

ALCONPAT Internacional

Founders members:

Liana Arrieta de Bustillos – **Venezuela**
Antonio Carmona Filho - **Brazil**
Dante Domene – **Argentina**
Manuel Fernández Cánovas – **Spain**
José Calavera Ruiz – **Spain**
Paulo Helene, **Brazil**

Board of Directors International:

President of Honor

Carmen Andrade Perdrix, **Spain**

President

Enio Pazini Figueiredo, **Brazil**

General Director

Pedro Castro Borges, **Mexico**

Executive Secretary

César Juárez Alvarado, **Mexico**

Technical Vice President

Pedro Garcés Terradillos, **Spain**

Administrative Vice President

Luis Álvarez Valencia, **Guatemala**

Treasurer

Jose Manuel Mendoza Rangel, **Mexico**

Manager

Enrique Cervera Aguilar, **Mexico**
Paulo Helene, **Brazil**

Revista ALCONPAT

Editor in Chief:

Dr. Pedro Castro Borges
Centro de Investigación y de Estudios Avanzados del
Instituto Politécnico Nacional, Unidad Mérida
(CINVESTAV IPN – Mérida)
Merida, Yucatan, **Mexico**

Co-Editor in Chief (2022-2023):

Dra. Edna Possan
Universidade Tecnológica Federal do
Paraná, Curitiba, **Brazil**

Executive Editor:

Dr. José Manuel Mendoza Rangel
Universidad Autónoma de Nuevo León,
Facultad de Ingeniería Civil
Monterrey, Nuevo León, **Mexico**

Associate Editors:

Dr. Manuel Fernández Cánovas
Universidad Politécnica de Madrid.
Madrid, **Spain**

Ing. Raúl Husni

Facultad de Ingeniería - Universidad de Buenos Aires.
Buenos Aires, **Argentina**

Dr. Paulo Roberto do Lago Helene

Universidade de São Paulo.

São Paulo, **Brazil**

Dr. José Iván Escalante García

Centro de Investigación y de Estudios Avanzados del
Instituto Politécnico Nacional (Unidad Saltillo)
Saltillo, Coahuila, **Mexico**.

Dra. Oladis Troconis de Rincón

Centro de Estudios de Corrosión

Universidad de Zulia

Maracaibo, **Venezuela**

Dr. Fernando Branco

Universidade Técnica de Lisboa

Lisboa, **Portugal**

Dr. Pedro Garcés Terradillos

Universidad de Alicante

San Vicente, **Spain**

Dr. Andrés Antonio Torres Acosta

Instituto Tecnológico y de Estudios Superiores de
Monterrey, Querétaro

Querétaro, **Mexico**

Dr. Filippo Ubertini

Universidad de Perugia,

Perugia, **Italy**

Dr. Ravindra Gettu

Instituto Indio de Tecnología de Madrás,

Chennai, **India**

RAV12N2, May – August 2022

Message from the Editor in Chief

**JOURNAL OF THE LATIN-AMERICAN
ASSOCIATION OF QUALITY CONTROL,
PATHOLOGY AND RECOVERY OF
CONSTRUCTION**

<http://www.revistaalconpat.org>

With great satisfaction, we present the second issue of the twelfth year of the ALCONPAT Journal.

The objective of the Journal is the publication of contributions on basic or applied research directly related to solving problems about quality control, pathology and recovery of constructions, with related case studies being welcome in these areas.

This V12N2 edition begins with a work from **Brazil**, where E. L. Machado and colleagues identify what criteria should be considered in the evaluation of school buildings, through a systematic review of the literature, consultation of government regulations and guidelines, and consultation with experts. The research was carried out in 3 stages: 1) systematic review of the literature and 2) review of national standards and guidelines to identify criteria and 3) weighting of criteria, by applying the Delphi method. 70 evaluation criteria were identified, which were grouped into 11 categories and weighted by consulting experts. The identification of criteria, as presented in this research, aims to contribute to the development of evaluation techniques and methods, to subsequently write a performance standard for school buildings.

In the second work, from **Mexico**, A. Moreno and colleagues make a review of the work done using marble powder as a substitute for cement, sand or fine aggregate in concrete, mortar and bricks. Research carried out in various parts of the world with different experimental procedures was reviewed. It is concluded that marble powder can be used as a partial substitute for cement or fine aggregate (up to 15%, depending on the material to be replaced), without affecting the compressive strength of the samples or pieces, and regardless of the shape. Therefore, marble dust not only helps to reduce the pollution it generates, but also to reduce its use as sand and dust, contributing to sustainable development.

The third work in this issue is from **Brazil**, where F. G. S. Ferreira and colleagues evaluate the impact of thermal curing and the use of particle packing in ultra-high performance cementitious composites (UHPC), with and without glass powder. For this, the specimens were molded with 0% and 50% glass powder (volumetric replacement for cement), in addition to two mixtures obtained through particle packing. The samples were subjected to thermal curing and moist curing to compare the effects. Tests of resistance to compression and absorption by capillarity were carried out. The results indicated that thermal curing provides a gain in initial strength. The application of particle packing in the mixing doses resulted in a significant improvement in the properties of the samples and the glass powder proved to be a viable substitute for cement.

In the fourth article from **Brazil**, R. R. C. Silva and C. Bertoldo simulate pathological manifestations in diaphragm walls through concrete made with different additions of synthetic polymer, proposing to obtain resistance and stiffness prediction models through the propagation of ultrasound waves. Compression tests were carried out to determine resistance and stiffness, as well as ultrasound tests by the direct and indirect method on concrete produced with different concentrations of synthetic polymer. The results obtained indicated a decrease in the mechanical and acoustic properties of the concrete with the increase in the concentration of synthetic polymer in its preparation. The models generated by the ultrasonic test were statistically significant, with a confidence level of 95%, and the correlations established in particular can be used in the detection of pathological manifestations in loco.

The fifth article, by R. Cattelan and colleagues, comes from **Brazil**, and they evaluate the influence of the eccentricity variations of the cables in models with post-tensioned flat slabs. The correct positioning of the tendons in the assembly of post-tensioned flat slabs is essential for the structural system to achieve adequate performance and safety. Four different architectural models with modification of the height of the cables at different points and quantity were analyzed. Pre-compression stresses, extreme stresses at the top and bottom, vertical displacements, load balancing and amount of passive steel in the slabs were evaluated. The ADAPT Floor Pro software was used for the analysis. The project follows the recommendations of NBR 6118:2014 and ACI 318:2019. For the evaluated models, it was found that the variation in the vertical eccentricity of the tendons at the base of the slab further reduces the values of the applied stresses, compared to the variation at the top.

The sixth work of this issue was written by Elia Alonso and colleagues from **Mexico**, in which they analyzed modifications presented by different stabilizers (lime, cement, prickly pear fiber, river lithics, volcanic lithics, sodium sulfate and gypsum) in properties and failure envelope of a remodeled natural clayey soil from Santiago Undameo, in Michoacán, Mexico. Granulometry, hydrometry, index tests, simple compression and Proctor test were performed on the clay soil. The variation in index and failure envelope properties was determined for the stabilized mixtures. The proposed additions improve the behavior of the highly plastic soil, reducing volumetric deformations and increasing its normal mechanical strength, shear strength and internal friction angle. The research contributes favorably to the restoration of historic-heritage earthen constructions, civil works, pathologies in buildings and construction technologies. The research was carried out in a laboratory under international regulations.

In the seventh paper, from **Brazil**, Ana Lin Ramos and Elton Bauer study the conditions of exposure to degrading agents in buildings located in different Brazilian bioclimatic zones. Knowing the action of weathering is essential to understand the degradation of facades. For this, eight cities were selected: Curitiba, Santa María, Florianópolis, Brasília, Niterói, Goiânia, Picos and Belém. A hygrothermal simulation construction model was defined to evaluate total radiation, thermal amplitude, thermal shock, temperature intensity

index and directed rainfall. As a result, critical condition zones are identified, providing exposure classifications. For agents of temperature and directed rain, the most exposed areas are Goiânia and Belém. The mildest exposure zones are Belém for temperature agent and Niterói for directed rain.

The eighth work is a case study from **Cuba**, where Alberto Hernández Oroza and colleagues make an evaluation through visual classification and non-destructive tests, the state of conservation of 32 wooden beams for reuse in the building restoration project. Narciso López of the Historic Center of Havana. For this, measurements of the moisture content, penetrometer, estimation of the modulus of elasticity and breaking stress by ultrasonic pulse velocity were made. The results showed that 66% of the beams were affected by rot, defibrillation and cracking. The tests carried out on the deteriorated beams made it possible to determine that, for a reliability of 95%, of the remaining 21 beams it was possible to reuse 17 of them with an average density of 0.4 g/cm³.

The ninth work in this number comes from **Brazil**. In this case study, G. Coni and colleagues present the study carried out in a Wastewater Pumping Station after severe degradation was observed. Biogenic sulfuric acid attack on sewage systems is widely studied in the literature, however, data on real construction situations are still quite limited. Analyzes of H₂S concentration in air, carbonation depth, compressive strength test, petrography, SEM/EDS, XRD and chemical determinations were performed on concrete cores extracted above the effluent level. Products identified on the surface were gypsum, jarosite, ferrous hydroxide, ferrous chloride, and possibly hisingerite. The results demonstrate the presence on the surface of both cement paste dissolution products and 16 mm steel bars located in the attacked region.

The tenth article that closes the edition was written by Alberto Hernández Oroza and colleagues from **Cuba**, who diagnose and propose a solution to the injuries present in the wooden floors of the Santa Clara Convent. To this end, non-destructive resistography and penetrometer tests, biological studies on the wood, and geomatic techniques for analysis of deformation and dimensioning of the beams were applied. The results of the diagnosis showed that 65% of the slab composed of 98 beams is affected by rot and xylophagous organisms. Density studies by comparison with reference values showed loss in wood hardness. The results conclude that the restoration implies the need to replace 17 beams, and the reinforcement of the right feet and sections of sliding beams.

It is important to mention that the ONCyTS of Brazil and Mexico have kept Revista Alconpat in their indexes of Quality Scientific Journals. In particular, in Mexico, the Alconpat Journal has been consolidated at an international level and the National System of Researchers (SNI) already considers it as a valid product for the promotion and permanence of its members. This has been a great achievement, the product of everyone's efforts, authors, reviewers and editorial committee. Similarly, it is important to mention that Revista Alconpat already belongs to the Directory of Open Access Journals (DOAJ), which is a definitive step to apply to new indexes. Alconpat is also making a significant financial investment so that all its issues are being marked in XML-Jats so that it can be evaluated in

more prestigious indexes. Congratulations and our thanks to all.

We are sure that the articles in this issue will constitute an important reference for those readers involved with questions of evaluation and characterization of materials, elements and structures. We thank the authors participating in this issue for their willingness and effort to present quality articles and meet the established deadlines.

On behalf of the Editorial Board

Pedro Castro Borges

Editor in Chief



CONTENT

Page

REVIEW

- Machado, E. L., Pasdiora, L., Santos, A. P. L., Santos Filho, M. L.:** Identification of criteria for evaluating school buildings. 143 - 161
- Moreno, A., Ponce P., Múzquiz, E., Avalos, F.:** Marble residues in construction materials: a review of the use of marble dust in mortars, concrete and bricks. 162 - 183

BASIC RESEARCH

- Ferreira, F. G. S., Dias, L. V., Soares, S. M., Castro, A. L.:** Influence of thermal curing in the physical and mechanical properties of ultra-high-performance concrete with glass powder. 184 - 199
- Silva, R. R. C., Bertoldo, C.:** Simulation of pathological manifestations in diaphragm wall through ultrasonic wave propagation. 200 - 209
- Cattelan, R., Cielo, L., Santos Lübeck, A., Neto, A. B. S.:** Analysis of the influence of variation of eccentricity of unbonded tendons on the structural behavior of post-tensioned flat slabs. 210 - 226
- Sánchez, A., Alonso, E., Martínez, W., Chávez, H., Navarrete, M., Arreola, M., Borrego, J., Equihua, L., Núñez, E., Miranda, O.:** Modifications of the rupture envelope in clayey soils with different volumetric stabilizer. 227 - 247

APPLIED RESEARCH

- Ramos, A. L., Bauer, E.:** Study of the facade degradation agents associated with temperature and driving rain in different Brazilian bioclimatic zones. 248 - 262

STUDY CASE

- Hernández Oroza, A., Berreo Alayo, E., Expósito Mendez, R.:** Non-destructive evaluation of the state of conservation of the wooden beams of the Narciso López building in the Historic Center of Havana for reuse in its restoration. 263 - 278
- Coni, G., Tafuri, A., Costa, A., Sakuma, G.:** Degradation of concrete through the formation of biogenic sulfuric acid in a Sewage Pumping Station (EEE). 279 - 295
- Hernández Oroza, A., Diomedes Almeida, A., Romeo Sáez, A., Cuétara Pérez, P. R.:** Diagnosis and solutions proposal to the damages present in the ceiling of the Convent of Santa Clara de Asís. 296 - 310



Identification of criteria for evaluating school buildings

E. L. Machado^{1*}, L. Pasdiora², A. P. L. Santos³, M. L. Santos Filho⁴

*Contact author: eduarda.jauck@gmail.com

DOI: <https://doi.org/10.21041/ra.v12i2.532>

Reception: 25/03/2021 | Acceptance: 12/02/2022 | Publication: 01/05/2022

ABSTRACT

The objective of this research is to identify which criteria should be considered in the evaluation of school buildings, through a systematic review of the literature, consultation of government standards and guidelines and consultations with experts. The research was carried out in 3 stages: 1) systematic review of the literature, 2) review of national standards and guidelines to identify criteria, and 3) weighting of criteria through the application of the Delphi method. 70 evaluation criteria were identified, which were grouped into 11 categories and weighted through consultation with experts. The identification of criteria as presented in this research, aims to contribute to the development of techniques and evaluation methods, to later compose a performance standard for school buildings.

Keywords: school infrastructure; performance of school buildings; school building evaluation criteria; systematic literature review; delphi.

Cite as: Machado, E. L., Pasdiora, L., Santos, A. P. L., Santos Filho, M. L. (2022), “*Identification of criteria for evaluating school buildings*”, Revista ALCONPAT, 12 (2), pp. 143 – 161, DOI: <https://doi.org/10.21041/ra.v12i2.532>

¹ Doutoranda do Programa de Pós-Graduação em Engenharia Civil, Universidade Federal do Paraná, Curitiba, Brasil.

² Programa de Pós-Graduação em Engenharia Civil, Universidade Federal do Paraná, Curitiba, Brasil.

³ Departamento de Engenharia de Produção, Universidade Federal do Paraná, Curitiba, Brasil.

⁴ Engenheiro Civil, Universidade Federal do Paraná, Curitiba, Brasil.

Contribution of each author

In this work, the 1st author contributed with the activities of applying the Delphi technique and discussion of the results, the 2nd author with the literature review activity, the 3rd author contributed with the original idea and direction of the research, and the 4th author contributed with the selection of specialists and review of regulations.

Creative Commons License

Copyright 2022 by the authors. This work is an Open-Access article published under the terms and conditions of an International Creative Commons Attribution 4.0 International License ([CC BY 4.0](https://creativecommons.org/licenses/by/4.0/)).

Discussions and subsequent corrections to the publication

Any dispute, including the replies of the authors, will be published in the first issue of 2023 provided that the information is received before the closing of the third issue of 2022.

Identificación de criterios para la evaluación de edificios escolares

RESUMEN

El objetivo de esta investigación es identificar qué criterios se deben considerar en la evaluación de edificios escolares, a través de una revisión sistemática de la literatura, consulta de normas y directrices gubernamentales y consultas a expertos. La investigación se llevó a cabo en 3 etapas: 1) revisión sistemática de la literatura, 2) revisión de normas y directrices nacionales para identificar criterios y 3) ponderación de criterios mediante la aplicación del método Delphi. Se identificaron 70 criterios de evaluación, los cuales fueron agrupados en 11 categorías y ponderados mediante consulta a expertos. La identificación de criterios, tal como se presenta en esta investigación, tiene como objetivo contribuir al desarrollo de técnicas y métodos de evaluación, para posteriormente redactar una norma de desempeño para edificios escolares.

Palabras clave: infraestructura escolar; desempeño del edificio escolar; criterios de evaluación de edificios escolares; revisión sistemática de literatura; delphi.

Identificação de critérios para avaliação de edificações escolares

RESUMO

O objetivo desta pesquisa é identificar quais critérios devem ser considerados na avaliação de edifícios escolares, por meio de uma revisão sistemática da literatura, consulta a normas e diretrizes governamentais e consultas a especialistas. A pesquisa foi realizada em 3 etapas: 1) revisão sistemática da literatura, 2) revisão de normas e diretrizes nacionais, para identificação dos critérios e 3) ponderação dos critérios, por meio da aplicação do método Delphi. Foram identificados 70 critérios de avaliação, que foram agrupados em 11 categorias e ponderados por meio da consulta a especialistas. A identificação dos critérios conforme apresentado nesta pesquisa, visam contribuir para o desenvolvimento de técnicas e métodos de avaliação, para posteriormente compor uma norma de desempenho para edifícios escolares.

Palavras-chave: infraestrutura escolar; desempenho de edifícios escolares; critérios de avaliação de edifícios escolares; revisão sistemática da literatura; delphi.

Legal Information

Revista ALCONPAT is a quarterly publication by the Asociación Latinoamericana de Control de Calidad, Patología y Recuperación de la Construcción, Internacional, A.C., Km. 6 antigua carretera a Progreso, Mérida, Yucatán, 97310, Tel.5219997385893, alconpat.int@gmail.com, Website: www.alconpat.org

Reservation of rights for exclusive use No.04-2013-011717330300-203, and ISSN 2007-6835, both granted by the Instituto Nacional de Derecho de Autor. Responsible editor: Pedro Castro Borges, Ph.D. Responsible for the last update of this issue, Informatics Unit ALCONPAT, Elizabeth Sabido Maldonado.

The views of the authors do not necessarily reflect the position of the editor.

The total or partial reproduction of the contents and images of the publication is carried out in accordance with the COPE code and the CC BY 4.0 license of the Revista ALCONPAT.

1. INTRODUCTION

The school environment and indoor spaces play a significant role in improving or obstructing teaching and learning processes. Well-designed, properly furnished and maintained school facilities contribute to better academic performance which positively reflects on student development (Hassanain; Ali Iftikhar, 2015).

As pointed out by Cardoso (2017), school infrastructure planners are faced with a scenario in which there is a need to create a comfortable and stimulating space for children. However, considering the Brazilian economic limitations, a transformation of this reality can be only with the construction of new units, so it is necessary to define strategies for the adaptation of existing buildings.

National and international studies point to many deficiencies in relation to the maintenance and conservation of school buildings (Norazman, Norsafiah, et al., 2019; Marques, De Brito, Correia, 2015; Mojela, Thwala; 2014; Mydin et al., 2014; Tan et al., 2014; Ali et al.; 2013; Shehab, Nouredine 2013; Soares Neto et al., 2013; Boothman, Higham, Horsfall, 2012; Asiya, 2012; Gomes and Regis; 2012)

Beauregard and Ayer (2018) highlight the importance of establishing a process to prioritize the installation maintenance work orders, thus seeking to optimize public resources. Therefore, the selection of the criteria to be evaluated becomes the first step to obtain this prioritization of the conservation activities of the schools.

The identification of criteria for evaluating buildings is a recurring theme in case studies related to quality control, pathology and building recovery, such as the research by Sotsek, Leitner and Santos (2019). As pointed out by Koleoso et al., (2013), measuring the performance of a building is the safest way to improve the economic, physical and functional development of a building, ensuring that its objectives are met.

Based on this scenario, this article aims to identify which criteria should be considered in the evaluation of school buildings, through a systematic review of the literature, consultation of national and international standards and consultations with specialists, aiming at the conservation of these buildings and guaranteeing the proper performance.

2. STANDARDS AND GUIDELINES FOR EVALUATING SCHOOL INFRASTRUCTURE IN BRAZIL

In Brazil, there are no specific standards for evaluating a school's infrastructure. However, there are rules for evaluating buildings in general, which can guide the evaluation of a school building. These standards are drawn up by the Brazilian Civil Construction Committee (ABNT/CB-002), which is responsible for standardizing the sector.

The main building evaluation standard is ABNT NBR 15575 (2013), “Performance of housing buildings”, which establishes the requirements and performance criteria that apply to housing buildings, seeking to meet user requirements that are: safety, habitability and sustainability.

This standard, however, does not apply to works in progress or buildings completed by the date of entry into force, nor to renovations, retrofits and temporary buildings.

In addition to ABNT NBR 15575 (2013), other standards that address the performance of buildings are ABNT NBR 14037 (2014) “Guidelines for the preparation of manuals for the use, operation and maintenance of buildings – Requirement for the preparation and presentation of contents”, ABNT NBR 5674 (2012) “Building maintenance – Requirements for the maintenance management system”, and ABNT NBR 16280 (2015) “Building renovation – Renovation management system – Requirements”.

Recently, another standard was elaborated, ABNT NBR 16747 (2020), "Building Inspection - Guidelines, concepts, terminology, requirements and procedure", which provides guidelines, requirements and procedures related to building inspection, aiming to standardize methodology, establishing methods and minimum steps of the activity. The standard will apply to buildings of any type, public or private, for global assessment of the building, fundamentally through sensory examinations by a qualified professional.

The "Prova Brasil" and the School Census have been the methods used to assess a school's infrastructure in terms of learning and performance.

The "Prova Brasil" is a census assessment, created by the National Institute of Educational Studies and Research (INEP) in 2005, to assess the quality of education offered by the Brazilian public education system; through standardized tests in the areas of Portuguese Language and Mathematics, it provides data for Brazil, federation units, municipalities and participating schools. In addition to the tests, students also answer a questionnaire on aspects related to socioeconomic and cultural origin and on school and study practices. Principals and teachers also respond to questionnaires involving aspects related to school resources, school organization and management, academic climate and pedagogical practices (Gomes and Regis, 2012).

In this test, the state of conservation of the items and equipment of the building (roof, walls, floor, entrance of the building, patio, corridors, classrooms, doors, windows, bathrooms, kitchen and hydraulic and electrical installations are evaluated, but it does not evaluate stairs, ramps and elevators, among others...), the number of classrooms that meet the criteria for adequate lighting and ventilation, aspects related to the safety of schools and students, among other aspects.

The School Census, on the other hand, offers different information about the school reality, presenting data on schools, classes, enrollment and teachers. Although these data are important, by themselves they would not reveal the state of conservation of the schools, since the infrastructure variables available in the School Census only indicate the presence or absence of certain items.

The School Census (INEP, 2019) is applied annually throughout Brazil, collecting information on various aspects of Brazilian schools, in particular enrollment and infrastructure. All levels of education are involved: kindergarten, elementary school, high school and Youth and Adult Education (EJA). Infrastructure data is divided into seven sections: power; services; dependencies; equipments; technology; accessibility and others.

3. METHOD

The development of this research was carried out in three different stages, as shown in Figure 1.

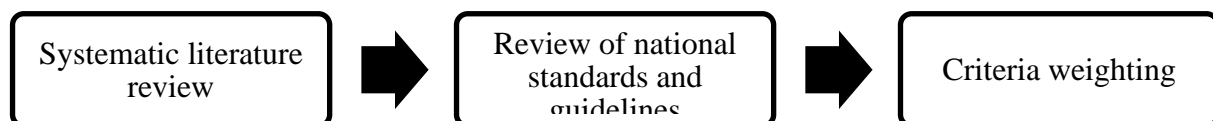


Figure 1. Steps of the research. Source: The authors.

3.1 Step 1

First, a systematic literature review (SLR) was conducted on scientific articles, seeking to identify which criteria for evaluating the performance of school buildings were most relevant in the academic environment. According to the research by Sampaio (2007), the following parts were defined to conduct the literature review:

- 1) Definition of the question - what criteria are used to evaluate the performance of educational buildings?
- 2) Searching for references – characterized by the definition of keywords and search strategies, in addition to the identification of the databases to be consulted. Table 01 shows the search strategies adopted. The search was carried out in four different databases, and limited to results in English and Portuguese. In addition, the search was restricted to finding the term only in the title, abstract and keywords of the documents.

Table 1. Search terms, sources used and respective results. Source: The authors.

Search Terms	Source	Results
“Educational Building Performance”	Scopus	88
	Periódicos CAPES	23
	Scielo	21
	Science Direct	188

3) Reviewing and selecting the studies - Based on the results found previously, the titles of documents that did not fit the criteria defined for conducting the research were evaluated and eliminated. The summaries of the remaining articles were then analyzed and those that dealt with performance in educational buildings were selected. Then the repeated documents were excluded, and the rest of the articles were read in full. The final selection excluded documents that did not include criteria and parameters for analyzing the performance of buildings. Through the backward procedure, in which the references of previously selected studies are consulted (DRESCH et al, 2015), one more article was added to the review.

After the selection of the studies, an analysis was carried out in order to identify the criteria addressed in the research to evaluate the performance of the school building. The data obtained are exposed in the results section.

3.2 Step 2

After analyzing the academic works consulted in the SLR, it was found by the authors that it would be necessary to carry out a more comprehensive search to identify which criteria should be used for the evaluation of school buildings. To complement the research, the following were also consulted:

- National standards; (references to international standards have been removed, based on the evaluators' suggestions)
- Federal and state government guidelines;
- Assessment instruments for Brazilian schools;

The presentation and synthesis of the results obtained are also addressed in the Results and Discussion section.

3.3 Step 3

In order to build a more consistent criteria framework, the Delphi method was also applied, in which specialists who work or worked as engineers in city halls are presented in Table 2. The objective of this step was to make the specialists reach a consensus on the importance of the previously identified criteria and assign grades to the criteria.

Table 2. Profile of the specialists who participated in the Delphi stage. Source: The authors.

Specialist	Occupation	Working time with performance of school buildings
A	Construction supervisor	Less than 1 year
B	Construction supervisor	Less than 3 years
C	Civil engineer	Less than 3 years
D	Construction Secretary (Retired)	More than 3 years
E	Civil Engineer I	Less than 1 year
F	Infrastructure supervisor	More than 08 years

To decide whether or not there was consensus after each round, equation (1) was used. (WILSON; PAN; SCHUMSKY, 2012):

$$CVR = (NE - N/2)/(N/2) \quad (1)$$

where:

CVR = Content Validity Ratio;

NE = number of experts who indicate that a parameter is essential; and

N = total number of specialists participating in the survey.

Consensus was considered when the CVR was greater than or equal to 0.29 and the method rounds were stopped. The technique was applied through online questionnaires, in three rounds. In the first one, the specialists received a questionnaire with the list of criteria obtained in the previous step, and they should indicate their importance on a scale from 1 to 4 (where 1 means little important and 4 very important). This scale was adopted to avoid the intermediate neutral term (3), from the five-point scale, which in previous experiences has shown to be an option for indecision in questionnaires. If they judged that the criterion was not relevant in the evaluation, it was possible to mark the option N/A (not applicable). In the second round, the averages obtained through the previous questionnaire were presented, and the experts were invited to reassess some criteria, whose consensus was not obtained in the first round. Finally, the third round presented the results obtained in the previous stage and, only for the criteria where there was still no consensus, a new reassessment was carried out.

4. RESULTS AND DISCUSSION

4.1 Step 1

This stage of the work is based on the results of the literature review on the important criteria for the evaluation of school units. The academic works consulted, resulting from the literature review, are listed in Table 3, according to the identified criteria.

Table 3. Articles consulted in the Literature Review. Source: The authors.

References	Criteria
Michael, Heracleous (2017)	Lighting levels, light distribution, visual comfort conditions, need to use artificial lighting
Khalil et al. (2016)	Spaces, window orientation, infrastructure, accesses, circulation areas, ergonomics, signs, emergency exits, probability of user contamination, common areas, materials, structural stability, information systems in building automation, electrical and plumbing services, prevention fire, roof, elevators, thermal comfort, artificial and natural lighting, garbage disposal, ventilation, acoustic comfort, cleaning
Driza, Park (2013)	Performance of water and electrical systems
Khalil et al. (2012)	Accessibility in buildings, location, users' perception of building problems
Mijakowski, Sowa (2017)	Indoor ventilation, temperature, humidity and CO2 concentration
El Asmar et al. (2014)	Layout, furniture, thermal comfort, indoor air quality, lighting, acoustic comfort, hydraulic efficiency, cleaning and maintenance
Zomorodian, Tahsildoost (2014)	Thermal and visual comfort
Bonomolo et al. (2017)	Natural lighting
Pellegrino et al. (2015)	Window orientation, external obstructions, dimensions, area of windows, depth of rooms, curtains and blinds, reflectance properties and external view.
Wang, Zamri (2013)	Thermal and acoustic comfort, indoor air quality, room layout, lighting
Karima, Altan (2016)	lighting systems, heating, air conditioning, natural lighting, security systems
Ali et al. (2016)	Surface temperature, relative humidity, light intensity, internal concentration of CO2
Khalil et al. (2011)	Visual and thermal comfort, ventilation
El Darwish, El-Gendy (2018)	Air temperature, relative humidity, radiant temperature, air speed
Ropi, Tabassi (2014)	Condition analysis of bathrooms, ceilings, doors, structures, walls and roofs
Wong, Jan (2003)	Thermal, spatial, visual, acoustic comfort, indoor air quality and building integrity

4.2 Step 2

At this stage, official standards and guidelines were consulted that could help in the elaboration of a list of criteria for the evaluation of school buildings. Table 4 lists the standards and guidelines consulted.

Table 4. Standards and guidelines consulted in the identification of evaluation criteria for school buildings. Source: The authors.

National Standards	Federal government guidelines		Assessment tools for Brazilian schools
Standards of the Brazilian Association of Technical Standards (ABNT)	1	Technical Guidelines Manual - v.2: Elaboration of school building projects: early childhood education (MEC, 2017)	Scholar Census (2019)
	2	Book of Requirements and Performance Criteria for Public Education Establishments (MEC, 2014)	
	3	Technical manual of architecture and engineering Guidance for designing construction projects for Early Childhood Education Centers. (MEC, 2009)	
	4	Minimum operating standards of the elementary school: implementation manual. (MEC, 2006a)	"Prova Brasil" (2017)
	5	Basic infrastructure parameters for early childhood education institutions. Brasilia. (MEC, 2006b)	
	6	Manual for Adequacy of School Buildings - Ministry of Education MEC (2005)	

All these norms, guidelines and academic works identified in Steps 1 and 2 were submitted to content analysis and it was noticed that there is no standard to organize the identified criteria. In this way, the authors created their own structure, seeking to organize them into groups that are related to each other. 70 criteria were identified, grouped into 11 categories, as shown in Table 5. This table also presents the ABNT standards related to the criteria identified in the systematic literature review.

Table 5. Criteria, norms and guidelines for the evaluation of school buildings. Source: The authors.

Category	Nº	Criteria	Standard NBR	Federal government guidelines						Scholar Census	"Prova Brasil"
				1	2	3	4	5	6		
installations	1	Roofs	15575-5	x	x	x	x		x		x
	2	Walls	15575-4	x	x	x	x	x	x		x
	3	Sports courts		x	x		x			x	x
	4	Playgrounds	16071-2	x			x			x	
	5	Gates, railings and walls		x	x	x	x				x
	6	Unpaved areas		x							

	7	Furniture	14006	x	x	x	x	x	x			
	8	Structures	6118	x	x	x	x		x			
	9	Parking		x	x	x			x			
	10	Stairs	9077	x	x	x						
	11	Ramps	9050	x	x	x			x			
	12	Elevators	13994			x			x			
Finishes	13	Wall paintings	13245	x	x	x	x	x	x			
	14	Coatings	16919	x	x	x	x	x	x			
	15	Floors	15575-3	x	x	x	x	x	x		x	
	16	Sockets	14136	x	x	x	x		x			
	17	Metals	10283	x	x	x			x			
	18	Frames (door and windows)	10821/ 10831	x	x	x		x	x	x		x
	19	Lining	14285/ 16382	x	x	x		x		x		
Fire security	20	Crockering	15097	x	x	x			x			
	21	fire extinguishers	12693	x		x			x		x	
	22	Escape routes	9077	x	x				x			
Thermal comfort	23	Signaling	13434	x	x	x			x			
	24	Adequacy of walls	15220-2	x	x			x	x	x		
	25	Thermal insulation of the roof	15220-2	x	x	x			x	x		
	26	Ventilation openings	15575-4	x	x	x		x	x	x		x
	27	Humidity in environments		x	x	x			x			
Acoustic comfort	28	Acoustic insulation of walls	15575-4	x	x	x			x			
	29	Noise pollution	10151	x	x	x			x			
Visual comfort	30	Natural lighting	15215	x	x	x	x	x	x		x	
	31	artificial lighting	5413	x	x	x	x	x	x		x	
Infrastructure	32	water installations	5626	x	x	x	x	x	x	x	x	
	33	sewer installations	8160	x	x	x	x	x	x	x	x	
	34	rainwater system	10844	x	x	x	x	x				
	35	electrical installations	5410	x	x	x		x	x	x	x	
	36	telecommunication systems	14691	x		x			x			

Sustainability	37	energy efficiency	ISO 50001		x	x			x		
	38	environmental management systems	ISO 14001	x	x	x			x		
	39	Waste destination		x	x	x			x		x
	40	Rain catchment management	15527	x	x				x		
Habitability	41	Ceilings height	15575	x	x	x	x			x	
	42	Tightness to sources of moisture	9575	x	x	x					
	43	signs of predation									x
	44	Pollutants in the indoor atmosphere		x	x						
	45	Suitability for people with reduced mobility	9050	x	x	x			x	x	x
	46	Environment cleanliness level		x	x	x			x	x	
	47	building aesthetics		x					x	x	
	48	school location		x	x	x			x		x
Safety (school and student)	49	Check-in and check-out of students									x
	50	Controlling the entry of strangers into the school						x		x	x
	51	Daytime surveillance						x			x
	52	Nighttime surveillance						x			x
	53	Surveillance on weekends and holidays						x			x
	54	Policing scheme to inhibit thefts, robberies and other forms of violence									

Table 6. Weighting of criteria for evaluating school buildings. Source: The authors.

Category	Nº	Criteria	Nota Delphi
installations	1	Roofs	4,0
	2	Walls	3,2
	3	Sports courts	3,0
	4	Playgrounds	2,5
	5	Gates, railings and walls	3,2
	6	Unpaved areas	1,7
	7	Furniture	3,3
	8	Structures	3,7
	9	Parking	1,0
	10	Stairs	3,0
	11	Ramps	3,5
	12	Elevators	1,8
Finishes	13	Wall paintings	2,7
	14	Coatings	3,0
	15	Floors	3,7
	16	Sockets	3,7
	17	Metals	3,0
	18	Frames (door and windows)	3,3
	19	Lining	3,3
	20	Crockering	3,0
Fire security	21	fire extinguishers	3,8
	22	Escape routes	4,0
	23	Signaling	4,0
Thermal comfort	24	Adequacy of walls	2,3
	25	Thermal insulation of the roof	3,3
	26	Ventilation openings	4,0
	27	Humidity in environments	3,3
Acoustic comfort	28	Acoustic insulation of walls	2,8
	29	Noise pollution	3,3
Visual comfort	30	Natural lighting	3,7
	31	artificial lighting	3,8
Infrastructure	32	water installations	3,2
	33	sewer installations	3,0
	34	rainwater system	2,8
	35	electrical installations	3,8
	36	telecommunication systems	2,8

Sustainability	37	energy efficiency	3,3
	38	environmental management systems	2,7
	39	Waste destination	3,8
	40	Rain catchment management	2,8
Habitability	41	Ceilings height	3,3
	42	Tightness to sources of moisture	4,0
	43	signs of predation	3,3
	44	Pollutants in the indoor atmosphere	2,7
	45	Suitability for people with reduced mobility	3,8
	46	Environment cleanliness level	3,7
	47	building aesthetics	2,7
	48	school location	2,2
Safety (school and student)	49	Check-in and check-out of students	3,8
	50	Controlling the entry of strangers into the school	4,0
	51	Daytime surveillance	2,8
	52	Nighttime surveillance	3,7
	53	Surveillance on weekends and holidays	3,3
	54	Policing scheme to inhibit thefts, robberies and other forms of violence	3,3
	55	Policing scheme to inhibit drug trafficking within the school	3,5
	56	Policing scheme to inhibit drug trafficking in the vicinity of the school	3,3
	57	Lighting outside the school	3,7
	58	Protection mechanisms for more expensive equipment	3,3
	59	Security in your surroundings	3,3
environments	60	Classrooms	4,0
	61	administrative rooms	3,0
	62	Teachers' room	3,3
	63	computer rooms	3,5
	64	laboratories	3,5
	65	Refectory	4,0
	66	DML	2,7
	67	Kitchen	3,7
	68	Terrace	3,2
	69	Library	3,2
	70	Bathrooms	4,0

Evaluating the school facilities, the elements of the buildings identified as important from consultation with specialists are: roof, structure, walls, gates, railings and walls, furniture, sports

courts, stairs and ramps, all with scores greater than 3. The other criteria, mentioned in the RSL and in the norms and guidelines consulted, were not considered by the specialists as important elements for evaluating the performance of the school building.

Regarding the category of finishes, the criteria were considered important (coatings, floors, sockets, metals, frames, ceiling and crockery), only the painting of the walls was given a score lower than 3.

The categories of “Thermal, acoustic and lighting comfort” are generally considered important criteria in evaluating the performance of the building, although the criteria for thermal and acoustic insulation of the walls receive scores below 3.

The “Fire Safety” category, an indispensable item in the Fire and Panic Prevention and Fighting System, is unanimous in terms of importance, in the opinion of experts.

Electrical and hydro-sanitary installations are the outstanding criteria in the infrastructure category. Regarding the Sustainability and Habitability categories, the criteria of "energy efficiency", "waste disposal", "ceiling height", "tightness to sources of moisture", "signs of depredation", "adequacy to people with reduced mobility (PMR)” and “level of cleanliness of the environments”.

In general, the security aspects of the facility, property and physical occupants, Category of “School and Student Safety”, despite being important in the experts' assessment, was mentioned only in the SAEB assessment. It is understood that this criterion is not related to the building structure, but to its functioning.

For the environments mentioned in the RSL studies and in the norms and guidelines, an exclusive category was assigned, since they are not criteria, but are important enough to compose the assessment of the building. The least important environment is the DML. This environment is related to the cleanliness and hygiene of the school, however, it is mentioned only in a school evaluation instrument and for the specialists, it has a score of 2.7 on a scale of 1 to 4.

5. FINAL CONSIDERATIONS

Since the school building is the main asset of the learning process and is expected to offer quality and safety environments to users, this article aimed to identify, through a literature review, government guidelines and consultation with experts, the criteria used in research to evaluate the performance of school buildings.

70 criteria were identified, which were grouped into 11 categories according to their correlations: facilities, finishes, fire safety, thermal, acoustic and visual comfort, infrastructure, sustainability, habitability, safety (of the school and the student) and environments.

It was observed with the research that the Brazilian standards and guidelines in relation to the performance and conservation of schools are very outdated, some standards are more than 20 years old, which points to a need to review these guidelines, in order to guarantee the performance of these buildings, avoiding those defects and pathological manifestations compromise the school infrastructure, especially now with the consequences of the pandemic experienced in the last two years.

Considering also that in Brazil there are no specific norms for the evaluation of school buildings, the identification and weighting of criteria that allow such evaluation, as presented in the study, is a first step and contributes to the development of techniques and evaluation methods, which later can form a performance standard for school buildings.

As a suggestion for future work, a literature review is indicated to identify evaluation methods for the criteria presented in this research.

6. REFERENCES

- Ali, A. S., Keong, K. C., Zakaria, N., Zolkafli, U., Akashah, F. (2013). The effect of design on maintenance for school buildings in Penang, Malaysia. *Structural Survey*. <https://doi.org/10.1108/SS-10-2012-0030>
- Ali, A. S., Zanzinger, Z., Debose, D., Stephens, B. (2016). Open Source Building Science Sensors (OSBSS): A low-cost Arduino-based platform for long-term indoor environmental data collection. *Building and Environment*, 100, 114-126. <https://doi.org/10.1016/j.buildenv.2016.02.010>
- Asiyai, R. I. (2012). Assessing school facilities in public secondary schools in Delta State, Nigeria. *African research review*, 6(2), 192-205. <https://doi.org/10.4314/afrrrev.v6i2.17>
- Associação Brasileira de Normas Técnicas. CB-002 - Comitê Brasileiro da Construção Civil. Disponível em: <<http://www.abnt.org.br/cb-02>>. Acessado em 20/05/2020.
- Associação Brasileira de Normas Técnicas (2017). *NBR 10821. Esquadrias para edificações Parte 2: Esquadrias externas - Requisitos e classificação*. Rio de Janeiro.
- Associação Brasileira de Normas Técnicas (2011). *NBR 10831: Projeto e utilização de caixilhos para edificações de uso residencial e comercial – Janelas*. Rio de Janeiro.
- Associação Brasileira de Normas Técnicas (1989). *NBR 10844: Instalações prediais de águas pluviais – Procedimento*. Rio de Janeiro.
- Associação Brasileira de Normas Técnicas (2013). *NBR 12693: Sistemas de proteção por extintores de incêndio*. Rio de Janeiro.
- Associação Brasileira de Normas Técnicas (2011). *NBR 13245: Tintas para construção civil — Execução de pinturas em edificações não industriais — Preparação de superfície*. Rio de Janeiro.
- Associação Brasileira de Normas Técnicas (2004). *NBR 13434: Sinalização de segurança contra incêndio e pânico - Parte 2: Símbolos e suas formas, dimensões e cores*. Rio de Janeiro.
- Associação Brasileira de Normas Técnicas (2020). *NBR 16919: Placas cerâmicas - Determinação do coeficiente de atrito*. Rio de Janeiro.
- Associação Brasileira de Normas Técnicas (2014). *NBR 14037: Diretrizes para elaboração de manuais de uso, operação e manutenção das edificações – Requisito para elaboração e apresentação dos conteúdos*. Rio de Janeiro.
- Associação Brasileira de Normas Técnicas (2021). *NBR 16071-2: Playgrounds Parte 2: Requisitos de segurança*. Rio de Janeiro.
- Associação Brasileira de Normas Técnicas (2012). *NBR 15200: Projeto de estruturas de concreto em situação de incêndio*. Rio de Janeiro.
- Associação Brasileira de Normas Técnicas (2005). *NBR 15215-1: Iluminação natural - Parte 1: Conceitos básicos e definições*. Rio de Janeiro.
- Associação Brasileira de Normas Técnicas (2008). *NBR 15220: Desempenho térmico de edificações - Parte 2: Método de cálculo da transmitância térmica, da capacidade térmica, do atraso térmico e do fator solar de elementos e componentes de edificações*. Rio de Janeiro.
- Associação Brasileira de Normas Técnicas (2013). *NBR 15.575-1: Edificações Habitacionais – Desempenho – Parte 1: Requisitos gerais*. Rio de Janeiro.
- Associação Brasileira de Normas Técnicas (2013). *NBR 15.575-2: Edificações Habitacionais – Desempenho – Parte 2: Requisitos para os Sistemas Estruturais*. Rio de Janeiro.
- Associação Brasileira de Normas Técnicas (2013). *NBR 15.575-3: Edificações Habitacionais – Desempenho – Parte 3: Requisitos para os Sistemas de Pisos*. Rio de Janeiro.
- Associação Brasileira de Normas Técnicas (2013). *NBR 15.575-4: Edificações Habitacionais – Desempenho – Parte 4: Requisitos para os Sistemas de Vedações Verticais internas e externas*. Rio de Janeiro.

- Associação Brasileira de Normas Técnicas (2013). *NBR 15.575-5: Edificações Habitacionais – Desempenho – Parte 5: Requisitos para os Sistemas de Coberturas*. Rio de Janeiro.
- Associação Brasileira de Normas Técnicas (2012). *NBR 16071-1: Playgrounds - Parte 1: Terminologia*. Rio de Janeiro.
- Associação Brasileira de Normas Técnicas (2015). *NBR 16280: Reforma em edificações – Sistema de gestão de reformas – Requisitos*. Rio de Janeiro.
- Associação Brasileira de Normas Técnicas (2020). *NBR 16747: Inspeção predial – Diretrizes, conceitos, terminologia, requisitos e procedimento*. Rio de Janeiro.
- Associação Brasileira de Normas Técnicas (2020). *NBR 5626: Instalação predial de água fria*. Rio de Janeiro.
- Associação Brasileira de Normas Técnicas (2012). *NBR 5674: Manutenção de edificações – Requisitos para o sistema de gestão de manutenção*. Rio de Janeiro.
- Associação Brasileira de Normas Técnicas (2014). *NBR 6118: Projeto de estruturas de concreto – Procedimento*. Rio de Janeiro.
- Associação Brasileira de Normas Técnicas (1998). *NBR 7200: Execução de revestimento de paredes e tetos de argamassas inorgânicas – Procedimento*. Rio de Janeiro.
- Associação Brasileira de Normas Técnicas (1999). *NBR 8160: Sistemas prediais de esgoto sanitário - Projeto e execução*. Rio de Janeiro.
- Associação Brasileira de Normas Técnicas (1983). *NBR 8214: Assentamento de azulejos - Procedimento*. Rio de Janeiro.
- Associação Brasileira de Normas Técnicas (2015). *NBR 9050: Acessibilidade a edificações, mobiliário, espaços e equipamentos urbanos*. Rio de Janeiro.
- Associação Brasileira de Normas Técnicas. *NBR 9077. Saídas de emergência em edifícios (em revisão)*. Rio de Janeiro.
- Associação Brasileira de Normas Técnicas (2010). *NBR 9575. Impermeabilização - Seleção e projeto*. Rio de Janeiro: ABNT, 2010.
- Associação Brasileira de Normas Técnicas (2015). *NBR ISO 14001: Sistemas de gestão ambiental – Requisitos com orientações para uso*. Rio de Janeiro.
- Beauregard, M. A., Ayer, S. K. (2018). Maintaining performance: Understanding the relationship between facility management and academic performance at K-12 schools in the State of Arizona. *Facilities*. Vol. 36 No. 11/12, pp. 618-634. <https://doi.org/10.1108/F-11-2017-0111>
- Bonomolo, M., Baglivo, C., Bianco, G., Congedo, P. M., Beccali, M. (2017). Cost optimal analysis of lighting retrofit scenarios in educational buildings in Italy. *Energy Procedia*, 126, 171-178. <https://doi.org/10.1016/j.egypro.2017.08.137>
- Boothman, C., Higham, A., Horsfall, B. (2012). Attaining zero defects within building schools for the future: a realistic target or a Sisyphean task?. In *Proceedings 28th Annual ARCOM Conference* (3-5). Disponível em: https://www.arcom.ac.uk/-docs/proceedings/ar2012-0991-1001_Boothman_Higham_Horsfall.pdf
- Cardoso, T. A. (2017). *Estruturação do processo decisório para reforma de edificações escolares públicas do ensino fundamental utilizando o método multicritério de apoio à decisão – construtivista (MCDA-C)*. 223f. Dissertação (mestrado) - Universidade Federal do Paraná, Setor de Tecnologia, Programa de Pós-graduação em Engenharia de Construção Civil.
- Dresch, A., Lacerda, D. P., Júnior, J. A. V. A. (2015). *Design science research: método de pesquisa para avanço da ciência e tecnologia*. Bookman Editora.
- Driza, P. J. N., Park, N. K. (2013). Actual energy and water performance in LEED-certified educational buildings. *Sustainability: The Journal of Record*, 6(4), 227-232. <https://doi.org/10.1089/SUS.2013.9850>

- El Asmar, M., Chokor, A., Srouf, I. (2014). Are building occupants satisfied with indoor environmental quality of higher education facilities? *Energy procedia*, 50, 751-760. <https://doi.org/10.1016/j.egypro.2014.06.093>
- El-Darwish, I. I., El-Gendy, R. A. (2018). Post occupancy evaluation of thermal comfort in higher educational buildings in a hot arid climate. *Alexandria engineering journal*, 57(4), 3167-3177. <https://doi.org/10.1016/j.aej.2017.11.008>
- Gomes, A., Regis, A. (2012). Desempenho e infraestrutura: mapeamento das escolas públicas da região metropolitana do Rio de Janeiro. In *Congresso Ibero-americano de Política e Administração da Educação* (Vol. 3). Disponível em: https://www.anpae.org.br/iberoamericano2012/Trabalhos/AdaildaGomesDeOliveira_res_int_GT1.pdf.
- Hassanain, M. A., Iftikhar, A. (2015). Framework model for post-occupancy evaluation of school facilities. *Structural Survey*. Vol. 33 No. 4/5, pp. 322-336. <https://doi.org/10.1108/SS-06-2015-0029>
- Instituto Nacional de Estudos e Pesquisas Educacionais Anísio Teixeira (INEP). *Censo Escolar*. Disponível em: <<http://portal.inep.gov.br/web/guest/censo-escolar>> Acessado em 26 nov. 2019.
- Karima, M., Altan, H. (2017). Interactive building environments: A case study university building in UAE. *Procedia Engineering*, 180, 1355-1362. <https://doi.org/10.1016/j.proeng.2017.04.298>
- Khalil, N., Husin, H. N., Nawawi, A. H. (2012). An analytical literature: Strategic improvement of sustainable building performance tool for Malaysia's Higher Institutions. *Procedia-Social and Behavioral Sciences*, 36, 306-313. <https://doi.org/10.1016/j.sbspro.2012.03.034>
- Khalil, N., Husin, H. N., Wahab, L. A., Kamal, K. S., Mahat, N. (2011). Performance Evaluation of Indoor Environment towards Sustainability for Higher Educational Buildings. *Online Submission*. US-China Education Review A 2 p188-195 2011. Disponível em: <https://eric.ed.gov/?id=ED524814>
- Khalil, N., Kamaruzzaman, S. N., Baharum, M. R. (2016). Ranking the indicators of building performance and the users' risk via Analytical Hierarchy Process (AHP): Case of Malaysia. *Ecological Indicators*, 71, 567-576. <https://doi.org/10.1016/j.ecolind.2016.07.032>
- Koleoso, H., Omirin, M., Adewunmi, Y., Babawale, G. (2013), "Applicability of existing performance evaluation tools and concepts to the Nigerian facilities management practice". *International Journal of Strategic Property Management*, 17(4), 361-376. <https://doi.org/10.3846/1648715X.2013.861367>
- Marques, B. A., de Brito, J., Correia, J. R. (2015). Constructive characteristics and degradation condition of Liceu secondary schools in Portugal. *International Journal of Architectural Heritage*, 9(7), 896-911. <https://doi.org/10.1080/15583058.2013.865814>
- Michael, A., Heracleous, C. (2017). Assessment of natural lighting performance and visual comfort of educational architecture in Southern Europe: The case of typical educational school premises in Cyprus. *Energy and Buildings*, 140, 443-457. <https://doi.org/10.1016/j.enbuild.2016.12.087>
- Mijakowski, M., Sowa, J. (2017). An attempt to improve indoor environment by installing humidity-sensitive air inlets in a naturally ventilated kindergarten building. *Building and Environment*, 111, 180-191. <https://doi.org/10.1016/j.buildenv.2016.11.013>
- Ministério da Educação (2014). *Diretrizes Técnicas para Apresentação de Projetos e Construção de Estabelecimentos de Ensino Público*. Caderno de Requisitos e Critérios de Desempenho para Estabelecimentos de Ensino Público, vol. 1. Programa PROINFÂNCIA.
- Ministério da Educação (2017). *Manual de Orientações Técnicas - v.2: Elaboração de projetos de edificações escolares: educação infantil*. Brasília.
- Ministério da Educação (2005). *Manual para Adequação de Prédios Escolares*. 5a Ed./Elaboração Carlos Alberto Araújo Guimarães, Cláudia Maria Videres Trajano, Erinaldo Vitério, Rodolfo Oliveira Costa, Willamy Mamede da Silva Dias – Brasília: Fundescola/DIPRO/FNDE/MEC.

- Ministério da Educação (2009). *Manual técnico de arquitetura e engenharia de Orientação para elaboração de projetos de construção de Centros de educação Infantil*. Elaboração Karen Gama Muller, Luiz Paulo Ferrero Filho, Débora Carvalho Diniz –Brasília.
- Ministério da Educação (2006a). *Padrões mínimos de funcionamento da escola do ensino fundamental: manual de implantação*. 2a impressão. Brasília.
- Ministério da Educação (2006b). *Parâmetros básicos de infra-estrutura para instituições de educação infantil*. Brasília.
- Mojela, W., Thwala, W. D. (2014). Maintenance of Public Schools Infrastructure in South Africa. In *Proceedings of the 17th International Symposium on Advancement of Construction Management and Real Estate* (pp. 1253-1261). Springer, Berlin, Heidelberg. https://doi.org/10.1007/978-3-642-35548-6_127
- Mydin, M. O., Salim, N. A., Tan, S. W., Tawil, N. M., Ulang, N. M. (2014). Assessment of significant causes to school building defects. In *E3S Web of Conferences* (Vol. 3, p. 01002). EDP Sciences. <https://doi.org/10.1051/e3sconf/20140301002>
- Norazman, N., Asma, N. S., Nashruddin, M., Irfan, A., Ani, C., Norhaslina, J. F., Muhamad, K. A. (2019). School Building Defects: Impacts Teaching and Learning Environment. *International Journal of Recent Technology and Engineering (IJRTE)*, 8, 22-29. <https://doi.org/10.35940/ijrte.B1005.0782S219>
- Pellegrino, A., Cammarano, S., Savio, V. (2015). Daylighting for Green schools: A resource for indoor quality and energy efficiency in educational environments. *Energy Procedia*, 78, 3162-3167. <https://doi.org/10.1016/j.egypro.2015.11.774>
- QEDU. (2018). *Infraestrutura: Dependências em escolas públicas de ensino fundamental regular*. Disponível em: <https://www.qedu.org.br/brasil/censo-escolar?year=2018&dependence=0&localization=0&education_stage=0&item=>> Acessado em: 06/05/2020.
- Ropi, R. M., Tabassi, A. A. (2014). Study on maintenance practices for school buildings in Terengganu and Kedah, Malaysia. In *MATEC Web of Conferences* (Vol. 10, p. 03003). EDP Sciences. <https://doi.org/10.1051/matecconf/20141003003>
- Shehab, T., Noureddine, A. (2014). Prioritization Model for Rehabilitation of Public School Buildings in California. *International Journal of Construction Education and Research*, 10(1), 58-75. <https://doi.org/10.1080/15578771.2013.805344>
- Sistema de Avaliação da Educação Básica (2017). *Questionário da Escola*. Disponível em: <<http://portal.inep.gov.br/web/guest/educacao-basica/saeb/instrumentos-de-avaliacao>>. Acesso em 20 abr. 2020
- Soares Neto, J. J., De Jesus, G. R., Karino, C. A., De Andrade, D. F. (2013). Uma escala para medir a infraestrutura escolar. *Estudos em Avaliação Educacional*, 24(54), 78-99. <https://doi.org/10.18222/eae245420131903>
- Sotsek, N. C., Leitner, D. S., Lacerda Santos, A. de P. (2018). Uma revisão sistemática dos critérios do Building Performance Evaluation (BPE). *Revista ALCONPAT*, 9(1), 1 - 14. <https://doi.org/10.21041/ra.v9i1.260>
- Tan, S. W., Mydin, M. O., Sani, N. M., Sulieman, M. Z. (2014). Investigation into Common Decay of Educational Buildings in Malaysia. In *MATEC Web Of Conferences* (Vol. 10, p. 05001). EDP Sciences. <https://doi.org/10.1051/matecconf/20141005001>
- Wang, C. C., Zamri, M. A. (2013). Effect of IEQ on occupant satisfaction and study/work performance in a green educational building: a case study. In *ICCREM 2013: Construction and Operation in the Context of Sustainability* (pp. 234-246). <https://doi.org/10.1061/9780784413135.022>

Wilson, F. R., Pan, W., Sschumsky, D. A. (2012). Recalculation of the critical values for Lawshe's content validity ratio. *Measurement and Evaluation in Counseling and Development*, 45(3), 197-210. <https://doi.org/10.1177/0748175612440286>

Zomorodian, Z. S., Tahsildoost, M. (2017). Assessment of window performance in classrooms by long term spatial comfort metrics. *Energy and Buildings*, 134, 80-93. <https://doi.org/10.1016/j.enbuild.2016.10.018>

Marble residues in construction materials: a review of the use of marble powder in mortars, concrete, and bricks

A. Moreno^{1*} , C. Ponce² , E. Múzquiz¹ , F. Avalos¹ 

*Contact author: nicolas.moreno@uadec.edu.mx

DOI: <https://doi.org/10.21041/ra.v12i2.522>

Reception: 17/11/2020 | Acceptance: 19/04/2022 | Publication: 01/05/2022

ABSTRACT

The objective of this work is to make a review of the results carried out using marble powder as a substitute for cement, sand, or fine aggregate in concrete, mortar, and bricks. Research carried out in various parts of the world with different experimental procedures was reviewed. It is concluded that marble powder can be used as a partial substitute for cement or fine aggregate (up to 15%, depending on the material to be replaced) without affecting the compressive strength of the samples or pieces regardless of their shape. Therefore, marble powder not only helps to reduce the pollution it generates but also to reduce its use as sand and powder, contributing to sustainable development.

Keywords: marble powder; brick; mortar; concrete; cement.

Cite as: Moreno, A., Ponce P., Múzquiz, E., Avalos, F., (2022), “*Marble residues in construction materials: a review of the use of marble powder in mortars, concrete, and bricks*”, Revista ALCONPAT, 12 (2), pp. 162 – 183, DOI: <https://doi.org/10.21041/ra.v12i2.522>

¹ Facultad de Ciencias Químicas Unidad Saltillo, Universidad Autónoma de Coahuila, Blvd. V. Carranza y José Cárdenas Valdés, C.P. 25280, Saltillo, México.

² Escuela de Arquitectura Unidad Torreón, Universidad Autónoma de Coahuila, Carretera Torreón - Matamoros km. 7.5. Ejido El Águila. Ciudad Universitaria. C.P. 27087. Torreón, Coahuila

Contribution of each author

In this work, the author Moreno, A. contributed with the conceptualization of the activity, the research, the methodology, the data collection and the writing of the original draft by 50%. Author Ponce, C. contributed 40% to validation, writing, review, and editing. The author Múzquiz, E. contributed 5% to validation, writing, revision and editing. Author Avalos, F., contributed 5% to data collection, writing, review, and editing.

Creative Commons License

Copyright 2022 by the authors. This work is an Open-Access article published under the terms and conditions of an International Creative Commons Attribution 4.0 International License ([CC BY 4.0](https://creativecommons.org/licenses/by/4.0/)).

Discussions and subsequent corrections to the publication

Any dispute, including the replies of the authors, will be published in the first issue of 2023 provided that the information is received before the closing of the third issue of 2022

Residuos de mármol en materiales para la construcción: una revisión del uso del polvo de mármol en morteros, concretos y ladrillos

RESUMEN

Este artículo tiene como objetivo hacer una revisión de los trabajos realizados usando polvo de mármol como sustitución de cemento, arena o agregado fino en concreto, mortero y ladrillos. Se revisaron investigaciones realizadas en varias partes del mundo con procedimientos experimentales diferentes. Se concluye que el polvo de mármol se puede usar como sustituto parcial de cemento o agregado fino (hasta por un 15 %, dependiendo del material a sustituir), sin afectar la resistencia a compresión de las muestras o las piezas, y sin importar la forma. Por lo tanto, el polvo de mármol no sólo ayuda a aminorar la contaminación que genera, sino que también a la reducción de uso como arena y polvillo, aportando al desarrollo sustentable.

Palabras clave: polvo de mármol; ladrillo; mortero; concreto; cemento

Resíduos de mármore em materiais de construção: uma revisão do uso do pó de mármore em argamassas, concreto e tijolos

RESUMO

O objetivo deste trabalho é fazer uma revisão dos trabalhos realizados utilizando pó de mármore como substituto do cimento, areia ou agregado miúdo em concreto, argamassa e tijolos. Pesquisas realizadas em várias partes do mundo com diferentes procedimentos experimentais foram revisadas. Conclui-se que o pó de mármore pode ser utilizado como substituto parcial do cimento ou agregado miúdo (até 15%, dependendo do material a ser substituído), sem afetar a resistência à compressão das amostras ou peças independentemente de sua forma. Portanto, o pó de mármore não só ajuda a reduzir a poluição que gera, mas também reduz seu uso como areia e pó, contribuindo para o desenvolvimento sustentável.

Palavras-chave: pó de mármore; tijolo; argamassa; concreto; cimento.

Información Legal

Revista ALCONPAT es una publicación cuatrimestral de la Asociación Latinoamericana de Control de Calidad, Patología y Recuperación de la Construcción, Internacional, A. C., Km. 6, antigua carretera a Progreso, Mérida, Yucatán, C.P. 97310, Tel.5219997385893, alconpat.int@gmail.com, Página Web: www.alconpat.org

Reserva de derechos al uso exclusivo No.04-2013-011717330300-203, eISSN 2007-6835, ambos otorgados por el Instituto Nacional de Derecho de Autor. Editor responsable: Dr. Pedro Castro Borges. Responsable de la última actualización de este número, Unidad de Informática ALCONPAT, Ing. Elizabeth Sabido Maldonado.

Las opiniones expresadas por los autores no necesariamente reflejan la postura del editor.

La reproducción total o parcial de los contenidos e imágenes de la publicación se realiza en apego al código COPE y a la licencia CC BY 4.0 de la Revista ALCONPAT.

1. INTRODUCTION

The Marble is a metamorphic rock composed of carbonates. In commercial terms, the word marble does not have a petrological meaning sometimes, the term is applied to rocks such as tuff, serpentine, and granite, although it often refers to calcareous rocks such as recrystallized limestone, dolomite, marble, onyx, and travertine (Coordinación General de Minería, 2014).

According to data from the United States Geological Survey (USGS) in 2018, Mexico is one of the world's largest producers of various non-metallic minerals. In 2019, the Directorate General of Mines (DGM) reported an increase of 4,663 million pesos from 2017 to 2018 in the national production of non-metallic minerals, which represents an increase of 23.9% (Servicio Geológico Mexicano, 2019).

China, India, and other countries, including Mexico, are the leading producers of dimensional rock. Dimensional rock includes a wide variety of rocks, including granite, limestone, and marble.

The marble production process begins with the extraction of the rock by mechanical means (saws), breaking large blocks, which will later be divided into smaller sizes for sale. This process is known as lamination.

The lamination process consists of cutting the block of rock to obtain slabs of 2 to 3 cm thick and is performed using saws with diamond inlays; then, the obtained slab is subjected to polishing to roughen the rough parts of the rock and polishing by means of abrasives and water. Once the polishing is finished, the plates are subjected to cuts to be sized according to the client's needs. Similarly, to meet the client's requirements, the product is subjected to a process of beveling, drying, or waxing. Finally, the product is packaged and shipped for national or international commercialization. (Coordinación General de Minería, 2014).

One ton of marble stone processed by vertical and horizontal cutting for block production and lamination produces 35% to 45% spillage or slurry of unused materials (Singh, et al., 2017).

This waste slurry, especially after drying, causes environmental hazards such as dust contamination, which occupies agricultural land and other nearby areas, rendering them infertile. (Singh, et al., 2017). In 2017, the world production of marble was 2,352,614 tons. (Servicio Geológico Mexicano, 2019), so, 941,045 tons of waste were generated, considering 40% of the processed product.

Due to the great problem generated by marble powder (waste disposal, contamination by calcium oxide (CaO), which is absorbed by the soil, causing it to become infertile), scientific research has been carried out for its application in the construction sector, either as a substitute for cement in mortars or concrete or also as a block or brick manufacturing applicable to construction systems in various parts of the world.

This paper reviews the work done using marble powder as a substitute for cement, sand, or fine aggregate in concrete, mortar, and bricks, with the purpose of reporting the ways in which it can substitute cement or fine aggregate to manufacture non-structural bricks, among other contributions.

2. MARBLE POWDER AS AN INPUT IN THE CONSTRUCTION INDUSTRY

This section evaluates the use of marble powder as an input in construction. An exhaustive review of published articles is conducted, and the results of each study on the application of marble powder in cement, mortar, concrete, and bricks are presented in a concise and detailed manner.

2.1 Marble powder as a partial cement substitute.

Marble powder has a high content of Calcium Carbonate (CaCO_3), which can be added to Portland cement-based mortars and concretes to increase the service life, functioning as a pore filler. (Singh, et al., 2017).

Other authors, on the contrary, think that the partial substitution of CaCO_3 produces chemical modifications, which result in changes in the mechanical and physical properties of the cement. (Tobón & Kazes Gómez, 2008).

Additions of between 3 and 5% of marble powder have been made to Portland cement pastes, and no changes in their mechanical behavior have been observed.

El-Sayed, Farag, Kandeel, Younes, and Yousef (2016) replaced 3, 4, and 5 wt% of the cement with marble powder, observing that, due to the high presence of calcium carbonate, it did not affect the properties of the cement. With the hardened cement pastes, compression tests were performed at ages of 1, 3, 7, 14, and 28 days; it was observed that the strengths increased proportionally to the age of curing from 1 to 28 days, as shown in Figure 1.

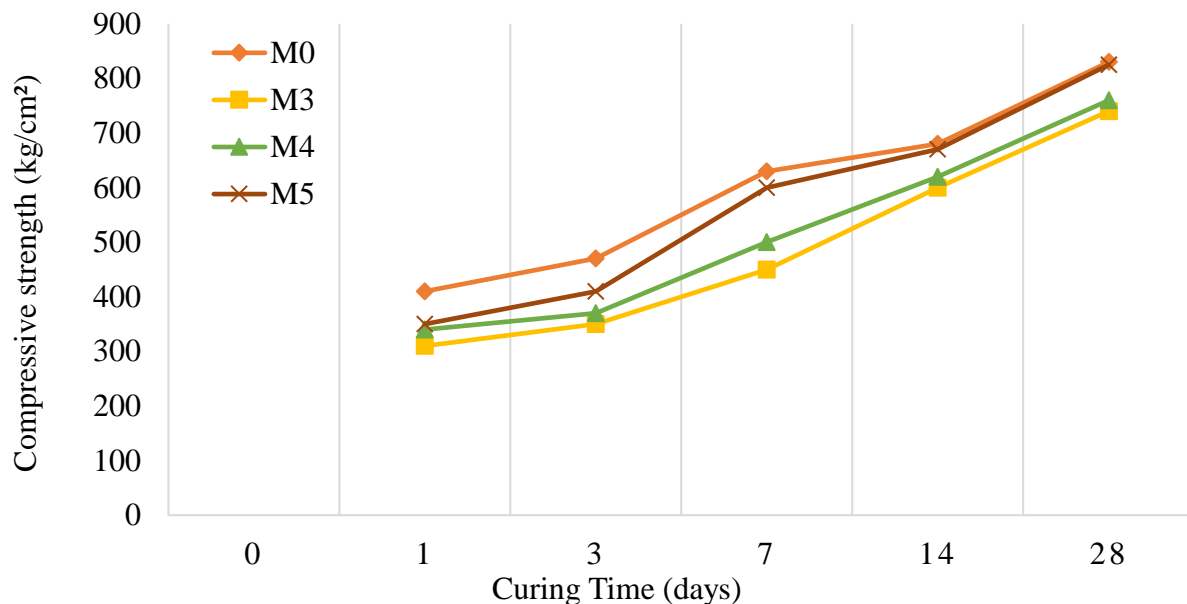


Figure 1. Compressive strength of hardened Portland cement pastes incorporating 3%(M3), 4% (M4), and 5%(M5) marble powder residues versus curing time. (El-Sayed, et al., 2016)

It was shown that the specimen with 5% (M5) of marble powder, at 28 days of curing, obtained the same compressive strength as the control specimen of ordinary Portland cement without additions. The other samples of 3 and 4 % cement substitution by marble powder have a lower compressive strength compared to M5 and M0.

With this, the use of marble powder in the cement industry becomes feasible due to the economic and ecological benefits that the use of a waste product represents.

Singh et al. (2017) mention that marble powder has a high content of Calcium Carbonate (CaCO_3), and this helps to increase the service life of cement-based pastes and concretes, while Tobon & Kazes Gome (2008) mention the opposite. El-Sayed, Farag, Kandeel, Younes, and Yousef (2016), show that substituting marble powder for cement in small quantities does not affect the compressive strength.

These studies show that the compressive strength of the specimens is not affected when a maximum of 5% of marble powder is replaced by cement. It is observed in the test result graphs that the increase in strength is similar in the specimens with and without marble powder.

2.2 Marble powder and its application in mortars.

Portland cement-based mortars are among the most widely used composite materials in the construction industry, and cement is the construction material that generates the most CO₂ pollution to the environment in its manufacturing process. For this reason, researchers have carried out experimental studies by partially replacing cement with marble powder to reduce its use. Corinaldesi, Moriconi, and Naik (2010) replaced 10% of the cement with marble powder from a reference sample and, in a second option, replaced 10% of the fine aggregate of the mortar (sand), as shown in Table 1. From each mixture, 3 bars of 40 x 40 x 160 mm were manufactured, from which cubes of 40 mm per side were obtained to perform compression tests at 3, 7, 28, and 56 days of curing.

Table 1. Mortar proportions (Corinaldesi, et al., 2010)

Mix	Ref	10% Cement	10% Sand
A/C	0.61	0.68	0.59
Water (kg/m ³)	275	276	266
Cement (kg/m ³)	450	405	450
Sand (kg/m ³)	1350	1350	1215
Marble powder (kg/m ³)	0	45	135

The results obtained are shown in Figure 2. It can be observed that the mixture with 10% cement replaced by marble powder showed a reduction in compressive strength. However, the marble powder used as a replacement for 10% sand obtained higher strength than the mixture with the replacement of marble powder by cement.

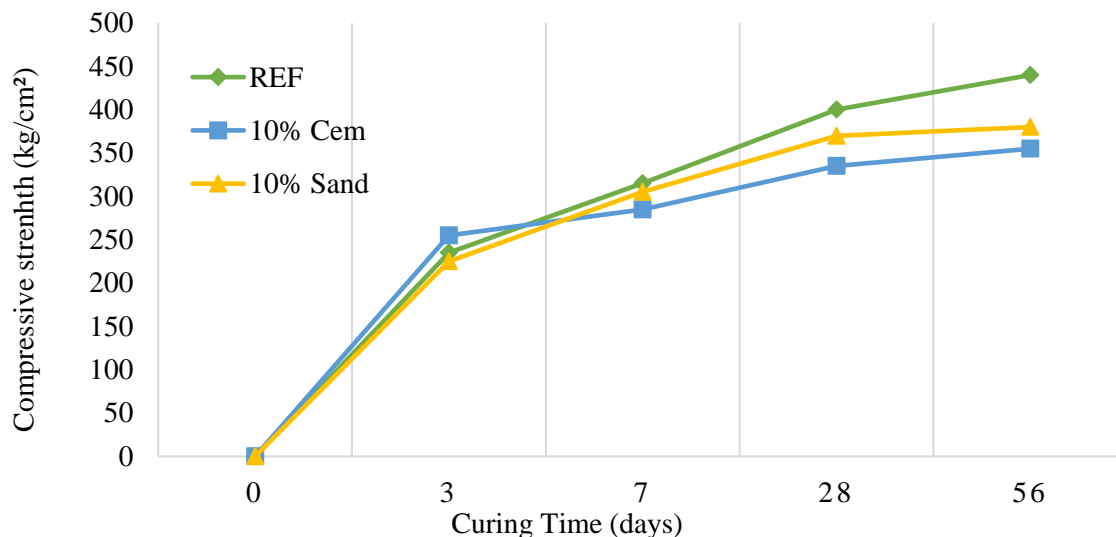


Figure 2. Compressive strength versus curing time for mortars with partial substitution of marble powder by cement and sand. (Corinaldesi, et al., 2010)

Li G. L. et al. (2019), propose the substitution with marble powder in two options for cement-based mortar. The first proposal is the partial substitution of cement in the mixture, without altering the water-cement ratio (w/c), and a second one in which a part of the cement and the water required for the manufacture of the mortar is replaced, changing the w/c ratio.

First, for each mortar mix, the volume of paste (volume of water, cement, expressed as a percentage of mortar volume) plus the volume of marble powder (expressed as a percentage of mortar volume) was set at 60%.

The marble powder was adjusted to 0, 5, 10, 10, 15, and 20 % and the respective paste volume was set to 60, 55, 50, 50, 45, and 40, to sum each of the mixes the 60 % set previously. The volume of fine aggregate was set at 40% of the total volume of the mortar (Figure 3). For the second proposal, the marble powder replaced 0, 5, 10, 10, 15, and 20% of the volume of cement, which was set at 100, 95, 90, 85, and 80%

It is important to emphasize that the volume of water in the mixture remains constant. (Figure 4). With each of the mixes, 3 cubes of 100 mm per side were made, and after 28 days of curing, compressive strength tests were carried out.

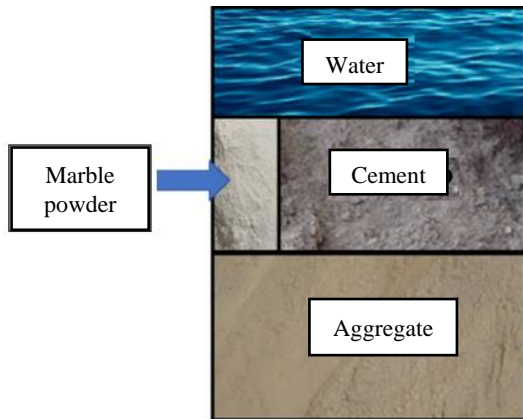


Figure 1. Cement replacement method (Li, et al., 2019)

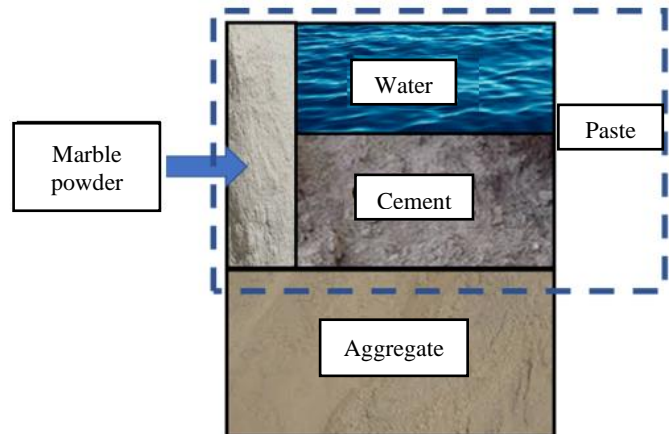


Figure 2. Paste replacement method (Li, et al., 2019)

The tests showed that in the mortar with paste replacement (cement and water) with a w/c ratio of 0.40 and increasing the volume of marble powder from 0% to 20% increased the cube strength from 607.75 to 730.12 kg/cm², in the w/c ratio of 0.55 increased the compressive strength from 402.79 to 543.51 kg/cm².

In mortar mixes where only the cement was partially replaced with marble powder from 0 to 5% and with a w/c ratio of 0.40, the cube strength increased from 607.75 to 610.81 kg/cm², and increasing the volume of marble powder from 0% to 20% showed a decrease in compressive strength from 607.5 to 488.44 kg/cm².

In the same case, but with a w/c ratio of 0.55, and replacing 0 to 10% of the cement with marble powder, the strength increased from 402.79 to 411.97 kg/cm², and with the replacement of 0% to 20% the cube strength decreased from 402.79 to 344.66 kg/cm². In the work done by Yamanel et al. (2019), they made mortars replacing 0, 5, 10, 10, 15, and 20 % of cement with marble powder and manufactured 40 x 40 x 160 mm prisms, cured for 28 days, before performing mechanical and durability tests on the samples (Table 2).

Table 1. Mortar Mix proportions. (Yamanel, et al., 2019)

Sample	Cement g	Marble powder g	Sand g	Water g
M-0	450.0	0.0	1350.00	225
M-5	427.5	22.5	1350.00	225
M-10	405.0	45.0	1350.00	225
M-15	382.5	67.5	1350.00	225
M-20	360.0	90.0	1350.00	225

At 28 days of curing, the compressive strength of the affected mixes at 5, 10, 15, and 20% is lower than that of the mix without cement substitution.

At 90 days of curing, the mix with a 5% replacement of marble powder to cement increased the compressive strength even more than the mix without marble powder (Figure 5).

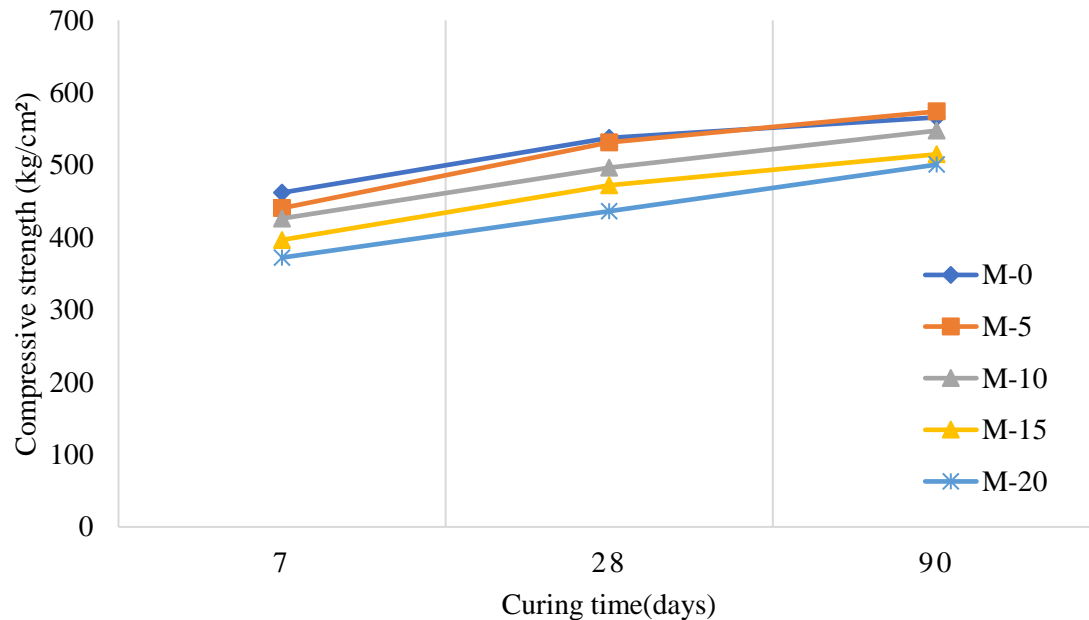


Figure 3. Compressive strength of mortars. (Yamanel, et al., 2019)

Figure 5. Compressive strength of mortars. (Yamanel, et al., 2019)

Toubal Seghir, N., et al. (2019) manufactured mortars with 3:1 sand-cement ratios and replaced at levels of 0%, 5%, 10%, and 15% of the weight of cement in the mortar with marble powder. A water/cement ratio of 0.5 (constant) was maintained. Compressive strength tests were performed with 50 mm cubes of the manufactured mortars, and were tested at 3, 7, 28, and 65 days. The samples were cured in open air, this study gave the following results: All samples up to 15% substitution obtained a lower compressive strength than the sample without marble powder; this decrease is attributed to the lack of curing, which caused voids and cracks within the samples, as well as a reduction in density of the samples.

Corinaldesi, Moriconi and Naik (2010) show that substituting marble powder for cement affects the compressive strength, and when marble powder is substituted for sand, it is not affected. Li G. L. et al (2010) show that increasing the substitution of marble powder for cement decreases the compressive strength and when the substitution is less, the strength is maintained or increased. Toubal Seghir, N et al. (2019) shows that to have good results in compressive strength, it is necessary to have a good curing of the specimens.

When marble powder is replaced by cement in mortars, in most cases, there is a decrease in compressive strength, especially at water/cement ratios lower than 0.5. When the water/cement ratio increases, the compressive strength of the samples also increases. Another important factor in the strength of the samples is curing; it is mentioned that when the samples are not cured, the strength at early ages is low.

2.3 Concrete with marble powder.

2.3.1 Marble powder as a partial substitute for fine aggregate in concrete.

The application of marble powder in concrete has also been sought, either as a partial substitute for cement or as a fine aggregate, without impairing compressive strength.

In 2010, Santos, Villegas, and Betancourt proposed the partial substitution of fine aggregate in concrete and the use of marble powder.

The proposal they made was the partial replacement of sand by marble powder in a 10 in 10 range, from 0-80 %, keeping fixed the w/c ratio, the weight of cement, and the weight of coarse aggregate, as shown in Table 3.

Table 2. Concrete dosages (Santos, et al., 2012)

Material		Control	M10	M20	M30	M40	M50	M60	M70	M80
Sand	kg/m ³	793	714	634	555	476	397	317	238	159
Marble powder	kg/m ³	0	79	159	238	317	397	476	555	634
Gravel	kg/m ³	1044	1044	1044	1044	1044	1044	1044	1044	1044
Water	kg/m ³	228	325	325	325	325	325	325	325	325
Cement	kg/m ³	325	325	325	325	325	325	325	325	325
a/c	kg/m ³	0.7	0.7	0.7	0.7	0.7	0.7	0.7	0.7	0.7

From the compressive strength tests applied to the above dosages at 7 and 28 days of curing, the following results were obtained and are shown in Figure 6.

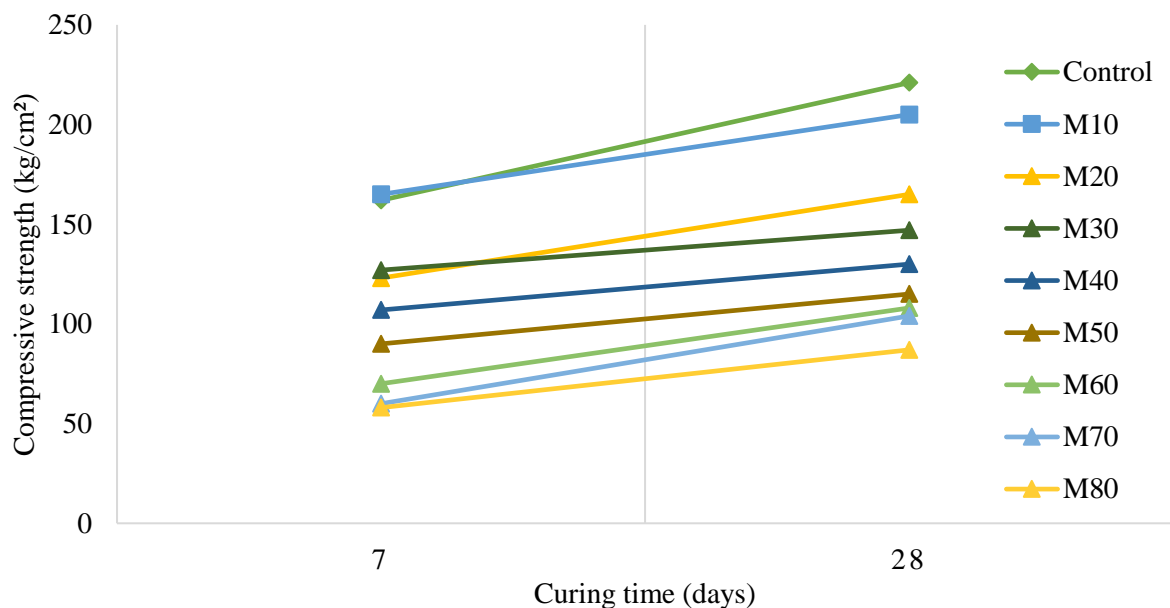


Figure 6. Compressive strength results from concretes with marble powder. (Santos, et al., 2012)

As the percentage of sand substitution by marble powder increases, the compressive strength decreases. Such loss of strength is like the percentage of marble powder, i.e., the M40 dosage has 40% less compressive strength compared to the control (Santos et al., 2012).

Hebnoub H. et al. (2011) partially substituted in proportions of 25%, 50%, 75%, and 100% marble powder for the fine aggregate; manufactured concrete cylinders and were cured and tested according to European Union (EU) standards. The samples were tested at 2, 14, 28, and 90 days of curing to determine their compressive strength. The results found by the authors reflected that the compressive strength at the 25, 50, and 75% substitution rates offered higher strength than the

control sample; the 100% substitution at ages 14 and 28 days presented lower strength than the sample without marble powder, but at the age of 90 days, the strength practically equaled the original sample.

Rahangdale, S. & Qureshi, S. (2018) conducted a study comparing the properties of a traditional concrete with one made with supplementary materials (fly ash for cement; stone and marble powder in partial replacement of fine aggregate).

Fourteen samples were manufactured, in the first three samples (1, 2, and 3), 35% of cement was replaced by fly ash, and 30% of the fine aggregate was replaced by stone and marble powder, in quantities of 20% - 10%, 15% - 15% and 10% - 20% respectively; the compressive strengths were lower than those recorded for the control concrete sample (35.58 N/mm²) varying at 28 days the strengths of 28.05, 28.87 and 30.35 N/mm².

In samples 4, 5, and 6, the amount of fly ash was maintained, but the amounts of stone and marble powder was increased to 40% as follows: 30-10%, 20-20%, 10-30%, obtaining the following strengths at 28 days: 27.25, 25.65 and 26.65 N/mm². From these results, it can be observed that the decrease shown in the compressive strength of series 1, 2 and 3 is maintained.

In samples 7, 8, and 9, the fly ash was reduced to 25%, and the substitution of fine aggregates in the same amount as in samples 1, 2, and 3 returned to 30%; the strengths recorded were 29.75, 32.04, and 35.45 N/mm², being higher than the previous ones but still below the original sample. In the following three samples (10, 11 and 12) the fly ash is maintained, at 25% and the percentage of substitution of the fine aggregate changes to 40% as in samples, 4, 5 and 6, the results obtained were 30.29, 31.54 and 29.87 N/mm², and once again it is observed that the compressive strengths decrease.

In sample 13, the fly ash was considered in a percentage of 22.5%, and in the fine aggregate 30% (10% marble stone and 20% marble powder). At 28 days, the compressive strength recorded was 35.49 N/mm², which is the highest of the samples analyzed, practically equal to the compressive strength of the control sample.

In the last sample (14), the fly ash replaced 20% of the cement, and in the 30% fine aggregate (10% marble stone and 20% marble powder) at 28 days, the registered resistance was 38.87 N/mm, increasing the compressive strength by 0.75%, being practically the same resistance as the reference sample.

Thus, with the dosages of sample 14, the use of cement is minimized; therefore, the authors recommend the use of supplementary materials to solve environmental problems and advance the sustainability of the development of the construction industry.

Verma, M., Kaushal, N. & Sharma, A. (2019) substituted fine aggregate in the manufacture of concrete in proportions of 0%, 5%, 10%, 15%, 20%, 25% and 30% by marble powder, and performed compression tests at 7 and 28 days of age. The results obtained in the sample without modifications were 19.10 and 24.73 N/mm² at 7 and 28 days, respectively.

In the 5% sample, an increase of 20.36 and 27.40 N/mm² was observed in 7 and 28 days, respectively. Similarly, in the 10% sample, an increase in resistance of 20.51 and 29.92 N/mm² was observed in 7 and 28 days, respectively.

From the samples with 15% to 30%, the compressive strengths showed a decrease with respect to the original sample with decreases at 7 days from 15.85 to 12.14 N/mm² and at 28 days from 24.44 to 18.07 N/mm², so it is determined that a partial substitution of the fine aggregate by up to 10% of marble powder generates a higher compressive strength.

In Giza, Egypt, Mostafa Shaaban (2020) carried out a study where he substituted in shotcrete percentages of 5, 10, 15, 15, 20, 25 and up to 30% of sand partially with marble powder. At seven days of age the samples tested for compressive strength with the partial substitution of 5% obtained a lower value than the sample without marble powder.

Samples from 10% presented an increase in compressive strength at 28 days of age (from 5% to

30%), due to the fineness of the marble powder that performs a filling effect in the concrete. It was also determined that the adhesion of the shotcrete increases proportionally to the greater substitution of marble powder for sand.

Ince, C. et al. (2020) used marble powder in pozzolanic concrete; the concrete was prepared with 20% silica fume replacing cement, and marble powder in fine aggregate replacement proportions of 10% and 20%, 15 cm diameter cylinders with a height of 30 cm were manufactured. The study lasted 1 year, and all the samples were cured under water. The compressive strength results show that the substitution of 20% silica fume increased the long-term compressive strength, this increase in strength is attributed to the pozzolanic activity of silica fume. As for the substitution of marble powder in the fine aggregate, the 20% substitution presents a slight decrease in compressive strength than that shown by the 10% substitution compared to the control sample without substitution. Both the 10% and 20% samples show an increase in compressive strength.

Santos, Villegas, and Betancourt (2010) and Rahangdale, S. & Qureshi, S. (2018) found that the higher the amount of marble powder the lower the compressive strength. Hebroub, H., et al. (2011) and Verma, M., Kaushal, N. & Sharma, A. (2019) show that more marble powder can be substituted without affecting the strength. Ince, C., et al. (2020) results show that the substitution of marble powder up to 20% in pozzolanic concrete can have an increase in compressive strength.

According to the authors of this section, it is mentioned that substituting marble powder for fine aggregate up to 10% does not affect the compressive strength since it does not increase or decrease when the substitution of marble powder for fine aggregate in concrete is increased. If the strength was to decrease considerably, it could be attributed to the fact that the marble powder up to 10% helps to cover pores that the fine aggregate can not do, and when it is greater than 10%, there is a lack of aggregate to help give strength to the concrete.

2.3.2 Marble powder as a partial substitute for cement in concrete.

High performance concretes have also been tested, in a study by Talah, Kharchi, and Chaid (2015). They developed two study mixes, the first as reference concrete (RC) and a second high performance concrete mix with marble powder (HPCMP) to which 15% of cement was replaced by marble powder. The dosages used are shown in Table 4.

Table 4. Mix proportions and properties of concrete. (Talah, et al., 2015)

Mix	Ratio a/c	Cement kg/m ³	Marble powder kg/m ³	Water kg/m ³	Sand kg/m ³	Gravel 3/8 kg/m ³	Gravel 8/16 kg/m ³
RC	0.5	400	0	200	788	163	886
HPCMP	0.5	340	60	200	788	163	886

The compressive strengths of each mix were evaluated on 160 x 320 mm cylinders at 7, 28, 90, 180, and 365 days of age. All samples were compacted using a vibrating table after demolding, the samples were divided into two equal groups and cured in the following conditions: in the first curing condition, the samples were immersed in water until the test age, while, in the second curing condition, they were immersed in aggressive water (5% CaCl₂) until the test age.

Figure 7 shows the compressive strength results of the mixes, according to the curing condition and age of the concrete.

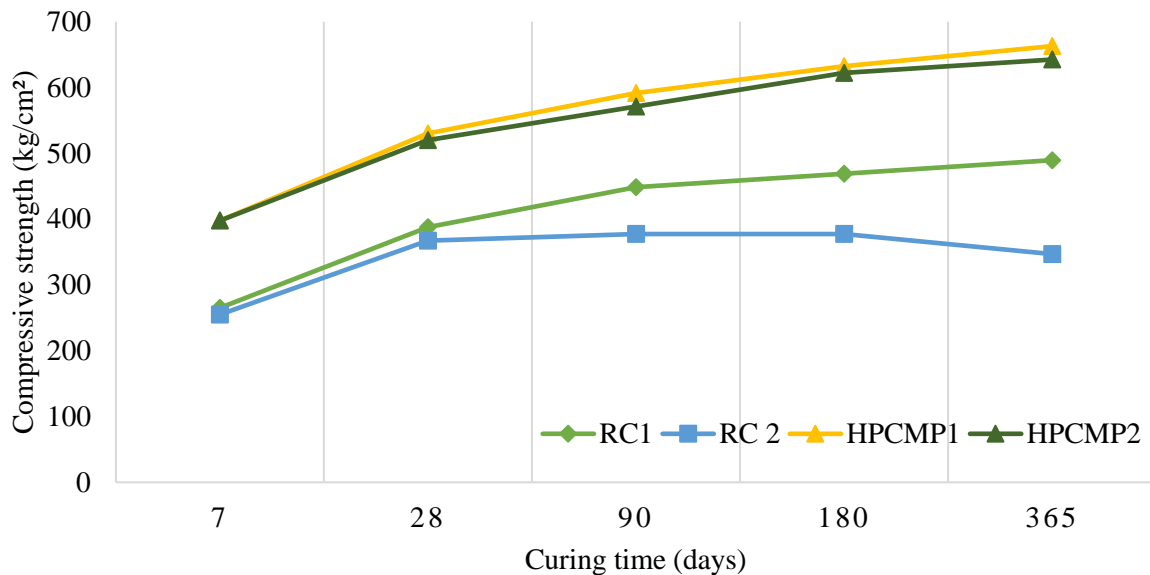


Figure 7. Evolution of compressive strength at different ages. (Talah, et al., 2015)

The result indicates that there was a systematic gain in compressive strength with marble powder content. It was observed that the ratio between the compressive strength of specimens subjected to water curing and those cured under aggressive conditions the reference concrete deviated up to 29%. However, this ratio for concretes containing marble powder is within a range of 3%, depending mainly on the marble powder content and test age. This implies that reference concretes are more sensitive to aggressive media than concrete with marble powder. (Talah et al., 2015).

In 2017 Singh, Srivastava, and Bhunia, performed tests on concretes by substituting 0, 10, 15, 15, 20, and 25% of the cement with marble powder, also experimenting with 3 w/c ratios 0.35, 0.4, and 0.45. The dosage of the concretes is shown in Table 5.

Ghorbani S. et al. (2018) proportionally replaced Portland cement type II with 0%, 5%, 10%, and 20% of marble powder, granite powder, or combination of both. The samples were subjected to curing and analyzed at 7 and 28 days of age. In the samples with marble powder and granite powder as a partial cement substitute, the compressive strength was not significantly affected, both at 7 days and 28 days. In the samples where only marble powder was substituted, the samples with 5 to 15% substitution showed an improvement in compressive strength, but not the 20% substitution, which showed a decrease in compressive strength of 0.94 and 0.96 times in both the marble powder and granite powder mixtures; in the samples where granite powder was substituted for cement, the 10% sample offered a higher strength between the ranges of 1.14 and 1.09 times of the sample without any substitution. The authors determined that the increase in compressive strength presented in this study is due to the improvement in the density of the samples due to the filling of their pores. Finally, as the age of curing increases, the loss of compressive strength decreases.

Mostafa Shaaban (2020) partially substituted cement for marble powder in the mix for the manufacture of shotcrete, in proportions of 5, 10, 15, 20, 25, up to 30%. The results obtained reported that the use of marble powder in any of the substitution proportions presented a decrease in compressive strength; in the samples with 5% substitution at early ages (7 days) presented a decrease in compressive strength of 5.4% in relation to the original sample, and at 28 days, a decrease that reached 23.4% in the samples with 30% marble powder substitution.

Babouri L. et al. (2020) used marble powder as a partial substitute for ordinary portland cement in the manufacture of concrete; the substitution percentages used were 5%, 10%, 15%, and 20%, and performed compressive strength tests at 2, 7, 14, and 28 days cured.

The samples with 5%, 10%, and 15% presented lower compressive strength results than the original sample without marble powder, but the sample with 5% marble powder, from day 2 to day 28 of the last test, showed an increase in strength, this increase in compressive strength is attributed to the fact that the marble powder reduces porosity, which is reflected in a sample with fewer voids, and, therefore, more resistant.

Table 5. Concrete mix proportions (Singh, Srivastava y Bhunia, 2017)

Ratio a/c	Mix	Cement kg/m ³	Marble powder %	Marble powder kg/m ³	Coarse aggregate kg/m ³	Fine aggregate kg/m ³	Water kg/m ³
0.35	Control	422	0	0	1278	689	148
	M10	379.8	10	42.2	1278	689	148
	M15	358.7	15	63.3	1278	689	148
	M20	337.6	20	84.4	1278	689	148
	M25	316.5	25	105.5	1278	689	148
0.40	Control	394	0	0	1257.2	707.2	158
	M10	354.6	10	39.4	1257.2	707.2	158
	M15	334.9	15	59.1	1257.2	707.2	158
	M20	315.2	20	78.8	1257.2	707.2	158
	M25	295.5	25	98.5	1257.2	707.2	158
0.45	Control	351	0	0	1183	858	158
	M10	315.9	10	35.1	1183	858	158
	M15	298.35	15	52.65	1183	858	158
	M20	280.8	20	70.2	1183	858	158
	M25	263.25	25	87.75	1183	858	158

The results of the compressive strength tests show an increase in strength in the mixes with 10% and 15% replacement with marble powder. This increase can be attributed to the fact that the marble powder helps to form denser mixes with less porosity. The mixes with 20 and 25% replacement percentages show a decrease in compressive strength, possibly due to the lack of cementitious material in the concrete.

The samples with a w/c ratio of 0.35 showed an increase in strength in the sample with 15% replacement (Figure 8). Similarly, at the same percentage of replacement but at the w/c ratio of 0.40, there is also an increase in compressive strength (Figure 9).

For the w/c ratio of 0.45, the compressive strength decreased compared to w/c ratios of 0.35 and 0.40 (Figure 10).

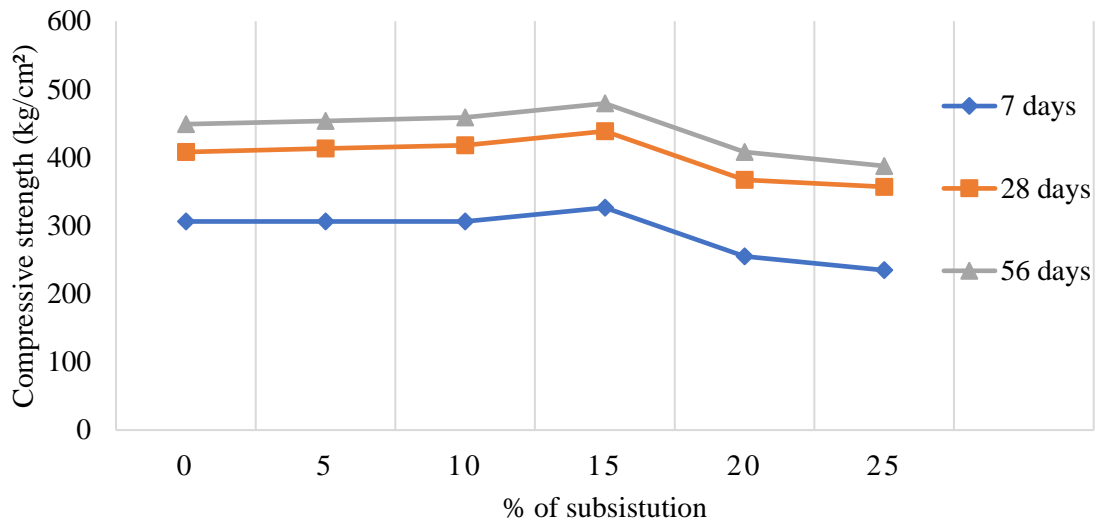


Figure 4. Compressive strength of concrete specimens with w/c ratio 0.35.

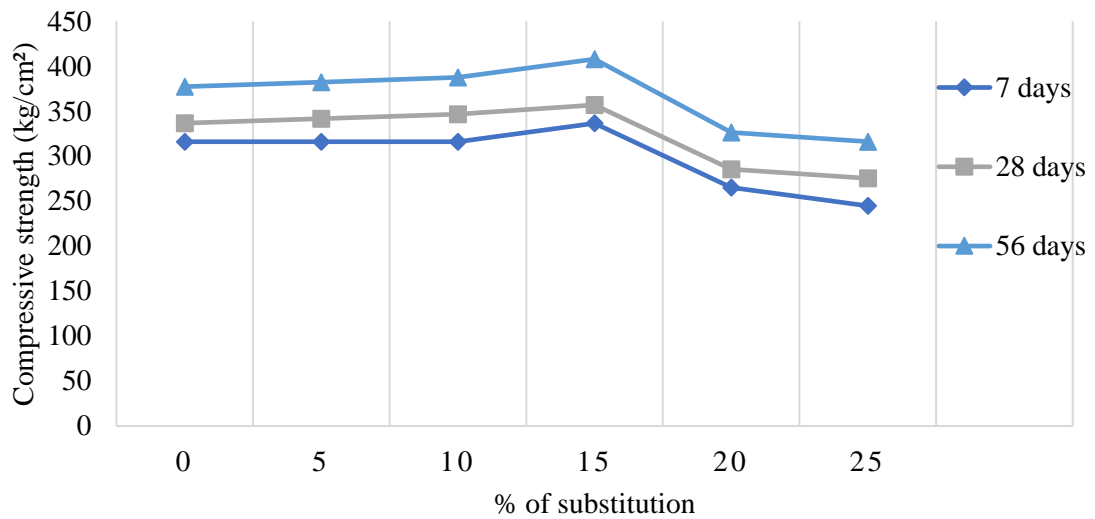


Figure 5. Compressive strength of concrete specimens with w/c ratio 0.40.

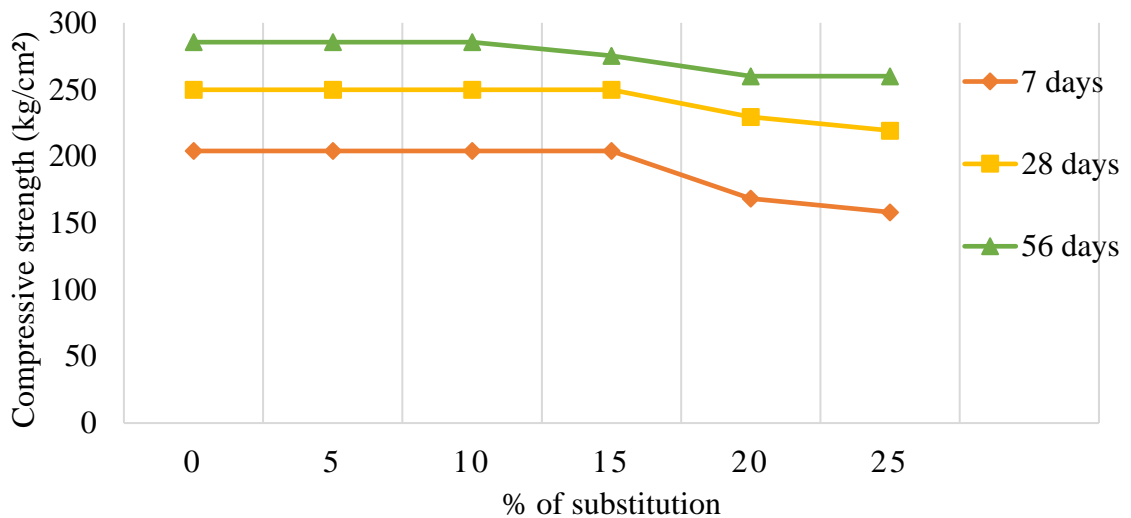


Figure 6. Compressive strength of concrete samples with w/c ratio 0.45.

Another research experimented with replacement of cement with marble waste at 0, 5, 10, and 20% and determined that the use of marble powder in concrete in the range of 10-15% increases the compressive strength. (Khodabakhshian, et al., 2018).

Wang, Y. et al. (2022) manufactured concrete by replacing cement with marble powder in proportions of 0%, 5%, 10%, 15%, 20%, and 25%, in samples of 150 mm cubes, performing compressive strength tests at 3, 7, 14 and 28 days of age, obtaining the following results: the control sample presented strengths of 23.8, 29.8, 33.1 and 35.0 MPa at 3, 7, 14 and 28 days respectively, the 5% samples at 3 days obtained a lower compressive strength than the original sample, the sample with 10% marble powder from 3 to 14 days, as well as the 5% sample, had a lower strength, but at 28 days it was 35.4 MPa, increasing by 1.14% with respect to the original sample. The other substitutions (15%, 20%, and 25%) showed up to 21.14% (28 days) lower compressive strength than the sample without marble powder.

Talah, Kharchi, and Chaid (2015) found that one can substitute marble powder for cement and have a gain in compressive strength if one has vibration to remove air in the fabrication of specimens. Ghorbani, S. et al. (2018), Mostafa Shaaban (2020), Babouri, L., et al., (Khodabakhshian, et al., 2018), and Wang, Y., et al. (2022) found that the range of substitution of marble powder for cement so that the compressive strength is not affected is 0 to 10 %.

From this section, it can be concluded that up to 10% of marble powder can be substituted for cement so that the compressive strength of the concrete is not affected. According to the test results, the compressive strength is affected when the marble powder substitution is greater than 10%.

2.4 Marble powder, concrete, mortar, and superplasticizers

Water-reducing additives (plasticizers) and high-range water-reducing additives (superplasticizers) contribute to increase durability and provide a reduction in the amount of water of at least 5%, decreasing the w/c ratio, and superplasticizers, at least 12%, and up to 40%.

Corinaldesi, Moriconi, and Naik (2010), in a reference sample, substituted 10% cement with marble powder and, in a second option, substituted 10% sand; in addition, an acrylic-based superplasticizer additive was added at a proportion of 0.5% of the weight of the cement, as shown in Table 6.

Three cubes obtained from 40 x 40 x 160 mm bars of each mixture were manufactured for compression tests at 3, 7, 28, and 56 days of curing.

Table 6. Proportions of mortar with superplasticizer.

Mix	Ref	10% Cement	10% Sand
A/C	0.48	0.49	0.53
Water (kg/m ³)	220	200	240
Cement (kg/m ³)	450	405	450
Sand (kg/m ³)	1350	1350	1215
Marble powder (kg/m ³)	0	45	135
Superplasticizer additive (kg/m ³)	2.25	2.02	2.25

Both samples reported higher compressive strength at early ages. At 28 days of age, the reference sample obtained higher strength; however, the use of the plasticizer provided an increase in compressive strength compared to the study carried out without the additive. (Figures 2 and 11).

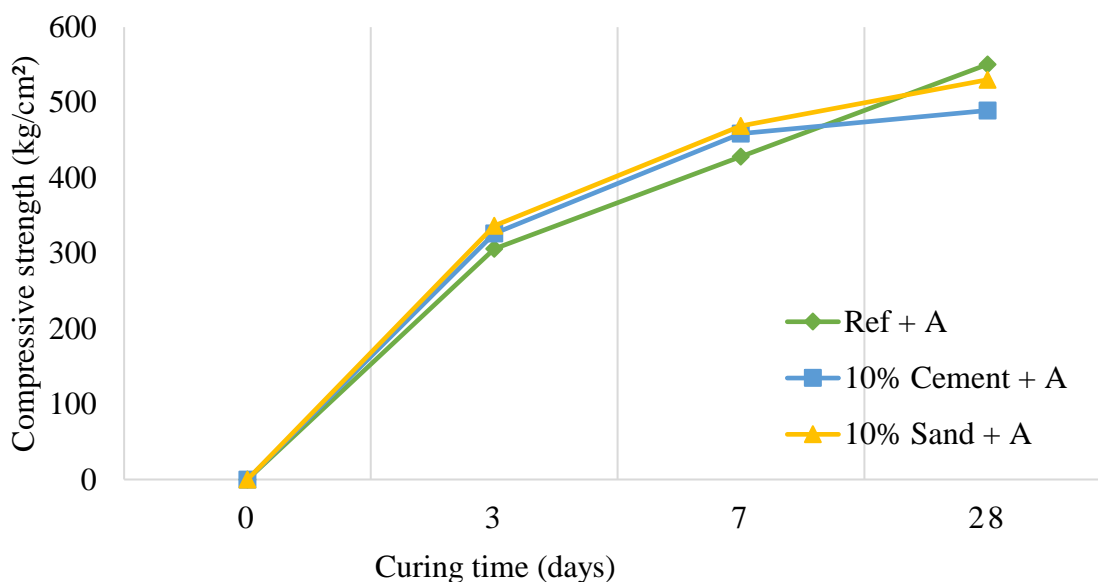


Figure 11. Compressive strength in relation to curing time in mortars with superplasticizer admixture.

In summary, when a superplasticizer is used in concrete, an increase in compressive strength is achieved. It can be said that marble powder can be substituted for cement in an amount greater than 10%, and a superplasticizer is applied to compensate for the resistance.

2.5 Previous experimental studies to elaborate bricks with marble powder.

Santos, Villegas, and Betancourt (2012) conducted a study proposing a series of dosages having marble powder as a base, the amount of cement in the samples varied, and the amount of water did not change (Table 7).

Table 7. Results of bricks based on marble powder. (Santos, et al., 2012)

Sample No.	Cement %	Water (c+RM) %	Resistance (kg/cm ²)	Absorption %
1	8	15	45.83	17
2	11	15	81.56	16
3	14	15	82.76	18

Cylinders of 15 cm in height and 7.5 cm in diameter were manufactured, as well as 5 cm cubes. They concluded that the shape of the bricks did not affect the results.

The results show that there is a significant influence on strength with an increase from 8 to 11% cement, but at a percentage higher than 11%, there is no increase in strength.

The results show that the absorption did not change as a function of the amount of cement.

Morales-Olán et al. (2015) propose the fabrication of a block of 14 x 20 x 40 cm section made with marble powder, tepezil, cement, and water. The dosage is shown in Table 8. The mixtures were compacted by vibration and pressing and were dried in the sun for 48 hours.

Table 8. Composition in percentage of materials in the evaluated mixtures.
(Morales-Olán , et al., 2015)

Material	M1 %	M2 %
Marble Waste	55	35
Tepezil	31	51
Cement	6	6
Water	8	8

The results obtained in the water absorption test show that sample 1 absorbs less water than sample 2. As for the compressive strength tests, sample 1 performs better than sample 2, as shown in Table 9.

Table 9. Percentage of water absorption and compressive strength of samples.
(Morales-Olán , et al., 2015)

Sample No.	Water absorption %	Resistance (kg/cm²)
1	19.43 ± 5.55	38.40 ± 1.84
2	23.91 ± 0.25	21.46 ± 3.25

With the results presented, sample 1 complies with the necessary characteristics indicated in NMXC-441-ONNCCE-2013 to work as a construction material for non-structural use. Another study carried out to produce bricks with marble powder was conducted by Nevárez and Rangel (2014). Table 10 shows the dosage used for the production of reference bricks, cured in the traditional way and saturated in water. Tables 11 and 12 report the results of the brick compression tests, with two options of cement quantity, 12 and 15%.

A preload of 100 kg/cm² was applied to all samples during the mold filling process for one minute, but the author does not explain the preloading process in his paper.

Table 10. Dosages that passed the compressive strength test.
(Nevarez & Rangel, 2014)

Component	Mixing at 12% cement	Mixing at 15 % cement
Marble powder	10 kg	10 kg
Cement	1.2 kg	1.5 kg
Sand	2 kg	2 kg
Water	2 l	2 l

Table 11. Result compressive strength of brick samples at 7, 14, or 28 days of curing 15% cement. (Nevarez & Rangel, 2014)

Sample No.	7 days of curing (kg/cm ²)	14 days of curing (kg/cm ²)	28 days of curing (kg/cm ²)
1	122.70	89.12	89.99
2	138.50	Witness	Witness
3	140.70	119.29	Witness
4	136.60	86.05	87.47
5	144.30	Witness	88.00
6	129.90	86.46	88.96
7	109.70	88.00	87.88
8	149.90	86.79	88.57
9	130.9	86.61	86.20
10	100.4	87.79	86.16

Table 12. Compressive strength results with 12% cement. (Nevarez & Rangel, 2014)

No. Dyas	Compressive strength (kg/cm ²)
7 days	107.00
14 days	107.15
28 days	95.55

For the case of 12% cement in the samples, it is concluded that the highest compressive strength occurs at early ages, i.e., at the age of 7 days, while for the age of 14 and 28 days, the strength decreases compared to 7 days, but the magnitude is maintained between 14 and 28 days. For the case of 15% cement, the compressive strength decreases compared to the 12% samples at the age of 7 days, but at the ages of 14 and 28 days, it increases, which indicates that for the amount of cement in small percentages, the strength increases at early ages and the higher percentages increase the strength at advanced ages.

Betancourt et al. (2015) elaborated a brick with Portland Cement Compound type I, drinking water, river sand, and marble powder in order to observe the behavior of different proportions and shapes of the samples, cubes of 5 x 5 x 5 x 5 cm, cylinders of 7.5 diameter and 15 cm high and tablets of 5 x 10 cm; the results of the compression tests are presented in Tables 13, 14 and 15 respectively.

Table 13. Compressive strength in cubes of 5 x 5 x 5 x 5 cm elaborated with marble powder base. (Betancourt Chávez, et al., 2015)

Mix #	Cement %	Lime %	Water %	Compressive strength kg/cm ²
1	25	0	20	76.60
2	22.5	2.5	20	60.00
3	20	5	20	52

Table 14. Compressive strength, in cylindrical elements of 7.5 x 15 cm elaborated with marble powder base. (Betancourt Chávez, et al., 2015)

Mix #	Cement %	Lime %	Wáter %	Compressive strength kg/cm ²
1	25	0	20	67.90
2	22.5	2.5	20	56.24
3	20	5	20	48.00

Table 15. Compressive strength of 5 x 10 cm tablets with marble powder and sand base material, pressed at 70 kg/cm². (Betancourt Chávez, et al., 2015)

Sample	Cement %	Sand %	Wáter %	Compressive strength kg/cm ²
1	8	0	20	28
2	10	20	20	76
3	10	30	20	90

Tables 13, 14, and 15 show the compressive strength results of cubes, cylinders, and tablets manufactured with marble powder in its highest percentage. The tables show the percentages of cement, sand, and water only, and the percentage that is missing to reach 100% in each piece is what corresponds to the marble powder.

The elements with a higher amount of cement showed better results in compression. The shape of the element does not significantly influence the results. With respect to the results in Table 15, it is observed that, by adding sand and compressing the sample, the compressive strength increases (Betancourt Chávez et al., 2015).

For the above dosages, it was considered that, of the weight of marble powder to be used, the percentages of cement, lime, sand, and water were used as indicated in tables 13, 14, and 15.

Moreno et al. (2020) manufactured bricks with a mixture based on marble powder, cement, water, and river sand (AR), they made 4 more mixtures, taking as a basis the dosage shown in Table 16.

Table 16. Dosage of marble brick with river sand (AR). (Moreno Juárez, et al., 2020)

Material	Quantity
Marble powder	15 kg
Cement	2.25 kg
River sand	3 kg
Water	7 l

In the first mix, river sand was added; in the second mix, 100% of the river sand was replaced by crushed limestone sand (AT); in the third mix, 100% of the river sand was replaced by silica sand (S); in the next mix, 66% of the river sand was replaced by silica sand (SR); in the last mix, 66% of the river sand was replaced by silica sand (RS); and the rest of the aggregate was replaced by silica sand (RS). The compression results at 28 days of curing, according to each mix, are shown in Figure 12.

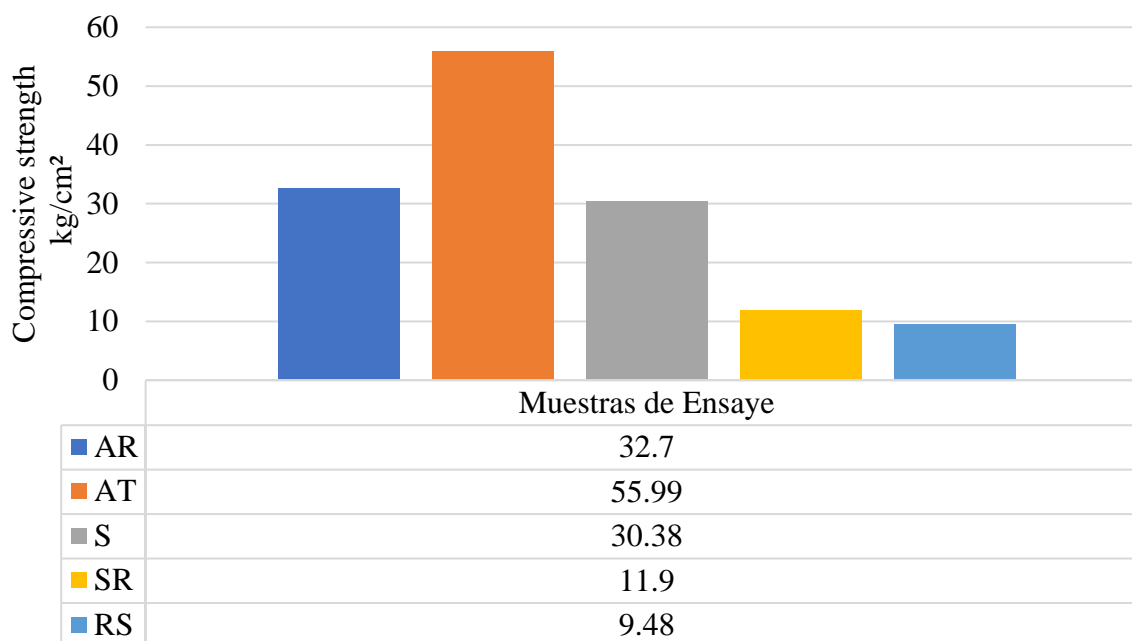


Figure 7. Compressive strength of test specimens. (Moreno Juárez, et al., 2020)

With the results presented, the AT mix performed better in compression (Figure 12) but does not have sufficient strength to work as a structural brick according to NMX-C-404-ONNCCE-2012. In Pakistan, Khan et al (2021) analyzed the performance of clay brick with partial substitution of marble powder at percentages of 0%, 5%, 10%, 15%, 20%, 25%, and 30%.

Three different brick factories in the region participated in the study; the results obtained were similar in each of the participating companies. They performed efflorescence, thermal conductivity, compressive strength, porosity, absorption, and density tests.

The density of the bricks in the original sample without marble powder was 1.55 g/cm^3 and decreased as the percentage of substitution increased until it reached 30%, with a density of 1.27 g/cm^3 . The samples did not show efflorescence. The porosity of the samples also increased according to the percentage of marble powder substitution, from 12.6% to 52.71%, this due to the release of Carbon Dioxide (CO_2), in addition, the Calcium Oxide (CaO), being expandable, causes porosity in the sample, therefore, it is also reflected an increase in the absorption of the samples from 18% to 36%. Given the increase in porosity in the bricks, the compressive strength is also affected considerably, decreasing the compressive strength from 18.06 MPa to 4.83 MPa. Khan et al. (2021) comment that Turkish and European standards indicate that a clay brick should have a minimum strength of 7 MPa, so a substitution of up to 20% marble powder for clay meets the compressive strength standard for brick. Due to the increased porosity of the bricks, the thermal conductivity decreased from 0.99 to 0.86 W/mK, and it is concluded that with this result, the pieces would work as thermal insulation.

Santos, Villegas, Betancourt (2012) and Khan et al. (2021) found good results in the compressive strength of bricks at low marble powder substitution contents and at higher percentages, the strength decreases, Morales-Olán et al (2015) show results where marble powder is combined with Tepezil, and it is shown that the higher the marble powder substitution, the higher the strength. Nevárez and Rangel (2014) have high compressive strengths in their bricks as long as there is a preload in the manufacture of the bricks, Betancourt et al. (2015) found that the compressive strength of the samples is proportional to the amount of cement, i.e., the more cement, the higher the strength. Moreno et al. (2020) in their research, used different types of sand, resulting in the best performance of limestone sand.

As a conclusion of this section, it is determined that marble powder bricks can be used as non-structural elements and as thermal insulation.

3. CONCLUSIONS

As a conclusion of this review, it can be mentioned that marble powder can be used in construction either to replace cement, to replace fine aggregate, or to manufacture non-structural bricks. It is a topic with a lot of potential where good results can be obtained if the research is deepened.

Marble powder as a partial substitute for cement in proportions no greater than 10-15% is shown to maintain or offer an increase in compressive strength in mortars, concrete, and brick manufacturing.

The addition of superplasticizers showed an increase in compressive strength in conventional concrete mixes, and the partial substitution of marble powder to cement does not affect the compressive strength in this condition.

Marble powder as the main agent for brick making, supplemented with sand and cement, is feasible for non-structural use in residential masonry construction.

On the other hand, reducing the amount of cement used in concrete and mortars projects a cost reduction because the difference in commercial value with respect to marble powder is greater in cement. This implies that using marble powder in the manufacture of bricks reduces the cost of the pieces.

The energy required in cement production is about 1.18 GJ/ton. Therefore, replacing 15% of cement substitution with marble powder reduces energy consumption by almost 1.05%.

With the reduction of cement content, the carbon footprint would show a reduction, so its use would show a positive impact on the environment.

For the manufacture of bricks, it is observed that if a compaction of the material is used in the manufacturing process, a higher compressive strength is achieved, it is also concluded that using crushed sand instead of river sand helps the strength of the pieces.

In the case of concrete, it has been proven that the loss of strength is proportional to the increase of marble powder substitution. It was shown that the maximum percentage of marble powder substitution by cement is 10 %, so that the resistance is not affected.

For the application of marble powder in mortars, it is concluded that it is similar to the application of marble powder in concrete or bricks, i.e., the compressive strength with low percentages of marble powder is not affected.

Based on the above, it is possible to continue studying the application of marble powder in mortars, concrete, and brick manufacturing. In the manufacture of bricks, it is only necessary to find the right dosage so that the pieces can be used as structural. To achieve this, it is necessary to continue studying this topic and find the right dosage and aggregates.

4. REFERENCES

Khodabakhshian, A., de Brito, J., Ghalehnovi, M., Shamsabadi, E. A. (2018), *Mechanical, environmental and economic performance of structural concrete containing silica fume and marble industry waste powder*. Construction and Building Materials, Volume 169, Pages 237-251, <https://doi.org/10.1016/j.conbuildmat.2018.02.192>.

Talah, A., Kharchi, F., Chaid, R. (2015), *Influence of Marble Powder on High Performance Concrete Behavior*, Procedia Engineering, Volume 114, Pages 685-690, <https://doi.org/10.1016/j.proeng.2015.08.010>

Betancourt Chávez, J. R., Lizárraga Mendiola, L. G., Narayanasamy, R., Olguín Coca, F. J., Sáenz López, A. (2015), *Revisión sobre el uso de residuos de mármol, para elaborar materiales para la*

- construcción. Revista de Arquitectura e Ingeniería, 9(3), 1-12, <https://www.redalyc.org/articulo.oa?id=193943013004>
- Coordinación General de Minería (2014). *Perfil del Mercado del Mármol*. Ciudad de México: Dirección General del Desarrollo Minero.
- Ferraz, D. F. (2016), *Aditivos reductores de agua para concreto premezclado*. Construcción y Tecnología en Concreto. <http://www.revistacyt.com.mx/pdf/mayo2016/experto.pdf>
- Ghorbani, S., Tahi, I., Tavakkolizadeh, M., Davodi, A., de Brito, J. (2018), *Improving corrosion resistance of Steel rebars in concrete with marble and granite waste dust as partial cement replacement*, Construction, and Building Materials, Vol. 185 Pages: 110-119, <https://doi.org/10.1016/j.conbuildmat.2018.07.066>.
- El-Sayed, H. A., Farag, A. B., Kandeel, A. M., Younes, A. A., Yousef, M. M. (2018), *Characteristics of the marble processing powder waste at Shaq El-Thoaban industrial area, Egypt, and its suitability for cement manufacture*, HBRC Journal, 14:2, 171-179, DOI: <https://doi.org/10.1016/j.hbrcj.2016.06.002>
- Hebhoub, H., Aoun, H., Belachia, M., Houari, H., Ghorbel, E. (2011), *Use of waste marble aggregates in concrete*. Construction and Building Materials, Vol. 25, No. 3, Pages: 1167-1171, <https://doi.org/10.1016/j.conbuildmat.2010.09.037>
- Ince, C., Hamza, A., Derogar, S., Ball, R. (2020), *Utilization of waste marble dust for improved durability and cost efficiency of pozzolanic concrete*, Journal of Cleaner Production, vol. 270, 122-213. <https://doi.org/10.1016/j.jclepro.2020.122213>
- Khan, Z., Gul, A., Ali Shah, S. A., Qazi, S., Wahab, N., Badshah, E., Naqash, T., Shahzada, K. (2021). *Utilization of Marble Wastes in Clay Bricks: A Step towards Lightweight Energy Efficient Construction Materials*. Civil Engineering Journal, Vol. 7, No. 09, September, 2021, Pages 1488-1500, <https://doi.org/10.28991/cej-2021-03091738>
- Li, L. G., Huang, Z. H., Tan, Y. P., Kwan, A. K. H., Chen, H. Y. (2019), *Recycling of marble dust as paste replacement for improving strength, microstructure and eco-friendliness of mortar*, Journal of Cleaner Production, Volume 210, Pages 55-65, ISSN 0959-6526, <https://doi.org/10.1016/j.jclepro.2018.10.332>.
- Singh, M., Srivastava, A., Bhunia, D. (2017), *An investigation on effect of partial replacement of cement by waste marble slurry*, Construction and Building Materials, Volume 134, Pages 471-488, ISSN 0950-0618, <https://doi.org/10.1016/j.conbuildmat.2016.12.155>.
- Singh, M., Choudhary, K., Srivastava, A., Sangwan, K. S., Bhunia, D. (2017), *A study on environmental and economic impacts of using waste marble powder in concrete*, Journal of Building Engineering, Volume 13, Pages 87-95, ISSN 2352-7102, <https://doi.org/10.1016/j.jobee.2017.07.009>.
- Morales-Olán, G., et. al. (2015), *Desarrollo de un bloque de construcción a base de desecho de corte generado por la industria marmolera*. Revista Congreso Nacional de Ingeniería y Tecnologías para el Desarrollo Sustentable, pp. 80-83.
- Moreno Juárez, A. N., Ponce Palafox, C., López Montelongo, A. M., Cárdenas Díaz, O. E. (2020), *Aplicación del polvo de mármol para fabricar ladrillo estructural con dimensiones tradicionales en la Comarca Lagunera utilizados en muros de vivienda*. Revista de Arquitectura e Ingeniería, 14(1),1-10. <https://www.redalyc.org/articulo.oa?id=193962633006>
- Nevarez, C., Rangel, L. (2014), *Estudio experimental realizado para elaborar ladrillos con residuos de mármol (polvo)*. Tesis Licenciatura, Gómez Palacio, Dgo.: Universidad Juárez de Estado de Durango UJED.
- Babouri, L., Biskri, Y., Khadraoui, F., El Mendili, Y. (2020), *Mechanical performance and corrosion resistance of reinforced concrete with marble waste*, European Journal of Environmental and Civil Engineering, <https://doi.org/10.1080/19648189.2020.1838952>
- Rahangdale, S., Qureshi, S. (2019), *Study of Compressive Strength of Cement Concrete with Stone*

- and Marble Dust*, International Journal of Science and Research (IJSR) ISSN: 2319-7064, Vol. 8, No. 1, January 2019, <https://www.ijsr.net/archive/v8i1/ART20194592.pdf>
- Sánchez Pérez, C. J., Castillejo Cans, M. A. (2018), Caracterización geomecánica de rocas dimensionables: casos faja dolomítica y esquistos verdes, yacimiento de canteras tacarigua, C.A. Jornadas de Investigación. Encuentro Académico Industrial. Facultad de ingeniería UCV (JIFI2018). <http://www.ing.ucv.ve/jifi2018/documentos/cienciatierra/CT-017.pdf>
- Santos, A., Villegas, N., Betancourt, J. (2012), *Residuo de mármol como insumo en la construcción civil: diagnóstico de la Comarca Lagunera*. Revista de la construcción, 11(2), 17-26. <https://dx.doi.org/10.4067/S0718-915X2012000200003>
- Shaaban, M. (2020), *The Effects of Marble Dust on the Rheological and Mechanical Properties of Shotcrete*, Engineering, Tehcnology & Applied Science Research, Vol. 10, No. 5, pp. 6334-6348. https://pdfs.semanticscholar.org/3c8f/4b16c8512037e6c97aed1b14d29efb89646d.pdf?_ga=2.66500078.1376494727.1650224112-2140534152.1650224112
- Servicio Geológico Mexicano (2019). Anuario Estadístico de la Minería Mexicana, 2018. Ciudad de México: Secretaría de Economía. PUBLICACIÓN NO. 48. https://www.gob.mx/cms/uploads/attachment/file/683099/Anuario_2018_Edicion_2019.pdf
- Tobón, J., Gomez, R. (2008). Desempeño del cemento pórtland adicionado con calizas de diferentes grados de pureza. Dyna. vol.75 no.156 Medellín Sep./Dic. 2008. http://www.scielo.org.co/scielo.php?script=sci_arttext&pid=S0012-73532008000300017
- Toubal Seghir, N., Mellas, M., Sadowski, Ł., Krolicka, A., Žak, A., Ostrowski, K. (2019), *The Utilization of Waste Marble Dust as a Cement Replacement in Air-Cured Mortar*. Sustainability, 11 (8), 22-15. <https://doi.org/10.3390/su11082215>
- Corinaldesi, V., Moriconi, G., Naik, T. R. (2010), *Characterization of marble powder for its use in mortar and concrete*, Construction and Building Materials, Volume 24, Issue 1, Pages 113-117, <https://doi.org/10.1016/j.conbuildmat.2009.08.013>.
- Verma, M., Kaushal, N., Assistant, A. (2019). *Waste marble Powder/Dust*.
- Wang, Y., Xiao, J., Zhang, J., Duan, Z. (2022), *Mechanical Behavior of Concrete Prepared with Waste Marble Powder*. Sustainability 14, 41-70. <https://doi.org/10.3390/su14074170>
- Yamanel, K., Durak, U., İlkentapar, S., Atabey, İsmail İsa, Karahan, O., Duran, C. (2019), *Influence of waste marble powder as a replacement of cement on the properties of mortar*. Revista de la Construcción. 18(2), 290–300. <https://doi.org/10.7764/RDLC.18.2.290>

Influence of thermal curing on the physical and mechanical properties of ultra-high-performance cementitious composites with glass powder

F. G. S. Ferreira^{1*} , L. V. Dias¹ , S. M. Soares² , A. L. Castro³ 

*Contact author: fgiannotti@ufscar.br

DOI: <https://doi.org/10.21041/ra.v12i2.546>

Reception: 13/07/2021 | Acceptance: 28/02/2022 | Publication: 01/05/2022

ABSTRACT

This paper discusses the impact of thermal curing and particle packing on ultra-high-performance concrete (UHPC) that used glass powder as a partial replacement of Portland cement. For this, specimens with 0% and 50% of glass powder (volumetric substitution to cement) were produced, as well as two mixtures obtained by particle packing. The samples were submitted to thermal and standard curing to compare the effects and tested for compression strength and capillary water absorption. The results show that thermal curing improves resistance expressively in the early ages while particle packing applied to the mix design improved significantly the concrete properties, indicating that glass powder is a viable substitute for cement.

Keywords: cementitious composite; thermal curing; particle packing; glass powder.

Cite as: Ferreira, F. G. S., Dias, L. V., Soares, S. M., Castro, A. L. (2022), "Influence of thermal curing on the physical and mechanical properties of ultra-high-performance cementitious composites with glass powder", Revista ALCONPAT, 12 (2), pp. 184 – 199, DOI: <https://doi.org/10.21041/ra.v12i2.546>

¹ Departamento de Engenharia Civil, Universidade Federal de São Carlos, São Carlos, Brasil.

² Instituto Federal de Educação, Ciência e Tecnologia de São Paulo, Caraguatatuba, Brasil.

³ Departamento de Engenharia de Estruturas, Universidade de São Paulo, Brasil.

Contribution of each author

In this work, the author L. V. Dias contributed with the activities of conceptualization, development, results and discussion, writing and preparation of the original text (30%); S. M. Soares contributed to the activities of conceptualization, development, results and discussion (30%); F. G. S. Ferreira contributed with conceptualization, supervision, discussion of results, writing and review (20%) and A. L. Castro contributed with conceptualization, supervision, discussion of results, writing and review (20%).

Creative Commons License

Copyright 2022 by the authors. This work is an Open-Access article published under the terms and conditions of an International Creative Commons Attribution 4.0 International License ([CC BY 4.0](https://creativecommons.org/licenses/by/4.0/)).

Discussions and subsequent corrections to the publication

Any dispute, including the replies of the authors, will be published in the first issue of 2023 provided that the information is received before the closing of the third issue of 2022.

Influência da cura térmica nas propriedades física e mecânica de compósitos cimentícios de ultra alto desempenho com pó de vidro

RESUMO

Este trabalho visa avaliar o impacto da cura térmica e do uso de empacotamento de partículas em compósitos cimentícios de ultra alto desempenho (CCUAD), com e sem pó de vidro. Para tanto, foram moldados corpos de prova com 0% e 50% de pó de vidro (substituição volumétrica ao cimento), além de dois traços obtidos através do empacotamento de partículas. As amostras foram submetidas a cura térmica e a cura úmida para comparação dos efeitos. Foram realizados ensaios de resistência à compressão e de absorção de água por capilaridade. Os resultados indicaram que a cura térmica proporciona ganho inicial de resistência, a aplicação do empacotamento de partículas na dosagem das misturas resultou em uma significativa melhoria nas propriedades das amostras e o pó de vidro se mostrou um substituto viável para o cimento.

Palavras-chave: compósitos cimentícios; cura térmica; empacotamento de partículas; pó de vidro

Influencia del curado térmico en las propiedades físicas y mecánicas del hormigón de ultra alto desempeño con polvo de vidrio

RESUMEN

Este trabajo tiene como objetivo evaluar el impacto del curado térmico y el uso de empaquetamiento de partículas en compuestos cementosos de ultra alto desempeño (UHPC), con y sin polvo de vidrio. Para ello, los cuerpos de prueba fueron moldeados con 0% y 50% de polvo de vidrio (reemplazo volumétrico al cemento), además de dos mezclas obtenidas a través del empaquetamiento de partículas. Las muestras fueron sometidas a curado térmico y curado húmedo para comparar los efectos. Se realizaron pruebas de resistencia a la compresión y absorción por capilaridad. Los resultados indicaron que el curado térmico proporciona ganancia de la resistencia inicial, la aplicación del empaquetamiento de partículas en las dosis de mezcla resultó en una mejora significativa en las propiedades de las muestras y el polvo de vidrio demostró ser un sustituto viable del cemento.

Palabras clave: compuestos cementosos; curado térmico; empaquetamiento de partículas; polvo de vidrio

Legal Information

Revista ALCONPAT is a quarterly publication by the Asociación Latinoamericana de Control de Calidad, Patología y Recuperación de la Construcción, Internacional, A.C., Km. 6 antigua carretera a Progreso, Mérida, Yucatán, 97310, Tel.5219997385893, alconpat.int@gmail.com, Website: www.alconpat.org

Reservation of rights for exclusive use No.04-2013-011717330300-203, and ISSN 2007-6835, both granted by the Instituto Nacional de Derecho de Autor. Responsible editor: Pedro Castro Borges, Ph.D. Responsible for the last update of this issue, Informatics Unit ALCONPAT, Elizabeth Sabido Maldonado.

The views of the authors do not necessarily reflect the position of the editor.

The total or partial reproduction of the contents and images of the publication is carried out in accordance with the COPE code and the CC BY 4.0 license of the Revista ALCONPAT.

1. INTRODUCTION

In the last decades, ultra-high-performance cementitious composites (UHPC) emerged to meet the growing demand for more durable structures with higher mechanical resistance. The first reference to the term is attributed to de Larrard and Sedran, in 1994 (Shi *et al.*, 2015), while referring to a composite with high mechanical resistance (greater than 150 MPa) and high durability (Alkaysi *et al.*, 2016; Wang *et al.*, 2019). To achieve these characteristics, a high cement consumption (about 1000 kg/m³) and a low water/cement ratio (w/c) (between 0.14 and 0.20) are required to allow reduced porosity, and the use of a superplasticizer additive to provide adequate workability to the material (Ganesh and Murthy, 2019). The inclusion of silica fume also changes workability while increasing the final strength due to the better filling of the voids and the generated pozzolanic reactions (Abbas *et al.*, 2015).

The application of particle packing models is necessary to determine the composition of special mixtures, such as UHPC, since they improve the mechanical properties and the durability of the cementitious composite, by increasing the matrix density (Castro and Ferreira, 2016). The packing concept also contributes to increasing density with the removal of coarse aggregate (Zhang *et al.*, 2019). Additionally, by removing the coarse aggregate, the internal voids and the transition zone are reduced while generating a more homogeneous distribution of tensions in the grains (Tutikian *et al.*, 2011).

The first published references on particle packing date back to 1892 and are attributed to Féret (Castro and Pandolfelli, 2009). In 1930, Furnas developed one of the first packing models, based on a discrete approach. Subsequently, a model based on continuous distributions was developed by Andreasen. Finally, Funk and Dinger (1994) analyzed both models and reported that the models proposed approximately the same solution. Therefore, the authors perfected their model that became known as Alfred's model, whose analysis is considered to generate the best results (Lopes, 2019).

The adopted curing procedure also influences the development of mechanical resistance in cementitious composites such as UHPC. Thermal curing procedures at temperatures between 90 and 400 °C, can maximize the composite mechanical strength due to the acceleration of pozzolanic reactions, improving the matrix microstructure (Ganesh and Murthy, 2019).

The main effect of thermal curing in concretes is linked with the increase in density generated by the greater amount of C-S-H produced (Bahedh and Jaafar, 2018). Such a process, when performed in a high humidity environment at 90 °C, increases significantly the concrete strength in the early ages (Heinz *et al.*, 2012). However, Terzian (2005) asserted that thermal curing procedures performed at temperatures above 70 °C can reduce concrete final strength between 10 and 20%.

The incorporation of mineral additions can provide a better particles packing and also contribute to the reduction of the environmental impact. The environmental impact of the cement manufacturing process is enormous since 0.8 tons of CO₂ is released to produce one ton of cement (Mehta and Ashish, 2020). To this end, the high consumption of cement required for producing UHPC has an extremely significant environmental impact. Therefore, looking for a viable replacement for cement that does not modify significantly the composite properties is interesting and desired. The glass powder characteristics allow its use as a possible substitute for cement due to the significant pozzolanic activity resulting from the high content of silica (SiO₂) and its amorphous structure, in addition to being abundant. In 2005, the USA generated 12.8 million tons of waste, of which only 2.75 million were recycled (Schwarz *et al.*, 2008) and, in 2007, the European Union generated about 25.8 Mt of glass waste (Abdollahnejad *et al.*, 2017). Furthermore, in 2008, Brazil consumed 5.5 kg of glass packaging per inhabitant, of which 80% have not been recycled (IPEA, 2012).

The main objective of this work is to evaluate the effects of thermal curing on UHPC specimens

with and without added glass powder.

2. PROCEDURE

2.1 Materials

This research used as binders Portland cement of high initial resistance (CPV ARI), silica fume, and glass powder consisting of ground recycled amber bottles that were subsequently sieved in the #200 mesh sieve (diameter less than 75 μm). Also, natural quartz sand was used as fine aggregate. Additionally, ground silica (SM200) was used as filler, the superplasticizer additive based on polycarboxylate provided adequate workability due to the low water/binder ratio used, and shrinkage reducing additive to avoid cracking of the matrix. The parameters of the granular materials used to produce the UHPCC are shown in Tables 1 to 4.

Table 1. Portland Cement physical characteristics.

Parameter		Method	Obtained value	Reference value, NBR 16697 (ABNT, 2018)
Specific gravity		NBR 16605 (ABNT, 2017)	3.16 g/cm ³	-
Initial setting time		NBR 16607 (ABNT, 2018)	135 min	≥ 60 min
Final setting time		NBR 16607 (ABNT, 2018)	210 min	≤ 600 min
Water for normal consistency		NBR 16606 (ABNT, 2018)	30.0%	-
% retained in 75 μm sieve		NBR 16372 (ABNT, 2015)	0.1%	$\leq 6.0\%$
Blaine surface area		NBR 16372 (ABNT, 2015)	665.0 m ² /kg	-
Compressive strength	1 day	NBR 7215 (ABNT, 2019)	27.5 MPa	≥ 14.0 MPa
	3 days		42.0 MPa	≥ 20.0 MPa
	7 days		48.7 MPa	≥ 34.0 MPa
	28 days		52.2 MPa	-

Table 2. Silica fume, glass powder and filler physical characteristics.

Parameter	Silica fume		Glass powder		Filler	
	Test results	Reference value NBR 13956-1	Test results	Reference value	Test results	Reference value
Specific gravity	2.25 g/cm ³	-	2.55 g/cm ³	-	2.70 g/cm ³	-
Moisture		≤ 3.0%	-	-	-	-
% retained in 45 µm sieve	Max. 10.0%	≤ 10.0%	-	-	-	-
Blaine surface area	247.0 m ² /kg	-	393.0 m ² /kg	-	234.0 m ² /kg	-
Pozzolanic activity index	Min. 105.0%	≥ 105.0%	6.4 MPa	6.0 MPa**	-	-

*tested according to the NBR 5751 (ABNT, 2015) method.

** Reference values from NBR 12653 (ABNT, 2015).

Table 3. Materials chemical composition.

Component	Materials (% mass)			
	Portland cement	Silica fume	Glass powder	Fine aggregate
Loss on ignition (LOI)	4.05 (≤ 6,50)*	3.60(≤ 6,00)**	0.58	0.58
Calcium oxide (CaO)	61.40	<0.20	9.10	0.071
Aluminum oxide (Al ₂ O ₃)	4.31	<0.20	3.70	3.40
Silicic anhydrous (SiO ₂)	23.00	94.10	74.00	94.00
Sulfur trioxide (SO ₃)	2.97 (≤ 4,5)*	-	-	-
Ferric oxide (Fe ₂ O ₃)	2.49	<0.50	0.42	0.67
Potassium oxide (K ₂ O)	0.96	1.28	0.56	1.20
Phosphoric oxide (P ₂ O ₅)	0.52	-	-	-
Strontium oxide (SrO)	0.27	<0.20	0.039	-
Chlorine ions (Cl ⁻)	0.12	-	-	-
Thorium dioxide (ThO ₂)	<0.01	<0.01	<0.01	<0.01
Uraninite (U ₃ O ₈)	<0.01	<0.01	<0.01	<0.01
Titanium dioxide (TiO ₂)	-	<0.20	-	0.35
Chromium oxide (Cr ₂ O ₃)	-	-	-	0.049
Magnesium oxide (MgO)	-	-	0.74	-
Rubidium oxide (Rb ₂ O)	-	-	0.016	-
Sodium oxide (Na ₂ O)	-	-	11.00	0.37

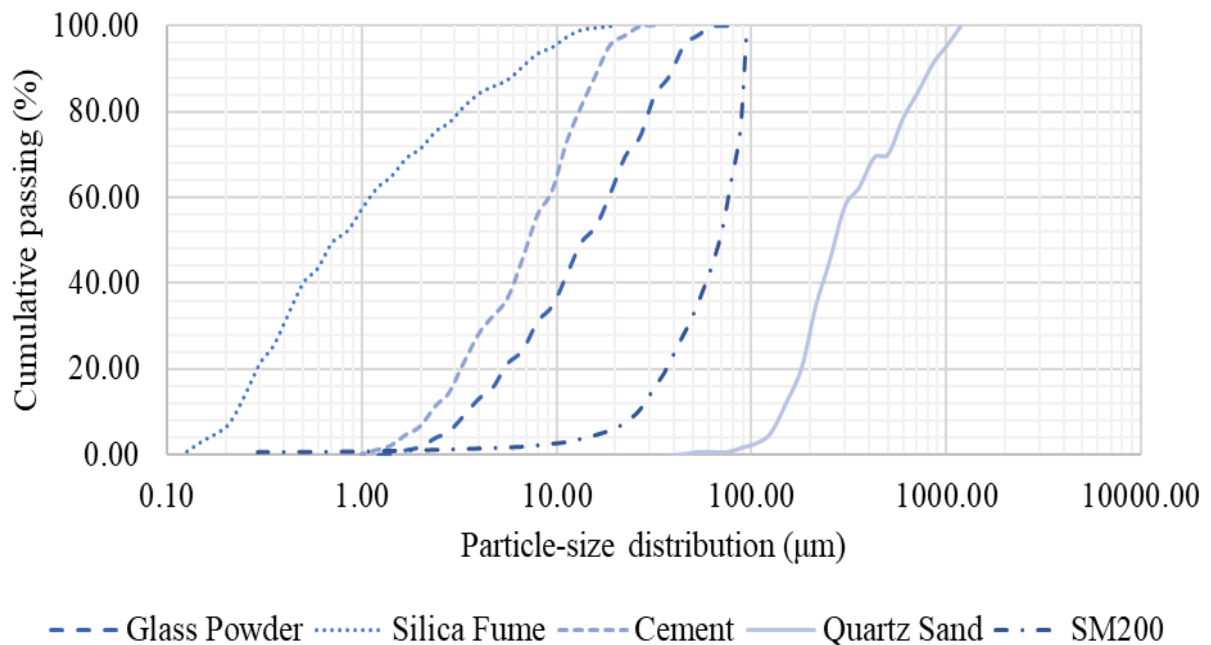
* Reference values of NBR 16697 (ABNT, 2018).

** Reference values of NBR 13956-1 (ABNT, 2012).

Table 4. Fine aggregate physical characteristics.

Parameters	Method	Obtained value
Water absorption	NBR 16916 (ABNT, 2021)	0.64%
Specific gravity	NBR 16916 (ABNT, 2021)	2.56 g/cm ³
Unit weighth	NBR 16972 (ABNT, 2021)	1475.78 kg/m ³
Unit weighth (compacted)	NBR 16972 (ABNT, 2021)	1617.83 kg/m ³
Organic impurities	NBR NM 49 (ABNT, 2006)	Clear solution than standard
Fine material passing through the 75 µm sieve, by washing	NBR 16973 (ABNT, 2021)	1.66%

Figure 1 shows the particle size distribution of cement, silica fume, glass powder, fine aggregate (quartz sand), and filler (SM200). The d₅₀ values of 0.8, 7, 15, 32, and 270 µm were determined for silica fume, cement, glass powder, filler, and fine aggregate, respectively.



2.2 Methodology

To produce all UHPCC mixtures, a fixed water/binder ratio of 0.18 was adopted. Initially, two mixtures were produced, a reference mix (REF), with 0% added glass powder, and a mix with 50% glass powder (GP50) as a volumetric replacement for cement; silica fume was added to both mixtures, at a ratio of 8% to the cement mass of the reference mix. Subsequently, the GP50 mix was optimized based on the particle packing concept, applying the Alfred model (Equation 1).

$$CPFT = \left(\frac{D_p^q - D_s^q}{D_L^q - D_s^q} \right) \times 100 \quad (1)$$

Where: CPFT is the cumulative percent finer than D_p , D_p is the particle diameter, D_L is the largest particle diameter in the size distribution, D_s is the smallest particle diameter in the size distribution, and q is a constant, designated per particle size distribution module.

The distribution coefficient value used for optimizing the GP50 mix was determined considering the discrete particle size distribution and the proportions of materials added in the mixtures. Thus, the experimental curve was obtained for the particle size distribution while the theoretical curve was obtained by applying the Alfred model. Through an iterative process to adjust the theoretical curve to the experimental curve, aiming to obtain the maximum correlation coefficient, the distribution coefficient value was determined ($q = 0.17$; $R^2 = 0.9913$).

The mixture composition was optimized by a mathematical process, which used as input data the discrete particle size distribution of the materials added to the mixture and the distribution coefficient determined for the GP50. Iteratively, the program calculates the diameter of the smallest and largest particles present in the mixture, providing the theoretical grain size distribution curve of the adopted packing model (Alfred model). Simultaneously, the content of each added material is adjusted to obtain the highest correlation coefficient between the theoretical and experimental curves. At the end of the process, the optimized mixture composition is given in terms of the mass percentage of each granular material added to the mixture.

Thus, a spreadsheet editor, using the solver tool, assisted the calculations of the optimal proportion of the materials constituting the optimized mixture, identified as GP50E. Figure 2 shows that the particle size range between the sand and the glass powder is not filled by any particle of the granular materials added initially. For this reason, to increase the packing efficiency of the selected mixture, the filler (SM200) was added to the list of materials that make up the mixture (Figure 3), generating a second optimized mixture based on the particle packing concept (GP50SM), applying the Alfred model and the determined distribution coefficient value.

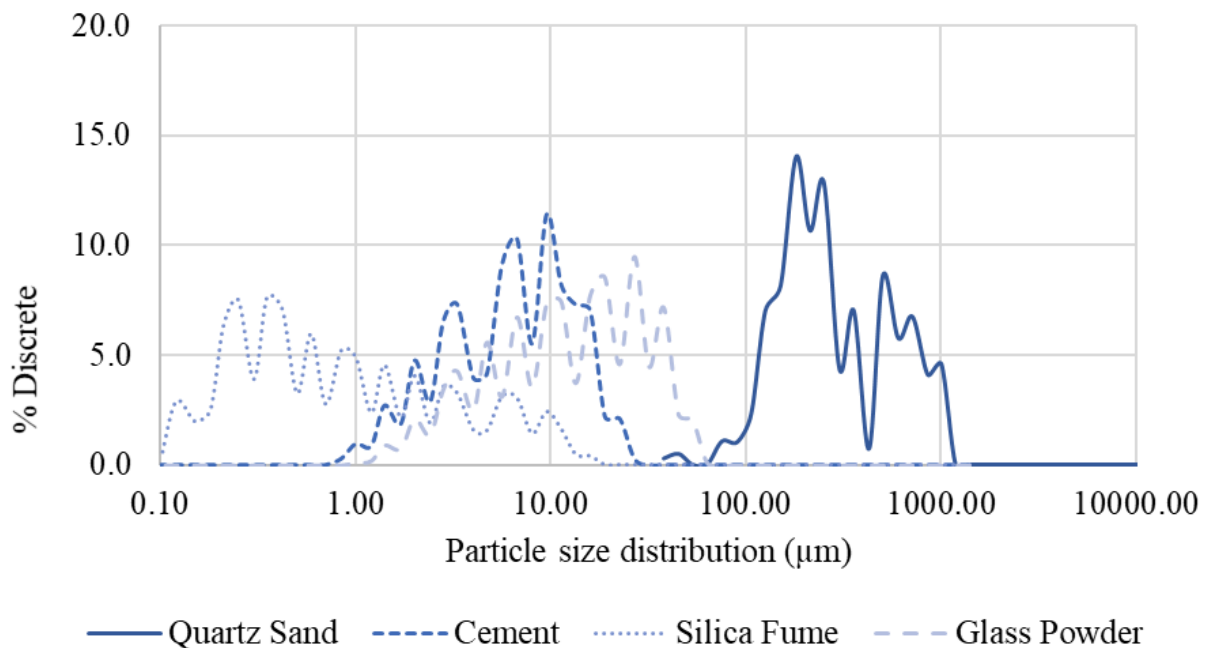


Figure 2. Discrete particle size distribution of materials without SM200.

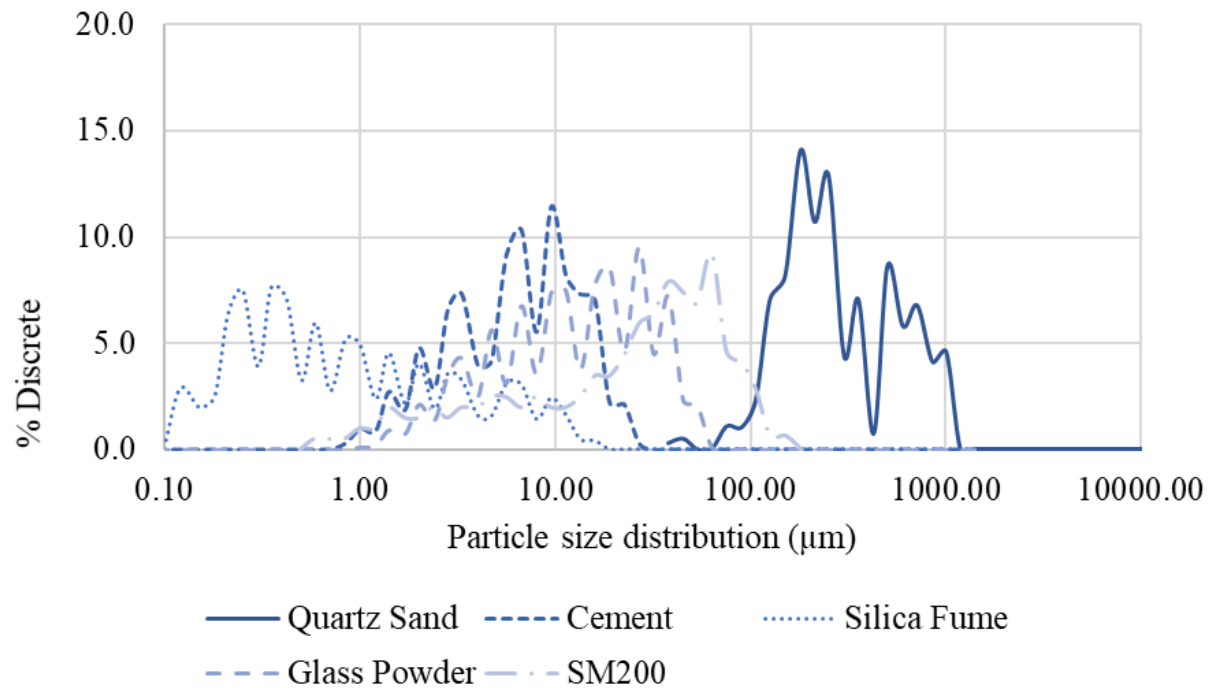


Figure 3. Discrete particle size distribution of materials with SM200.

Table 5 shows the unitary mix cementitious composites (in mass), the consistency index, and the cement consumption for the studied mixtures. Consistency was measured according to NBR 13276 (ABNT, 2016). It is noteworthy that the content of the superplasticizer additive was determined to obtain a consistency of (380 ± 10) mm (fluid consistency) for the REF and GP50 mixtures, maintaining the same superplasticizer content when producing the optimized mixtures to reduce the variables in the process. The shrinkage-reducing additive content was determined following the manufacturer's recommendations. The compatibility between the binders and the additives was verified through the mini-slump test (Kantro, 1980).

Table 5. Mixtures proportion, consistency index and cement consumption of UHPCC.

Mixtures	Cement	Silica fume	Glass powder	Fine aggregate	Filler	Water	SP*	RR**	Consistence index (mm)	Cement consumption (kg/m ³)
REF	1	0.08	0	1.07	0	0.18	0.02	0.01	380	1,000
GP50	1	0.16	0.81	2.15	0	0.18	0.04	0.02	385	500
GP50E	1	0.43	0.46	2.11	0	0.18	0.04	0.02	345	510
GP50SM	1	0.29	0.40	2.01	0.30	0.18	0.04	0.02	323	514

*Superplasticized additive.

**Shrinkage reducing additive.

Then, cylindrical specimens of 50 mm x 100 mm were manually molded, following a material mixing procedure developed during the research and suitable for each different mix (Figure 4). When producing the GP50SM mix, the glass powder and filler were weighed separately, packed in the same package, and homogenized for about 2 minutes before being added to the mixture.

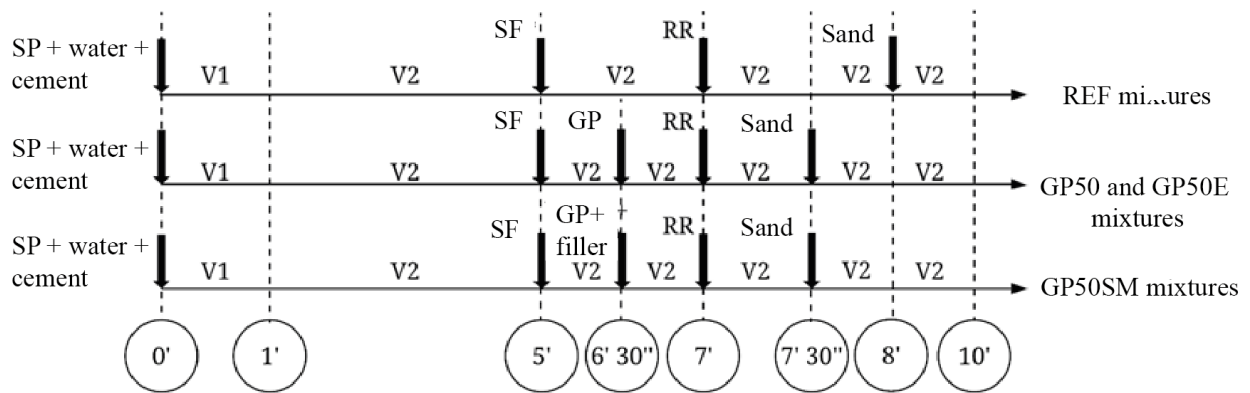


Figure 4. The mixing procedure, in which V1 and V2 represent, respectively, the low and high speeds of the mortar mixer/pump/machine.

After molding, the specimens were placed in an air-conditioned chamber for approximately 48 hours, until demolding. The specimens were then submitted to the respective curing procedures. For thermal curing (TC), the specimens were placed in an appropriate container/tank filled with water, ensuring that all were fully submerged. This container was placed in an unventilated oven heated to $(90 \pm 5)^\circ\text{C}$ for two hours, corresponding to a heating rate of approximately 35°C/h . After 24 hours in the oven, all specimens were removed and taken to an air-conditioned room, where they remained for 24 hours. Finally, the specimens were placed in a container filled with lime-saturated water until the testing ages. Another group of specimens was submitted to immersion curing (IC), which consists of immersion in lime-saturated water.

Then, the mechanical resistance of the specimens was determined at the ages of 7, 28, and 180 days, for a total of 8 specimens per mixture (4 for TC and 4 for IC) using the axial compression test, according to NBR 5739 (ABNT, 2018). Additionally, capillary water absorption was evaluated at 28 days of age, for 6 specimens per mix (3 for TC and 3 for IC), according to NBR 9779 (ABNT, 2012). The obtained results were analyzed using Analysis of Variance (ANOVA) and $F > \text{Critical}$ indicated significant statistical differences in the group, the means were compared by Tukey test to verify which sample was significantly different.

3. RESULTS AND DISCUSSIONS

3.1 Compressive strength

Figure 5 shows graphically the compressive strength results for the studied mixtures. The values are the average of four individual values obtained from the specimens tested at the ages of 7, 28, and 180 days.

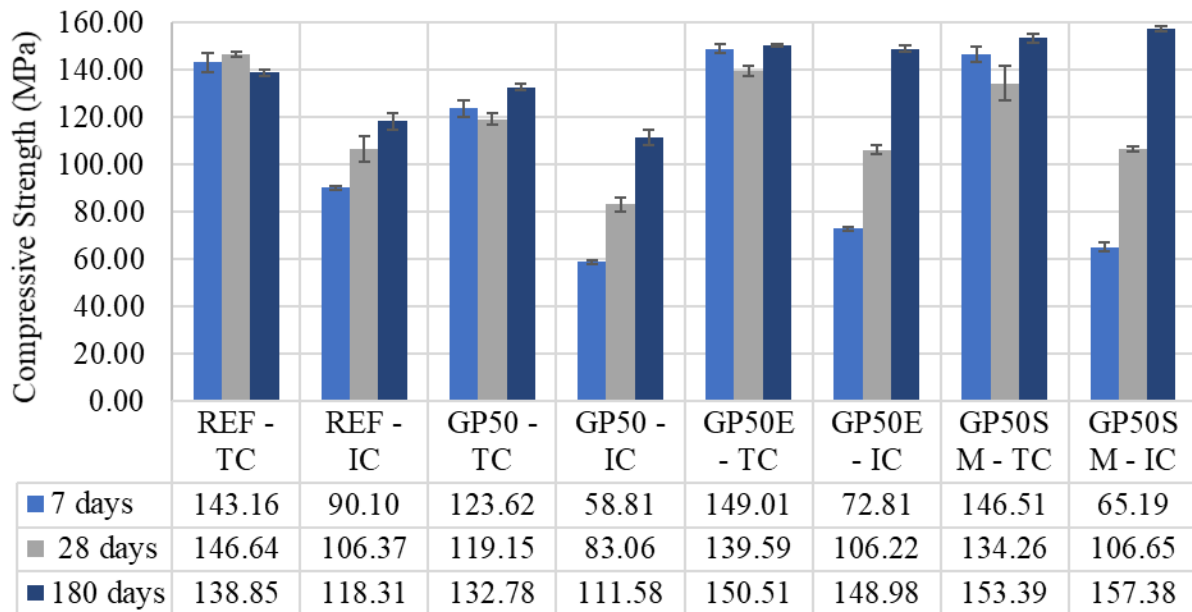


Figure 5. Compressive strength of the UHPCC mixtures.

At 7 days of age, the comparison of different cure types shows that the resistance values are about 2 times higher for specimens submitted to TC compared to IC, except for the REF mix, whose resistance is about 1.6 times higher. This resistance gain can be attributed mainly to the acceleration of the cement hydration reactions and the pozzolanic reactions of the added minerals, and the exposure to a temperature of $(90 \pm 5) ^\circ\text{C}$ during the thermal curing process. However, at 180 days, this gain is not so significant since the TC/IC ratio varied between 0.97 and 1.17. This result can be explained by the fact that the thermal cure only accelerates the process to reach the composite final strength, thus having little impact on the resistance in later ages, especially in mixtures optimized through the packing of particles. Likewise, other authors evaluated the performance of UHPCC mixtures under different curing conditions and observed similar behavior. Heinz *et al.* (2012) compared the mechanical performance of UHPCC using cubic specimens submitted to thermal and immersion curing and reported that resistance values of 136.3 MPa (IC) increased to 232.5 MPa (TC) at 7 days of age (1.76 times greater) whereas, at 28 days, resistances of 216.1 MPa (IC) increased to 232.8 MPa (TC) (1.08 times greater). Sokolovicz (2020) investigated the behavior of UHPCC specimens obtained by packing particles and reported resistances 1.25 times greater at 7 days and 1.13 at 28 days, to those submitted to thermal curing compared to immersion curing. Additionally, the loss of resistance in specimens submitted to TC, between 7 and 28 days (Fig. 5), is not significant according to the ANOVA statistical analysis and the Tukey test. Melo (2000) attributed this resistance loss to the changes in concrete microstructure caused by the accelerated process of cement hydration, but resistance improves again due to the pozzolanic activity of silica fume at more advanced ages (180 days). Additionally, Du and Tam (2015) verified that the pozzolanic reactions of the glass powder are slower compared to the cement hydration process, which may have also contributed to the later recovery of the resistance of the specimens with added fine material.

Initially, the samples optimized via particle packing had no significant resistance gain compared to traditionally dosed mixtures. At 7 days of age, the resistance of the GP50E and GP50SM specimens is lower than the reference but statistically equal to the resistance of the GP50 mix. This fact can be explained by the lower cement consumption of the GP50, GP50E and GP50SM mixtures compared to the REF mixture, which probably impaired the mechanical performance of these mixtures in the early ages. At more advanced ages, a significant compressive strength gain is

observed for the optimized samples. Lopes (2019) also investigated concrete optimized via particle packing and observed significant strength gains after 28 days of age, attributing them to the strengthening transition zones due to mineral additions. Similarly, this justification can also be applied to this case since the optimized mixtures consumed high amounts of silica fume. Sokolovicz (2020) evaluated the mechanical behavior of UHPCC packaged, submitted to wet curing, and reported resistances of 115.30, 138.60 and 158.9 MPa, at 7, 28 and 91 days, respectively. In this case, resistance developed more uniformly over time, probably explained by the fact that the specimens consumed less silica fume and the non-use of glass powder, which has slower pozzolanic activity, as previously mentioned. It is also observed that the author reported a final resistance close to that obtained in the present study.

It is noteworthy that the development of compressive strength of the studied UHPCC occurs as a function of cement hydration and the pozzolanic reaction of silica fume and glass powder. Depending on the type and content of mineral addition used and the curing regime adopted, a significant gain in strength can occur at ages greater than 28 days (as can be seen in Figure 5 for compressive strength at 180 days), a fact that must be considered in the design of concrete structures.

3.2 Water absorption

Figure 6 shows graphically the results of the capillary water absorption test obtained for the studied mixtures. The values are the average of three individual measurements obtained from the specimens tested at 28 days.

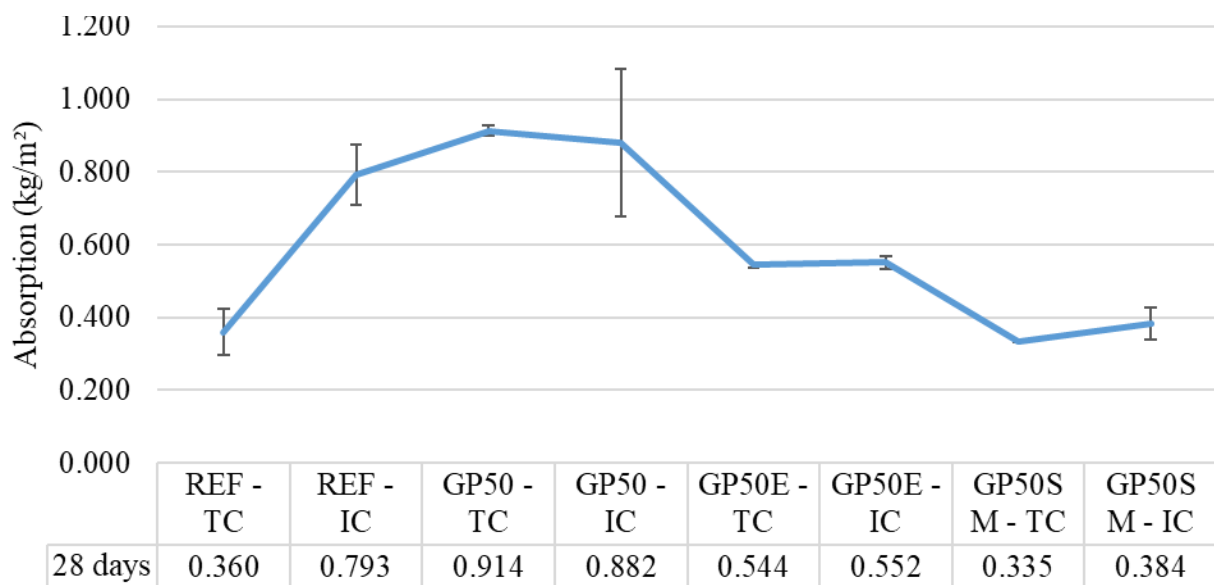


Figure 6. Capillary water absorption of the studied UHPCC mixtures.

Figure 6 shows that the lowest levels of water absorption by capillarity were recorded for the specimens optimized via particle packing, considering the use of SM200 (GP50SM). This result can be explained by the filler effect provided by the material, which provides a more dense and homogeneous microstructure while generating a disconnected pore structure and reducing the water absorption by the material (Tam *et al.*, 2012). Also, the optimized samples (GP50E and GP50SM), in general, absorbed less water than those traditionally dosed, which can be explained by the better filling of the voids provided by the particle packing and by the high consumption of silica fume which, in addition to the filler effect, provides an additional amount of CSH due to the pozzolanic reaction, blocking the pores present in the material (Tam *et al.*, 2012). This effect also explains why, in general, the samples submitted to TC show less absorption than those submitted

to IC, since this curing procedure increases the C-S-H amount in the early ages due to the acceleration of cement hydration reactions.

It is worth mentioning the great dispersion of results observed for some studied UHPCC, as is the case of the REF-IC and GP50-IC. As the capillary water absorption values obtained for these mixtures are very low (0.793 kg/m² for REF-IC and 0.882 kg/m² for GP50-IC), a small difference between the values obtained for the specimens can result in a high standard deviation, as observed in the present study, corresponding to coefficients of variation of 10.4% and 26.0%, respectively. It is noteworthy, however, that the test procedure in NBR 9779 (ABNT, 2012) was not suitable to be applied to UHPCC, since due to the low amount of pores present in the concrete microstructure, the specimens did not present significant mass differences after long periods in the oven or exposed to water.

3.3 Statistical analysis

Tables 6 to 9, presented below, show the statistical analysis results of the mechanical resistance and capillary water absorption of the studied UHPCC mixtures. Yes indicates a statistically significant difference between samples whereas No indicates no statistically significant difference between samples.

Table 6. Mechanical resistance at 7 days - significant difference ($F = 68.87$ and $F_{obtained} = 2.42$).

	REF - IC	GP50 - TC	GP50 - IC	GP50E - TC	GP50E - IC	GP50SM - TC	GP50SM - IC
REF - TC	Yes	No	Yes	No	Yes	No	Yes
REF - IC		Yes	Yes	Yes	No	Yes	Yes
GP50 - TC			Yes	Yes	Yes	Yes	Yes
GP50 - IC				Yes	No	Yes	No
GP50E - TC					Yes	No	Yes
GP50E - IC						Yes	No
GP50SM - TC							Yes

According to Table 6, it is possible to observe that there was a significant difference in the values of compressive strength (at 7 days of age) of the samples submitted to TC, compared to the samples after IC. The incorporation of glass powder provided a significant decrease in the mechanical strength of the UHPCC.

Table 7. Mechanical resistance at 28 days - significant difference ($F = 9.07$ and $F_{obtained} = 2.42$).

	REF - IC	GP50 - TC	GP50 - IC	GP50E - TC	GP50E - IC	GP50SM - TC	GP50SM - IC
REF - TC	Yes	No	Yes	No	Yes	No	Yes
REF - IC		No	No	Yes	No	No	No
GP50 - TC			Yes	No	No	No	No
GP50 - IC				Yes	No	Yes	No
GP50E - TC					Yes	No	No
GP50E - IC						No	No
GP50SM - TC							No

At 28 days of age (Table 7), it is possible to observe that the mixtures GP50-TC, GP50SM-TC and GP50SM-IC did not present significant differences in relation to most of the studied UHPCC. For the GP50SM mixture, with the incorporation of silica fume, glass powder and filler, the curing procedure (TC or IC) did not imply significant differences in terms of mechanical resistance. The samples with glass powder incorporation and submitted to TC showed no significant differences compared to the reference sample after TC (REF-TC).

Table 8. Mechanical resistance at 180 days - significant difference ($F = 19.84$ and $F_{obtained} = 2.42$).

	REF - IC	GP50 - TC	GP50 - IC	GP50E - TC	GP50E - IC	GP50SM - TC	GP50SM - IC
REF - TC	Yes	No	Yes	No	No	No	Yes
REF - IC		No	No	Yes	Yes	Yes	Yes
GP50 - TC			Yes	No	No	Yes	Yes
GP50 - IC				Yes	Yes	Yes	Yes
GP50E - TC					No	No	No
GP50E - IC						No	No
GP50SM - TC							No

According to Table 8, it is possible to observe that there was a significant difference in the values of compressive strength (at 180 days of age) of the samples submitted to TC, compared to the samples after IC in the REF and GP50 mixtures. In the others, the curing procedure did not significantly interfere with resistance. In the samples submitted to TC, the incorporation of glass powder did not provide a significant difference in the compressive strength of the UHPCC.

Table 9. Water absorption at 28 days - significant difference.

	REF - IC	GP50 - TC	GP50 - IC	GP50E - TC	GP50E - IC	GP50SM - TC	GP50SM - IC
REF - TC	Yes	Yes	Yes	No	No	No	No
REF - IC		No	No	Yes	Yes	Yes	Yes
GP50 - TC			No	Yes	Yes	Yes	Yes
GP50 - IC				Yes	Yes	Yes	Yes
GP50E - TC					No	No	No
GP50E - IC						No	No
GP50SM - TC							No

According to Table 9, it is possible to observe that there was no significant difference in the water absorption values of the samples submitted to TC, compared to the samples after IC, except for the sample without glass powder (REF). The incorporation of glass powder did not provide a significant difference in the water absorption of the UHPCC submitted to TC (except for the GP50 mixture). As for the mixtures with better particle packing (GP50E and GP50SM), the decrease in the values of capillary water absorption was significant, when compared to the GP50 mixture, regardless of the curing procedure.

4. CONCLUSIONS

Given the obtained data, it can be concluded that:

1. The adopted thermal curing procedure is feasible and beneficial since concrete strength increased in early and more advanced ages, especially if applied to cementitious composites with added glass powder.
2. The particle packing model used to optimize the mixtures increased the concrete strength and reduced water absorption effectively; these effects became more pronounced at more advanced ages.
3. The use of ground silica (SM200) did not generate significant strength gains. However, the observed reduction of water absorption validates its use.
4. The high levels of glass powder (50%) added tend to decrease the mechanical strength of the UHPCC by 35%, 22% and 5% compared to the reference composite at 7, 28 and 180 days, respectively, indicating the feasibility of using glass powder as a partial substitute for cement.
5. The water absorption test following the method recommended in the NBR 9779 (ABNT, 2012) is not ideal for evaluating the performance of the UHPCC mixtures. Therefore, it is recommended to elaborate another procedure more appropriate for low porosity and/or permeability composites.

5. ACKNOWLEDGMENTS

To the National Council for Scientific and Technological Development (CNPq) for the financial support to this research and to the Institute of Technological Research of the State of São Paulo (IPT), for assisting the characterization tests of the binders.

6. REFERENCES

- Abbas, S., Soliman, A. M., Nehdi, M. L. (2015), *Exploring mechanical and durability properties of ultra-high-performance concrete incorporating various steel fiber lengths and dosages*. Construction and Building Materials. 75: 429–441. <https://doi.org/10.1016/j.conbuildmat.2014.11.017>
- Abdollahnejad, Z., Kheradmand, M., Pacheco-Torgal, F. (2017), *Short-Term Compressive Strength of Fly Ash and Waste Glass Alkali-Activated Cement-Based Binder Mortars with Two Biopolymers*. Journal of Materials in Civil Engineering. 29(7). [https://doi.org/10.1061/\(ASCE\)MT.1943-5533.0001920](https://doi.org/10.1061/(ASCE)MT.1943-5533.0001920)
- Alkaysi, M., El-Tawil, S., Liu, Z., Hansen, W. (2016), *Effects of silica powder and cement type on durability of ultra-high-performance concrete (UHPC)*. Cement and Concrete Composites. 66: 47-56. <https://doi.org/10.1016/j.cemconcomp.2015.11.005>
- Associação Brasileira de Normas Técnicas. (2018). *NBR 5739: Concreto – Ensaio de compressão de corpos de prova cilíndricos*. Rio de Janeiro.
- Associação Brasileira de Normas Técnicas. (2015). *NBR 5751 Materiais pozolânicos – Determinação da atividade pozolânica com cal aos sete dias*. Rio de Janeiro.
- Associação Brasileira de Normas Técnicas. (2019). *NBR 7215: Cimento Portland - Determinação da resistência à compressão de corpos de prova cilíndricos*. Rio de Janeiro.
- Associação Brasileira de Normas Técnicas. (2012). *NBR 9779: Argamassa e concretos endurecidos - Determinação da absorção de água por capilaridade*. Rio de Janeiro.
- Associação Brasileira de Normas Técnicas. (2013). *NBR 11579: Cimento Portland - Determinação do índice de finura por meio da peneira 75 μm (n^o200)*. Rio de Janeiro.

- Associação Brasileira de Normas Técnicas. (2016). *NBR 13276: Argamassa para assentamento e revestimento de paredes e tetos – Determinação do índice de consistência*. Rio de Janeiro.
- Associação Brasileira de Normas Técnicas. (2012). *NBR 13956-1: Sílica ativa para uso com cimento Portland em concreto, argamassa e pasta. Parte 1: Requisitos*. Rio de Janeiro.
- Associação Brasileira de Normas Técnicas. (2010). *NBR 15895: Materiais pozolânicos – Determinação do teor de hidróxido de cálcio fixado – Método Chapelle modificado*. Rio de Janeiro.
- Associação Brasileira de Normas Técnicas. (2015). *NBR 16372: Cimento Portland e outros materiais em pó - Determinação da finura pelo método de permeabilidade ao ar (método de Blaine)*. Rio de Janeiro.
- Associação Brasileira de Normas Técnicas. (2017). *NBR 16605: Cimento Portland e outros materiais em pó - Determinação da massa específica*. Rio de Janeiro.
- Associação Brasileira de Normas Técnicas. (2018). *NBR 16606: Cimento Portland - Determinação da pasta de consistência normal*. Rio de Janeiro.
- Associação Brasileira de Normas Técnicas. (2018). *NBR 16607: Cimento Portland - Determinação dos tempos de pega*. Rio de Janeiro.
- Associação Brasileira de Normas Técnicas. (2018). *NBR 16697: Cimento Portland - Requisitos*. Rio de Janeiro.
- Associação Brasileira de Normas Técnicas. (2021). *NBR 16916: Agregado miúdo - Determinação da densidade e da absorção de água*. Rio de Janeiro.
- Associação Brasileira de Normas Técnicas. (2021). *NBR 16972: Agregados - Determinação da massa unitária e do índice de vazios*. Rio de Janeiro.
- Associação Brasileira de Normas Técnicas. (2021). *NBR 16973: Agregados - Determinação do material fino que passa pela peneira de 75 μm por lavagem*. Rio de Janeiro.
- Associação Brasileira de Normas Técnicas. (2001). *NBR NM 49: Agregado miúdo - Determinação de impurezas orgânicas*. Rio de Janeiro.
- Bahedh, M. A., Jaafar, M. S. (2018), *Ultra High-Performance Concrete Utilizing Fly Ash as Cement Replacement under Autoclaving Technique. Case Studies in Construction Materials*. 9. <https://doi.org/10.1016/j.cscm.2018.e00202>
- Castro, A., Ferreira, F. (2016), *Effect of particle packing in the durability of high performance concretes*. *Revista Ingeniería de Construcción*. 31(2):91 – 104. <http://dx.doi.org/10.4067/S0718-50732016000200003>
- Castro, A. L., Pandolfelli, V. C. (2009), *Revisão: Conceitos de dispersão e empacotamento de partículas para a produção de concretos especiais aplicados na construção civil*. *Cerâmica*. 55:18-32. <https://doi.org/10.1590/S0366-69132009000100003>
- De Larrard, F., Sedran, T. (1994), *Optimization of ultra-high performance concrete by the use of a packing model*. *Cement and Concrete Research*. 24(6):997-1009. [https://doi.org/10.1016/0008-8846\(94\)90022-1](https://doi.org/10.1016/0008-8846(94)90022-1)
- Melo, A. B. (2020), *“Influência da cura térmica (vapor) sob pressão atmosférica no desenvolvimento da microestrutura dos concretos de cimento Portland”*, Tese (Doutorado), Universidade de São Paulo, p. 296.
- Du, H., Tan, K. H. (2014). *Effect of particle size on alkali-silica reaction in recycled glass mortars*. *Construction and Building Materials*. 66: 275-285. <https://doi.org/10.1016/j.conbuildmat.2014.05.092>
- Funk, J. E.; Dinger, D. R. (1994), *Predictive process control of crowded particulate suspensions: applied to ceramic manufacturing*. New York: Springer Science Business Media.
- Ganesh, P., Murthy, A. R. (2019), *Tensile behaviour and durability aspects of sustainable ultra-high performance concrete incorporated with GGBS as cementitious material*. *Construction and Building Materials*. 197:667-680. <https://doi.org/10.1016/j.conbuildmat.2018.11.240>
- Heinz, D., Urbonas, L., Gerlicher, T. (2012), *“Effect of Heat Treatment Method on the Properties*

- of UHPC” in: M. Schimdt, E. Fehling, C. Glotzbach, S. Fröhlich, S. Piotrowski (Eds.), *Ultra-High Performance Concrete and Nanotechnology in Construction*, HiperMat, Kassel, HE, (Germany), pp. 283-290.
- Instituto de Pesquisa Econômica Aplicada (IPEA). (2012), “*Diagnóstico dos Resíduos Sólidos Urbanos*”. Disponível em: <https://www.ipea.gov.br/portal/images/stories/PDFs/relatoriopesquisa/121009_relatorio_residuos_solidos_urbanos.pdf>. Acesso em: 27 de março de 2020.
- Kantro, D. (1980), *Influence of Water-Reducing Admixtures on Properties of Cement Paste—A Miniature Slump Test*. Cement, Concrete and Aggregates. 2(0):95-102. <https://doi.org/10.1520/CCA10190J>.
- Lopes, H. M. T. (2019), “*Aplicação do conceito de empacotamento de partículas na otimização de dosagem de concretos de cimento Portland*”, Dissertação (Mestrado), Universidade de São Paulo, p. 172.
- Mehta, A., Ashish, D. K. (2020), *Silica fume and waste glass in cement concrete production: A review*. Journal of Building Engineering. <https://doi.org/10.1016/j.jobbe.2019.100888>
- Schwarz, N., Cam, H., Neithalath, N. (2008), *Influence of a fine glass powder on the durability characteristics of concrete and its comparison to fly ash*. Cement & Concrete Composites. 30: 486–496. <https://doi.org/10.1016/j.cemconcomp.2008.02.001>
- Shi, C., Wu, Z., Xiao, J., Wang, D., Huang, Z., Fang, Z. (2015), *A review on ultra-high-performance concrete: Part I. Raw materials and mixture design*. Construction and Building Materials. 101:741-751. <https://doi.org/10.1016/j.conbuildmat.2015.10.088>
- Sokolovicz, B. C. (2020), “*Avaliação das propriedades mecânicas e microestrutura de concreto de ultra alto desempenho com adições minerais e resíduos industriais*”, Tese (Doutorado), Universidade Federal de Santa Maria, p. 358.
- Tam, C. M., Tam, V. W. Y., Ng, K. M. (2012). *Assessing drying shrinkage and water permeability of reactive powder concrete produced in Hong Kong*. Construction and Building Materials. 26:79-89. <https://doi.org/10.1016/j.conbuildmat.2011.05.006>
- Terzian, P. (2005), *Concreto pré-fabricado*. In: Isaia G. C. “*Concreto Ensino Pesquisas e Realizações*”, São Paulo, IBRACON, v.2.
- Tutikian B., F., Isaia, G. C., Helene, P. (2011), *Concreto de Alto e Ultra-Alto Desempenho*. In: Isaia, G. C. “*Concreto: Ciência e Tecnologia*”, São Paulo, IBRACON.
- Wang, X., Yu, R., Song, Q., Shui, Z., Liu, Z., Wu, S., Hou, D. (2019), *Optimized design of ultra-high-performance concrete (UHPC) with a high wet packing density*. Cement and Concrete Research. 126. <https://doi.org/10.1016/j.cemconres.2019.105921>
- Zhang, H., Ji, T., Lin, X. (2019), *Pullout behavior of steel fibers with different shapes from ultra-high performance concrete (UHPC) prepared with granite powder under different curing conditions*. Construction and Building Materials. 211: 688-702. <https://doi.org/10.1016/j.conbuildmat.2019.03.274>

Simulation of pathological manifestations in diaphragm wall through ultrasonic wave propagation

R. R. C. Silva^{1*} , C. Bertoldo² 

*Contact author: rodrigoroferiodoutorado@gmail.com

DOI: <https://doi.org/10.21041/ra.v12i2.564>

Reception: 01/11/2021 | Acceptance: 19/02/2022 | Publication: 01/05/2022

ABSTRACT

This research aimed to simulate pathological manifestations in diaphragm wall using concrete produced with different additions of synthetic polymer, in order to obtain models of strength and stiffness prediction through ultrasound wave propagation. Compression tests were performed to determine strength and stiffness, as well as ultrasound tests by direct and indirect method on concrete produced with different concentrations of synthetic polymer. The results suggested a decrease in the mechanical and acoustic properties of concrete with the increase in the concentration of synthetic polymer. The models generated by the ultrasonic test were statistically significant, at 95% confidence level, and the correlations established in concrete can be applied in the detection of pathological manifestations in loco.

Keywords: diaphragm wall ultrasonic wave propagation; strength and stiffness.

Cite as: Silva, R. R. C., Bertoldo, C. (2022), "*Simulation of pathological manifestations in diaphragm wall through ultrasonic wave propagation*", Revista ALCONPAT, 12 (2), pp. 200 – 209, DOI: <https://doi.org/10.21041/ra.v12i2.564>

¹Laboratory of Nondestructive Testing - University of Campinas, Campinas/SP, Brasil.

Contribution of each author

In this study, Silva, R. R.C., contributed to the acquisition of financing activity, methodology, research, preparation of the experimental program of samples, draft and original writing, Pedroso, C.B. contributed to the conceptualization, methodology, supervision, and analysis of data.

Creative Commons License

Copyright 2022 by the authors. This work is an Open-Access article published under the terms and conditions of an International Creative Commons Attribution 4.0 International License ([CC BY 4.0](https://creativecommons.org/licenses/by/4.0/)).

Discussions and subsequent corrections to the publication

Any dispute, including the replies of the authors, will be published in the first issue of 2023 provided that the information is received before the closing of the third issue of 2022.

Simulación de manifestaciones patológicas en muro pantalla mediante propagación de pulso ultrasónico

RESUMEN

El objetivo de esta investigación fue simular manifestaciones patológicas en muros pantalla a través de hormigones elaborados con diferentes adiciones de polímero sintético, proponiendo obtener modelos de predicción de resistencia y rigidez a través de la propagación de ondas de ultrasónica. Se realizaron ensayos de compresión para determinar resistencia y rigidez, así como ensayos de ultrasonido por el método directo e indirecto sobre hormigones producidos con diferentes concentraciones de polímero sintético. Los resultados obtenidos indicaron una disminución de las propiedades mecánicas y acústicas del hormigón con el aumento de la concentración de polímero sintético en su confección. Los modelos generados por la prueba ultrasónica fueron estadísticamente significativos, con un nivel de confianza del 95%, y las correlaciones establecidas en concreto pueden ser utilizadas en la detección de manifestaciones patológicas in loco.

Palabras clave: muros pantalla; propagación de pulso ultrasónico; fuerza y rigidez.

Simulação de manifestações patológicas em parede diafragma através de propagação de ondas ultrassônicas

RESUMO

O objetivo dessa pesquisa foi simular manifestações patológicas em parede diafragma através de concretos produzidos com diferentes adições de polímero sintético, propondo obter modelos de predição de resistência e rigidez através de propagação de onda de ultrassom. Foram realizados ensaios de compressão para determinação da resistência e rigidez, assim como ensaios de ultrassom pelo método direto e indireto em concretos produzidos com diferentes concentrações de polímero sintético. Os resultados obtidos indicaram queda nas propriedades mecânicas e acústicas do concreto com o aumento da concentração de polímero sintético em sua confecção. Os modelos gerados pelo ensaio ultrassônico foram estatisticamente significativos, ao nível de confiança em 95%, podendo, as correlações estabelecidas em concreto, serem utilizadas na detecção de manifestações patológicas in loco.

Palavras-chave: parede diafragma; propagação de ondas ultrassônicas; resistência e rigidez

Legal Information

Revista ALCONPAT is a quarterly publication by the Asociación Latinoamericana de Control de Calidad, Patología y Recuperación de la Construcción, Internacional, A.C., Km. 6 antigua carretera a Progreso, Mérida, Yucatán, 97310, Tel.5219997385893, alconpat.int@gmail.com, Website: www.alconpat.org

Reservation of rights for exclusive use No.04-2013-011717330300-203, and ISSN 2007-6835, both granted by the Instituto Nacional de Derecho de Autor. Responsible editor: Pedro Castro Borges, Ph.D. Responsible for the last update of this issue, Informatics Unit ALCONPAT, Elizabeth Sabido Maldonado.

The views of the authors do not necessarily reflect the position of the editor.

The total or partial reproduction of the contents and images of the publication is carried out in accordance with the COPE code and the CC BY 4.0 license of the Revista ALCONPAT.

1. INTRODUCTION

As civil constructions have been increasing in recent decades, studies have investigated ways to facilitate the execution of major constructions that face difficulties due to unstable soils in which they are located. According to Hachich et al. (2019), the use of a containment system with diaphragm wall which consists of open trench in the ground filled with reinforced concrete stabilized by the synthetic use of polymeric fluids or bentonite clay is one of the alternatives to assist in the excavation of soils.

The use of synthetic polymer in excavations has great advantages over traditional forms of soil stabilization, such the use of bentonite. According to Mota (2010), the economic aspect is an advantage, because polymers although its cubic meter is more expensive than bentonite clay require less amounts of product to obtain better yields than traditional forms (bentonite clay). According to Mota (2010), the environmental factor is also noteworthy, mainly because of some properties of polymers, namely: their high solubility, chemical sensitivity, and ultraviolet ray actions that end up fragmenting their polymer chains and, therefore, preventing bioaccumulations. Thus, the use of polymers as stabilizers in excavations do not affect the environment (Mota 2010).

Studies conducted by Mota (2010) found that the highly concentrated synthetic polymer can be used specifically to chemically interact with all types of soil as the basis of its stabilization. Its molecular structure allows for total water solubility, without changing its primary role of active chemical bonding in the stabilization of soil particles.

The use of this polymer during excavations should follow the recommendations of ABNT-NBR 6122 (2019), with concrete density ranging from 2.1 to 2.8 g/cm³ and minimum cement consumption of 400 kg/m³, and stabilizing fluid as polymer with water pH between nine and 12, density from 1.005 g/cm³ to 1.1 g/cm³ and sand content up to 4.5%. According to Djelal et al. (2020) one of the pathologies found on the diaphragm wall is related to the mixture of polymer fluid during concreting, increasing the infiltration of groundwater from the soil after the execution of the panels, compromising the concrete ability to resist compression.

In loco diaphragm walls are extremely difficult to be assessed, especially regarding the addition of synthetic polymer, and its influence in the quality of the concrete. The ultrasound test is one tests that do not damage the concrete containment system as suggested Silva (2020). Studies conducted by Savaliya et al. (2014), through ultrasound test in concrete structures, demonstrate that the method is able to accurately detect pathologies, identifying defects and its specific location.

Considering the aforementioned aspects, our project used non-destructive ultrasonic wave propagation tests, directly and indirectly, simulating in loco inspection to verify its sensitivity in predicting mechanical (strength and stiffness) and physical (water absorption) properties of concrete made with different concentrations of synthetic polymer.

Thus, this research aimed to simulate pathological manifestations in diaphragm wall with different quantities of synthetic polymer in the concrete, proposing models of prediction of strength and stiffness obtained through ultrasound wave propagation tests to evaluate this containment system in loco.

2. EXPERIMENTAL PROGRAM

For the research, concrete were made with CII-F cement proportions following the ABNT-NBR 11578 (1997): medium sand and gravel 01 (1:1.8:2.5), and the cement was measured in mass, aggregates by volume and water-cement ratio of 0.6, as specified for concrete structures as diaphragm walls (ABNT- NBR 6122, 2019). Considering the standard mixture, different percentages of synthetic polymer 0%, 20%, 40%, and 60% of granulated anionic polymer and high molecular weight > 21 million and long chains used for flocculation were added in relation to the

cement mass (Figure 1a). The characterization of the aggregates was carried out according to the recommendations of the standards for fine aggregate NBR (NM 248, 2003; NM 52, 2009; NM 45, 2006) and coarse aggregate NBR (NM 248, 2003, NM 53, 2003, NM 45, 2006). After 28 days, the samples were subjected to the immersion absorption test, according to the specifications of ABNT-NBR 9778 (2015).

Table 1 shows the characterization of aggregates within the limits of acceptability, according to ABNT - NBR 7211 (2009).

Table 1. Results of the physical characterization of fine and coarse aggregates.

Aggregate	Specific Mass (kg/m ³)	Unit mass (kg/m ³)	Maximum diameter (mm)	Fineness modulus
Granite	2650	1500	25	6.75
Sand	2590	1310	4.8	1.89

The addition of synthetic polymer presented a behavior similar to the addition of water to the concrete, especially when assessing workability (Slump Test values) and density, that is, the increment in polymer quantity increased workability and reduced the density (Table 2).

Table 2. Slump Test and medium density values of concrete produced with different synthetic polymer quantities.

Quantity	Slump Test (mm)	Average density (kg.m ⁻³)
0%	180	2223
20%	210	2097
40%	250	1934
60%	260	1900

After the Slump tests, 12 cylindrical specimens (100 mm in diameter and 200 mm in length) and one prismatic specimen (400 x 400 x 300 mm³) were molded for each mixture simulating part of a finished diaphragm wall, totaling 48 cylindrical and four prismatic specimens. After 28 days, the cylindrical samples were ultrasound-tested by direct wave propagation method (Figure 1b) and prismatic samples by indirect method (Figure 1c), representing the in loco inspection.

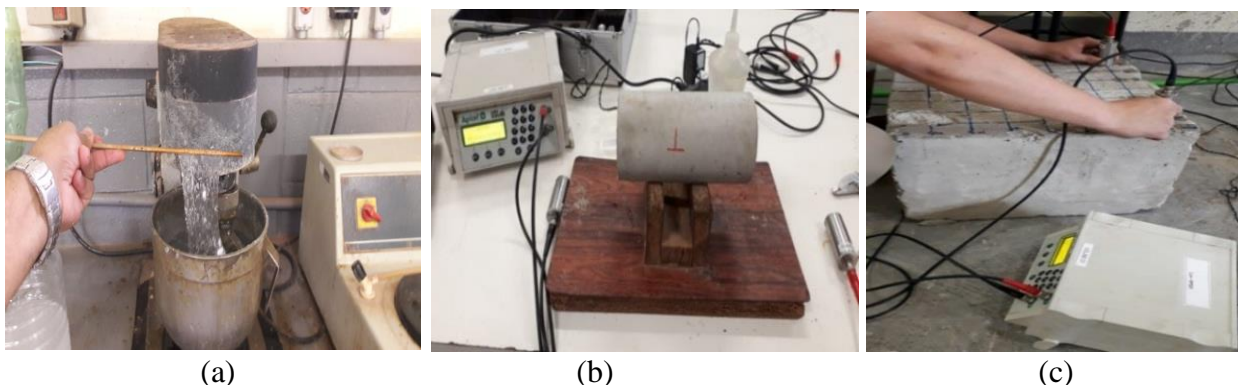


Figure 1. (a) Synthetic polymer, (b) cylindrical samples subjected to direct ultrasound test (c)

prismatic samples subjected to indirect ultrasound test. Source: authors (2021).

For the tests, ultrasound equipment (USLAB, Agricef, Brazil) and 45 KHz-frequency longitudinal transducers of flat faces were used. With the propagation times of ultrasound waves (t), it was possible to calculate, for each distance between transducers (L), the direct propagation velocity of ultrasound waves (V_D), using the equation proposed by ABNT NBR 8802 (2019), as in Equation (1).

$$V = \frac{L}{t} \quad (1)$$

After 28 days, the mass of each specimen was also determined using a precision scale, and with a digital caliper its dimensions were obtained to calculate the volume and the density. From the direct velocity and density of the concrete (ρ), the stiffness coefficient was determined (2).

$$C_{LL} = \rho \cdot V_D^2 \quad (2)$$

The prismatic samples, which represent the feasibility of inspection of a finished diaphragm wall using the indirect wave propagation method, were tested according to the methodology proposed by the ABNT-NBR 8802 (2019). The ABNT proposes a way of measuring the ultrasonic propagation velocity by indirect transmission mode (VI), whose procedure consists of calculating the velocity through a propagation time graph versus distance between transducers Figure (2).

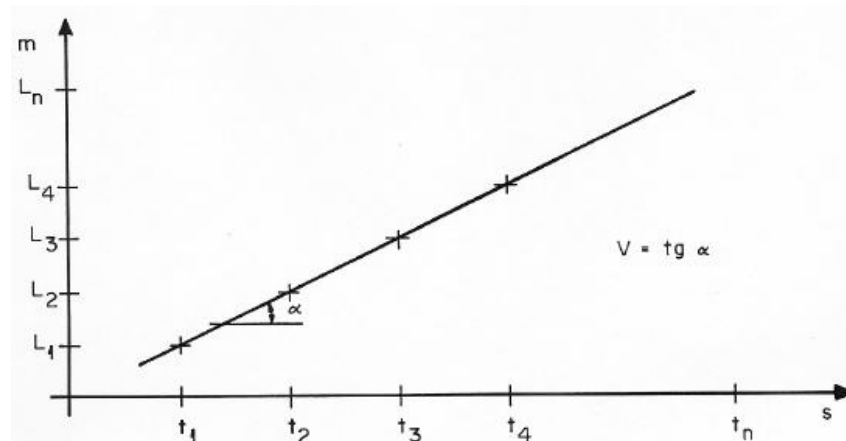


Figure 2. Determination of the propagation velocity of ultrasound waves by indirect method.

Source: ABNT-NBR 8802 (2019).

The specimens were then subjected to a compression test in a EMIC machine to determine the strength (f_c - ABNT-NBR 5739, 2018) and the elastic modulus (E_{ci} - ABNT-NBR 8522, 2017). The results of the tests were used in the creation of models to predict the mechanical properties based on the propagation velocity of ultrasound waves.

The results of f_c and E_{ci} and the parameters of propagation of ultrasound velocity waves (V_D), (V_I) and (C_{LL}) were used to analyze regressions in order to verify the existence of statistically significant models between mechanical properties and acoustic properties, obtained through ultrasound wave propagation tests.

3. RESULTS AND DISCUSSIONS

The mechanical (f_c and E_{ci}) and acoustic properties (C_{LL} , V_D , and V_I) of the concrete also reduced as polymer quantities increased, a fact related to increased porosity (amount of voids) of the concrete. Table 3 shows the tests performed on the 12 concrete samples for each studied mixture.

Table 3. Minimum, maximum, and mean values of strength (f_c), elasticity (E_{ci}), Stiffness Coefficient (C_{LL}) direct (V_D) and indirect velocity (V_I) for the mixtures produced with different polymer quantities.

Quantities	f_c (MPa)	E_{ci} (GPa)	C_{LL} (GPa)	V_D (m.s ⁻¹)	V_I (m.s ⁻¹)
	Min. Max. Mean	Min. Max. Mean	Min. Max. Mean	Min. Max. Mean	Min. Max. Mean
0%	16.9; 20.5; 17.41	19.58; 27.80; 23.28	27.23; 34.38; 30.16	3485; 3885; 3680	2437; 2855; 2639
20%	8.32; 9.6; 8.80	11.44; 16.13; 13.10	19.87; 22.42; 21.26	3095; 3230; 3185	2421; 2628; 2520
40%	5.53; 6.78; 6.17	5.80; 9.85; 7.48	9.81; 17.29; 13.14	2386; 2788; 2615	1886; 2518; 2127
60%	4.13; 4.96; 4.60	2.03; 3.13; 2.95	7.88; 15.69; 12.83	2040; 2858; 2528	804; 1085; 935

To avoid dispersion of the we used the mean of the results of strength, stiffness, and acoustic parameters for statistical analyses. The linear regression models evaluated by analysis of variance (ANOVA) were statistically significant at the 95% confidence level (P -value < 0.05), and the best models for predicting concrete strength (f_c) and stiffness (E_{ci}) properties were obtained based on the stiffness coefficient (C_{LL}) (Table 4).

The models found are within the ranges of coefficients of determination (R^2) found in the literature regarding mechanical tests and wave propagation. For the prediction of f_c , the R^2 in the studies conducted by Mohamad et al. (2016) and Silva et al. (2020), ranged from 60 to 98% and, for E_{ci} , from 50 to 96%, (Giacon et al., 2010; Mohamed et al., 2016, and Silva et al., 2020). Correlations between the stiffness parameters (C_{LL}) and the mechanical properties of strength (f_c) and elastic modulus (E_{ci}) obtained in ultrasound and compression tests were found by Giaccon et al., (2010) and Silva (2020), with linear models and R^2 values ranging from 85% to 97% for E_{ci} and from 79% to 95% for f_c .

Absolute error values of the strength and elastic modulus of the concrete range from 25% to 50% when based on models with wave propagation parameters (Bungey and Millard, 2006). In our research, the absolute errors found (9.70% to 20% – Table 4) are below those found in the literature, suggesting that the models for predicting strength and stiffness are valid in the evaluation of the quality of concrete used in diaphragm walls, using acoustic parameters of wave propagation.

Table 4. Correlation models between direct velocity (V_D), indirect velocity (V_I) and stiffness coefficient (C_{LL}) parameters with compressive strength (f_c) and initial Elastic Modulus (E_{ci}).

Parameter	Model	P-Value	R ² (%)	Estimation error	Absolute error* (%)
$f_c \times V_D$	$f_c = -20.34 + 0.0098 * V_D$	0.03	92.81	1.70	18.40
$f_c \times V_I$	$f_c = -5.25 + 0.0068 * V_I$	0.04	81.65	1.87	20.3
$f_c \times C_{LL}$	$f_c = -3.96 + 0.68 * C_{LL}$	0.025	97.46	1.57	9.70
$E_{ci} \times V_D$	$E_{ci} = -35.13 + 0.015 * V_D$	0.01	96.91	1.83	18.90
$E_{ci} \times V_I$	$E_{ci} = -11.68 + 0.012 * V_I$	0.04	89.00	1.90	20.60
$E_{ci} \times C_{LL}$	$E_{ci} = -8.56 + 1.05 * C_{LL}$	0.020	97.97	2.14	12.37

*Relationship between estimated error and mean value.

Table 5 shows the results obtained from immersion absorption and the longitudinal velocity of the tested samples after saturation. Notably, the addition of synthetic polymer increased water absorption (Table 5), leaving more voids (pores) after the drying process. This aspect occurs because of the release of internal curing, which leads to the swell of polymer particles, changing the porous structure of cement (Araújo and May, 2019).

Table 5. Absorption values by immersion and average direct velocity (V_D), for the shapes produced with different additions of synthetic polymer.

Sample	Absorption	V_D ($m.s^{-1}$)
0%	12.0	3087
20%	12.4	2777
40%	17.3	2291
60%	18.4	1846

Note that, due to the change in the absorbed volume of water, changes in acoustic properties are observed (Tables 3 and 5). Also, it can be noted that the velocities of sound propagation decrease as the amount of polymer used increases; the voids found in dry concrete are a significant factor in the transmission of sound waves, since the ultrasonic pulse velocity is lower in the air than in solids (Godinho, et al., 2020), thus explaining the increase in the amount of pores, reducing the propagation velocity of ultrasonic waves in the specimens.

The regression between ultrasound velocity and absorption showed a model with R² of 92% (Figure 3) and P-Value of $0.04 < 0.05$, demonstrating that there is a statistically significant relationship between the parameters, with a 95% confidence level, obtained through ANOVA. The outcomes suggest that the wave propagation method is sensitive to the increase of water content inside the samples, caused by increased porosity after drying the synthetic polymer within the cement, decreasing its ultrasound velocity. Thus, the concrete will present more voids (pores) and, therefore, absorbing more water and presenting lower density and mechanical properties. Water is the main erosive agent in concrete, therefore concrete performance as a barrier to reduce the transport of potentially corrosion-causing agents is related to its porosity (Dudhal, 2016; Liu et al., 2020; Matiko, 2000).

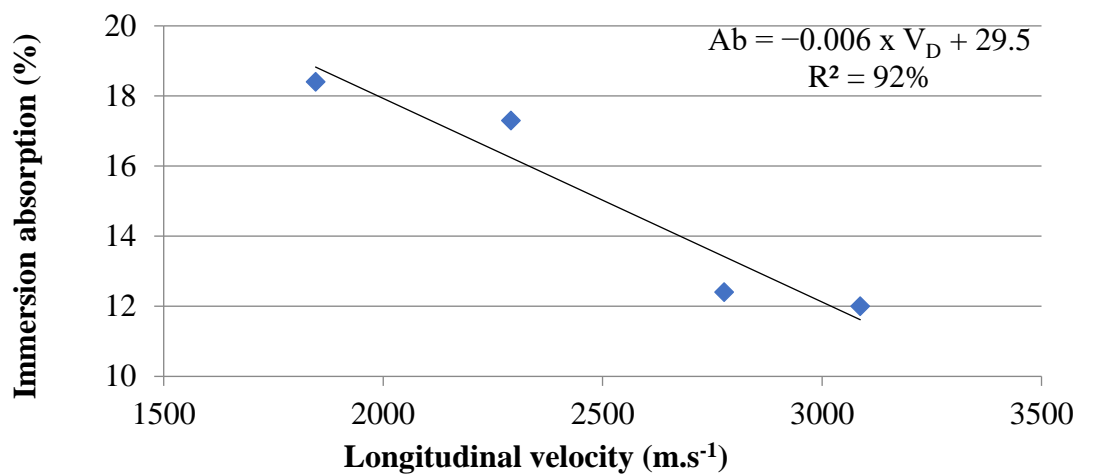


Figure 3. Regression model between immersion absorption and longitudinal velocity.
Source: Authors (2021).

The polymer aggregates and forms a film on the surface of cement particles during the hydration, avoiding additional contact between cement and water, increasing the cement porosity, thus affecting the compressive strength and elastic modulus of polymer-added concrete (Liu et al., 2020).

Our research corroborates with the literature. Table 3 shows a 26% reduction for the mean values of f_c and 13% for the mean values of E_{ci} , after an 18% increase in absorption for concrete samples with the addition of 60% of synthetic polymer in relation to the samples without it (Table 5).

The models obtained can be used as a non-destructive alternative test to estimate mechanical and physical properties, such as water absorption in samples and diaphragm wall structures, verifying the infiltration of groundwater from the soil mass after the execution of the panels, a fact that may compromise concrete ability to resist compression.

4. CONCLUSIONS

The increment in the concentration of synthetic polymer used in the different concrete mixtures increased its workability, reducing its density and its mechanical (f_c and E_{ci}) and acoustic (V_D , V_I , and C_{LL}) properties.

The models of prediction of mechanical properties by ultrasound velocity were statistically significant, showing coefficients of determination higher than 80% and errors inferior to those found in the literature.

Thus, the sensitivity of the direct or indirect ultrasound wave propagation test is demonstrated, for concrete with physical and mechanical properties similar to those used in our research, and the correlations established here in concrete samples can be used to support the detection of in loco pathological manifestations.

Moreover, the increase in synthetic polymer content in the production of concrete directly interferes with the amount of water absorption and, consequently, in the acoustic properties of the material.

5. ACKNOWLEDGEMENTS

The authors thank the São Paulo Research Foundation (FAPESP) for funding the various research group projects, which made possible the facilities and infrastructure used in this research. The authors thank the Espaço de Escrita Pro-Reitoria de Pesquisa – Universidade Estadual de Campinas

for the linguistic services provided.

6. REFERÊNCIAS BIBLIOGRÁFICAS

- Associação Brasileira de Normas Técnicas (1997). *NBR 11578: Cimento Portland Composto*. Rio de Janeiro.
- Associação Brasileira de Normas Técnicas (2003). *NBR NM 248: Agregados: Determinação da composição granulométrica*. Rio de Janeiro.
- Associação Brasileira de Normas Técnicas (2006). *NBR NM 45: Agregados: Determinação da massa unitária e do volume de vazios*. Rio de Janeiro. 2006.
- Associação Brasileira de Normas Técnicas (2009). *NBR NM 53: Agregado graúdo – Determinação da massa específica, massa específica aparente e absorção de água*. Rio de Janeiro.
- Associação Brasileira de Normas Técnicas (2009). *NBR NM 52: Determinação da massa específica de agregados miúdos por meio de frasco Chapman*. Rio de Janeiro.
- Associação Brasileira de Normas Técnicas (1998). *NBR NM 67: Concreto: determinação da consistência pelo abatimento do tronco de cone*. Rio de Janeiro.
- Associação Brasileira de Normas Técnicas (2005). *NBR 9778: Argamassa e concreto endurecidos – Determinação da absorção de água por imersão – Índice de vazios e massa específica*. Rio de Janeiro.
- Associação Brasileira de Normas Técnicas (2009). *NBR 7211: Agregados para concreto - Especificação*. Rio de Janeiro.
- Associação Brasileira de Normas Técnicas (2016). *NBR 5738: Concreto: Procedimento para moldagem e cura de corpos de prova*. Rio de Janeiro.
- Associação Brasileira de Normas Técnicas (2018) *NBR 5739: Ensaio de compressão de corpos-de-prova cilíndricos de concreto*. Rio de Janeiro.
- Associação Brasileira de Normas Técnicas (2017). *NBR 8522: Concreto – Determinação dos módulos estáticos de elasticidade e de deformação à compressão*. Rio de Janeiro.
- Associação Brasileira de Normas Técnicas (2019). *NBR 8802: Concreto Endurecido – Determinação da velocidade de propagação da onda ultra-sônica*. Rio de Janeiro.
- Araújo, C. M. M, May, C. A. (2019). *Durabilidade de concretos de alta resistência com adição de polímero superabsorvente e nano partículas de sílica*. Monografia de projeto final em engenharia civil; Brasília; p. 124.
- Bungey J., Millard, S. (2006). *Testing of concrete in structures*. 3 ed. London: Blackie Academic e Professional.
- Djelal, C., Vanhove, Y., Azzi, A., Madec, O. (2020). *Recommendation for concrete mix design to prevent bleed channels on diaphragm walls*. European Journal of Environmental and Civil Engineering, p.1-13.
- Giacon Jr, M., Goncalves, R., Soriano, J., Amalfi, G. (2010). *Caracterização do concreto utilizando ultrassom*. In: XXVIII CONAENDI - Congresso de Ensaio Não Destrutivos e Inspeção, Santos - SP. Anais CONAENDI 2010. v. 1. p. 1-9.
- Godinho, J. P., Junior, T. F. S; Medeiros, M. H. F; Silva, M. S. A. (2020). *Factors influencing ultrasonic pulse velocity in concrete*: 13. ed. Curitiba: Revista Ibracon de Estruturas e Materiais.
- Hachich, W. et al. (2019). *Fundações: Teoria e Prática*. 2ª ed. São Paulo, Pini.
- Liu, B., Shi, J., Sun, M., He, Z., Xu, H., Tan, J. (2020). Mechanical and permeability properties of polymer-modified concrete using hydrophobic agent. *Journal of Building Engineering*, v. 31, p. 101337. <https://doi.org/10.1016/j.jobe.2020.101337>.
- Matiko, N. N. S. (2000). *Análise da porosidade e de propriedades de transporte de massa em concretos*. FAPESP.
- Mohammed, T. U., Rahman, M. N. (2016). *Effect of types of aggregate and sand-to-aggregate*

- volume ratio on UPV in concrete*. Construction and Building Materials, v. 125, p. 832-841. <https://doi.org/10.1016/j.conbuildmat.2016.08.102>.
- Savaliya, K. D., Thaker, K. K., Dave, U. V. (2014). *Comparison between Different Methods of Ultrasonic Pulse Velocity Tests on Concrete*. International Journal of Engineering Research and Applications (IJERA), (March), p. 41–44.
- Silva, R. R. C. (2020). *Propagação de ondas de ultrassom em sistemas de contenção par obras de terra*. Tese de Doutorado. UNICAMP - Universidade Estadual de Campinas. p.113.
- Silva, R. R. C., Gonçalves, R., Bertoldo, C. P. (2020). *Classification and inspection of reinforced concrete elements for use in retaining walls using ultrasound tests*. Construction and Building Materials, v. 262, p. 120010. <https://doi.org/10.1016/j.conbuildmat.2020.120010>.
- Hirde, S. K., Dudhal, Omprakash S. (2016). *Review on polymer modified concrete and its application to concrete structures*. International Journal of Engineering Research, ISSN, v. 3. P.766-769. <https://doi.org/10.17950/ijer/v5i3/053>.

Numerical analysis of the effect of variation of eccentricity of unbonded post-tensioned tendons on the structural behavior of flat slabs

R. Cattelan^{1*}, L. Cielo¹, A. Lübeck¹, A. B. S. Santos Neto¹

*Contact author: rogerio@ufsm.br

DOI: <https://doi.org/10.21041/ra.v12i2.570>

Reception: 11/11/2021 | Acceptance: 26/02/2022 | Publication: 01/05/2022

ABSTRACT

In this study, the effect of variations of eccentricity of tendons in unbonded post-tensioned flat slabs was evaluated. The correct positioning of strands in the assembly of unbonded post-tensioned flat slabs is essential for the structural system to achieve adequate performance and safety. Four different slab models were analyzed with variations in the height of the strands at different positions providing the change in eccentricity and increases in the number of tendons. Pre-compression stresses, stresses on the bottom and top faces, center vertical displacements, load balancing and passive reinforcement of the slabs were evaluated. The ADAPT Floor Pro commercial software was used for the analyses with the design conforming with standard NBR 6118:2014 and recommendations from standard ACI 318:2019. For the models evaluated, it was found that the variation in the eccentricity of the strands in the bottom face of the slab reduced the applied stresses more than variations in the top face.

Keywords: post-tensioned concrete, unbonded tendons, strand eccentricity.

Cite as: Cattelan, R., Cielo, L., Santos Lübeck, A., Neto, A. B. S. (2022), "Numerical analysis of the effect of variation of eccentricity of unbonded post-tensioned tendons on the structural behavior of flat slabs", Revista ALCONPAT, 11 (2), pp. 210 – 226, DOI: <https://doi.org/10.21041/ra.v12i2.570>

¹ Universidade Federal de Santa Maria, Av. Roraima nº 1000 Cidade Universitária Bairro - Camobi, Santa Maria - RS, 97105-900, Brazil.

Contribution of each author

All authors contributed equally in the conception and definition of the methodology. Author Cielo contributed to the numerical model (100%), analysis and discussion of results (25%) and writing (100%). Author Lima contributed with advising (50%), analysis and discussion of results (25%) and proofreading (34%). Author Santos Neto contributed with advising (50%), analysis and discussion of results (25%) and proofreading (33%). Author Lübeck contributed with analysis and discussion of results (25%) and proofreading (33%).

Creative Commons License

Copyright 2021 by the authors. This work is an Open-Access article published under the terms and conditions of an International Creative Commons Attribution 4.0 International License ([CC BY 4.0](https://creativecommons.org/licenses/by/4.0/)).

Discussions and subsequent corrections to the publication

Any dispute, including the replies of the authors, will be published in the first issue of 2023 provided that the information is received before the closing of the third issue of 2022.

Análise da influência da variação da excentricidade de cordoalhas engraxadas no comportamento estrutural de lajes lisas protendidas

RESUMO

Neste estudo, avaliou-se a influência de variações de excentricidade dos cabos em lajes lisas protendidas. O correto posicionamento das cordoalhas na montagem de lajes lisas protendidas é imprescindível para que o sistema estrutural alcance desempenho e segurança adequados. Analisou-se quatro modelos diferentes com modificação da altura dos cabos em diferentes pontos e quantidades. Foram avaliadas tensões de pré-compressão, tensões nas faces inferior e superior, flechas, balanceamentos de cargas e armaduras passivas. Utilizou-se o programa ADAPT Floor Pro para as análises, sendo o dimensionamento regido pela NBR 6118:2014 e recomendações do ACI 318:2019. Constatou-se que a variação na excentricidade vertical das cordoalhas na face inferior da laje, reduzem mais os valores das tensões, em comparação com a variação na face superior.

Palavras-chave: Concreto Protendido, Protensão Não Aderente, Excentricidade de Cordoalhas.

Análisis de la influencia de la variación de excentricidad de tendones no-adherentes en el comportamiento estructural de losas planas postensadas

RESUMEN

En este estudio se evaluó la influencia de las variaciones de excentricidad de los cables en modelos con losas planas postensadas. El correcto posicionamiento de los tendones en el montaje de losas planas postensadas es fundamental para que el sistema estructural logre un adecuado rendimiento y seguridad. Se analizaron cuatro modelos arquitectónicos diferentes con modificación de la altura de los cables en diferentes puntos y cantidad. Se evaluaron tensiones de pre compresión, tensiones extremas en el tope y base, desplazamientos verticales, balanceo de carga y cantidad de acero pasivo de las losas. Para el análisis se utilizó el software ADAPT Floor Pro. El proyecto sigue las recomendaciones de la NBR 6118:2014 y ACI 318:2019. Para los modelos evaluados, se encontró que la variación en la excentricidad vertical de los tendones en la base de la losa reduce aún más los valores de las tensiones aplicadas, en comparación con la variación en el tope.

Palabras clave: hormigón postensado; postensión no-adherente; excentricidad de los tendones.

Legal Information

Revista ALCONPAT is a quarterly publication by the Asociación Latinoamericana de Control de Calidad, Patología y Recuperación de la Construcción, Internacional, A.C., Km. 6 antigua carretera a Progreso, Mérida, Yucatán, 97310, Tel.5219997385893, alconpat.int@gmail.com, Website: www.alconpat.org

Reservation of rights for exclusive use No.04-2013-011717330300-203, and ISSN 2007-6835, both granted by the Instituto Nacional de Derecho de Autor. Responsible editor: Pedro Castro Borges, Ph.D. Responsible for the last update of this issue, Informatics Unit ALCONPAT, Elizabeth Sabido Maldonado.

The views of the authors do not necessarily reflect the position of the editor.

The total or partial reproduction of the contents and images of the publication is carried out in accordance with the COPE code and the CC BY 4.0 license of the Revista ALCONPAT.

1. INTRODUCTION

The use of unbonded tendons in building construction is frequent in developed countries like the USA and Australia, as well as parts of the Middle East, Southeast Asia, United Kingdom and in some South American countries. The choice of its use is due to excellent structural performance and economic advantages (Aalami, 2000; Santos, 2017; Silva *et al.*, 2018).

Unbonded tendons were included in standard ACI 318 of the American Concrete Institute from 1963 and onwards after its use in several construction projects around the world (Aalami, 2000; Kang and Bondy, 2008). In Brazil, the use of unbonded tendons in post-tensioned flat slabs started only in 1997 (Carvalho, 2017). This was partially driven by architectural designs with wide spans and reduced number of pillars and beams in upscale residential buildings (Santos, 2017; Almeida, 2001; Loureiro, 2006). Other decisive factors that promoted the effective application of post-tension concrete in civil construction were the development of high strength steel, advancements in design software and its relative ease of execution (Carvalho, 2017; Loureiro, 2006).

Prestressing has economic benefits and improves performance throughout the projected service life (PSL) and structural safety of concrete. In particular, it improves durability as the prevention or decrease in fissuring inhibits corrosion and ensures greater protection to the reinforcement (NBR 6118, 2014; Cholfe and Bonilha, 2018; Silva, 2003).

In flat slabs with post-tensioned unbonded tendons, the strands are usually placed in a parabolic arch which produces an eccentricity with respect to the center of the slab. This allows an increase in the loads applied to the strands and also increases the load balancing capacity (Pfeil, 1984; Vicente and Albino, 1994). The basic principle of load balancing is to allow the vertical portion of the tendons stress to balance out part of the dead load and result in a structure subjected only to compressive stresses (Silveira, 2002; Aalami, 1990; Aalami and Bommer, 1999). In order to accomplish this, vertical tendon placement must be as close as possible as projected. Incorrect vertical placement could lead to negative consequences such as different center deflection from predicted values and, in more severe cases, even structural collapse (Silva *et al.*, 2018; Aalami and Bommer, 1999; Romanichen and Souza, 2019).

In order to ensure vertical strand placement in accordance to projected values, spacers are used in regular intervals. Mass-produced spacers are made from plastic or steel with rigorous quality control with respect to height. However, in some exceptional cases, spacers are manufactured *in situ* with folded steel bars and inadequate quality control, resulting in variations in height (Loureiro, 2006; Aalami, 2014). Furthermore, other factors such as improper handling of the reinforcement or damage to it during pouring of concrete can lead to breaking or displacement of spacers as shown in Figure 1. Even with proper quality control, there is a human factor that can result in incorrect placement of spacers during tendon assembly. The end result of all these factors are strands placed at heights and eccentricities different than projected.

The incorrect placement of strands can lead to slab fissuring, excessive vertical displacements and loading stresses different from predicted to the point of exceeding projected limits of tension and compression in the structural element. Further effects can occur such as concrete flaking and acceleration of steel corrosion due to insufficient cover (Souza, 2018; Xin and Xianyan, 2012).



Figure 1. Concrete pouring example: (a) workers in direct contact with the reinforcement and (b) damaged and out of position spacer.

The correct vertical positioning of strands in accordance with projected values during the assembly stage has been cited as the main factor affecting system performance (Carvalho, 2017; Souza Junior and Oliveira, 2016; Caro *et al.*, 2013). Cauduro (2002) recommended a maximum tolerance of ± 5 mm in vertical variations of stand placement for slabs of less than 200 mm thick and ± 10 mm for slabs between 200 mm and 600 mm thick. The most critical locations were the low and high points in the curvature, while horizontal position was not as crucial but excessive variation should be avoided. However, acceptable variations in absolute deviation, which were independent of structural geometry and applied loads, could still lead to an unsafe structural condition. Variations in tendon eccentricity could have an effect depending on slab thickness, relative eccentricity error, span width between pillars and applied load.

This study evaluated the effect of variations in eccentricity of tendons in flat, post-tensioned slabs. Several models were tested with different spans and relative error in eccentricity. The post-tensioned slabs were projected in accordance with standard ABNT NBR 6118:2014 and recommendations from ACI 318:2019.

2. METHODOLOGY

2.1 Slab Geometry and Strand Layout

The structural models consisted of a single slab supported directly by pillars and without beams as shown in Figure 2. The span between pillars was constant for each model. Four models were manufactured with spans of 7.0 m x 7.0 m to 10.0 x 10.0 m in 1 m increments and were designated M7, M8, M9 and M10. The slab thickness varied for each model and were defined approximately as $L/42$ (ACI 318, 2019), where L is the span between pillars. The characteristics of each model are shown in Table 1.

Strand layout concentrated tendons along the larger direction (in this case, Strands 1 through 3 in the x-direction) and a more regular distribution was applied in the perpendicular direction (in this case, Tendons 1 through 27 in the y-direction) as seen in Figure 3. The analyses were exclusive to central Strand 2 in the x-direction since it concentrated the most loads and should be the most affected by variations in eccentricity of each model. The number of tendons in central Strand 2 for models M7, M8, M9 and M10 were 10, 17, 25 and 33, respectively. Also shown in Fig.3 are the locations of the pillars, labeled P1 through P12.

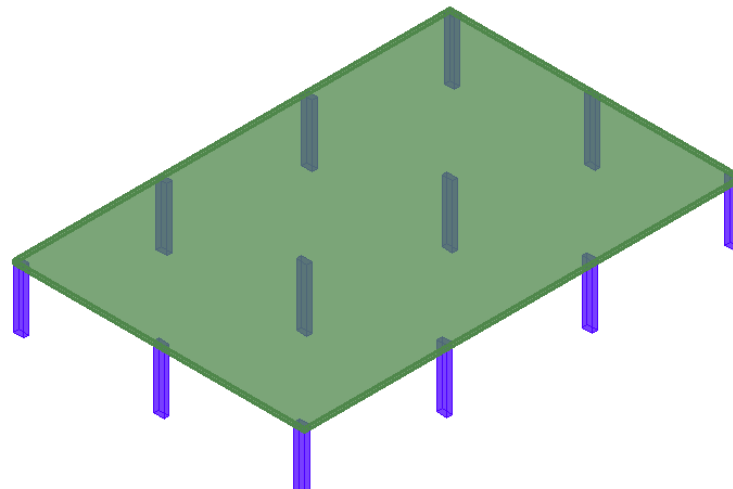


Figure 2. Sample structural model of post-tensioned slab for analysis.

Table 1. Model designations and dimensions

	Designation	Span between pillars	Slab thickness
Model	M7	7.0 m x 7.0 m	170 mm
	M8	8.0 m x 8.0 m	190 mm
	M9	9.0 m x 9.0 m	210 mm
	M10	10.0 m x 10.0 m	240 mm

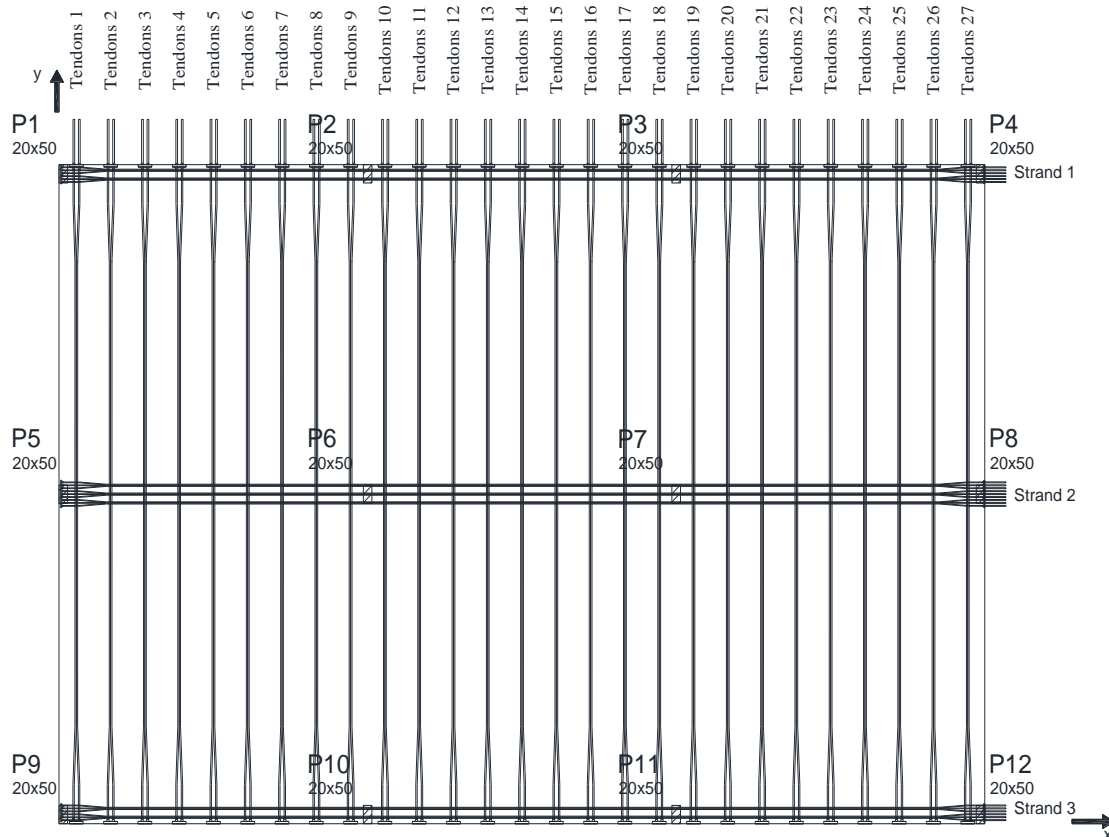


Figure 3. Layout of unbonded tendons and strands in a model post-tensioned slab.

The variations in eccentricity are shown schematically in Figure 4. Concave down eccentricities curving towards the top of the slab were placed on locations above pillars while concave up eccentricities towards the bottom of the slab were placed in the span between pillars. Three test cases of variation of eccentricity were tested. In the first case, only concave down eccentricity (designated “Top”) was reduced over pillars P6 and P7. In the second case, only concave up eccentricity in was reduced in the span between pillars (designated “Bottom”). In the third case, a simultaneous decrease in eccentricity in both locations was applied in order to obtain a critical combination (designated “Critical”).

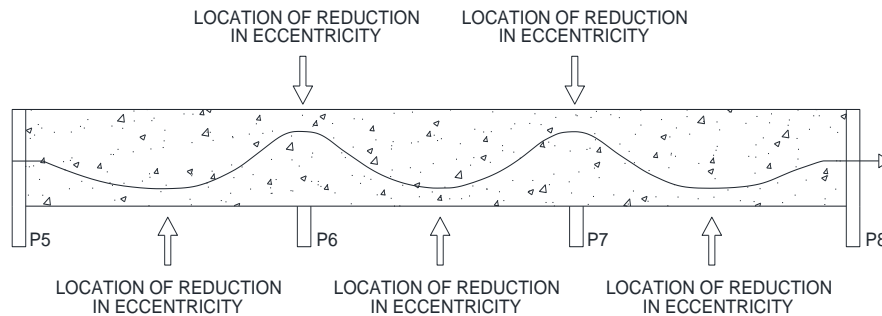


Figure 4. Variation of eccentricity along center Strand 2 and locations of reduction of eccentricity.

A total of 4 variations of eccentricity were applied to each of the 4 models shown in Table 1, designated hypothesis H1 through H4. The variations in eccentricity were of 5 mm, 10 mm, 15 mm and 20 mm. These variations were selected because projected spacer heights are usually listed in 5 mm increments and it would also allow easier and practical verification *in loco*. Additionally, Cauduro (2002) established that decreases in eccentricity should be limited to 5 mm and 10 mm for slab thicknesses equal or larger than the ones of this study. The variations of eccentricity and their designations are shown in Table 2.

Table 2. Designations of variations in eccentricity of this study.

Variation	Designation	Decrease in eccentricity (mm)
Reference	H0	0
Hypothesis 1	H5	5
Hypothesis 2	H10	10
Hypothesis 3	H15	15
Hypothesis 4	H20	20

For the analysis, the spans with decreased eccentricity were labeled “First” between P5 and P6, “Central” between P6 and P7 and “Final” between P7 and P8. These are shown in Figure 5.

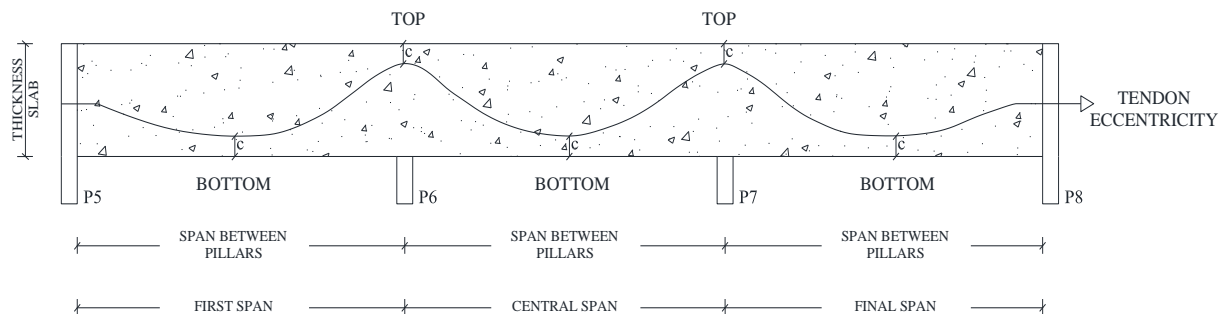


Figure 5. Designation of spans with variations of eccentricity.

2.2 Materials and Reference Parameters

Concrete covers were 2.5 cm for slabs with passive reinforcements and 3.0 cm for active reinforcements. In the numerical models, a C35 class concrete was adopted with a f_{ck} of 35.0 MPa and modulus of elasticity (E) of 39.7 GPa. The tendons used were CP 190 RB ($f_{ptk} = 1,900$ MPa), nominal diameter of 12.7 mm and nominal steel area of 100.9 mm².

A variable (over)load of 2.5 kN/m² was applied to the slab, which corresponded to the minimum value recommended in standard NBR 6120 (ABNT, 2019). A dead load consisting of the structure's own weight based on slab thickness and a permanent load of 1.0 kN/m² representing other materials was also present.

The numerical analysis considered three fundamental parameters: minimum pre-compression strength, tensile normal stress limit and maximum vertical displacement. Other criteria such as load balance and final displacements were adjusted once these fundamental parameters were reached. Afterwards, the slabs were loaded in order to test projected service life (PSL) and useful service life (USL). The pre-compression stress at any point in the slab was kept at a minimum of 1.0 MPa in accordance with ACI 318 (ACI, 2019) and NBR 6118 (ABNT, 2014). In pre-testing, models in which the pre-compression stress of 1.0 MPa was insufficient to produce the tensile normal stress limit or maximum vertical displacements, the number of tendons was increased until these parameters were reached.

Whenever possible, a load balance parameter between 60% and 80% of the permanent load was adopted. This range of values was commonly used in slabs of residential and commercial buildings and parking garages (Loureiro, 2006).

A limited stress was defined in accordance with standard NBR 6118 (ABNT, 2014). As described, the tension stress of a flat slab was defined as sufficient for fissure formation at PSL (f-PSL) from a combination of loads under any class of environmental aggression. In this case, the normal compressive stress applied to the concrete when stressing was limited to 15.75 MPa while the f-PSL threshold stress was 21.0 MPa in accordance with standard ACI 318 (ACI, 2019).

Standard NBR 6118 (ABNT, 2014) defined minimum measurable vertical displacements in beams and slabs as $L/250$, where L is the span in between pillars. This value was used as a limit in the numerical models before variations in eccentricity of the strands were introduced. After the variations in eccentricity were introduced, analyses were performed to confirm which models were still within limits. Through this methodology, passive reinforcements, strand placement and maximum acceptable strand eccentricity were determined for each model. Passive bottom and top reinforcements were determined for the models based on criteria from standard NBR 6118 (ABNT, 2014). The combined criteria and limits used in the slabs are presented in Table 3.

2.3 Slab Analysis

Slabs were analyzed with Adapt Floor 2017 PRO commercial software. This program specialized in the design and analysis of post-tensioned concrete structures with a finite element method. The program evaluated the effects of post-tensioning in accordance with geometry and loading on the strands.

Adapt Floor 2017 PRO provided automatic mesh generation with user input on the size of elements. Two maximum element sizes were tested in this study and the results showed no significant differences. Consequently a maximum element size of 500 mm was used for all analyses. A sample mesh for model M8 is shown in Figure 6.

Table 3. Model criteria and limits with references.

Criteria	Limit	Parameter	Units	Reference
Pre-compression stress	Minimum	1.0	MPa	NBR 6118, ACI 318
Top and bottom tensile stress	Maximum	3.38	MPa	NBR 6118
Maximum compression stress at post-tensioning	Maximum	15.0	MPa	ACI 318
Maximum compression stress for f-PSL	Maximum	21.0	MPa	ACI 318
Load balance	Recommended	60 a 80	%	Loureiro (2006), Hanai (2005)
Vertical displacement	Maximum	L/250	-	NBR 6118

Slab model analysis made use of support lines aligned with pillar positions. Each support line defined “design sections” with average stress values which compiled stresses from surrounding areas delimited by the support lines.

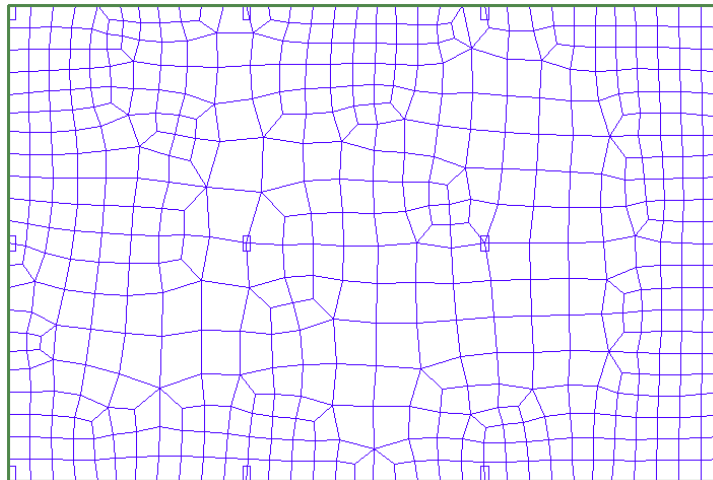


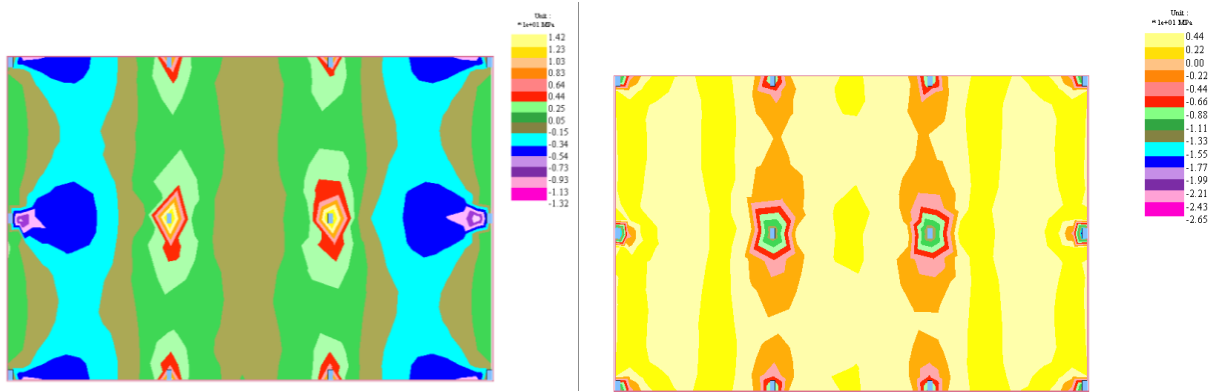
Figure 6. Finite element mesh for slab model M8.

Figure 7 shows normal stresses in the x-direction on the top and bottom faces of the slab for the most frequent combination in model M8.

3. RESULTS AND DISCUSSION

3.1 Pre-compression stresses

Table 4 presents pre-compression normal stress values on the slabs. No variations in stress were identified with respect to changes in the vertical position of the strands but rather with respect to the number of tendons and applied load. As the span between pillars increased, an increasing number of tendons were necessary to balance the models, resulting in a corresponding increase in pre-compression stress. The shortest span Model M7 presented stresses in between 1.0 MPa and 1.11 MPa while the longest span Model M10 had stresses between 1.43 MPa and 1.60 MPa.



(a) Top face (b) Bottom face
 Figure 7. Normal stresses in the x-direction for slab model M8 (MPa).

Table 4. Pre-compression normal stresses on the slab (MPa).

Model		M7												
Case		Reference	Top				Bottom				Critical			
Hypothesis			H5	H10	H15	H20	H5	H10	H15	H20	H5	H10	H15	H20
Span	Primeiro	1.00	1.00	1.00	1.00	1.00	1.00	1.00	1.00	1.00	1.00	1.00	1.00	1.00
	Central	1.11	1.11	1.11	1.11	1.11	1.11	1.11	1.11	1.11	1.11	1.11	1.11	1.11
	Último	1.01	1.01	1.01	1.01	1.01	1.01	1.01	1.01	1.01	1.01	1.01	1.01	1.01
Modelo		M8												
Stress		Reference	Top				Bottom				Critical			
Hypothesis			H5	H10	H15	H20	H5	H10	H15	H20	H5	H10	H15	H20
Span	First	1.27	1.27	1.27	1.27	1.27	1.27	1.27	1.27	1.27	1.27	1.27	1.27	1.27
	Central	1.36	1.36	1.36	1.36	1.36	1.36	1.36	1.36	1.36	1.36	1.36	1.36	1.36
	Last	1.31	1.31	1.31	1.31	1.31	1.31	1.31	1.31	1.31	1.31	1.31	1.31	1.31
Model		M9												
Case		Reference	Top				Bottom				Critical			
Hypothesis			H5	H10	H15	H20	H5	H10	H15	H20	H5	H10	H15	H20
Span	First	1.53	1.53	1.53	1.53	1.53	1.53	1.53	1.53	1.53	1.53	1.53	1.53	1.53
	Central	1.75	1.75	1.75	1.75	1.75	1.75	1.75	1.75	1.75	1.75	1.75	1.75	1.75
	Last	1.53	1.53	1.53	1.53	1.53	1.53	1.53	1.53	1.53	1.53	1.53	1.53	1.53
Model		M10												
Case		Reference	Top				Bottom				Critical			
Hypothesis			H5	H10	H15	H20	H5	H10	H15	H20	H5	H10	H15	H20
Span	First	1.43	1.43	1.43	1.43	1.43	1.43	1.43	1.43	1.43	1.43	1.43	1.43	1.43
	Central	1.60	1.60	1.60	1.60	1.60	1.60	1.60	1.60	1.60	1.60	1.60	1.60	1.60
	Last	1.50	1.50	1.50	1.50	1.50	1.50	1.50	1.50	1.50	1.50	1.50	1.50	1.50

3.2 Maximum normal stresses on the slab

Normal tensile stresses on the bottom face of the slab are shown in Table 5 for all models. Despite changes to eccentricity through vertical position of the strands, all models were within the maximum limit of 3.38 MPa for f-PSL set by standard NBR 6118 (ABNT, 2014). In the case of the “Central” span of the Reference model, compressive stresses were found on the bottom face of the slab due to higher prestresses when compared to the “First” and “Final” spans. Less variation in stresses were observed for the variations of eccentricity of the “Top” cases when compared to the “Bottom” cases. Still, “Critical” combination cases produced the most unfavorable stresses.

Results for the stresses in the top face of the slab are summarized in Table 6. Stresses that exceeded the limit set by standard NBR 6118 (ABNT, 2014) were highlighted in yellow. Only stresses of the “Top” cases and hypothesis H5 were within the limit of 3.38 MPa. Decreases in eccentricity of the “Bottom” cases produced a greater increase in normal tensile stresses along the top face of the slab, especially in the regions supported by the pillars when compared to other locations. Models M7 and M9 with hypothesis H5 were the only slabs in which variations of eccentricity of the “Bottom” cases had normal tensile stresses lower than the limit of 3.38 MPa. Furthermore, no normal stresses for the most frequent “Critical” combination cases in all hypotheses of variations in eccentricity were below the 3.39 MPa limit for f-PLS.

Table 5. Normal tensile stresses at the bottom face of the slabs (MPa).

Model		M7												
Case	Reference	Top				Bottom				Critical				
Hypothesis		H5	H10	H15	H20	H5	H10	H15	H20	H5	H10	H15	H20	
Span	First	2.37	2.39	2.42	2.45	2.47	2.45	2.54	2.63	2.72	2.48	2.60	2.71	2.83
	Central	-0.15	-0.12	0.00	0.05	0.12	-0.10	0.00	0.02	0.05	-0.03	0.09	0.22	0.36
	Final	2.52	2.55	2.58	2.60	2.63	2.61	2.69	2.78	2.86	2.63	2.75	2.86	2.97
Model		M8												
Case	Reference	Top				Bottom				Critical				
Hypothesis		H5	H10	H15	H20	H5	H10	H15	H20	H5	H10	H15	H20	
Span	First	2.52	2.55	2.71	2.74	2.77	2.66	2.76	2.87	2.98	2.68	2.83	2.97	3.12
	Central	-0.62	-0.5	-0.5	-0.4	-0.3	-0.6	-0.5	-0.4	-0.4	-0.5	-0.3	-0.2	0.01
	Final	2.48	2.51	2.54	2.57	2.61	2.58	2.69	2.79	2.9	2.62	2.75	2.89	3.03
Model		M9												
Case	Reference	Top				Bottom				Critical				
Hypothesis		H5	H10	H15	H20	H5	H10	H15	H20	H5	H10	H15	H20	
Span	First	2.64	2.65	2.71	2.74	2.77	2.66	2.76	2.87	2.98	2.68	2.83	2.97	3.12
	Central	-1.49	-1.4	-1.3	-1.2	-1.1	-1.3	-1.2	-1.1	-1	-1.2	-1	-0.8	-0.6
	Final	2.63	2.66	2.72	2.74	2.78	2.67	2.79	2.9	3.01	2.71	2.82	3.01	3.16
Model		M10												
Case	Reference	Top				Bottom				Critical				
Hypothesis		H5	H10	H15	H20	H5	H10	H15	H20	H5	H10	H15	H20	
Span	First	2.70	2.73	2.77	2.80	2.83	2.81	2.91	3.01	3.12	2.84	2.97	3.10	3.24
	Central	-1.41	-1.33	-1.24	-1.15	-1.07	-1.34	-1.27	-1.20	-1.13	-1.26	-1.10	-0.93	-0.77
	Final	2.69	2.73	2.76	2.79	2.82	2.80	2.90	3.01	3.11	2.83	2.97	3.10	3.24

Table 6. Normal tensile stresses at the top face of the slabs (MPa).

Model		M7												
Case		Reference	Top				Bottom				Critical			
Hypothesis			H5	H10	H15	H20	H5	H10	H15	H20	H5	H10	H15	H20
Span	P5	3.04	3.12	3.21	3.29	3.37	3.15	3.25	3.36	3.46	3.23	3.42	3.61	3.80
	P6	3.26	3.33	3.41	3.48	3.56	3.36	3.45	3.55	3.65	3.43	3.61	3.78	3.96
Model		M8												
Case		Reference	Top				Bottom				Critical			
Hypothesis			H5	H10	H15	H20	H5	H10	H15	H20	H5	H10	H15	H20
Span	P5	3.28	3.38	3.47	3.56	3.65	3.40	3.52	3.65	3.77	3.50	3.71	3.93	4.14
	P6	3.08	3.18	3.28	3.37	3.47	3.21	3.33	3.46	3.58	3.30	3.53	3.75	3.97
Model		M9												
Case		Reference	Top				Bottom				Critical			
Hypothesis			H5	H10	H15	H20	H5	H10	H15	H20	H5	H10	H15	H20
Span	P5	3.09	3.19	3.29	3.40	3.51	3.24	3.34	3.42	3.55	3.26	3.49	3.72	3.95
	P6	3.13	3.22	3.31	3.45	3.53	3.29	3.42	3.56	3.57	3.39	3.64	3.88	4.12
Model		M10												
Case		Reference	Top				Bottom				Critical			
Hypothesis			H5	H10	H15	H20	H5	H10	H15	H20	H5	H10	H15	H20
Span	P5	3.28	3.37	3.47	3.56	3.66	3.40	3.52	3.65	3.77	3.50	3.71	3.93	4.15
	P6	3.23	3.32	3.42	3.52	3.65	3.33	3.47	3.65	3.77	3.45	3.67	3.88	4.11

3.3 Vertical Displacements Deslocamentos verticais

Table 7 presents vertical displacements for the model slabs. Models M7 and M8 had displacements of 28.0 mm and 32.0 mm, respectively. These displacements occurred for all hypotheses and were within the limits set by standard NBR 6118 (ABNT, 2014). For all variations in eccentricity in the “Top” case, model M9 had displacements lower than 36 mm only in the “Central” span while Model M10 had displacements of less than 40.0 mm. Both of these values were limits set by standard NBR 6118 (ABNT, 2014)

Table 7. Vertical displacements on all model slabs (mm).

Model		M7												
Case	Reference	Top				Bottom				Critical				
Hypothesis		H5	H10	H15	H20	H5	H10	H15	H20	H5	H10	H15	H20	
Span	First	18.5	18.8	19.0	19.2	19.4	19.1	19.6	20.1	20.7	19.3	20.0	20.8	21.5
	Central	5.4	5.8	6.3	6.6	7.0	5.7	6.0	6.3	6.6	6.1	6.9	7.5	8.2
	Final	19.1	19.3	19.4	19.6	19.8	19.6	20.1	20.6	21.1	19.8	20.4	21.1	21.8
Model		M8												
Case	Reference	Top				Bottom				Critical				
Hypothesis		H5	H10	H15	H20	H5	H10	H15	H20	H5	H10	H15	H20	
Span	First	24.2	24.4	24.7	24.9	25.2	24.9	25.6	26.3	27.0	25.1	26.1	27.2	28.0
	Central	4.8	5.1	5.5	6.5	7.1	5.3	5.6	6.1	7.1	5.8	6.7	7.7	8.7
	Final	23.9	24.2	24.6	24.8	25.1	24.7	25.5	26.3	30.0	25.0	26.1	27.1	28.1
Model		M9												
Case	Reference	Top				Bottom				Critical				
Hypothesis		H5	H10	H15	H20	H5	H10	H15	H20	H5	H10	H15	H20	
Span	First	35.7	35.9	36.5	36.8	37.1	36.1	36.7	37.0	37.9	36.3	36.8	37.9	39.2
	Central	5.0	5.8	6.6	7.4	8.1	6.5	7.1	7.6	8.3	7.3	8.4	9.7	10.9
	Final	35.6	35.9	36.2	36.7	37.0	36.0	36.3	36.8	37.6	36.1	36.5	37.7	39.0
Model		M10												
Case	Reference	Top				Bottom				Critical				
Hypothesis		H5	H10	H15	H20	H5	H10	H15	H20	H5	H10	H15	H20	
Span	First	35.4	35.7	36.4	38.0	39.0	36.3	37.2	38.1	40.1	36.9	39.3	41.6	42.5
	Central	2.7	3.3	5.0	8.9	10.1	3.3	5.9	9.0	10.3	4.0	6.6	9.9	12.0
	Final	34.8	35.2	35.9	37.4	38.3	35.8	36.7	37.6	39.6	36.1	38.9	40.0	42.1

The effects of changes in eccentricity on displacement are better understood graphically from Figure 8. In the figure, the vertical axis contained the f/L ratio, which represented the equivalent center span displacement in denominator format: for example $L/430$ with $L/250$ being the limit. The horizontal axis contained the relative eccentricities, which were the variation in height of the strand (eccentricity) with respect to slab thickness. The dashed lines were placed in order to visually separate the slab models. The relative eccentricity (or its variation) could have more or less of an effect depending on the case study: examining the trends of Figure 8, it could be noted that, for all slab models, the “Critical” hypothesis produced the most variations in displacement.

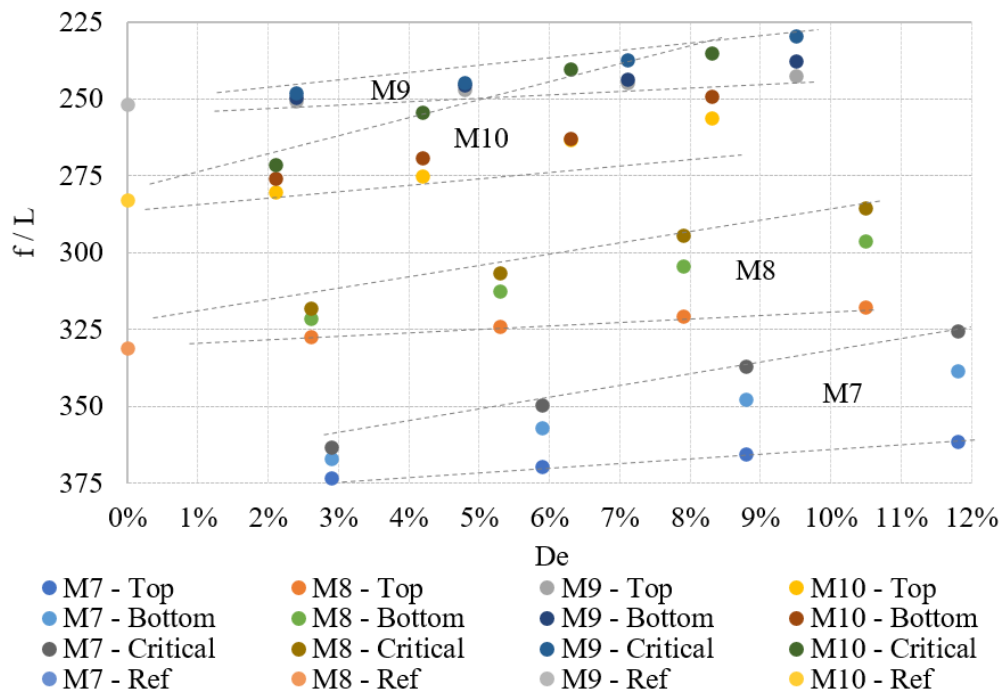


Figure 8. Relative displacement with respect to relative eccentricity for all slab models.

For slab models M9 and M10, the “Top”, “Bottom” or “Critical” eccentricity positions had less of an effect than for models M7 and M8. The amplitude of variation of the center displacement increased as relative eccentricity increased. In the “Critical” case of model M9, the increase in relative eccentricity from 2.4% to 9.5% resulted in an increase in relative displacement from L/248 to L/230. For comparison, in the “Critical” case of model M7, the increase in relative eccentricity from 2.9% to 11.8% resulted in an increase in relative displacement from L/363 to L/325.

3.4 Load Balancing

Load balancing values increased when strands were inserted in order to attain the normal tensile stress limits at the top and bottom faces of the slab and in pre-compression. Table 8 shows a summary of load balancing values for all models. Only model M7 reached the recommended value between 60% and 80% of Loureiro (2006) and Aalami (2014). In the other models, load balance varied between 59% and 95% of permanent loads.

Table 8. Load balancing on all slab models (%).

Model		M7												
Case		Reference	Top				Bottom				Critical			
Hypothesis			0.5	1.0	1.5	2.0	0.5	1.0	1.5	2.0	0.5	1.0	1.5	2.0
Span	First	73	73	72	72	71	73	72	72	71	72	71	70	69
	Central	74	72	71	69	68	72	71	69	68	71	68	64	61
	Final	80	79	79	78	77	79	78	77	75	78	76	74	72
Model		M8												
Case		Reference	Top				Bottom				Critical			
Hypothesis			0.5	1.0	1.5	2.0	0.5	1.0	1.5	2.0	0.5	1.0	1.5	2.0
Span	First	82	81	80	79	78	81	80	78	77	80	78	75	73
	Central	92	89	87	84	82	89	87	84	82	87	82	77	72
	Final	87	87	86	85	84	86	84	83	81	85	82	80	78
Model		M9												
Case		Reference	Top				Bottom				Critical			
Hypothesis			0.5	1.0	1.5	2.0	0.5	1.0	1.5	2.0	0.5	1.0	1.5	2.0
Span	First	88	87	86	85	83	60	59	57	56	60	57	54	52
	Central	94	92	90	88	85	61	60	58	57	60	56	53	50
	Final	87	86	85	84	83	59	58	57	56	58	56	54	52
Model		M10												
Case		Reference	Top				Bottom				Critical			
Hypothesis			0.5	1.0	1.5	2.0	0.5	1.0	1.5	2.0	0.5	1.0	1.5	2.0
Span	First	97	96	95	94	93	95	93	91	89	94	91	88	85
	Central	93	92	90	88	86	92	90	88	86	90	86	83	79
	Final	88	87	87	86	85	87	95	83	81	86	83	80	77

3.5 Passive Reinforcement

Table 9 shows bottom passive reinforcement results for the slab models.

Table 9. Bottom passive reinforcement results

Model	Hypothesis and Cases					
	Reference		H5 - Top		H5 - Bottom	
	First and Final span	Central span	First and Final span	Central span	First and Final span	Central span
	Steel area (cm ² /m)		Steel area (cm ² /m)		Steel area (cm ² /m)	
M7	2.54	2.11	2.54	2.11	2.64	2.22
M8	2.72	2.10	2.72	2.10		
M9	3.26	2.40	3.26	2.40		
M10	3.74	2.46	3.74	2.46		

In the case of hypothesis H5 and “Top” case, bottom passive reinforcements were unchanged with respect to Reference values. Changes in reinforcement were observed within a model but in different spans.

Table 10. Top passive reinforcement results

Model	Hypothesis and Cases		
	Reference	H5 - Top	H5 - Bottom
	Steel area (cm ² /m)		
M7	7.4	7.4	7.7
M8	10.5	10.5	
M9	12.2	12.2	
M10	15.6	15.6	

Table 10 shows results for the top passive reinforcement for all slab models. Similar to Table 9, the passive reinforcement rate used to cancel negative flexing remained unchanged for all models under hypothesis H5 and “Top” case with respect to Reference values. This was a consequence of the 5 mm reduction in height of the spacers over the pillars not inducing sufficient loads to demand an increase in steel. On the other hand, the variation of eccentricity in the “Bottom” case for model M7 resulted in an increase in reinforcement rate over the pillars to provide additional effect against negative flexing when compared to the Reference model with the same span.

4. CONCLUSIONS

This study analyzed four models of post-tensioned flat slabs with variations in the span between pillars and in strand eccentricity. The variations in eccentricity simulated errors in assembly and positioning of vertical spacers. Pre-compression stresses, normal tensile stresses in the top and bottom faces, load balancing and vertical displacements were analyzed. Top and bottom passive reinforcements were also analyzed.

A decrease in eccentricity of the strands had a direct effect on the slab loads: its main effect was a decrease in the ratio of normal stresses supported by post-tensioning. The decrease in eccentricity of the “Bottom” case had a stronger negative impact than a variation of eccentricity of the “Top” case and affected normal stress control, load balancing criteria and displacements.

Only model M7 with variations in eccentricity from hypothesis H5 were within limits set by standard NBR 6118 (ABNT, 2014) for the “Top” and “Bottom” cases. On other hand, models M8, M9 and M10, with variations in eccentricity from hypothesis H5 for the “Top” case presented normal tensile stresses below the 3.38 MPa limit of standard NBR 6118 (ABNT, 2014).

Pre-compression stresses in the structural element were affected only by the number of tendons and the load applied to them. There were no effects of variations in vertical height of spacers.

Vertical displacements of the slabs were affected by variations in eccentricity. Models M7 and M8 remained below the L/250 limit of standard NBR 6118 (ABNT, 2014) for all hypothesis of variations of eccentricity tested.

Load balancing criteria remained within recommended limits only for Model M7. However, since these criteria were complementary and not standardized, the other models could be acceptable for use nonetheless.

Reinforcement rate for top and bottom reinforcements were unchanged between the Reference model and all models with variations in eccentricity from hypothesis H5 and “Top” case.

The maximum variation of relative eccentricity so that the parameters of this study remained with established limits was 2.1% for the “Top” case. This was obtained by comparing the variation in eccentricity with respect to slab thickness.

Overall, results showed that flat post-tensioned slabs with unbonded tendons of type CP 190 RB, diameter of 12.7 mm and span between pillars between 7.0 m to 10.0 m could have a maximum

tolerance of 5 mm in a decrease of vertical height of strands in the top face of the slab (“Top” case). This result was more restrictive than found in reference studies.

5. REFERENCES

- Aalami, B. O. (1990), *Load Balancing: A Comprehensive Solution to Post - Tensioning*. ACI Structural Journal: 662-670.
- Aalami, B. O. (2014), “*Post-Tensioned Manual*”. California: ADAPT, v.1, p. 500.
- Aalami, B. O. (2000), *Structural Modeling of Post-Tensioned Members*. Journal of Structural Engineering. Vol. 126 N°. 2: 157-162.
- Aalami, B. O., Bommer, A. (1999), “*Design Fundamentals of Post-Tensioned Concrete Floors*”. Post-Tensioning Institute (PTI), Farmington Hills, USA.
- Almeida, S. R. M. (2001), “*Contribuição ao projeto ótimo de cabos em vigas de concreto protendido*”. Tese de Doutorado. Pontifícia Universidade Católica do Rio de Janeiro. <https://doi.org/10.17771/PUCRio.acad.2058>.
- American Concrete Institute (2019). *ACI 318 - Building Code Requirements for Structural Concrete*. Farmington Hills, MI.
- Associação Brasileira de Normas Técnicas. (2019). *NBR 6120: Ações para o cálculo de estruturas de edificações*. Rio de Janeiro.
- Associação Brasileira de Normas Técnicas. (2014). *NBR 6118: Projeto de estruturas de concreto – Procedimento*. Rio de Janeiro.
- Caro, L. A., Vargas J. R. M., Ros, P. S. (2013), *Prestress losses evaluation in prestressed concrete prismatic specimens*. Engineering Structures. Vol. 48, p. 704-715. <https://doi.org/10.1016/j.engstruct.2012.11.038>.
- Carvalho, R. C. (2017), “*Estruturas em concreto protendido: cálculo e detalhamento*”. Ed. Pini. São Paulo, Brasil, p. 448.
- Cauduro, E. L. (2002), “*Manual para a boa execução de estruturas protendidas usando cordoalhas de aço engraxadas e plastificadas*”. São Paulo, Brasil.
- Cavaco, E. S., Bastos, A., Santos, F. A. (2017), “*Effects of corrosion on the behaviour of precast concrete floor systems*”. Journal Construction and Building Materials. N. 145: 411-418. <https://doi.org/10.1016/j.conbuildmat.2017.04.044>.
- Cholfe, L., Bonilha, L. (2018), “*Concreto protendido: teoria e prática*”. Oficina de Textos. São Paulo, Brasil, p. 360.
- Hanai, J. B. (2005), “*Fundamentos do Concreto Protendido*”. E-book. São Carlos.
- Kang, T., Bondy, K. B. (2008), *Recommendations for Design of Post-Tensioned Slab-Column Connections Subjected to Lateral Loading*. PTI Journal, Post Tensioning Institute. Vol. 6, nº 1.
- Loureiro, G. J. (2006), *Projeto de Lajes Protendidas com Cordoalhas Engraxadas*. Revista Ibracon de Estruturas e Materiais, ed. 44.
- Pfeil, W. (1984), “*Concreto Protendido – Introdução*”. LTC. Rio de Janeiro.
- Romanichen, R. M., Souza, R. A. (2019), *Reinforced concrete corbels strengthened with external prestressing*. Revista Ibracon de Estruturas e Materiais. V. 12. N. 4, p. 812 – 831. <https://doi.org/10.1590/S1983-41952019000400006>.
- Santos, J. S. D. (2017), “*Desconstruindo o Projeto Estrutural de Edifícios: Concreto Armado e Protendido*”. 1ª. ed. São Paulo: Oficina de Textos. p. 127.
- Silva, G., Prata, B., Albuquerque, A. (2018), *Análise da eficiência dos sistemas estruturais para edifícios em concreto*. Ambiente Construído. Vol. 18, n. 1, p. 313-325. <https://doi.org/10.1590/s1678-86212018000100223>.
- Silva, R.C. (2003), “*Vigas de concreto armado com telas soldadas: análise teórica e experimental da resistência à força cortante e do controle da fissuração*”. Tese de doutorado. Escola de

Engenharia de São Carlos, Universidade de São Paulo. p. 328.

Silveira, M. C. A. (2002). “*Práticas de Projeto e Execução de Edificações Protendidas com Cordoalhas Engraxadas e Plastificadas*”. Revista Ibracon de Estruturas e Materiais. 44º Congresso Brasileiro do Concreto. Belo Horizonte.

Souza, F. A. (2018), “*Radier simples, armado e protendido – Teoria e Prática*”. Editora Catarse. São Paulo, Brasil, p. 312.

Souza Junior, O. A., Oliveira, D. R. C. (2016), “*Influence of the tendon’s layout on the shearing resistance of prestressed concrete beams*”. Revista Ibracon de estruturas e materiais. Vol. 9, N. 5. p. 765 – 795. <https://doi.org/10.1590/S1983-41952016000500008>.

Vicente, C. M. D. S., Albino, J. P. D. C. (1994), “*Lajes em Concreto Armado e Protendido*”. Editora da Universidade Federal Fluminense. Rio de Janeiro, Brasil, p. 584.

Xin, F., Xianyan, Z. (2012). “*Experimental research on crack width of retard bonded partially prestressed concrete beams*”. International Conference on Advances in Civil Infrastructure Engineering. Hunan.

Modifications of the rupture envelope in clayey soils with different volumetric stabilizer

A. Sánchez¹ , E. Alonso^{1,2*} , W. Martínez² , H. Chávez² , M. Navarrete² ,
M. Arreola² , J. Borrego² , L. Equihua² , E. Núñez² , O. Miranda²

*Contact author: elia.alonso@umich.mx

DOI: <https://doi.org/10.21041/ra.v12i2.595>

Reception: 01/03/2022 | Acceptance: 19/04/2022 | Publication: 01/05/2022

ABSTRACT

The modifications of seven different stabilizers (lime, cement, nopal fibers, river sand, volcanic sand, sodium sulphate and gypsum) on a clayey soil of Santiago Undameo, in Michoacan, Mexico, were analyzed to observe the changes in the properties and the rupture envelope. Sieve analysis, hydraulic sedimentation, index properties, compressive strength and Proctor were performed to the natural soil; while the variation of the index properties and the rupture envelope were determined for the stabilized mixtures. The additions improved the behavior of the high plasticity soil, diminishing the volumetric deformations and increasing the mechanical resistance, shear strength and angle of internal friction. This research contributes positively to the restoration of earthen heritage buildings, civil works, construction pathologies and construction technologies. The research was performed in the laboratory under international standards.

Keywords: soil stabilization; mechanical properties; shear strength; cohesion; angle of internal friction; restoration.

Cite as: Sánchez, A., Alonso, E., Martínez, W., Chávez, H., Navarrete, M., Arreola, M., Borrego, J., Equihua, L., Núñez, E., Miranda, O. (2022), “Modifications of the rupture envelope in clayey soils with different volumetric stabilizer”, Revista ALCONPAT, 12 (2), pp. 227 – 247, DOI: <https://doi.org/10.21041/ra.v12i2.595>

¹ Faculty of Architecture, Universidad Michoacana San Nicolás de Hidalgo, Morelia, Mexico

² Materials Department, Faculty of Civil Engineering, Universidad Michoacana San Nicolás de Hidalgo, Morelia, Mexico

Contribution of each author

In this work, the experimentation was carried out by O. Miranda (50%), L. Equihua (25%), E. Nuñez (25%); the bibliographic search activity O. Miranda (25%), L. Equihua (25%), A. Sanchez (25%) and E. Alonso (25%); the information extraction activity by E. Nuñez (20%), J. Borrego (20%), A. Sanchez (20%), E. Alonso (20%), W. Martinez (20%); analysis and discussion of results by M. Navarrete (25%), M. Arreola (25%), J. Borrego (25%), H. Chavez (25%); the writing of the document by A. Sanchez (20%), H. Chavez (20%), W. Martinez (20%), M. Navarrete (20%) and M. Arreola (20%); the revision of the text by E. Alonso (20%), H. Chavez (20%), M. Arreola (20%), M. Navarrete (20%) and J. Borrego (20%); figure design and format adaptation by W. Martinez (25%), L. Equihua (25%), E. Nuñez (25%) and O. Miranda (25%); English translation A. Sanchez (100%).

Creative Commons License

Copyright 2022 by the authors. This work is an Open-Access article published under the terms and conditions of an International Creative Commons Attribution 4.0 International License ([CC BY 4.0](https://creativecommons.org/licenses/by/4.0/)).

Discussions and subsequent corrections to the publication

Any dispute, including the replies of the authors, will be published in the first issue of 2023 provided that the information is received before the closing of the third issue of 2022.

Modificaciones de la envolvente de falla en suelos arcillosos con distintos estabilizadores volumétrico

RESUMEN

Se analizaron modificaciones presentadas por distintos estabilizadores (cal, cemento, fibra de nopal, líticos de río, líticos volcánicos, sulfato de sodio y yeso) en propiedades y envolvente de falla de un suelo arcilloso natural remoldeado de Santiago Undameo, en Michoacán, México. Al suelo arcilloso se le realizó granulometría, hidrometría, pruebas índice, compresión simple y prueba Proctor; a las mezclas estabilizadas se determinó la variación en propiedades índice y envolvente de falla. Las adiciones propuestas mejoraron el comportamiento del suelo altamente plástico, disminuyendo las deformaciones volumétricas e incrementando su resistencia mecánica normal, al cortante y ángulo de fricción interna. La investigación contribuye favorablemente a la restauración de construcciones de tierra histórico-patrimoniales, obra civil, patologías en edificaciones y tecnologías constructivas. La investigación fue realizada en laboratorio bajo normatividad internacional.

Palabras clave: estabilización de suelos; propiedades mecánicas; cortante; cohesión; ángulo de fricción interna; restauración.

Modificações do envelope de ruptura em solos argilosos com diferentes estabilizadores volumétricos

RESUMO

Foram analisadas as modificações apresentadas por diferentes estabilizantes (cal, cimento, fibra de figueira-da-índia (palma), líticos fluviais, líticos vulcânicos, sulfato de sódio e gesso) nas propriedades e envoltório de ruptura de um solo argiloso natural remodelado de Santiago Undameo, em Michoacán, México. Granulometria, hidrometria, testes de índice, compressão simples e teste de Proctor foram realizados no solo argiloso. A variação nas propriedades de índice e envoltório de ruptura foram determinadas para as misturas estabilizadas. As adições propostas melhoraram o comportamento do solo altamente plástico, reduzindo deformações volumétricas e aumentando sua resistência mecânica normal, resistência ao cisalhamento e ângulo de atrito interno. A pesquisa contribui favoravelmente para a restauração de construções de terra do patrimônio histórico, obras civis, patologias em edifícios e tecnologias de construção. A pesquisa foi realizada em laboratório utilizando normas internacionais.

Palavras-chave: estabilização do solo; propriedades mecânicas; resistência ao cisalhamento; coesão; ângulo de atrito interno; restauração.

Legal Information

Revista ALCONPAT is a quarterly publication by the Asociación Latinoamericana de Control de Calidad, Patología y Recuperación de la Construcción, Internacional, A.C., Km. 6 antigua carretera a Progreso, Mérida, Yucatán, 97310, Tel.5219997385893, alconpat.int@gmail.com, Website: www.alconpat.org

Reservation of rights for exclusive use No.04-2013-011717330300-203, and ISSN 2007-6835, both granted by the Instituto Nacional de Derecho de Autor. Responsible editor: Pedro Castro Borges, Ph.D. Responsible for the last update of this issue, Informatics Unit ALCONPAT, Elizabeth Sabido Maldonado.

The views of the authors do not necessarily reflect the position of the editor.

The total or partial reproduction of the contents and images of the publication is carried out in accordance with the COPE code and the CC BY 4.0 license of the Revista ALCONPAT.

List of acronyms (by order of appearance in the document)

Abbreviation	Meaning
CEB	Compressed Earth Block
UU	Unconfined Undrained
CS	Control Sample
L	Lime
PC	Portland Cement
NF	Nopal Fibres
RS	River Sand
VS	Volcanic Sand
SS	Sodium Sulphate
G	Gypsum
USCS	Unified Soil Classification System
A	Activity
PI	Plasticity Index
LL	Liquid Limit
PL	Plastic Limit
LC	Linear Contraction
VC	Volumetric Contraction
CH	Fat Clay
CL	Lean Clay
MH	Elastic Silt
ML	Silt
OH	Organic Clay
OL	Organic Silt

1. INTRODUCTION

Clayey soils, commonly known as clays, are employed for many applications, including the use as construction materials, being essential elements for our society since the first stages of civilization till our modern era. Different construction elements and components, like adobes, have been found in distinct cultures and places; with examples of exceptional antiquity in both the American and the European continents (Mauricio, et al., 2021). We can find important examples of the use of clayey soils: as impermeable elements in the core of the dams and water bodies for agricultural and irrigation purposes, production of Portland cement, building of land routes and roadways, to manufacture ceramic elements and components, for the vernacular and earthen architecture, to restore historical and heritage constructions, artificial wetlands, water cleaning and treatment, among many others.

Due to the easy availability and abundance of material in many regions of the world, clayey soils have an excellent appreciation because of their sustainable properties and the low energetic and environmental impact that they produce (Costa et. al., 2019). Clays are by definition mineral sediments constituted mainly by hydrous aluminium phyllosilicates with a fine and divided particle size. Additionally, clays have excellent binding properties, so they have been used historically as cementitious materials (Sanchez-Calvillo, et al., 2021).

In Mexico, we can find different types of clays, and they have been used for construction purposes over time; particularly, in the State of Michoacan, we can find the presence of clays in construction components like adobes, ceramic bricks, union mortars and earthen refurbishments, among many others. Santiago Undameo, a locality positioned in the northeast of the State of Michoacan has one of the most important clay quarries of the region, due to the proximity to the capital of the state, Morelia (See Figure 1). The Historic Centre of Morelia, a UNESCO World Heritage Site, has more than 1000 heritage buildings and monuments, all of them built with traditional and colonial construction techniques, with a widespread use of clayey soil and other local materials of the region.



Figure 1. (a) Location of Michoacan within Mexico; (b) Location of the municipality of Morelia, including Santiago Undameo, within the State of Michoacan

The soils taken from this locality have an important proportion of clay minerals, which have high plasticity properties that generate instability and relevant volumetric deformations in contact with water; this situation causes pathologies in the buildings and the civil engineering constructions. Historically, a great variety of materials has been employed as stabilizers of the clays, to diminish the high hygroscopic plasticity presented and consequently reducing the lineal and volumetric contractions in presence of water (Daneels et al., 2020). This stabilization is essential for the earthen construction and architecture areas, and the bases and subbases of flexible paving; the

stabilizations help to enhance the durability of these structures while improves the mechanical resistances (Laborel-Préneron et al., 2021), being all these properties very well appreciated in the construction field.

The research interest lies in the complexity of the studied soils in Santiago Undameo, since historically they have presented high plasticity and consequently great volumetric deformations, which have big affectation on the stability of the existing constructions of the studied region.

On the other hand, the earthen architecture in the state of Michoacan, despite its wealth, variety and cultural importance, has been relegated and abandoned, therefore it is essential to do more research works about this sustainable resource with easy access for the communities. Besides, to understand the behaviour of these clayey soils in combination with different stabilizers, will help to improve the actions of intervention, restoration and understanding of the existing pathologies.

There are plenty of materials used as stabilizers for construction purposes, many of them with a background of scientific research: lime (Taallah y Guettala, 2016; Navarro Mendoza et. al., 2019), portland cement (Dao et al., 2018; Jitha et. al., 2020), nopal fibres (Ige y Danso, 2020; Li Piani, 2020), rivers sand, volcanic sand, sodium sulphate and gypsum (hemihydrate calcium sulphate) (Martínez, et al., 2018).

The stabilizations with cement, lime and alkaline solutions are the most usual at global level (Abhilash, et al., 2022), furthermore, other research works have explored the use of sugarcane bagasse ashes as an alternative to improve the behaviour of soils in their physical properties like confinement, densification and volumetric stability; and the chemical properties from the reactions of the stabilizer agent (cement or lime) with water (Moraes et al., 2015; Ojeda Farías et al., 2018). We can find an extensive bibliography about the utilization of fibres and vegetative materials, mainly to avoid the shrinkage and cracking of compact construction elements, like the adobes, helping to increase their mechanical capacities (Yetgin, et al., 2008); multiple relevant research works achieved to improve the properties of these masonries (Sharma, et al., 2015; Araya-Letelier, et al., 2021). However, the modern development of upgraded earthen construction techniques, like the CEB (Compressed Earth Block) has allowed to search for new solutions including fibres with diverse origin in combination with other stabilizers like PC or L (Nagaraj, et al., 2014; Taallah y Guettala, 2016; Navarro Mendoza, et al., 2019).

In Mexico, the use of products derived from the *opuntia ficus indica*, commonly known as nopal, is very common for construction purposes, both in mucilage and fibres presentation. One of the most usual ways to use the mucilage is to boil the cacti plant and adding the liquid obtained to the construction mortar mixtures, being a solution recommended by the heritage regulatory institutions to restore historical buildings and monuments. With this methodology there have been proved increases in the mechanical resistance and the workability of the mortars (Martínez et al., 2008). In addition, correlation studies with other additions and stabilizers of historical use have shown an even better mechanical behaviour with the addition of this mucilage (Alonso et al., 2002).

In this research, seven stabilizer materials were employed to improve the behaviour of a clayey soil from Santiago Undameo as a control sample (CS). The stabilizers were: lime (L), Portland cement (PC), dehydrated pulverized fibres of cactus *opuntia ficus indica* (NF), river sand (RS), volcanic sand (VS), sodium sulphate (SS), and gypsum (hemihydrate calcium sulphate) (G). To measure the changes generated on the studied soil, there were performed unconsolidated undrained triaxial shear tests (UU), hydraulic classifier test, sieve analysis, the Standard Proctor test for both the CS and the stabilized mixtures. The analyses of the samples will provide significant information which helps to improve the earthen architecture and the construction systems which use clays as construction materials, both for modern construction works and conservation of architectural heritage.

2. MATERIALS AND METHODS

The soil samples of this research were obtained from the clay quarry of Santiago Undameo, a locality near Morelia, the capital of the State of Michoacan, in Mexico. The quarry is located within the coordinates $19^{\circ}42'$ latitude North and $101^{\circ}11.4'$ longitude West, near the shore of the Cointzio dam (See Figure 2), where local people produce adobes and handmade ceramic bricks (See Figure 3), which generate the rural dwellings of the near communities. After the sampling of the materials and taking the specimens, they were brought to the materials laboratory “Ing. Luis Silva Ruelas” of the Faculty of Civil Engineering of the UMSNH, where the experimentation was performed.



Figure 2. Location of the material quarry in Santiago Undameo (Source: Google Earth, 2022).



Figure 3. (a) Quarry with clayey soils in Santiago Undameo; (b) Manufacturing of ceramic and earthen construction components.

All the trials proposed in this document were executed in triplicate. The tests were fulfilled first with the control samples of the original soil, and later with the mixtures of clays and different stabilizers. Table 1 shows the stabilizers employed for this research, as well as the percentage by weight utilized for the mixtures.

Regarding the coarse material, the RS was provided from the quarry “El Cuervo” in the locality of Huajumbaro, Mexico, with coordinates: longitude 100.742500 degrees, latitude 19.403333 degrees and 1800 masl; this material is a silicic aggregate with round morphology. On the other hand, the VS was extracted from the quarry “Joyitas”, also located in Michoacan, Mexico, with coordinates: longitude 101.380000 degrees, latitude 19.730000 degrees and 2082 masl; this aggregate is an andesite with irregular morphology.

It is important to note that in previous research works each one of the stabilizers was tested and scanned in percentages of 1, 2, 3, 4, 5, 6, 7, 8, 9 and 10 % by weight of the soil (Flores Rentería, 2010), to assess the optimum content for each one of them. The better results for each stabilizer are shown in Table 1.

Table 1. Percentages of the stabilizers by weight.

Stabilizers	% Stabilizer
L	3.0
PC	3.0
NF	0.5
RS	10.0
VS	10.0
SS	0.5
G	6.0

For this research there were performed many tests and trials to characterize the clayey soils, which are shown in Table 2. All the experimentation was fulfilled in the laboratory “Ing. Luis Silva Ruelas” from the Faculty of Civil Engineering, UMSNH.

Table 2. Testing and standards followed in the present research.

Test	Standard
Atterberg limits and Unified Soil Classification System USCS	ASTM D2487-17 ASTM D4318-17
Mechanical analysis of soils	ASTM C136/C136M-19
Hydraulic classifier	ASTM D7928-17
Unconsolidated undrained (UU) triaxial test	ASTM D2850-15 UNE-EN ISO 17892-8:2019
Proctor standard test variant A	ASTM D698-12
Particle size < mesh n° 200	ASTM D421-85(2007) W2016
Particle size > mesh n° 200	ASTM D 422-63(2007) W2016

The UU triaxial compression test was performed with three different confinements (σ) for each one of the samples studied, as it can be spotted in Table 3. Once the specimens failed, they were left in the oven for 24 hours at 105 +/-5 °C to obtain the humidity parameter according the standards.

Table 3. UU triaxial test and confinement strength applied.

Sample	Confinement strength (kgf/cm ²)
1	$\sigma_3 = 0.3$
2	$\sigma_3 = 0.6$
3	$\sigma_3 = 0.9$

The particle size distribution of the control sample (CS), for the material retained by the mesh ASTM n° 200 was performed following the ASTM D421-85 (2007) W2016; while the material which passed through the ASTM n° 200 mesh was analysed with the hydraulic sedimentation apparatus, with an approximate length time of one week to take regular readings according to the ASTM D 422-63 (2007) W2016 standard. To classify the samples of the clayey soil the USCS system was followed with the ASTM D-2487-17 standard, being the most extended procedure in geotechnical practice.

The shearing resistance was obtained by the Mohr-Coulomb failure criterion, a theory constituted in 1773 which allows to determine the cohesion (c) and the internal friction angle (ϕ).

On the other hand, to obtain the reconstituted specimens for the UU triaxial tests, the stabilizers were added to the natural soil, homogenizing and matching the reconstitution by means of the maximum specific gravity ($\gamma_{dm\acute{a}x}$) and the optimum water content ($\omega_{\acute{o}pt}$), obtained with the Standardized Proctor test (variant A). The optimum water content ($\omega_{\acute{o}pt}$) is the content of water accomplished with the greater accommodation of the particles and the minimum void ratio ($e_{m\acute{i}n}$); while the great volumetric weight of the dry material, for a determined level of compaction is designated as the maximum specific gravity ($\gamma_{dm\acute{a}x}$).

The activity index (A) of the clays was obtained with the hydrometer test (ASTM D 422-63, 2016), by means of the equation (1). Figure 4 shows the variation of A as a function of different clay minerals.

$$A = \frac{PI}{\% \text{ of clay by weight smaller than } 2\mu m} \quad (1)$$

Where:

A= Activity of the clay

PI = Plasticity Index

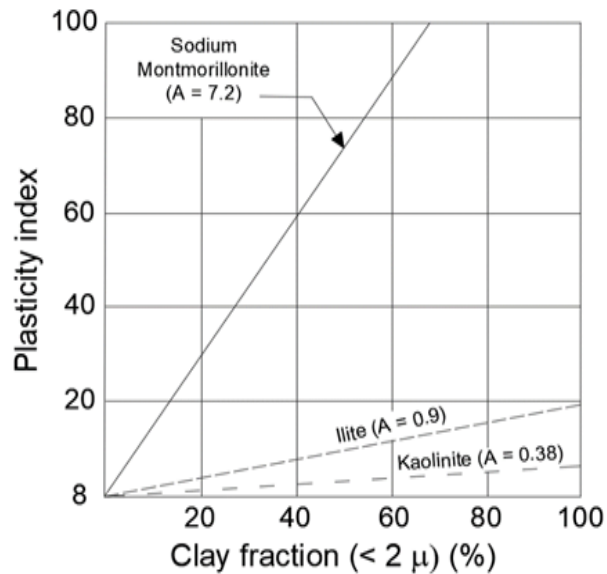


Figure 4. Activity and correlation between PI and the clay fraction <math>< 2 \mu\text{m}</math> (%) (Skempton, 1953).

3. RESULTS AND DISCUSSION

In this research, the modification of the rupture envelope of clayey soils with different volumetric stabilizers was studied. Therefore, in the next section the results obtained will be analysed and discussed, first considering the results of the tests performed on the natural reconstituted soil acting as a control sample (CS); and subsequently correlating the results of the stabilized mixtures with the seven different additions.

3.1 Analyses of the samples from the original soil

The results of the index properties are shown in Table 4, including humidity (ω), LL, PL, PI, LC and VC respectively.

Table 4. Index properties of the Santiago Undameo soils.

Material	ω (%)	LL (%)	PL (%)	PI (%)	LC (%)	VC (%)
CS	51.15	52.20	19.51	32.69	12.93	42.27

The Figure 2 shows both the results obtained from the sieve analysis, performed with ASTM meshes; and the fine material particle size, which was performed with the hydrometer analysis. The A of the clay was obtained with the last test.

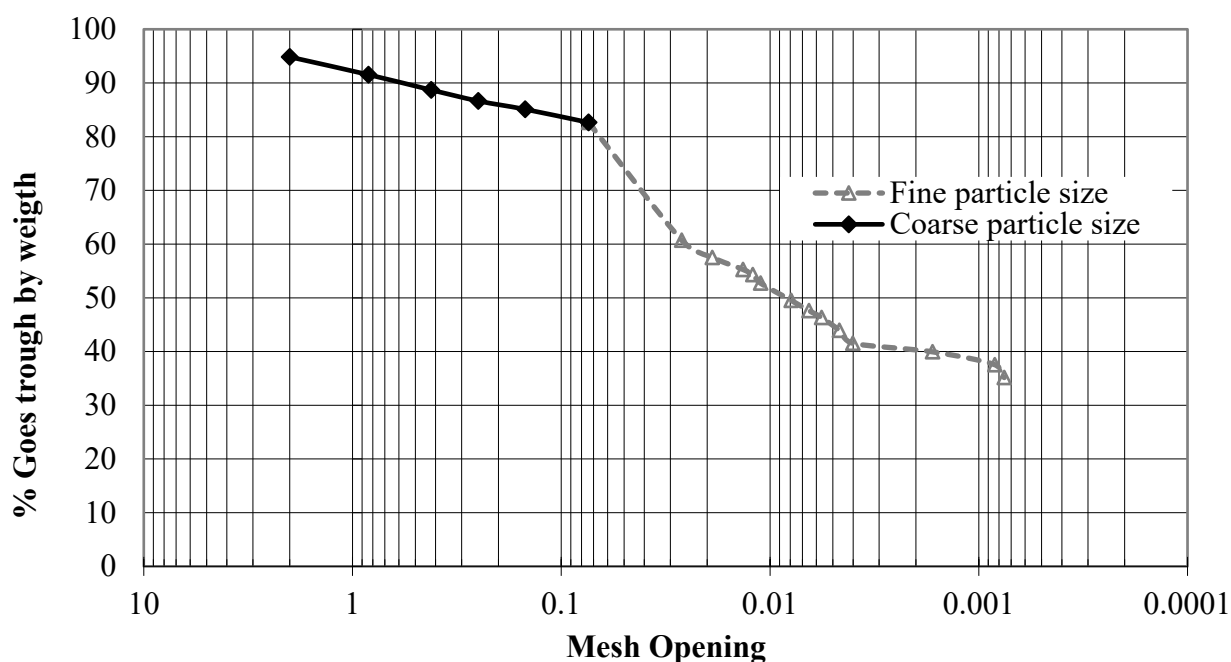


Figure 5. Particle size analysis combining coarse and fine soils of the original simple

The results of the particle size analysis showed that the 82% of the soil material went through the ASTM n° 200 mesh, classifying it as a fine soil. Also, the values of LL and PI locate the material within CH zone (See Figure 6). The hydrometer analysis was performed to obtain the fine particle size and determine the A of the clays. In Figure 4 we can see how the percentage of material going through 2 μ m size is about 40%, which indicates a significant proportion of micrometric material in the clayey soils of Santiago Undameo.

From the PI obtained, 32.7%, there was calculated an A of 0.81 (See Equation 1). According to Skempton (1953) the corresponding clay mineral is an illite (See Figure 4), which presents a much lower A than montmorillonites for instance. Nevertheless, illites have some drawbacks for construction due to their tendency to collapse and because they suffer great volumetric changes in presence of water, being problematic for civil engineering structures (Mirjalili et. al., 2020).

3.2 Analyses of the mixtures of clayey soils with different stabilizers

To classify the clayey material (the percentage of material which passes through the ASTM mesh n° 200) with different stabilizers, the technical personal of the laboratory performed the Atterberg limits trial. The results of the test are displayed in the plasticity chart (See Figure 6) where the position of the natural soil and the mixtures reflect their classification according the USCS. The natural soil from Santiago Undameo is classified as a CH, which matches the results of the A presented by the material. All the mixtures can be found in the CL zone, being evidence of the change of properties provided by the stabilizers; nevertheless, the mixture with NF is located in the limit between high plasticity and low plasticity, which means that it wouldn't be the best solution for some construction or restoration purposes. On the other hand, the combination with 0.5% SS was classified as CL (See Figure 6), presenting the greater reduction of the LL from 55.2% to 40.2% (See Table 5).

In the case of non-heritage stabilized clays (because it is easier to obtain more quantifications than patrimonial samples), it is possible to find correlation equations (Parisi et al., 2020; Vasic et al., 2020) with the results of the different physicomechanical tests (Olacia et al., 2020; Rodríguez et al., 2018; Lan et al., 2020). The correlation equations allow to estimate some parameters, to either

validate mathematical models or to find math relations between variables with statistically acceptable correlation coefficients. These correlations are useful to estimate parameters in engineering projects which include the use of clayey soils. Some researchers have found and proposed correlation equations with the variables of soils for practical purposes (Akkaya, Özvan, y Özvan, 2019; Chompoorat et al., 2022; Wang et al., 2021; Wu et. al., 2022).

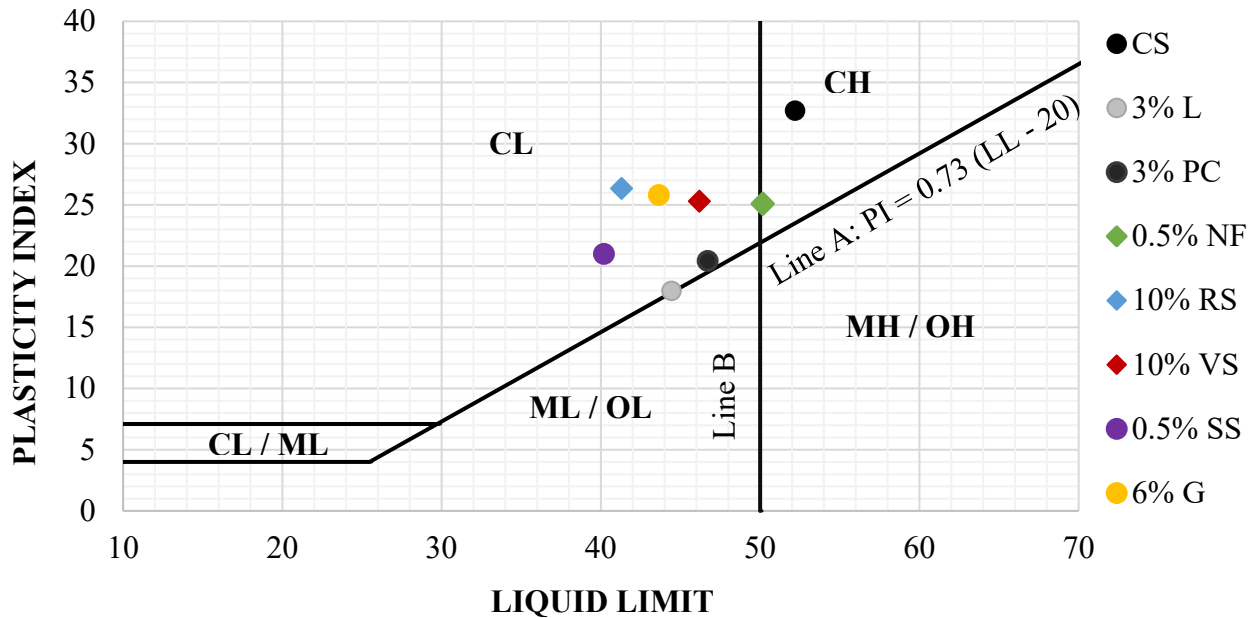


Figure 6. Plasticity chart with location of the original sample and the mixtures with stabilizers.

Table 5. Index properties of the original soil and the mixtures with different stabilizers.

Material	ω (%)	LL (%)	PL (%)	PI (%)	LC (%)	VC (%)
CS	51.15	52.20	19.51	32.69	12.93	42.27
3 % L	44.28	44.44	26.47	17.97	12.05	43.52
3% PC	46.67	46.71	26.29	20.42	12.33	45.46
0.5% NF	49.38	50.17	25.08	25.09	14.86	54.90
10 % RS	41.10	41.30	14.96	26.34	12.31	41.71
10% VS	46.06	46.19	20.89	25.34	10.04	42.98
0.5% SS	40.71	40.20	19.20	20.99	11.02	40.27
6% G	44.44	43.64	17.84	25.80	12.26	44.72

Figure 7 reveals the ensemble of index properties of each one of the stabilized mixtures and the natural soil. From the graph, it is noted that the stabilizers diminish the optimum water content (ω), the LL and the PI; on the other hand, the stabilizers also produce an irregular behaviour of the PL, LC and VC, which could be caused by the particular properties of each one of the stabilizers. For these three index properties (PL, LC and VC) the results obtained were both superior and inferior than the natural soil used as a control sample.

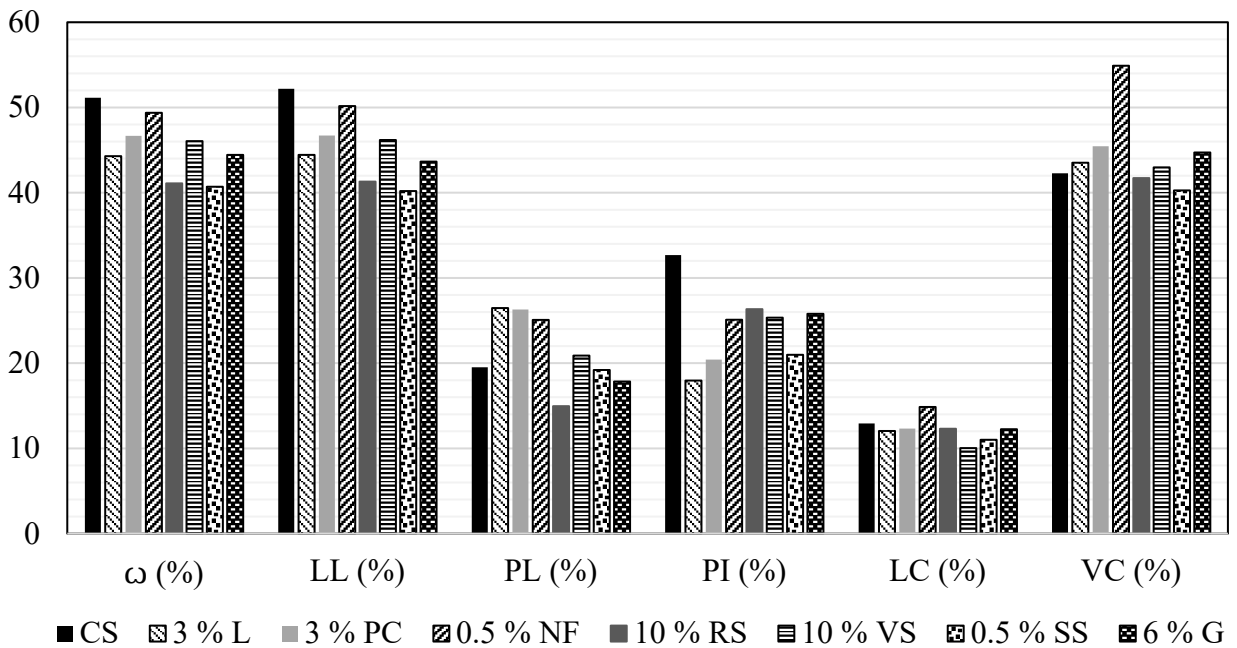


Figure 7. Index properties of the natural soil and the stabilized mixtures.

The Standard Proctor test determines the necessary content of water (ω_{opt}) to reach the maximum specific gravity ($\gamma_{dm\acute{a}x}$) through mechanical compaction (See Figure 8). In this case, it can be clearly noted the effect of the stabilizers on the necessary water content and the increase or decrease of the maximum specific gravity. The Figure 8 shows both, the behaviour of the CS and the stabilized mixtures with different colours, with the greater results corresponding to the RS and the lowers to L. The optimum water contents to achieve the maximum specific gravity are shown in Figure 9.

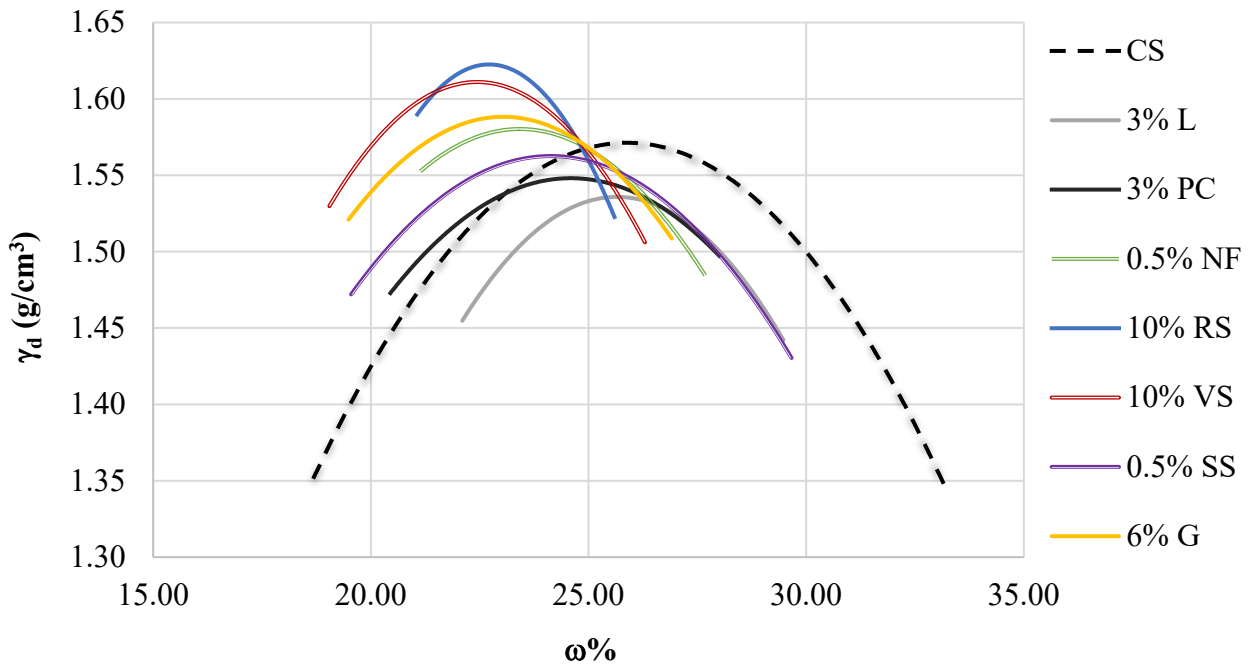


Figure 8. Results of the Standard Proctor test (variant A).

Figure 9 displays the results of the Standard Proctor test (Variant A), allowing to perceive the effect of the different stabilizers regarding the maximum specific gravity ($\gamma_{dm\acute{a}x}$) and the optimum water content (ω_{opt}) through the compaction of the samples in the laboratory. Reading the graph, we can observe the clear reduction of the optimum water content with the addition of L, PC and NF; this decrease also involves a related reduction of the specific gravity, which could be caused by the workability and plasticity properties of these materials, keeping in mind that water acts as a lubricant for the accommodation of the clay particles. Both L and PC are known to maintain a fluidity degree for certain time to provide facility of application during construction works; also, this behaviour has been monitored for lime and cement mortars which incorporate NF (Díaz-Blanco, et al., 2019; Knapen y Van Gemert, 2009; Ramírez-Arellanes et al., 2012).

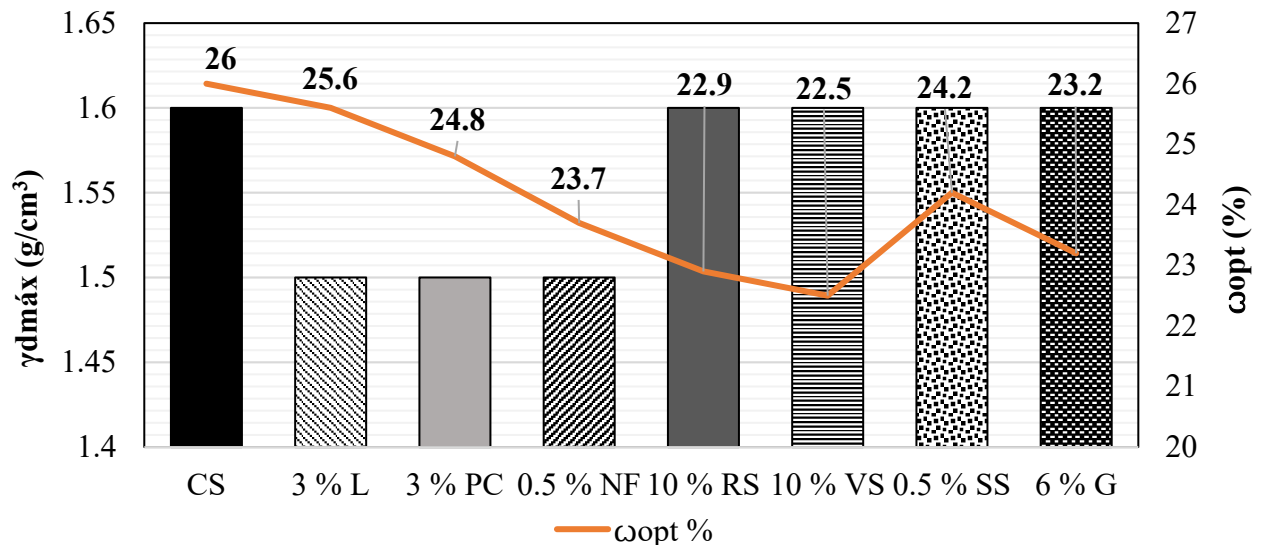


Figure 9. Results of the Standard Proctor test (Variant A) regarding the optimum water content.

Regarding the coarse materials, it is clear that they do not change their physical properties in presence of water, therefore they not change or inflict on the ω_{opt} ; nevertheless, they do decrease the $\gamma_{dm\acute{a}x}$ of the natural soil, which can be attributed to the particle size, porosity and density, as they occupy more volume than the original sample of soil. The SS can behave to some extent as lithic material if the water is aggregated at room temperature, and the dissolution of the sample can be slower than the time necessary to perform the test.

Figure 9 also reveals small changes in the $\gamma_{dm\acute{a}x}$ parameter (Miranda, 2017), while the main differences between the stabilizers can be noted in the optimal water content ω_{opt} . The water content is also necessary to later obtain the e_{min} parameter.

3.3 Unconsolidated Undrained triaxial test (UU)

To perform the UU triaxial tests there were used reconstituted specimens, for the eight cases considering the natural soil and the seven stabilizers. For the fulfilment of the trial a total of 144 specimens were tested (See Figure 10).

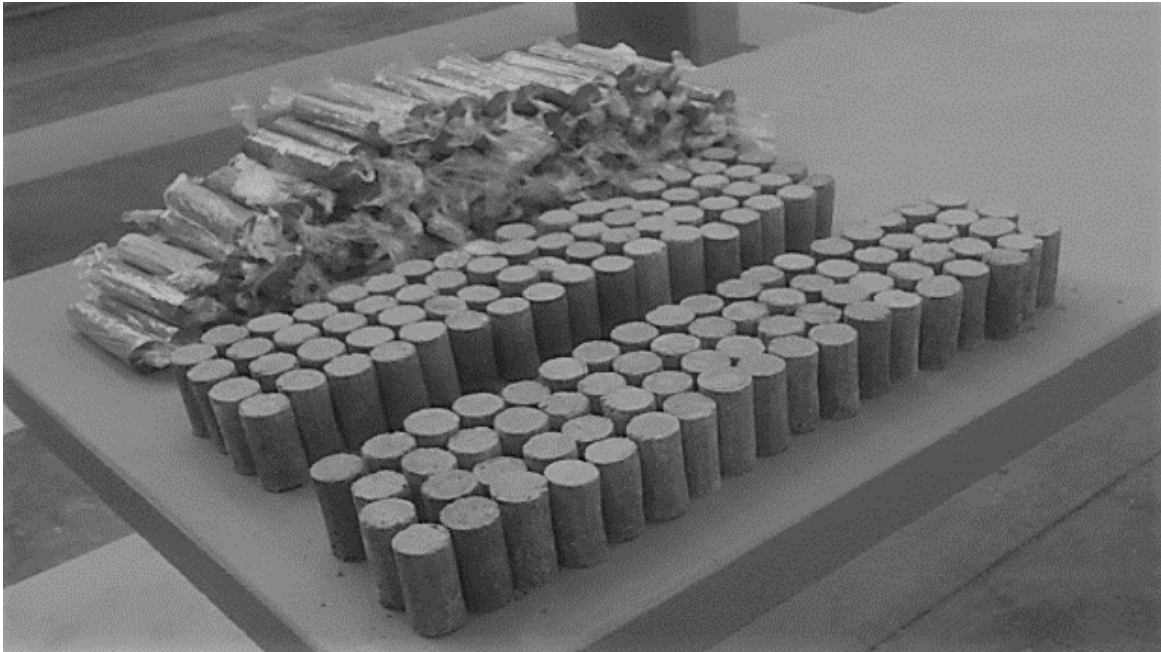


Figure 10. 144 specimens of clay mixtures with different stabilizers ready for the triaxial test UU (Miranda, 2017).

In Figure 11 we can see the correlation between the Deviator Stress (σ_d) and the Unitary Strain (ϵ), data that indicates us the failure mode of every combination of the clayey soil and stabilizers. The samples which presented an improvement in the plasticity (CL) also presented changes in their expansibility behaviour. This behaviour of the mixtures is really meaningful, as it can improve these materials and impact positively on construction purposes, being clever implementations on field work and many other applications.

Practically all the mixtures improved their behaviour regarding the compression strength and strains. It is clear that the 6% G mixture enhances the material rigidizing it, and increasing the mechanical compression resistance, which is noted in the greater grade of its curve.

The stabilization of soils with gypsum is not very common in practical purposes and the information about its use is scarce; nevertheless, the results shown provide certainty about its utilization. It is known that the G is soluble in water, for this reason thorough protective measures are required. After the G samples we can find the mixtures with L, RS and PC with similar behaviours; these materials are very usual for the stabilization of soils, therefore the improvement was expected. For instance, the mixtures with L produce a reaction between the lime and the water which diminish the permeability of the soil and increase the loading capacity in few hours, building a structural layer strong and flexible (Reginaldo et al., 2018).

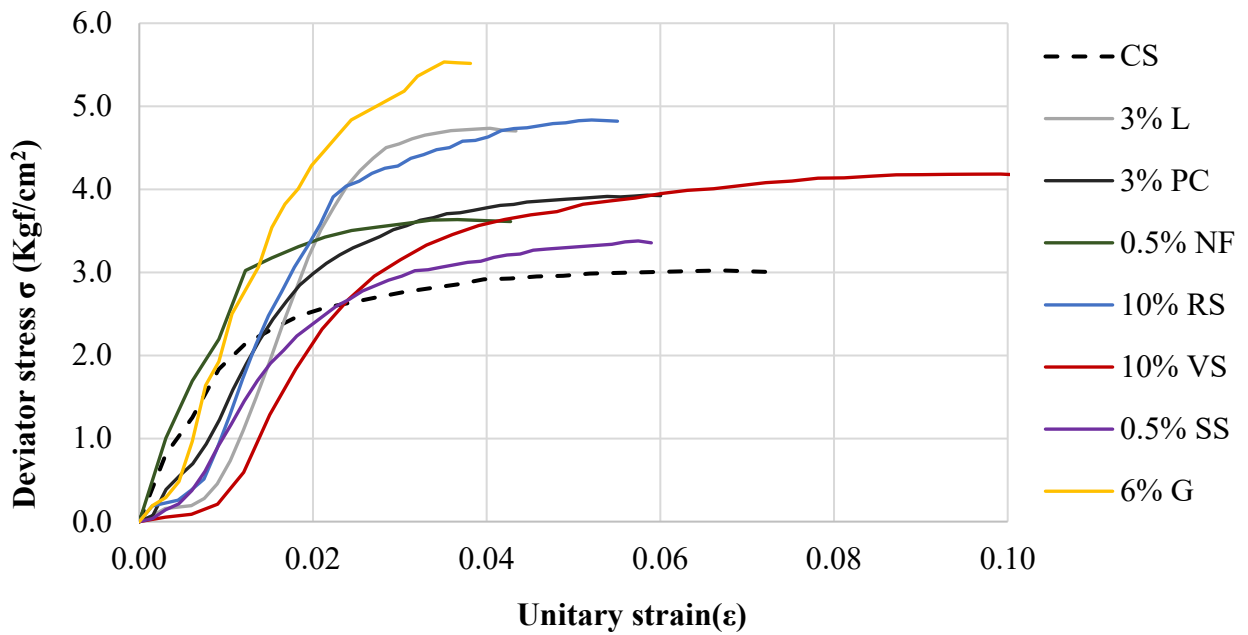


Figure 11. Stress-strain diagram curves.

Figure 12 displays an example of rupture envelope, using at least 3 Mohr's circles to determine the tendency of the envelope line, and with it, calculate the cohesion (c) and the internal friction angle (ϕ).

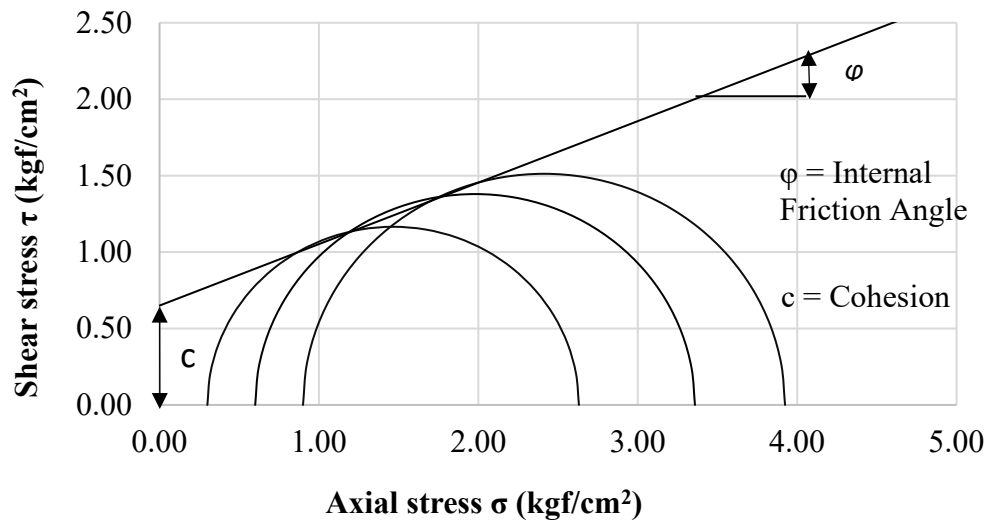


Figure 12. Rupture envelope obtained for the original soil (in situ), $c = 0.65 \text{ kgf/cm}^2$ y $\phi = 22^\circ$.

In order to simplify the display and graphic representation of the rupture envelopes, the Figure 13 presents the set of results of the CS and the stabilized clayey soils without showing the 3 respective Mohr's circles which produced the envelope.

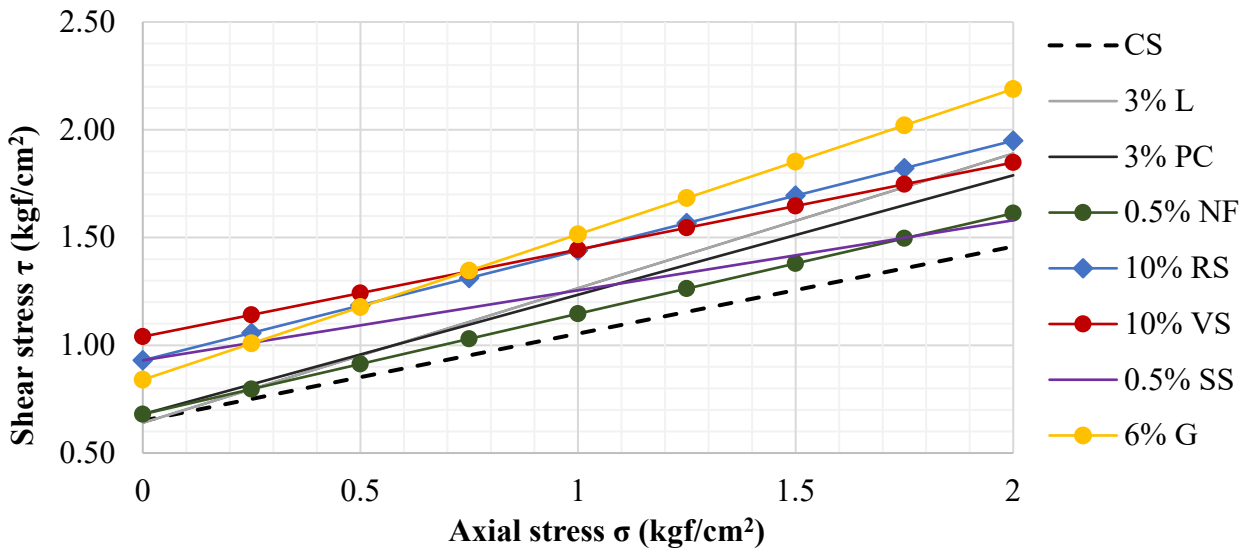


Figure 13. Correlative of the rupture envelopes of the control sample and the mixtures with stabilizers.

In Figure 14 it can be spotted how all the stabilizers employed increase the cohesion to a greater or lesser extent. The variation on the improvement degree of the cohesion (c) depends on the particular properties of each stabilizer regarding the prime materials and the natural clayey soil. In this trial the most outstanding materials were RS, VS, SS and G. Regarding the internal friction angle (ϕ), it can be observed that the performance is inversely proportional to the cohesion: the better results correspond to L, PC and G; these three stabilizers are materials which react chemically in presence of water and form new mineral phases with more mechanical resistance, which has a positive impact on the ϕ value. It is very interesting the fact that G impacts positively on both variables, being the only stabilizer with this behaviour.

It is important to mention that the increase of the internal friction angle is more important than the increase of cohesion, being a property highly appreciated in soils for building purposes. This is because the improve in the mechanical resistance can be easily lost with the presence and contact of water next to the soil particles, therefore, the capability of resistance become more important due to the cohesion between the clay particles.

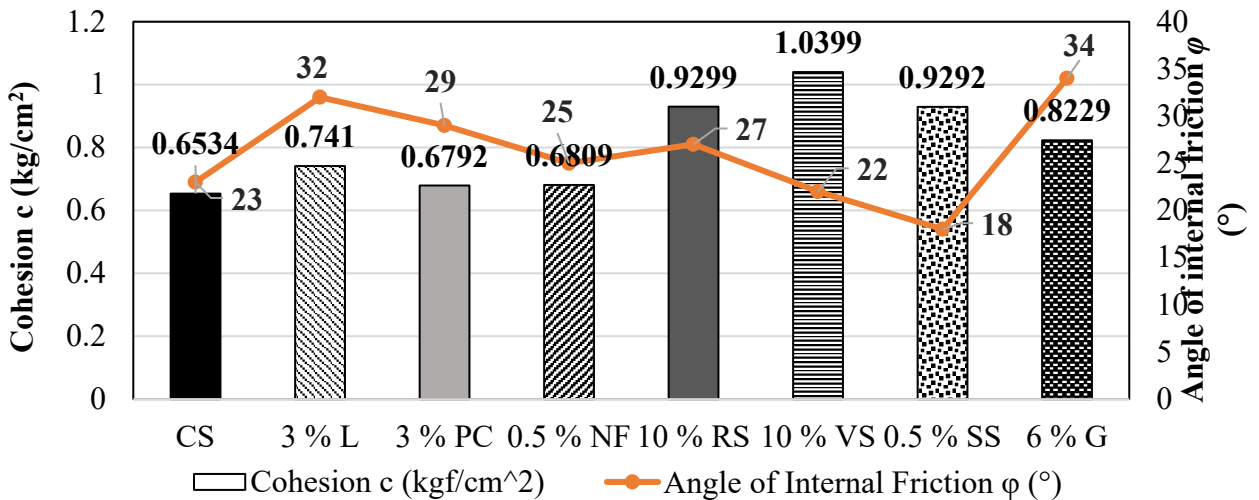


Figure 14. Cohesion (c) and internal friction angle (ϕ) values of the original sample and the mixtures with stabilizers.

4. CONCLUSIONS

The results shown in this manuscript correspond only to the study of the clayey soils of Santiago Undameo, in Michoacan, Mexico. It is important to underline that the extrapolation of these results to similar materials must be cautious and rely on the direct experimentation. The methodology proposed in this research and the innovation degree of some tests for clayey soils can be extremely useful for many applications in construction materials and for the restoration of heritage and historical buildings.

The rupture envelopes lines obtained with the control simple (the natural soil without any stabilization) allowed to determine the change on the maximum stress withstander, by means of the cohesion (c) and the angle of internal friction (ϕ) parameters. These two were obtained for each one of the stabilizers used, being the main contribution of the research.

Regarding the benefits of the stabilization, while improving the behaviour of soils we are impacting positively the environment, due to the several ecological and economic benefits we can achieve. For example, we can reduce or eliminate the transportation costs of the materials employed in a construction, which increase with the distance to the exploitation site. On the other hand, with the stabilization, we can achieve those certain materials which don't meet the standard requirements (a common situation with the materials extracted on site), reach the necessary resistance for their performance as pavement structures for instance. Regarding these civil engineering uses we can improve the behaviour of the soils, while reducing the thickness of the structures, which will decrease substantively the budget of the road paving works and a lesser operation of the quarries. The results shown that six of the stabilizers added to the clayey soils modified the USCS classification, from CH to CL. The 3% L sample showed the best improvement, since the mixture located between the region of the silts and the low plasticity clays in the chart. On the other hand, the NF addition modified next to nothing the properties of the clay, being located in the limit between high and low plasticity materials. The additions provide many other changes in the properties of soils, nevertheless, the plasticity is one of the most important due to the problems explained in the introduction of the article presented by the earthen constructions, the infrastructures or the heritage buildings and monuments.

With the rupture envelopes, it was observed a change of the cohesion c and the internal friction angle ϕ , which translates into an increase of the mechanical resistance of the mixtures. In this respect, the stabilizers which produced a higher friction between the soil particles (greater ϕ) were G, L, PC, RS and NF respectively. Conversely, VS did not provide any increase in the mechanical properties, as the internal friction angle (ϕ) was very similar to the natural soil; additionally, the SS was not very successful for this purpose.

The addition of certain stabilizers guarantees a meaningful increase of the mechanical properties of expansive soils. In the case of Santiago Undameo, the addition of L and G provided an improvement of the physical and mechanical properties. These two materials diminish the plasticity while enhancing the workability of the construction systems, being very desirable qualities for building and restoration purposes, with minimal aesthetic and colorimetric changes. Both L and G require lesser production energy than other industrial stabilizers, therefore they generate a minor environmental impact, being sustainable materials.

In the case of the adobes of the vernacular Mexican heritage and its restoration, these structures have several conservation problems and also difficulties for the stabilization of the materials. For these traditional systems, L continues to be the best choice for the stabilization of clays, in contrast with the PC, which is not suitable for these uses. Nevertheless, the PC has demonstrated utility for many other uses regarding soils, for example the manufacturing of CEB, a construction technology with low environmental impact which can achieve remarkable mechanical resistances and also presents a better behaviour in presence of water due to its compaction process.

Finally, we can conclude that the seven proposed additions, being analysed in laboratory under the international standards ASTM, improved the behaviour of a high plasticity soil. The stabilizers diminished the volumetric and lineal deformations and increased the mechanical resistance and the angle of internal friction of the mixtures. This research contributes beneficially to the improvement of clayey soils for purposes like the restoration of earthen heritage constructions, civil engineering, pathologies in buildings and construction technologies.

5. ACKNOWLEDGEMENTS

The authors thank the financial support given by the Coordinación de la Investigación Científica and the materials laboratory “Ing. Luis Silva Ruelas” of the Faculty of Civil Engineering of the UMSNH; the CONACYT through the project PRONACES 321260; and the Program Programa de Becas Nacionales; the SEP (Secretaría de Educación Pública) with the programs Prodep/Promep. The authors also acknowledge the inestimable technical support of the engineers O. S. Miranda Leal, F. J. Jerónimo Rodríguez, J. I. Bocanegra Torres, and P. García Díaz during the mechanical quantifications, as well as the technicians of the laboratory LANCIC-UNAM during the micro-characterization of the materials.

6. REFERENCES

- Abhilash, H. N., Hamard, E., Beckett, C. T., Morel, J.-C., Varum, H., Silveira, D., Ilampas, R. (2022), Chapter 4. Mechanical Behaviour of Earth Building Materials. In A. Fabbri, J.-C. Morel, J.-E. Aubert, Q.-B. Bui, D. Gallipoli, B. V. Venkatarama Reddy (Eds.), “*Testing and Characterisation of Earth-based Building Materials*”, Springer, cap. 4, pp. 127-180. doi: https://doi.org/10.1007/978-3-030-83297-1_4
- Akkaya, İ., Özvan, A., Özvan, E. E. (2019), *A new empirical correlation between pressuremeter modules (EM) and shear wave velocity (Vs) for clay soils*. Journal of Applied Geophysics. 171(103865). <https://doi.org/10.1016/j.jappgeo.2019.103865>
- Alonso, E., Martínez-Gomez, L., Martínez, W., & Castano, V. M. (2002), *Preparation and Characterisation of Ancient-Like Masonry Mortars*. Advanced Composite Letters. 11(1). doi: <https://doi.org/10.1177/096369350201100105>
- Araya-Letelier, G., Antico, F. C., Burbano-García, C., Concha-Riedel, J., Norambuena-Contreras, J., Concha, J., & Saavedra Flores, E. I. (2021), *Experimental evaluation of adobe mixtures reinforced with jute fibers*. Construction and Building Materials. 276(122127). doi: <https://doi.org/10.1016/j.conbuildmat.2020.122127>
- Asociación Española de Normalización y Certificación (AENOR). (1998). *UNE 103402: Determinación de los Parámetros Resistencia de Una Muestra de Suelo en el Equipo Triaxial*.
- Asociación Española de Normalización (AENOR) (2019), *UNE-EN ISO 17892-8:2019 Investigación y ensayos geotécnicos; Ensayos de laboratorio de suelos, Parte 8: ISO 17892-8:2018 Ensayo triaxial sin consolidación y sin drenaje*.
- ASTM International (2019), *ASTM C136/C136M-19 Standard Test Method for Sieve Analysis of Fine and Coarse Aggregates*. doi: https://doi.org/10.1520/C0136_C0136M-19
- ASTM International (2017), *ASTM D7928-17 Standard Test Method for Particle-Size Distribution (Gradation) of Fine-Grained Soils Using the Sedimentation (Hydrometer) Analysis*. doi: <https://doi.org/10.1520/D7928-17>
- ASTM International (2017). *ASTM D2487-17 Standard Practice for Classification of Soils for Engineering Purposes (Unified Soil Classification System)*. doi: <https://doi.org/10.1520/D2487-17>
- ASTM International (2017). *ASTM D4318-17e1 Standard Test Methods for Liquid Limit, Plastic Limit, and Plasticity Index of Soils*. doi: <https://doi.org/10.1520/D4318-17>

- ASTM International (2021). *ASTM D698-12e2 Standard Test Methods for Laboratory Compaction Characteristics of Soil Using Standard Effort (12 400 ft-lbf/ft³(600 kN-m/m³))*. doi: <https://doi.org/10.1520/D0698-12R21>
- ASTM International (2015). *ASTM D2850-15 Standard Test Method for Unconsolidated-Undrained Triaxial Compression Test on Cohesive Soils*. doi: <https://doi.org/10.1520/D2850-15>
- ASTM International. (2007) *ASTM D421-85 Standard Practice for Dry Preparation of Soil Samples for Particle-Size Analysis and Determination of Soil Constants (Withdrawn 2016)*.
- ASTM International (1998). *ASTM D 422-63 (Reapproved 1998) Standard Test Method for Particle-Size Analysis of Soils*.
- Chompoorat, T., Thepumong, T., Khamplod, A., Likitlersuang, S. (2022), *Improving mechanical properties and shrinkage cracking characteristics of soft clay in deep soil mixing*. Construction and Building Materials. 316(125858). <https://doi.org/10.1016/j.conbuildmat.2021.125858>
- Costa, C., Cerqueira, Â., Rocha, F., & Velosa, A. (2019), *The sustainability of adobe construction: past to future*. International Journal of Architectural Heritage. 13: 639-647. doi: <https://doi.org/10.1080/15583058.2018.1459954>
- Daneels, A., Romo de Vivar, A., Chávez, L., Reyes, M., Tapia, E., León, M., . . . Otero, F. J. (2020), *Bitumen-stabilized earthen architecture: The case of the archaeological site of La Joya, on the Mexican Gulf Coast*. Journal of Archaeological Science: Reports, 34(A). doi: <https://doi.org/10.1016/j.jasrep.2020.102619>
- Díaz-Blanco, Y., Menchaca-Campos, C., Rocabrano-Valdés, C. I., Uruchurtu-Chavarín J. (2019), *Influencia de un aditivo natural (mucílago de nopal) en las propiedades electroquímicas del acero de refuerzo del concreto*. Revista ALCONPAT. 9 (3): 260- 276. doi: <http://dx.doi.org/10.21041/ra.v9i3.429>
- Flores Rentería, A. (2010), “*La norma ASTM D6276 como instrumento de estabilización de suelos para fines patrimoniales*”. Bachelor Thesis, Faculty of Civil Engineering, Universidad Michoacana San Nicolás de Hidalgo.
- Kalifala, D., Ouedraogo, M., Millogo, Y., Aubert, J. E., Gomina, M. (2018), *Thermal, hydric and mechanical behaviours of adobes stabilized with cement*, Construction and Building Materials. <https://doi.org/10.1016/j.conbuildmat.2017.10.001>
- Knapen, E., Van Gemert, D. (2009), *Cement hydration and microstructure formation in the presence of water-soluble polymers*. Cement and Concrete Research. 39(1): 6-13. doi: <https://doi.org/10.1016/j.cemconres.2008.10.003>
- Ige, O. and Danso, H. (2021), *Physico-mechanical and thermal gravimetric analysis of adobe masonry units reinforced with plantain pseudo-stem fibres for sustainable construction*. Construction and Building Materials. 273(121686). <https://doi.org/10.1016/j.conbuildmat.2020.121686>
- Jitha P. T., Sunil Kumar B., Raghunath, S. (2020), *Strength development and masonry properties of geopolymer stabilised soil-LPC (lime-pozzolana cement) mixes*. Construction and Building Materials. 250(118877). <https://doi.org/10.1016/j.conbuildmat.2020.118877>
- Laborel-Préneron, A., Faria, P., Aubert, J.-E., Magniont, C. (2021), *Assessment of Durability of Bio-based Earth Composites*. Recent Progress in Materials. 3(2). doi:10.21926/rpm.2102016
- Lan Guanqi, L., Yihong Wan, Y., Xin, L., Liu, Y. (2020), *Shear test method analysis of earth block masonry mortar joints*. Construction and Building Materials. 264 (119997). <https://doi.org/10.1016/j.conbuildmat.2020.119997>
- Li Piani, T., Weerheijm, j., Peroni, M., Koene, L., Krabbenborg D., Solomos, G., Sluys, L. J. (2020), *Dynamic behaviour of adobe bricks in compression: The role of fibres and water content at various loading rates*, Construction and Building Materials. 230(117038). <https://doi.org/10.1016/j.conbuildmat.2019.117038>

- Martínez, W., Alonso, E. M., Rubio, J. C., Bedolla, J. A., Velasco, F. A., Torres, A. A. (2008), *Comportamiento Mecánico de Morteros de Cal Apagada Artesanalmente, Adicionados con Mucilago de Cactácea y Ceniza Volcánica, para su uso en Restauración y Conservación de Monumentos Coloniales*. Revista de la Construcción. 7(2): 93-101.
- Martínez, W., Torres-Acosta, A. A., Alonso-Guzmán, E. M., Chávez, H. L., Lara, C., Bedolla, A., Ruvalcaba, J. L. (2018), *Colorimetry of clays modified with mineral and organic additives*. Revista ALCONPAT. 8(2):163-177. <https://doi.org/10.21041/ra.v8i2.277>
- Mauricio, A. C., Grieseler, R., Heller, A. R., Kelley, A. R., Rumiche, F., Sandweiss, D. H., Viveen, W. (2021), *The earliest adobe monumental architecture in the Americas*. PNAS, 118(48). doi: <https://doi.org/10.1073/pnas.2102941118>
- Miranda Leal O. S. (2017), “*Envolvente de falla en arcilla de Santiago Undameo, con diferentes estabilizadores; realizados en la máquina triaxial Soiltest t-500*”. Bachelor Thesis, Faculty of Civil Engineering, Universidad Michoacana San Nicolás de Hidalgo.
- Mirjalili, A., Eslami, A., Morshed, R. (2020), *Experimental investigation into the effect of vertical loading on in-plane cyclic behavior of adobe walls*. Construction and Building Materials. 264(120706). <https://doi.org/10.1016/j.conbuildmat.2020.120706>
- Moraes, J. C., Akasaki, J. L., Melges, J. L., Monzó, J., Borrachero, M. V., Soriano, L., . . . Tashima, M. M. (2015), *Assessment of sugar cane straw ash (SCSA) as pozzolanic material in blended Portland cement: Microstructural characterization of pastes and mechanical strength of mortars*. Construction and Building Materials. 94: 670-677. doi: <https://doi.org/10.1016/j.conbuildmat.2015.07.108>
- Nagaraj, H. B., Sravan, M. V., Arun, T. G., & Jagadish, K. S. (2014), *Role of lime with cement in long-term strength of Compressed Stabilized Earth Blocks*. International Journal of Sustainable Built Environment. 3(1): 54-61. doi: <https://doi.org/10.1016/j.ijbsbe.2014.03.001>
- Navarro Mendoza, E. G., Sánchez Calvillo, A., Alonso Guzmán, E. M. (2019), “*Estabilización de suelos arcillosos con cal para firmes y blocks*”. In C. Neves, Z. Salcedo Gutiérrez, O. Borges Faria (Eds.), 19° Seminario Iberoamericano de Arquitectura y Construcción con Tierra, FUNDASAL / PROTERRA). San Salvador: El Salvador, pp. 284-291.
- Ojeda Fariás, O. F., Baltazar Zamora, M. Á., Mendoza Rangel, J. M. (2018), *Influence of sugar cane bagasse ash inclusion on compacting, CBR and unconfined compressive strength of a subgrade granular material*. Revista ALCONPAT. 8(2): 194-208. doi: <https://doi.org/10.21041/ra.v8i2.282>
- Olacia, E., Pisello, A. L., Chiodo, V., Maisano, S., Frazzica, A., Cabeza, L. F. (2020), *Sustainable adobe bricks with seagrass fibres. Mechanical and thermal properties characterization*. Construction and Building Materials. 239(117669). <https://doi.org/10.1016/j.conbuildmat.2019.117669>
- Parisi, F., Balestrieri, C., Varum, H. (2019), *Nonlinear finite element model for traditional adobe masonry*. Construction and Building Materials. 223: 450-462. <https://doi.org/10.1016/j.conbuildmat.2019.07.001>
- Pérez Nora, A., Bucio, L., Lima, E., Soto, E., Cedillo, C. (2016), *Identification of allophane and other semi-crystalline and amorphous phases on pre-Hispanic Mexican adobe earth bricks from Cholula, Mexico*. Microchemical Journal. 126(349-358). <https://doi.org/10.1016/j.microc.2015.12.033>
- Rodríguez-Mariscal, J. D., Solís, M., Cifuentes, H. (2018), *Methodological issues for the mechanical characterization of unfired earth bricks*. Construction and Building Materials. 175: 804-814. <https://doi.org/10.1016/j.conbuildmat.2018.04.118>
- Ramírez-Arellanes, S., Cano-Barrita, P. F. de J., Julián-Caballero, F., Gómez-Yañez, C. (2012), *Propiedades de durabilidad en concreto y análisis microestructural en pastas de cemento con*

- adición de mucilago de nopal como aditivo natural*. *Materiales de Construcción*. 62(307): 327–341. doi: <https://doi.org/10.3989/mc.2012.00211>
- Reginaldo-Sérgio, P., Fabiano-Emmert, E., Pereira-Miguel A. G. (2018), *Soil Stabilization with Lime for the Construction of Forest Roads*. *Floresta e Ambiente*. 25(2). <https://doi.org/10.1590/2179-8087.007715>
- Sanchez-Calvillo, A., Alonso-Guzman, E. M., Martinez-Molina, W., Navarrete-Seras, M. A., Ruvalcaba-Sil, J. L., Navarro-Ezquerria, A., Mitrani, A. (2021), *Characterization of adobe blocks: Point-load assessment as a complementary study of damaged buildings and samples*. *Heritage*. 4(2): 864-888. doi: <https://doi.org/10.3390/heritage4020047>
- Secretaría de Comunicaciones y Transportes (SCT) (2007), *M-MMP-1-07/07. Límites de Consistencia*.
- Secretaría de Comunicaciones y Transportes (SCT) (2006), *M-MMP-1-09/06. Métodos de muestreo y prueba de materiales. Compactación AASHTO*.
- Sharma, V., Vinayak, H. K., & Marwaha, B. M. (2015), *Enhancing sustainability of rural adobe houses of hills by addition of vernacular fiber reinforcement*. *International Journal of Sustainable Built Environment*. 4(2): 348-358. <https://doi.org/10.1016/j.ijbsbe.2015.07.002>
- Skempton, A. W. (1953). “*The colloidal activity of clays*”. In: *Proceedings of the third international conference on soil mechanics and foundation engineering*. ICOSOMEF, Zurich: Switzerland, pp. 57-61.
- Taallah, B., Guettala, A. (2016), *The mechanical and physical properties of compressed earth block stabilized with lime and filled with untreated and alkali-treated date palm fibers*. *Construction and Building Materials*. 104(1): 52-62. doi: <https://doi.org/10.1016/j.conbuildmat.2015.12.007>
- Vasic M.V., Pezo, L. L., Radojevic, Z. (2020), *Optimization of adobe clay bricks based on the raw material properties (mathematical analysis)*. *Construction and Building Materials*. 244(118342). <https://doi.org/10.1016/j.conbuildmat.2020.118342>
- Wang, C., Li, S., He, X., Chen, Q., Zhang, H., & Liu, X. (2021), *Improved prediction of water retention characteristic based on soil gradation and clay fraction*. *Geoderma*. 404(115293). <https://doi.org/10.1016/j.geoderma.2021.115293>
- Wu, B., Li, L., Xu, L., Li, X. (2022), *Modelling sheet erosion on steep slopes of clay loess soil using a rainfall simulator*. *Biosystems Engineering*. 216:1-12. <https://doi.org/10.1016/j.biosystemseng.2022.01.017>
- Yetgin, Ş., Çavdar, Ö., Çavdar, A. (2008), *The effects of the fiber contents on the mechanic properties of the adobes*. *Construction and Building Materials*. 22(3): 222-227. <https://doi.org/10.1016/j.conbuildmat.2006.08.022>

Study of the facade degradation agents associated with temperature and driving rain in different Brazilian bioclimatic zones

A. L. Ramos^{1*} , E. Bauer² 

*Contact author: analin.ramos@gmail.com

DOI: <https://doi.org/10.21041/ra.v12i2.560>

Reception: 10/01/2022 | Acceptance: 01/04/2022 | Publication: 01/05/2022

ABSTRACT

Therefore, the aim is to study the conditions of exposure to these degradation agents in buildings located in different Brazilian bioclimatic zones. Knowing the action of weathering is essential to understand the facades degradation. For this purpose, eight cities were selected: Curitiba, Santa Maria, Florianópolis, Brasília, Niterói, Goiânia, Picos and Belém. A model building was defined for hygrothermal simulation to assess total radiation, temperature range, thermal shock, intensity index temperature and driving rain. As a result, zones of critical conditions are identified, providing exposure rankings. For temperature agents and directed rain, the most exposed cities are Goiânia-GO and Belém-PA, respectively. Finally, the mildest exposure zones are Belém-PA for temperature agent and Niterói-RJ for driving rain.

Keywords: degradation; facades; ceramic coating; bioclimatic zones; temperature.

Cite as: Ramos, A. L., Bauer, E. (2022), "*Study of the facade degradation agents associated with temperature and driving rain in different Brazilian bioclimatic zones*", Revista ALCONPAT, 12 (2), pp. 248 – 262, DOI: <https://doi.org/10.21041/ra.v12i2.560>

¹ Aluna de mestrado PECC, Universidade de Brasília, Brasília, Brasil.

² Professor Doutor do PECC, Universidade de Brasília, Brasília, Brasil.

Contribution of each author

In this work, Ana Lin Ramos contributed to the activity of structuring and writing the text (100%), analysis and discussion of the results (100%). Elton Bauer contributed to the activity data collection (100%), supervision (100%) and correction of the text (100%).

Creative Commons License

Copyright 2022 by the authors. This work is an Open-Access article published under the terms and conditions of an International Creative Commons Attribution 4.0 International License ([CC BY 4.0](https://creativecommons.org/licenses/by/4.0/)).

Discussions and subsequent corrections to the publication

Any dispute, including the replies of the authors, will be published in the first issue of 2023 provided that the information is received before the closing of the third issue of 2022.

Estudio de la acción de los agentes de degradación de fachadas asociados a la temperatura y la lluvia dirigida en diferentes zonas bioclimáticas brasileñas

RESUMEN

El objetivo es estudiar las condiciones de exposición a estos agentes degradantes en edificios ubicados en diferentes zonas bioclimáticas brasileñas. Conocer la acción de la meteorización es fundamental para comprender la degradación de las fachadas. Para ello, se seleccionaron ocho ciudades: Curitiba, Santa María, Florianópolis, Brasília, Niterói, Goiânia, Picos y Belém. Se definió un modelo de construcción de simulación higrotérmica para evaluar radiación total, amplitud térmica, choque térmico, índice de intensidad de temperatura y lluvia dirigida. Como resultado, se identifican zonas de condiciones críticas, proporcionando clasificaciones de exposición. Para agentes de temperatura y lluvia dirigida, las zonas más expuestas son Goiânia y Belém. Las zonas de exposición más suaves son Belém para agente de temperatura y Niterói para lluvia dirigida.

Palabras clave: degradación; fachadas; revestimiento cerámico; zonas bioclimáticas; temperatura.

Estudo da ação de agentes de degradação de fachadas associados à temperatura e a chuva dirigida em diferentes zonas bioclimáticas brasileiras

RESUMO

Logo, objetiva-se investigar as condições de exposição a agentes de degradação em edifícios localizados em diferentes zonas bioclimáticas brasileiras. Estudar a ação do intemperismo é essencial para compreender a degradação das fachadas. Selecionou-se oito cidades representativas de cada Zona: Curitiba, Santa Maria, Florianópolis, Brasília, Niterói, Goiânia, Picos e Belém. Definiu-se um edifício modelo para simulação higrotérmica para avaliação da radiação total, amplitude térmica, choque térmico, índice de intensidade da temperatura e chuva dirigida. Como resultado, são identificadas as zonas de condições críticas, que são classificadas em função de sua gravidade. Para temperatura e chuva dirigida, as cidades mais expostas são Goiânia-GO e Belém-PA, respectivamente. As de exposição mais amenas são Belém-PA para agente de temperatura e Niterói-RJ para chuva dirigida.

Palavras-chave: degradação; fachadas; revestimento cerâmico; zonas bioclimáticas; temperatura.

Legal Information

Revista ALCONPAT is a quarterly publication by the Asociación Latinoamericana de Control de Calidad, Patología y Recuperación de la Construcción, Internacional, A.C., Km. 6 antigua carretera a Progreso, Mérida, Yucatán, 97310, Tel.5219997385893, alconpat.int@gmail.com, Website: www.alconpat.org

Reservation of rights for exclusive use No.04-2013-011717330300-203, and ISSN 2007-6835, both granted by the Instituto Nacional de Derecho de Autor. Responsible editor: Pedro Castro Borges, Ph.D. Responsible for the last update of this issue, Informatics Unit ALCONPAT, Elizabeth Sabido Maldonado.

The views of the authors do not necessarily reflect the position of the editor.

The total or partial reproduction of the contents and images of the publication is carried out in accordance with the COPE code and the CC BY 4.0 license of the Revista ALCONPAT.

1. INTRODUCTION

The facade is a constructive element aimed at protecting the building from the external environment and becoming, thus, greatly exposed to factors such as solar radiation, driving rain, and temperature. Such exposure allows a complex degradation process involving agents of different nature that can act in synergy, affecting the performance and useful life of the building components and materials through different degradation mechanisms (Bauer et al., 2021).

The ceramic claddings commonly used on facades are associated with a specific degradation process characterized mainly by tile detachment (Bauer et al., 2015; Pacheco and Vieira, 2017) in addition to cracking, lack of ceramic-substrate adhesion, and expansion of substrates due to humidity or thermal variations (Bezerra et al., 2018). In this case, the layers making up the cladding system have different properties (thermal expansion coefficients, modulus of elasticity, thermal conductivity, etc.) and, thus, the action of agents associated with temperature becomes highly relevant (Gaspar and Brito, 2011).

Additionally, the varying surface temperature of the cladding can cause physical changes in the facade sealing system (Silva, 2000). This degradation mechanism results from the effect of expansion and contraction due to temperature variations and non-homogeneous increments that cause shear stresses, generating a separation tendency at the system interface (Saraiva, 1998). As a result, the detachments and cracks that appear in the ceramic claddings can be intensified by the fatigue caused by thermomechanical efforts derived from temperature variations, in addition to restrictions on deformation (Barbosa, 2013).

The weighted thermal amplitude, represented by the Temperature Intensity Index, as well as solar radiation and thermal shocks are used as a representative value of the thermal amplitude and indicative of a greater degradation. The I_{TI} constitutes an analysis of the thermal amplitude that yields a weighted measurement concerning frequency (Nascimento, 2016) and thermal shock, which are punctual events characterized by a high difference in surface temperature in a short time interval (Zanoni, 2015).

The driving rain acting under the facades is considered a highly relevant agent (Nascimento et al., 2016). This action results from the association between rain and wind and is one of the main sources of water on building facades. Without the action of the wind, the rain would fall vertically without wetting significantly the walls (Zanoni, 2015). However, due to the action of the wind, the rain hits mainly the top and sides of buildings. And, although ceramic claddings suffer less significantly from the precipitation incidence compared to the mortar system (Bauer et al., 2018), it should be considered in hygrothermal simulations to understand the degradation process.

The degradation of ceramic cladding systems is mainly characterized by ceramic detachment, even though the degradation process changes for different geographical locations (Souza, 2019). Therefore, it is necessary to study the conditions of exposure to the actions of climatic agents to understand the different conditions triggering the degradation process in different regions.

As a continental country, Brazil has climatic variations throughout its territory. For this reason, ABNT NBR 15220-3 (2005) establishes the Brazilian bioclimatic zoning by classifying 330 cities according to their climate into eight bioclimatic zones. These zones are defined as homogeneous geographic regions regarding climate elements that interfere with the built environment and human comfort relationship. Buildings and their elements located in different zones are subject to different exposure conditions to the climate agents that cause the degradation process.

The objective of the proposed investigation is to analyze the action of degradation agents associated with temperature and driving rain on the facades of buildings located in different Brazilian bioclimatic zones. Therefore, the hygrothermal simulation performed using the WUFI Pro 6.5 software, a useful tool for studying degradation (Bauer et al., 2018; Gonçalves et al., 2018), allowed to obtain data on incident solar radiation, surface temperature and driving rain on the North facades

of a model building subjected to the different climatic conditions of each zone.

2. METHODS

2.1 Details of the model building.

In this study, the model building is 20m high with a 63.5% absorbance ceramic cladding system (Dornelles, 2007) corresponding to the dark red color, chosen to highlight the effects of temperature, since dark colors present higher surface temperature when exposed to radiation (Uchôa et al., 2016). This model building is placed in different cities located in the eight Brazilian bioclimatic zones as established in the ABNT NBR 15220-3 (2005). Table 1 shows the chosen cities and the corresponding bioclimatic zone.

Table1. City, State and the different bioclimatic zones.

Z1	Z2	Z3	Z4	Z5	Z6	Z7	Z8
Curitiba-PR	Santa Maria-RS	Florianópolis-SC	Brasília-DF	Niterói-RJ	Goiânia-GO	Picos-PI	Belém-PA

2.2 Simulation

The hygrothermal simulation in the WUFI Pro 6.5 software is used to evaluate the action of climatic agents on the facades in each city. The software allows entering data such as simulation period, configuration, orientation and inclination of the construction system, coefficients of driving rain and transfer to the surface, initial conditions of temperature and relative humidity, as well as interior and exterior climatic conditions (Freitas, 2011). The simulation output yields the hourly values of total radiation incident on the facades, surface temperature and precipitation.

The simulation was performed for one year period, between 01/01/2019 and 01/01/2020. The outdoor weather conditions of each city are defined based on the Typical Meteorological Year (TMY) files from the EPW/ANTAC database (Roriz, 2012). Table 2 contains the values adopted for the surface transfer coefficients.

Table 2. Transfer coefficients to the external surface adopted in the simulation.

Coefficient	Unit	Value
Thermal Resistance (left side)	m ² K/W	0.058
Absorption (Shortwave Radiation)	-	0.635
Soil Reflectivity	-	0.2
Incident rain reduction factor	-	0.7

In the study, because all cities studied are below the equator, we chose to analyze only the North facade of each building, which is critical for the incidence of solar radiation. The simulated construction system consists of ceramic cladding, cementitious plastering mortar, ceramic block, internal mortar, and the main monitoring point on the cladding surface. Figure 1 shows the system launched in the program.

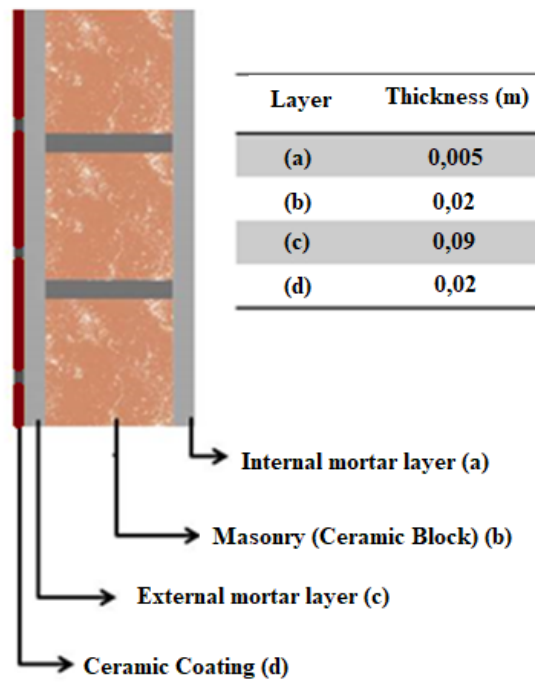


Figure 1. Evaluated constructive system: (a) ceramic tile; (b) external mortar/plaster; (c) ceramic block; (d) internal mortar.

The properties of the materials used in the constructive system layers had already been determined in previous tests conducted by other researchers. The lab tests determined apparent specific mass; porosity; water vapor permeability to calculate the water vapor diffusion resistance factor; water absorption coefficient or capillarity coefficient; and hygroscopic curve. The test results are described in detail in the LEM-UnB Internal Report (Bauer et al., 2015). Table 3 summarizes these results.

Table 3. Summary of material properties.

Properties	Ceramic Block	Ceramic Tile	Plaster Mortar
Apparent specific mass (kg/m ³)	578	1730	1830
Porosity (m ³ /m ³)	0.486	0.29	0.2604
Permeability to water vapor (kg/(m.s.Pa))	8.38. 10 ⁻¹²	1.66. 10 ⁻¹²	7.9. 10 ⁻¹²
Water absorption coefficient (kg/m ² .√s)	0.09	0.001	0.089

2.3 Degradation agents associated with temperature.

2.3.1 Total radiation, maximum and minimum surface temperature and maximum thermal amplitude.

Equation 1 uses surface temperature data to determine the maximum and minimum temperatures, as well as the daily thermal amplitudes over the simulation period. Furthermore, the daily solar radiation data observed on each facade are added to determine the solar radiation accumulated on the facade over the simulation period.

$$\Delta T = t_{\max} - t_{\min} \quad (1)$$

Where ΔT is the thermal amplitude, t_{\max} is the daily maximum surface temperature of the facade, and t_{\min} is the daily minimum surface temperature of the facade.

2.3.2 Thermal shock

Thermal shock is also analyzed in the study of the effects associated with temperature (Zanoni, 2015). For this purpose, the occurrence frequency of the events called full and attenuated thermal shock is determined for all facades during the simulation year. Full thermal shock is defined by a surface temperature difference greater than 8 °C in a 1-hour interval, whereas attenuated thermal shock consists of the same temperature difference verified in a 2-hour interval. The equations for full (2) and attenuated (3) thermal shock are:

$$\Delta T_{ch} = t_n - t_{n-1} \quad (2)$$

$$\Delta T_{ch} = t_n - t_{n-2} \quad (3)$$

The results are shown in graphs of annual occurrence frequency (%) calculated from the relationship between the total number of occurrences of thermal shocks and the number of hours in a year.

2.3.3 Weighted Thermal Amplitude

To analyze the effects associated with temperature, the weighted thermal amplitude expressed as I_{IT} is calculated for all facades, considering the effects of cycles and surface temperature values reached in the systems (Nascimento, 2016). The I_{IT} is established based on temperature variations and their frequency of occurrence in a given pre-established interval. To do so, the variation range of thermal amplitude is divided into four equal intervals, represented by average amplitude values. The I_{IT} is calculated as a weighted average from the frequency values verified for the climate of Brasilia in the given time interval of one year in this study.

Table 4 shows the ranges of the thermal amplitude variation distributed in four equal intervals (Nascimento, 2016) as follows: below 11.5°C (range 1) to greater than 27.7°C (range 4). Finally, I_{IT} is calculated as shown in (4).

Table 4. Thermal amplitude ranges considered for calculating I_{IT} .

Range	$\Delta T(^{\circ}\text{C})$	ΔT mean ($^{\circ}\text{C}$)
4	>27.7	31.8
3	19.7 a 27.7	23.7
2	11.5 a 19.6	15.6
1	< 11.5	7.5

$$I_{IT} = \sum \frac{\Delta T_{mean} \times f_n}{f_{total}} \tag{4}$$

Where I_{IT} is the temperature intensity index (°C), ΔT_{mean} is the amplitude of the average temperature in the range of occurrence (°C), f_n is the occurrence frequency of range “n” of ΔT , and f_{total} is the frequency of all occurrences of the four study ranges in the year, i.e., $f_{total} = 365$.

2.3.4 Driving rain

The driving rain is studied using the WUFI software, in which hourly values of precipitation, wind speed and direction are obtained for a total of 8760 hours and used as input data in the computer simulations (Zanoni, 2015). From this, the intensity of driving rainfall is calculated using equation (5).

$$R_{wdr} = R_2 \cdot R_h \cdot V \cdot \cos(D - \theta) \tag{5}$$

Where R_{wdr} is the intensity of driving rain (mm/h); R_h is precipitation on a horizontal surface (mm); R_2 is the coefficient dependent on the location on the facade (s/m); V is the hourly average of wind speed at a height of 10m (m/s); D is wind direction (angle from the North); θ facade orientation measured as the angle between the north and the direction normal to the wall.

In the WUFI quantification methodology, the value of R_2 depends on the building height and the location of the study area of the facade as shown in Table 5. In this study, we adopted the value of 0.2 for tall buildings, upper part taller than 20 m. The simulation output data are the values of precipitation incidents on the facades while the annual accumulated driving rain expressed as l/m² is calculated.

Table 5. R_2 values tabulated in the WUFI quantification methodology.

Height	R_2
Small building, height up to 10 m	0.07
Tall building, lower part up to 10 m	0.05
Tall building, middle part between 10 and 20 m	0.1
Tall building, upper part greater than 20 m	0.2

3. RESULTS

3.1 Total radiation, maximum surface temperature and maximum thermal amplitude.

The results of the total incident radiation and the absolute maximum surface thermal amplitudes on the North facades of the eight zones are shown in Figure 2. It is noted that the highest values occur in Z6 (38.15°C) followed by Z2 (37.5°C) and Z1 (37.15°C), whereas the lowest value is found in Z8 (22.64°C) and intermediate values were observed in the other zones. The highest solar radiation incidence is observed in Z4 (1,014,409 W/m²) followed by Z6 (995,347 W/m²) while Z8 has the lowest value (743,527 W/m²). Additionally, the solar radiation incidence is associated with the temperature gain on each facade, especially in the Z8 and Z6 zones, except for Z4, which had the highest radiation incidence and the third lowest thermal amplitude.

Total radiation is critical in Z4 and Z6, whereas exposure conditions are milder in Z8, despite being

close to the equator and represented by Belém, in PA. This result is because the solar radiation incident on the facade is only a portion of the horizontal global solar radiation (consisting of the direct, diffuse and reflected components) (Silva, 2011) dependent, therefore, on facade orientation and slope.

The surface temperature and the thermal amplitude at the surface result from the interaction between solar radiation and the rise in air temperature throughout the day, thus being better indicators of hygrothermal variations than the total incident solar irradiation (Zanoni, 2015). In this case, Z6 and Z7 are critical zones, as they have a higher thermal amplitude (Figure 2) and higher surface temperature (Figure 3) throughout the year, respectively.

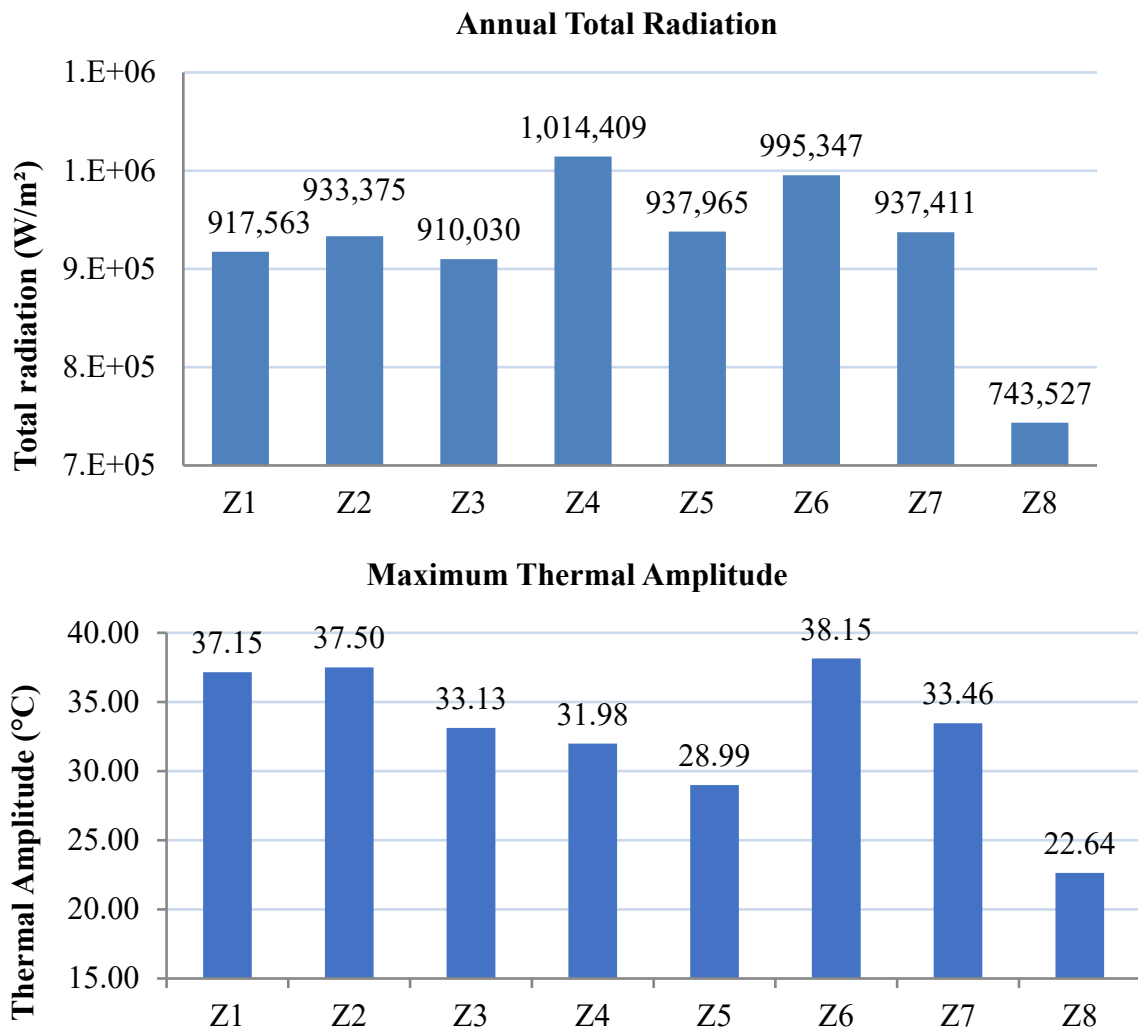


Figure 2. Total accumulated radiation and maximum thermal amplitude in the simulation year.

The annual maximum and minimum temperatures for each of the studied facades are shown in Figure 3. It is noted that the lowest temperatures, measured when there is no incident radiation on the facade, vary greatly in the studied buildings. The lowest temperatures of 2.99°C, 5.48°C and 6.98°C were measured for Z2, Z1 and Z3, respectively. Meanwhile, Z8, despite having a lower incidence of total radiation on the facade, has a higher minimum (22.07°C) and a lower maximum (46.16°C) temperature, which is consistent with reduced thermal amplitudes, as shown in Figure 2. In this case, it is emphasized that the surface temperature is linked not only to the incidence of radiation on the facade but also to the air temperature (ASHRAE, 2009; Lamberts et al., 2011).

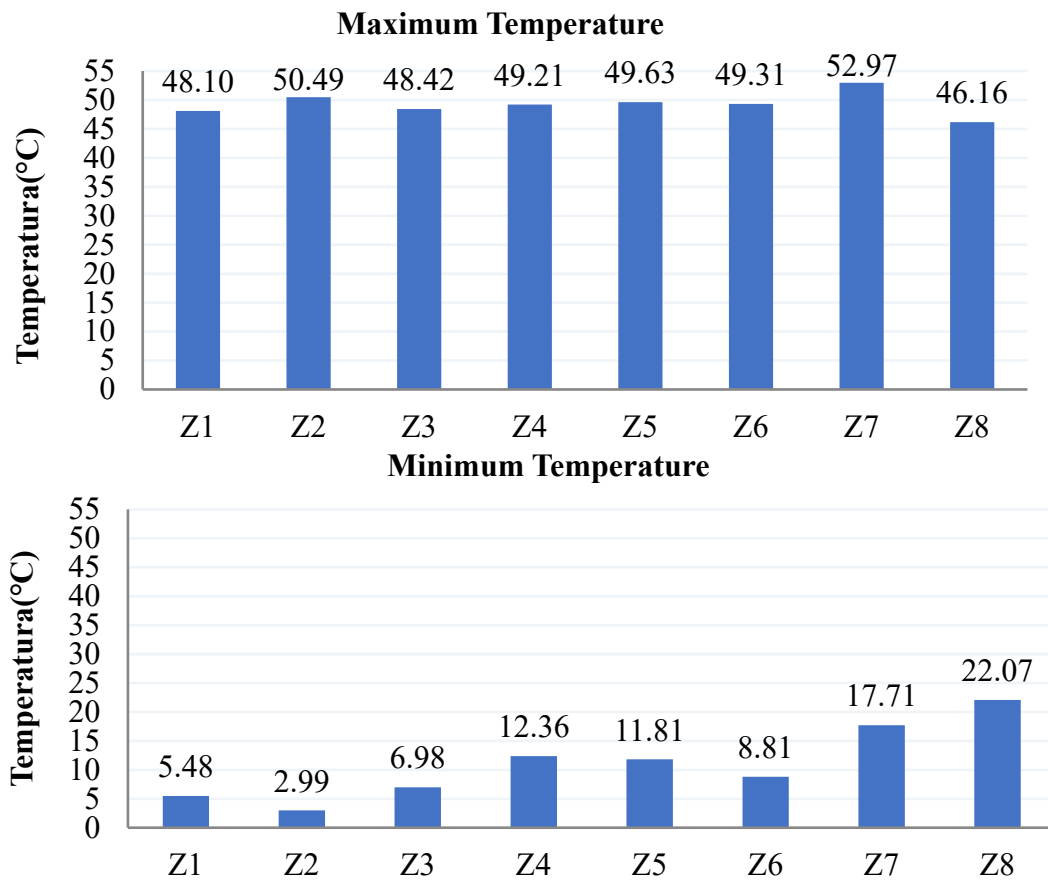


Figure 3. Absolute maximum and minimum surface temperatures for each bioclimatic zone in the studied year.

3.2 Thermal shock.

Figure 4 shows the occurrence frequency of full thermal shocks on all facades. The highest frequency is observed in Z6, in which 1.59% of the measurements are characterized as full thermal shocks, followed by Z1 (0.92%) and Z4 (0.79%). Zones Z5 and Z7 had the lowest frequencies 0.16% and 0.19%, respectively.

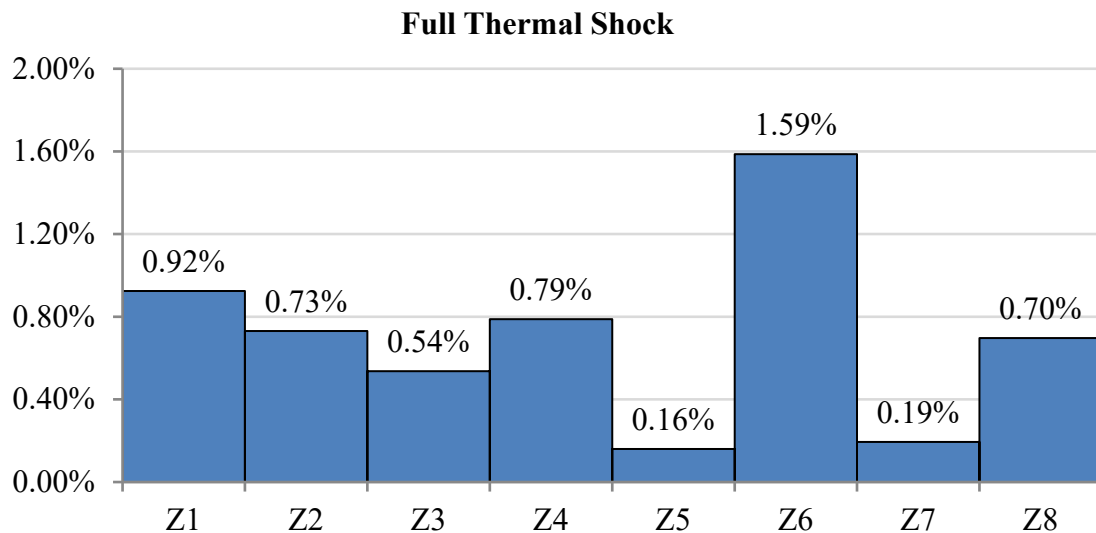


Figure 4. Frequency of occurrence of full thermal shock during one year.

The full thermal shock peaks are more frequent between May and July, according to Table 6. The monthly distribution of the number of shocks over a year indicates the month with the highest frequency of thermal shocks for each zone. Thus, the data show that the occurrence frequency of full thermal shocks peaked in zones Z1 and Z5 in July; Z3, Z4, Z6 and Z7 in June; and Z2 and Z8 in May. In zones 1 to 7, thermal shocks decreased from October to March, reaching zero in one or more months during this period except for Z8, where thermal shock events are better distributed throughout the year.

Table 6. Number of monthly full thermal shock events during one simulation year.

Full thermal shock													
	Jan	Feb	Mar	Apr	May	Jun	Jul	Aug	Sept	Oct	Nov	Dec	sum
Z1	1	1	1	9	14	18	25	9	1	1	0	1	81
Z2	0	1	0	4	21	10	7	12	7	0	0	2	64
Z3	1	0	0	1	6	25	14	0	0	0	0	0	47
Z4	1	1	0	4	17	23	19	0	0	1	0	3	69
Z5	0	0	0	0	1	5	6	1	1	0	0	0	14
Z6	4	1	3	10	13	53	38	12	0	0	1	4	139
Z7	0	1	3	3	2	6	2	0	0	0	0	0	17
Z8	5	5	6	7	10	5	2	3	1	4	5	8	61

The frequency of attenuated shocks is shown in Figure 5. the highest frequency of 13.65% is observed in Z6, followed by Z4 with 10.88%. Z8, Z5 and Z2 have the lowest frequency values of 2.84%, 3.35% and 4.95%, respectively. It is noteworthy that Z6 has approximately 5 times more attenuated shocks than Z8. The frequency is also high in Z4 and Z1 (10.88% and 10.31%, respectively) followed by Z3 and Z7 (8.75% and 8.60%).

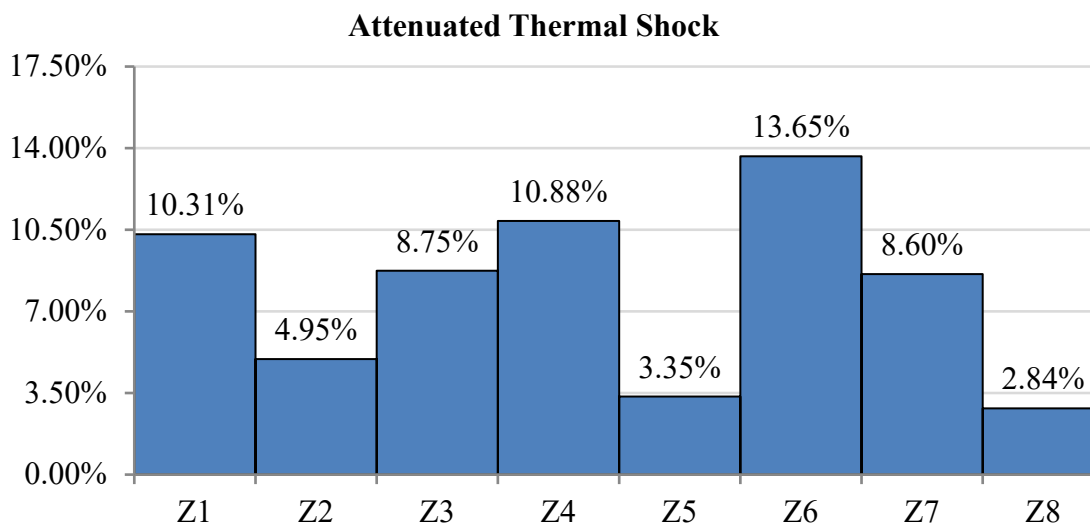


Figure 5. Frequency of attenuated thermal shock observed in one simulation year.

The annual distribution shows higher occurrence from May to August, as observed in Table 6. Only Z5 has two months without the occurrence of thermal shocks (November and December). The occurrence peaked in Z2 and Z8 in May; Z4 and Z6 in June; Z1, Z5 and Z7 in July; and Z3 in August. The occurrences in Z8 are better distributed throughout the year, varying from 12 in September to 32 in May. Meanwhile, in other areas, variation between the months of lowest and highest occurrence is greater, such as in Z6, where it varied from 14 events in November to 211 events in June.

Table 7. Monthly frequency of attenuated thermal shock events over a simulation year.

Attenuated Thermal Shock													
	Jan	Feb	Mar	Apr	May	Jun	Jul	Aug	Sept	Oct	Nov	Dec	sum
Z1	13	24	64	112	146	103	190	114	78	46	4	9	903
Z2	6	14	39	65	85	38	50	62	44	27	1	3	434
Z3	6	25	72	106	127	115	76	128	73	28	5	5	766
Z4	6	18	52	120	148	182	177	143	71	16	10	10	953
Z5	2	1	5	32	46	56	82	44	22	3	0	0	293
Z6	27	33	76	121	175	211	207	170	84	56	14	22	1196
Z7	10	11	32	80	155	145	157	114	40	3	2	4	753
Z8	18	15	22	29	32	20	29	19	12	18	14	21	249

The results show that zones with critical exposure have the highest frequency of thermal shock and those exposed to milder conditions have the lowest frequency. Zone Z6 stands out since it presented the highest frequency for both full and attenuated thermal shocks. Finally, Z5 had a reduced frequency of both thermal shocks considered while Z8 had a lower frequency of attenuated shocks.

3.3 Weighted Thermal Amplitude.

Figure 6 shows the I_{IT} results for all facades in each bioclimatic zone. The results take into account the temperature gradient during one year of simulation. As noted in the results of maximum thermal amplitude and thermal shock, Z6 presents critical values (22.55) regarding the action of temperature agents. Also, Z8 and Z5 have the lowest I_{IT} values (16.53 and 16.55) whereas Z2, Z4 and Z7 present high values, and zones Z3 and Z1 present intermediate values.

IIT

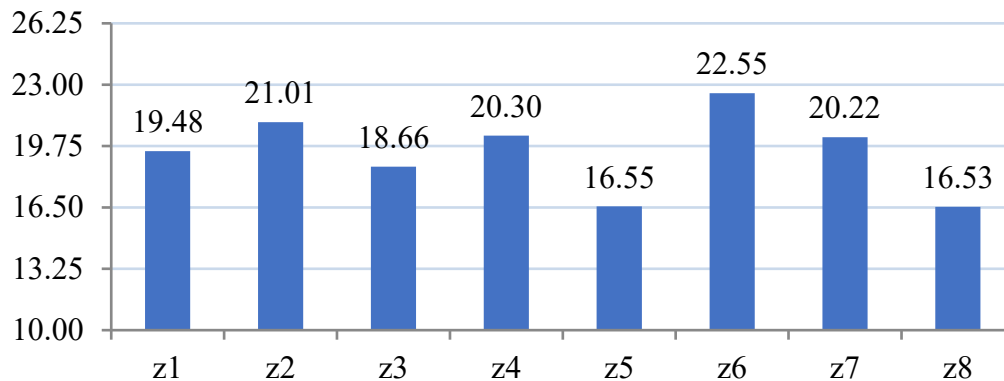


Figure 6. I_{IT} values for all bioclimatic zones.

Thermal variations on the facades cause deformations in the cladding system and induce fatigue stresses as a result of its cyclic nature. Thus, thermal variations are related to anomalies in facade cladding, especially concerning ceramic detachment and cracking (Silva, 2014; Souza, 2016). I_{IT} is considered a reference value for comparing degradation levels between cities that demonstrates the severity of exposure to the thermal degradation agent. Therefore, higher values indicate greater exposure and greater potential for degradation and decreasing useful life.

The I_{IT} is considered adequate to correlate the degradation of facades (Nascimento, 2016), and, based on these index values, we ranked the facades regarding exposure to temperature, according to severity. Then, in descending order, the areas of greatest severity were: Z6-Z2-Z4-Z7-Z1-Z3-Z5-Z8.

3.4 Driving rain.

Figure 7 shows the incidence of total annual rainfall (l/m²) on the same North-facing facades to complete the analysis of the degradation agents. Note that Z8 has a critical total annual rainfall (113.15 l/m²), the value is about 6 times higher than the lower incidence observed in Z5 (18.2 l/m²), in contrast to the previous results. Rainfall is also high in Z4 (100.12 l/m²) and Z3 (71.72 l/m²) compared to the others. Finally, Z1 (52.19 l/m²) and Z6 (59.67 l/m²) present intermediate values while Z2 (35.57 l/m²) and Z7 (30.57 l/m²) have a lower incidence of rain.

Total Annual driving Rain

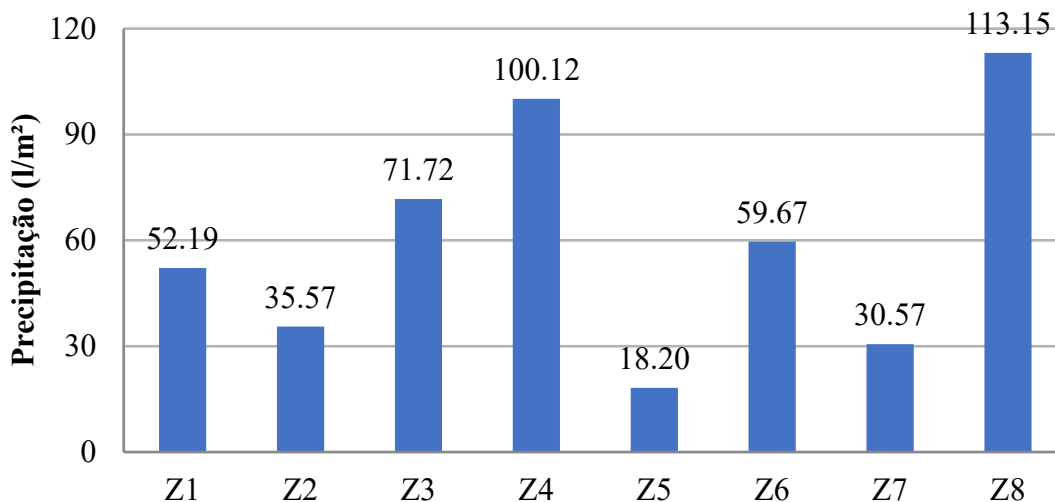


Figure 7. Accumulated driving rainfall in all bioclimatic zones during one year.

It is noteworthy that driving rain results from the action of winds on the precipitation (Freitas, 2011; Zanoni, 2015), therefore, it depends on wind speed and direction. The Northern rainfall incidence is highest in Brasilia and Goiania (Zanoni et al., 2014; Zanoni et al., 2018; Andrade et al., 2021; Melo and Carasek, 2011). The Eastern rainfall incidence is highest in Curitiba (Batista et al., 2017) while the Southern rainfall is most common in Florianópolis (Giango et al., 2010; Giongo, 2007). In this case, the results presented do not necessarily represent the orientation of critical exposure to moisture from the rain, but the orientation adopted as a reference, North.

4. CONCLUSION

This study investigated the action of degradation agents associated with temperature driving rain on the facades of buildings located in Brazilian cities from different bioclimatic zones. In this context, it was possible to identify areas that are critical regarding the exposure to degradation agents as a way of contributing to the knowledge of the different conditions that trigger the degradation process in Brazil. The results allowed us to identify the following patterns:

- Zone Z6 represented by Goiânia-GO had the most critical response to the exposure conditions regarding thermal amplitude, attenuated and full thermal shock, and temperature intensity index;
- Zone Z8 represented by Belém-PA, despite exhibiting a milder response to exposure conditions to the agents associated with temperature (solar radiation, thermal amplitude, attenuated thermal shock and temperature intensity index) is critical for exposure to the driving rain.
- Zones Z1, Z2, Z3, Z5 and Z7 represented by Curitiba-PR, Santa Maria-RS, Florianópolis-SC, Niterói-RJ and Picos-PI, respectively, presented similar values of total annual radiation incidence on the North facade. However, zones Z1 and Z2 present higher thermal amplitudes compared to the others.
- Regarding driving rain and considering the annual precipitation values, the North facades in Z8 (Belem-PA) and Z4 (Brasília-DF) presented higher exposure while Z5 had the mildest exposure.
- It is concluded that the North facades analyzed in the 8 Brazilian bioclimatic zones have different exposure conditions to agents associated with temperature and driving rain. These parameters affect building durability since the synergy between degradation agents acting on the facades accelerates the degradation, compromising building performance and affecting useful life. In addition, as a contribution, the study ranks the studied regions regarding the severity of exposure to temperature and, therefore, with greater potential for degradation and decreasing useful life. In descending order, the most exposed zones are: Z6-Z2-Z4-Z7-Z1-Z3-Z5-Z8 represented by the cities Goiânia-Santa Maria-Brasília-Picos-Curitiba-Florianópolis-Niterói-Belém.

5. ACKNOWLEDGEMENTS

We are grateful to the PECC (Postgraduate program in structures and civil construction) University of Brasília, and the DMMPROJECT (Degradation: Measurement and Modelling). This study was financed in part by the Coordenação de Aperfeiçoamento de Pessoal de Nível Superior - Brasil (CAPES) – Finance Code 001, by the Conselho Nacional de Desenvolvimento Científico e Tecnológico (CNPq), and by Academic Dean Graduate Studies (DPG) of the University of Brasilia (UnB).

6. REFERENCES

- Andrade, D., Kardec, T., Bauer, E.(2021). “*Sinergia dos agentes higrotérmicos na degradação de fachadas*”. In: XVII Congresso Internacional sobre Patologia e Reabilitação das construções, 2021, Fortaleza.
- ASHRAE - American Society of Heating (2009), *Refrigerating and Air-Conditioning Engineers*, Inc. Handbook 2009 -Fundamentals. Atlanta, artigo 2SPPC1017, pp. 199–212, 2017.
- Associação Brasileira de Normas Técnicas (2005). *NBR 15220-3: Desempenho térmico de edificações Parte 3: Zoneamento bioclimático brasileiro e diretrizes construtivas para habitações unifamiliares de interesse social*. Rio de Janeiro.
- Barbosa, A. S. (2013), “*Estudo Numérico-Computacional e Analítico do Choque Térmico em Fachadas de Edificações*”. Dissertação (Mestrado). Masters Thesis, Programa de Pós-Graduação em Estruturas e Construção Civil, Universidade de Brasília, Brasília-DF.
- Batista, G., Rufato, R., Miranda, D., Giordano, D. Medeiros, M. (2017), “*Análise do índice de chuva dirigida em cidades do Paraná e sua importância no projeto de fachadas de edifícios*”. IN: Simpósio Paranaense de Patologia das construções, 2017.
- Bauer, E., Aidar, L. A. G., Piña, A. B. S. (2018), “*Estudo do transporte de água oriunda da chuva dirigida em fachadas – aplicação com o emprego da simulação higrotérmica*”. IN: Construção, 2018, Brasília, Livro de Atas.
- Bauer, E., Castro, E. K., Silva, M. N. B. (2015), “*Estimativa da degradação de fachadas com revestimento cerâmico: estudo de caso de edifícios de Brasília*”. *Cerâmica*, v. 62, p. 151-159. <https://doi.org/10.1590/0366-69132015613581786>
- Bauer, E., Mota, L., Souza, J. (2021). “*Degradação de fachadas revestidas em argamassas nos edifícios de Brasília, Brasil*”. *Ambiente Construído*, Porto Alegre, v. 21, n. 4, p. 23-43. <http://dx.doi.org/10.1590/s1678-86212021000400557>
- Bauer, E., Nascimento, M. L. M., Castro, E. K.(2015), “*Parâmetros e ensaios físicos de materiais e componentes da fachada. Relatório interno*” – Laboratório de Ensaio de Materiais (LEM) – UnB/ENC.
- Bezerra, L. M., Uchôa, J. C., Araújo, J. A., Bonilla, J. (2018), “*Experimental and Numerical Investigation of Fatigue in Base-Rendering Mortar Used in Façades Undergoing Thermal Cycles*”. *Journal of Materials in Civil Engineering*. v. 30. n. 8. pp.1-14. [https://doi.org.ez54.periodicos.capes.gov.br/10.1061/\(ASCE\)MT.1943-5533.0002319](https://doi.org.ez54.periodicos.capes.gov.br/10.1061/(ASCE)MT.1943-5533.0002319)
- Dornelles, K. A., Roriz, M. (2007), “*A ilusão das cores na identificação da absorvância solar de superfícies opacas*”. In: IX ENCAC E VII ELACAC, 2007, Ouro Preto. Anais. Ouro Preto: ANTAC.
- Freitas, A. S. S. L. A. (2011), “*Avaliação do comportamento hidrotérmico de revestimentos exteriores de fachadas devido à acção da chuva incidente*”, Masters Thesis. Faculdade de Engenharia da Universidade do Porto. Porto, Portugal. 170 p.
- Gaspar, P., Brito, J. (2005), “*Mapping Defect Sensitivity in External Mortar Renders*”. *Journal of Construction and Building Materials*, v. 19(8), p. 571-578, 2005. <https://doi.org/10.1016/j.conbuildmat.2005.01.014>
- Giongo, M. (2007), “*Análise do nível de exposição das edificações à chuva dirigida para Florianópolis*”. Masters Thesis, Universidade Federal de Santa Catarina, 2007.
- Giango, M., Padaratz, I. J., Lamberts, R. (2011), “*Determinação da exposição à chuva dirigida em Florianópolis, SC: índices de chuva dirigida e métodos semi-empíricos*”. *Ambiente Construído*, v. 11, n. 1, p. 7-23. <https://doi.org/10.1590/S1678-86212011000100002>
- Lamberts, R (2011). “*Desempenho térmico de edificações. Apostila da disciplina ECV 5161 do LABEEE-Laboratório de Eficiência Energética em Edificações*”. Universidade Federal de Santa Catarina, Florianópolis, 2011.

- Melo, C. M., Carasek, H. (2011), “Índices de chuva dirigida direcional e análise do nível de umedecimento em fachadas de edifício multipavimentos em Goiânia, GO”. *Ambiente Construído*, v. 11, n. 3, p. 23-37. <https://doi.org/10.1590/S1678-86212011000300003>
- Moscoso, Y. F. M. (2013), “Estudo numérico e experimental de tensões atuantes na argamassa colante de fachadas de edificações sob ação da fadiga termo-mecânica”. Masters Thesis, Universidade de Brasília, Brasília. p. 142.
- Nascimento, M. (2016), “Aplicação da simulação higrotérmica na investigação da degradação de fachadas de edifícios”, Masters Thesis, Universidade de Brasília, Brasília, 2016.p. 127
- Nascimento, M. L. M., Bauer, E., de Souza, J. S. (2016), “Wind-driven rain incidence parameters obtained by hygrothermal simulation”. *Journal of Building Pathology and Rehabilitation* 1, 5. <https://doi.org/10.1007/s41024-016-0006-5>.
- Pacheco, C. P., Vieira, G. L. (2017), “Análise quantitativa e qualitativa da degradação das fachadas com revestimento cerâmico”. *Cerâmica*, v. 63, p. 432-445. <https://doi.org/10.1590/0366-69132017633682156>
- Roriz, M. (2012), “Correções nas Irradiâncias e Iluminâncias dos arquivos EPW da Base ANTAC”. Grupo de Trabalho sobre Conforto e Eficiência Energética de Edificações. ANTAC – Associação Nacional de Tecnologia do Ambiente Construído. São Carlos – SP.
- Saraiva, A. G. (1998), “Contribuição ao Estudo de Tensões de Natureza Térmica em Sistemas de Revestimento Cerâmico de Fachada”. Masters Thesis. Universidade de Brasília. Brasília, Brasil. 164 p.
- Silva, A., Dias, J. L., Gaspar, P. L., Brito, J. (2011), “Service life prediction models for exterior stone cladding”. *Building Research and Information*, 39(6): 637-653, 2011. <https://doi.org/10.1080/09613218.2011.617095>
- Silva, M. N. B. (2000), “Avaliação Numérica com o Método dos Elementos Finitos das Tensões Termo-Mecânicas em Sistemas de Revestimento de Fachadas”. Universidade de Brasília. Brasília, Brasil. 218 p.
- Souza, J. (2019), “Impacto dos fatores de degradação sobre a vida útil de fachadas de edifícios”, Doctoral thesis, Universidade de Brasília, Brasília, Brasil, p. 101.
- Uchôa, J. C. B., Bezerra, L. M., Brito, M. A. N., Júnior, A. C. M., Silva, W. T. M. (2016), “análise de tensões internas em sistemas de revestimentos Cerâmicos de fachadas no distrito federal devido a Carregamentos térmicos utilizando modelagem MEF 3D”. IN: XXXVII Iberian Latin-American Congress on Computational Methods in Engineering, Brasília, DF, Brazil, November 6-9.
- Zanoni, V. (2015), “Influência dos agentes climáticos de degradação no comportamento higrotérmico de fachadas em Brasília”. Doctorial Thesis, Universidade de Brasília, Brasília, 2015. p. 253.
- Zanoni, V., Sánchez, J., Bauer, E. (2014), “Chuva dirigida: um estudo da iso 15927-3 no contexto brasileiro. In: XV Encontro Nacional de Tecnologia do Ambiente Construído, 2014, Maceió-AL.
- Zanoni, V., Sánchez, J., Bauer, E. (2018), “Avaliação de métodos para quantificação de chuva dirigida nas fachadas das edificações”. *PARC Pesquisa em Arquitetura e Construção*, Campinas, SP, v. 9, n. 2, p. 122-132, jun. 2018. ISSN 1980-6809. <https://doi.org/10.20396/parc.v9i2.8650260>

Non-destructive evaluation of the wooden beams from the Narciso López building in the Historic Center of Havana for reuse in its restoration

A. Hernández Oroza^{1*} , E. Berreo Alayo¹, R. Expósito Mendez¹

*Contact author: ahernandez@proyectos.ohc.cu

DOI: <https://doi.org/10.21041/ra.v12i2.585>

Reception: 01/02/2022 | Acceptance: 08/04/2022 | Publication: 01/05/2022

ABSTRACT

The objective of the study was to evaluate, through visual classification and non-destructive tests, the state of conservation of 32 wooden beams for reuse as a restoration project for a historic building. For this, measurements of the moisture content, penetrometer, estimation of the modulus of elasticity and breaking stress by ultrasonic pulse velocity were made. The results showed that 66% of the beams were affected by rot, defibration and cracking. The tests carried out on the deteriorated beams made it possible to determine that, for a reliability of 95%, of the remaining 21 beams it was possible to reuse 17 of them with an average density of 0.4 g/cm³.

Keywords: restoration; wooden beams; decay; penetrometer; ultrasound.

Cite as: Hernández Oroza, A., Berreo Alayo, E., Expósito Mendez, R. (2022), “Non-destructive evaluation of the wooden beams of the Narciso López building in the Historic Center of Havana for reuse in its restoration”, Revista ALCONPAT, 12 (2), pp. 263 – 278, DOI: <https://doi.org/10.21041/ra.v12i2.585>

¹Departamento de Diagnóstico y Levantamiento. Empresa Filial RESTAURA, Oficina del Historiador de La Habana, La Habana Vieja, Cuba.

Contribution of each author

In this work, the author A. H. Oroza contributed to the research design (100%), text writing (60%), results discussion (100%) and revision (100%). The author E. Berrio Alayo contributed to the writing of the text (40%) and the processing of the data obtained (100%). The author R. Expósito Mendez contributed to the activity of recording the measurements (100%). All authors contributed equitably to the execution of the measurements and the development of the investigation.

Creative Commons License

Copyright 2022 by the authors. This work is an Open-Access article published under the terms and conditions of an International Creative Commons Attribution 4.0 International License ([CC BY 4.0](https://creativecommons.org/licenses/by/4.0/)).

Discussions and subsequent corrections to the publication

Any dispute, including the replies of the authors, will be published in the first issue of 2023 provided that the information is received before the closing of the third issue of 2022.

Evaluación no destructiva de las vigas de madera del edificio Narciso López del Centro Histórico de La Habana para reuso en su restauración

RESUMEN

El estudio tuvo como objetivo evaluar, a través de clasificación visual y ensayos no destructivos, el estado de conservación de 32 vigas de madera para su reuso como proyecto de restauración de un edificio histórico. Para esto se realizaron mediciones del contenido de humedad, penetrómetro, estimación del módulo de elasticidad y tensión de rotura mediante velocidad del pulso ultrasónico. Los resultados mostraron que el 66% de las vigas presentaban afectación por pudrición, desfibramiento y fisuración. Los ensayos realizados a las vigas deterioradas permitieron determinar que, para una confiabilidad del 95%, de las restantes 21 vigas era posible reutilizar 17 de ellas con una densidad promedio de 0.4 g/cm³.

Palabras clave: restauración; vigas de madera; deterioro; penetrómetro; ultrasonido.

Avaliação não destrutiva das vigas de madeira do edifício Narciso López no Centro Histórico de Havana para reutilização em sua restauração

RESUMO

O objetivo do estudo foi avaliar, por meio de classificação visual e ensaios não destrutivos, o estado de conservação de 32 vigas de madeira para reaproveitamento como projeto de restauração de um edifício histórico. Para isso, foram feitas medições do teor de umidade, penetrômetro, estimativa do módulo de elasticidade e tensão de ruptura por velocidade de pulso ultrassônico. Os resultados mostraram que 66% das vigas foram afetadas por apodrecimento, desfibramento e fissuração. Os ensaios realizados nas vigas deterioradas permitiram determinar que, para uma fiabilidade de 95%, das restantes 21 vigas foi possível reaproveitar 17 delas com densidade média de 0,4 g/cm³.

Palavras-chave: restauração; vigas de madeira; deterioração; penetrômetro; ultrassom.

Legal Information

Revista ALCONPAT is a quarterly publication by the Asociación Latinoamericana de Control de Calidad, Patología y Recuperación de la Construcción, Internacional, A.C., Km. 6 antigua carretera a Progreso, Mérida, Yucatán, 97310, Tel.5219997385893, alconpat.int@gmail.com, Website: www.alconpat.org

Reservation of rights for exclusive use No.04-2013-011717330300-203, and ISSN 2007-6835, both granted by the Instituto Nacional de Derecho de Autor. Responsible editor: Pedro Castro Borges, Ph.D. Responsible for the last update of this issue, Informatics Unit ALCONPAT, Elizabeth Sabido Maldonado.

The views of the authors do not necessarily reflect the position of the editor.

The total or partial reproduction of the contents and images of the publication is carried out in accordance with the COPE code and the CC BY 4.0 license of the Revista ALCONPAT.

1. INTRODUCTION

The use of wood as a construction material has its origins in the first human settlements, with the formation of primitive shelters. The benefits of its properties in terms of handling, durability, hardness, resistance and color have led to its use throughout the history of mankind, both for artistic and constructive creation. In buildings where the use of this material has a structural performance, which influences the safety of the building and its tenants, it is necessary to carry out periodic evaluations of the integrity of the wood through inspections and tests (Szostak et al., 2020; Zielińska and Rucka, 2021). Factors such as the low global availability of structural timber, the decrease in the diameter of the trunks of wood species that makes them less industrially usable, together with the need to preserve the historical memory of buildings, have led to the development of regulations, methodologies and assessment techniques for the evaluation of the quality and state of conservation of this material (Documento Básico SE-M, 2019; Manavella et al., 2019; Salazar et al., 2018; UNE 56544, 2011).

To make the intervention on timber structures as less invasive as possible, the application of ultrasonic pulse velocity tests (UPV), resistography, screw extraction or penetrometer allow reliable results to be obtained from *in-situ* measurements, and the evaluation of the state of conservation of wooden structural elements. Their application makes it possible to estimate parameters such as density, breaking stress, and modulus of elasticity for reuse or replacement in accordance with project requirements. Although the use of these techniques offers advantages in terms of classification safety based on their results, the visual evaluation of timber, as an acceptance criterion, remains currently the most widely used method, fundamentally due to its low cost compared to the use of equipment, and the ease that wood offers to show its characteristics and damages on its surface.

The buildings of the Historic Center of Havana constructed before the 20th century have in common the use of wood as a structural element to support floors and roofing, where beam and plank systems are combined, with beam and slab by plank. These woods, at the time they were sawn for exploitation as a structural element, were not classified by their characteristics due to the lack of regulations in this regard, so criteria such as the width of the growth rings, cracks, resin bags, gems, deformations and biological alterations were not taken into account in a standardized way. In this sense, current valid standards (DIN EN 338:2016-07, 2016; ISO 9709:2018, 2018; UNE 56544, 2011), establish rejection criteria that would lead to the total or partial substitution of timber elements that, after having been used for more than a century, have demonstrated their durability and bearing capacity, since this standards are designed for new wood.

However, when it comes to reusing structural timber elements for rehabilitation and heritage conservation, the combined use of visual and analytical criteria is important, since the latter can provide better success criteria compared to visual classification, as was proven by (Rello et al., 2007) where they obtained that through UPV it is possible to reach up to 72% with respect to the 53% of success in wood quality. Over the years of exploitation, construction materials suffer different forms of deterioration that, in the case of wood, begin fundamentally due to the presence of humidity since it is a hygroscopic and porous material. In this sense, several researchers (Bratasz et al., 2010; Sotomayor Castellanos, 2015) have shown the influence of water content on the conservation of wood and its properties. According to (Arriaga et al., 2006), the modulus of elasticity, might vary by 2% for humidity ranges between 5% and 30%.

Based on the aforementioned considerations and the need to evaluate the possible reuse of wooden beams in historic buildings, this work aims to present the results of the evaluation of the state of conservation of the wooden beams of the first level support between the axes 5-6:A-C of the Narciso López building (Figures 1 and 2), located in the Historic Center of Havana. It was built in 1858 and has 4 levels, of which the ground floor and mezzanine are made of stone walls, while the

upper floors are made of masonry. The floors are supported by pine wood beams (*pinus sp.*). The restoration processes started in 2019 required a pathological diagnosis, for the first time since the construction of the property, to determine its possible use and thus preserve, as far as possible, the original elements of the building.



Figure 1. Narciso López Building. Source: Arch. Fernando Salinas Documentation Center, Restaura, OHCH

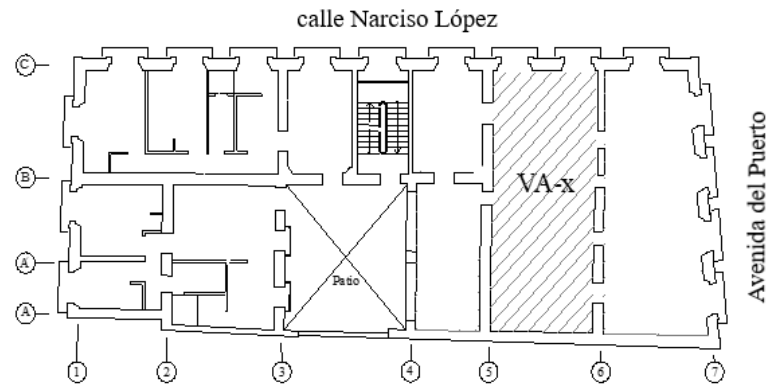


Figure 2. Plan view of the first level of the building. Signage of the study area. Own elaboration

2. EXPERIMENTAL PROCEDURE

The study began with the removal of the floor and the dismantling of all the beams. This enables detailed inspection on all sides (Figures 3 y 4), fundamentally in the area of the heads, which, being embedded in the walls, show greater deterioration due to rot by increase of moisture inside the joints (Figures 5 y 6). This first stage makes it possible to record the position, length, direction and sense of each fissure, crack, rot and/or defibration present in the beams, for which the distance of the lesion with respect to the head was taken as a reference (Figure 7). Additionally, the test areas that have the ideal conditions for carrying out the measurements were identified. In areas where there are cracks or deterioration due to different forms of rot (brown, soft, etc.) it is not possible to carry out measurements because a correct transmission or confinement of the signal is not achieved from the emitter to the receiver, or the results obtained are altered by the presence of microbial films that affect the physical-chemical composition of the wood, degrading its structure and density. On the other hand, impact or penetration techniques have the drawback that they should not be applied on irregular surfaces that influence the moment of impact of the drill bit, either due to its deformation, alteration in the angle of entry or lack of wood to offer a density value representative of the real properties of the structural element. For the preparation of the test areas, two sections were selected for each beam, free of surface lesions.

Subsequently, each beam was identified using the code (VA-x), where x represents a consecutive number, starting from 1. The local has a total of 32 wooden beams, which support each other axes 5-6. To determine the dimensions, a tape measure was used, and the measurements of width, depth and length were recorded (Table 1). The heads of the beams were identified with the letters A and B (Figure 8).



Figure 3. Stage of detailed inspection in beam mounted on wood supports



Figure 4. Inspection and visual classification of disassembled beams



Figure 5. State of the beam heads

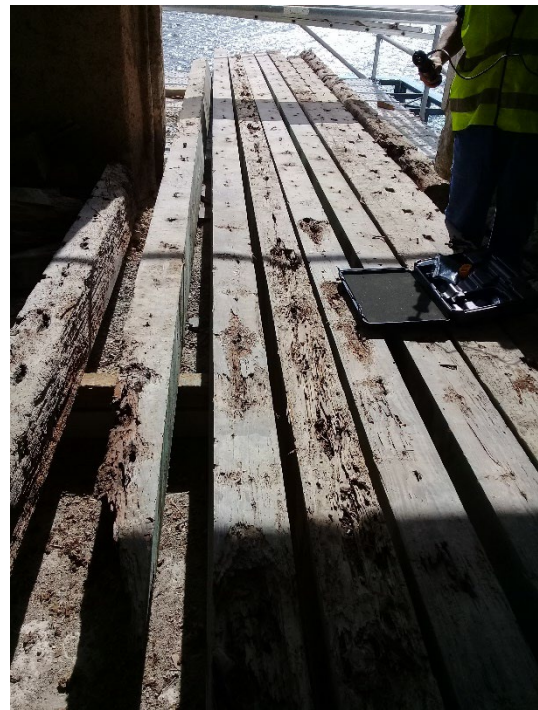


Figure 6. Disassembled beams with different pathological manifestations



Figure 7. Measure of the affected beam section with Steel tape



Figure 8. Identification of wooden beams

2.1 Non-destructive test applied

The tests applied consisted of estimating the density (ρ), breaking stress (f_k) and dynamic modulus of elasticity (MOE), by combining the penetrometer and UPV techniques. For both it is necessary to make adjustments with respect to the moisture content, for which the value of 12% is taken as a reference. In the case of the penetrometer, to determine the density at 12% humidity, the adjustment equation used was (Kuklík, 2007):

$$\rho_{12} = -0.027102 * t_{p,12} + 0.727987 \quad (1)$$

$$t_{p,12} = t_p(1 - 0.007\Delta w) \quad (2)$$

$$\Delta w = w - 12 \quad (3)$$

Where:

ρ_{12} = wood density at 12% humidity; g/cm^3

$t_{p,12}$ = depth of penetration in the wood with 12% humidity; mm

t_p = depth of penetration in the tested wood; mm

w = wood moisture at the time of measurement; %

For the measurement of UPV, the equipment used was Proceq Pundit Lab+, with 54 KHz conical transducers (Figure 9). They were placed perpendicular to the fibers (Figure 10) and the distance between them was programmed in the equipment for each beam. The adjustment was made at 12% humidity using the following equation (Liñán et al., 2011):

$$VPU_{12} = 27.5(w - 12) + VPU \quad (4)$$

Where:

UPV_{12} = ultrasonic pulse rate referred to 12% humidity; m/s

w = wood moisture at the time of measurement; %

UPV= measured ultrasonic pulse velocity; m/s



Figure 9. Application of UPV tests on wooden beams

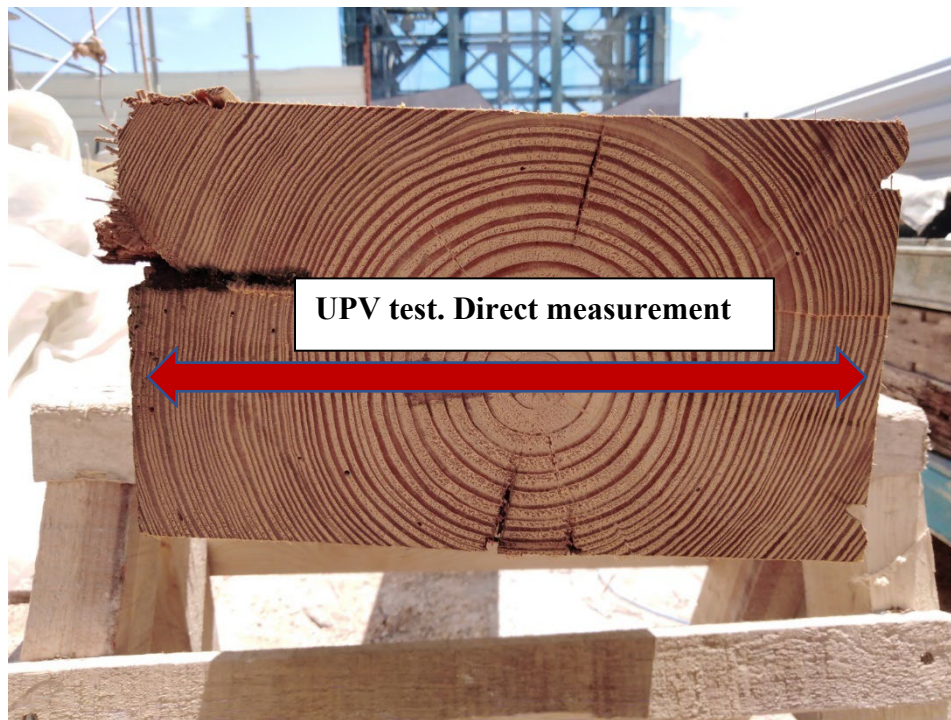


Figure 10. UPV application diagram perpendicular to the fiber

Based on the same criteria, the basic breaking stress (f_k) and the limit for determining the state of conservation of the wooden beams were calculated:

$$f_k = (0.212VPU_{12} - 183.09) * 1/10 \quad (5)$$

Where:

f_k = breaking strain; MPa

UPV_{12} = ultrasonic pulse rate referred to 12% humidity; m/s

From the UPV measurements and the density estimation values obtained, the dynamic modulus were calculated by applying the equation used by (Alquicira and Castellanos, 2021; Ettelaei et al., 2018):

$$MOE = \rho * VPU_{12}^2 \quad (6)$$

Where:

MOE= dynamic modulus of elasticity; N/m²

ρ = density; Kg/m³

VPU_{12}^2 = ultrasonic pulse rate referred to 12% humidity; m/s

To measure the humidity on the timbers, the Delmhorst's TotalCheck thermo-hygrometer was used (Figure 11).



Figure 11. Surface moisture measurement with Delmhorst's TotalCheck thermo-hygrometer equipment

3. RESULTS AND DISCUSSION

3.1 Visual Assessment

Of the 32 beams inspected, eleven of them did not show any type of injury (Table 1). In accordance with the visual classification requirements of the standard (UNE 56544, 2011), 4 beams categorized as ME-1 and 7 as ME-2 (Table 2). The rest of the beams are classified as Rejected considering the recurring damage from cracks and longitudinal fissures, rotting and splintering, mainly in the area of the heads up to a distance of approximately 40 cm. However, as it is a rehabilitation project that intends to use the original beams, with the exception of VA-18, all of them need to be re-evaluated through the proposed tests.

Table 1. Results of the inspection to the wooden beams.

ID	Wide (cm)	Timber cant (cm)	Length (cm)	Damages
VA-1	15	19.5	312	Splintered by UND at 70 cm from head A.
VA-2	16	20	320	Discontinuous longitudinal cracks in the middle of the depth of the LAS, from head B to a length of 250 cm.
VA-3	18	20	309	Longitudinal discontinuous cracks in the middle of the depth.
VA-4	17.5	20	295	Shredded in TOE throughout the length of the beam.
VA-5	17.5	20	310	Discontinuous longitudinal cracks and fissures by LAS, in the middle of the depth. Shredded by TOS from head B to a length of 70 cm.
VA-6	14	20	304	Crack in the LAS, from head B to a length of 20 cm in the middle of the superelevation.
VA-7	12.5	20	304	Longitudinal crack in the middle of the depth of both lateral faces, from head A to a length of 90 cm.
VA-8	12.5	20	310	Longitudinal cracks from head B to a length of 60 cm in the upper half of the LAS. LAS rot from head A, up to a length of 70 cm.
VA-9	14.5	20	309	No damages were observed.
VA-10	15.5	20	310	Longitudinal fissure in the upper half of the LAS, along the entire length. Superficial shredding by LAS, 90 cm from head B.
VA-11	17.5	21	310	No damages were observed.
VA-12	17	20	310	
VA-13	11.5	21.5	476	Shredded by the TOS affecting 5 cm of the width of the LAS and 2-3 cm of the height.
VA-14	11.5	21.5	475	No damages were observed.
VA-15	11.5	21.5	472	Longitudinal fissure in the middle of the depth of the LAS throughout the length.
VA-16	12	22	480	No damages were observed.
VA-17	13	21.5	480	Shredded by TOS at 30 cm from head B, up to a length of 60 cm.
VA-19	13	21	480	No damages were observed.
VA-18	Widespread decay			
VA-20	12	20	480	No damages were observed.
VA-21	11.5	20	480	
VA-22	11.5	21	480	Discontinuous longitudinal cracks and fissures by LAS throughout the span of the beam in the lower half of the depth. Shredded by TOS from 160 cm from head A, up to a length of 200 cm.

VA-23	15	20	299	Superficial defibration in the upper third of the LAS, from head B to a length of 40 cm.
VA-24	14	19.5	297	No damages were observed.
VA-25	15.5	20	306	
VA-26	18	20	305	
VA-27	17	20	305	Shredded throughout the upper edge of the LAS.
VA-28	15	20	310	Longitudinal cracks by TOS throughout the light.
VA-29	14.5	20	310	Softening and defibering by TOS, throughout the length.
VA-30	14.5	20	310	Discontinuous longitudinal fissures by the LAS.
VA-31	16.5	20	362	Shredded in head A and B by the TOS up to a length of 40 cm respectively.
VA-32	11	21	361	Shredded by TOS affecting 3 cm of the depth along the entire length.
Abbreviations used: UND: underside LAS: lateral side TOS: top side TOE: top edge				

Table 2. Visual classification of wooden beams.

Visual quality (UNE 56544, 2011)	Amount of wooden beams
ME-1	4
ME-2	7
Rejected	21

The visual inspection allowed to determine the extension of the damage on the surface, but not its depth in the mass of the wood, except in cases where the rot is very advanced. Injuries due to rot or deep cracks towards the interior of the beams can lead to the loss of the bearing capacity of the element and cause its fracture.

In accordance with (Nuere, 2007), in cases in which the deterioration can lead to the invalidation of the element to fulfill the structural function assigned to it in the whole, the decision must be made whether to replace or reinforce the beams. The application of these criteria to each beam will depend on the combined analysis of the visible lesions, and the results obtained by non-destructive techniques (Table 3). The removal of a wooden element will necessarily require its replacement by another of similar dimensions that meets the requirements of visual classification and resistance class, so as not to affect the load requirements for the project.

3.2 Application of non-destructives assays

To carry out the penetrometer and UPV tests, two points were prepared on each beam. In each one, 5 readings were recorded, for a total of 10 results for each element. Figure 12 shows a summary of values in some of the beams tested.

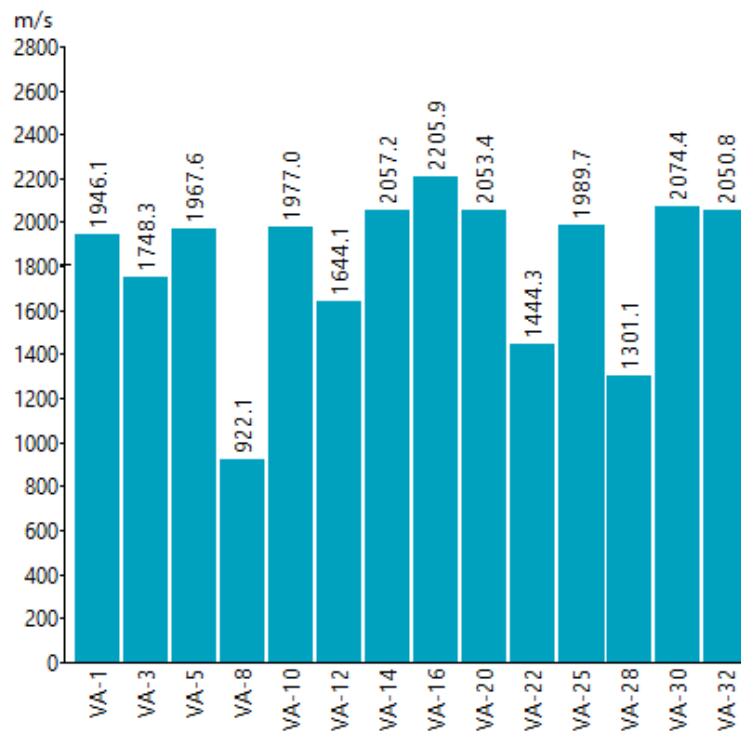


Figure 12. Summary of UPV measurements at a test point for wood beams.
Data extracted from software Proceq PunditLink

The criteria for estimating wood deterioration based on UPV results were established in accordance with (Liñán et al., 2011), in which it is established that:

- UPV > 1400 m/s: sound wood (SW)
- UPV < 1400 m/s: damaged wood (DW)

Table 3: Average results of measurements and applied calculations.

ID	w (%)	TP (mm)	TP ₁₂ (mm)	p ₁₂ (g/cm ³)	UPV ₁₂ (m/s)	fk (MPa)	MOE (MN/m ²)	Criteria
VA-1	13.3	10.5	10.4	0.45	2011.58	24.34	1804.33	SW
VA-2	12.3	10.0	10.0	0.46	2143.33	27.13	2101.57	SW
VA-3	11.8	12.0	12.0	0.40	2020.32	24.52	1642.40	SW
VA-4	14.3	12.0	11.8	0.41	1972.75	23.51	1587.83	SW
VA-5	17.9	9.5	9.1	0.48	1930.15	22.61	1792.52	SW
VA-6	13.7	9.5	9.4	0.47	2108.75	26.40	2105.94	SW
VA-7	15.8	9.5	9.2	0.48	2565.00	36.07	3140.70	SW
VA-8	15.2	10.5	10.3	0.45	921.20	1.22	381.70	DW
VA-9	19.9	11.3	10.7	0.44	2147.25	27.21	2022.57	SW
VA-10	12.2	10.7	10.7	0.44	1865.80	21.25	1526.17	SW
VA-11	14.6	9.0	8.8	0.49	2043.00	25.00	2038.96	SW
VA-12	18.1	12.3	11.8	0.41	1733.55	18.44	1228.72	SW
VA-13	17.8	10.7	10.3	0.45	2375.50	32.05	2538.05	SW
VA-14	14.9	12.3	12.1	0.40	2101.05	26.23	1771.94	SW
VA-15	15.6	11.7	11.4	0.42	2019.70	24.51	1708.71	SW
VA-16	19.3	11.0	10.4	0.45	2336.25	31.22	2429.38	SW

VA-17	15.7	12.0	11.7	0.41	2273.55	29.89	2125.43	SW
VA-18	Beam discarded due to advanced decay							
VA-19	17.0	10.3	9.9	0.46	2126.00	26.76	2072.85	SW
VA-20	15.4	10.3	10.1	0.46	2066.10	25.49	1944.34	SW
VA-21	15.6	11.0	10.7	0.44	2126.20	26.77	1977.26	SW
VA-22	14.4	10.7	10.5	0.44	1485.10	13.18	976.75	SW
VA-23	14.4	10.0	9.8	0.46	2165.10	27.59	2163.45	SW
VA-24	13.1	9.3	9.2	0.48	1995.55	24.00	1903.02	SW
VA-25	12.0	10.7	10.7	0.44	1996.20	24.01	1745.33	SW
VA-26	13.2	10.0	9.9	0.46	2073.90	25.66	1975.23	SW
VA-27	16.2	10.7	10.4	0.45	2015.70	24.42	1814.24	SW
VA-28	18.4	12.7	12.1	0.40	1397.50	11.32	779.66	DW
VA-29	15.7	11.7	11.4	0.42	1960.35	23.25	1610.61	SW
VA-30	14.5	11.7	11.5	0.42	2193.75	28.20	2004.15	SW
VA-31	14.6	12.0	11.8	0.41	1914.30	22.27	1497.63	SW
VA-32	13.9	9.7	9.6	0.47	1960.15	23.25	1800.43	SW

In the UPV results obtained, only two beams (VA-8 and VA-28) show values below the established limit of 1400 m/s, being classified as "deteriorated wood". This may be due to fungal infestation from rotting, softening and spalling in the wood having spread into the beams, which is reflected in the wave transmission velocity output between the transducers. With the years of exploitation of the building it is not possible to determine the causes for which these beams suffered a deterioration considerably higher than the rest. It is possible that its location coincided with that of humid areas such as bathrooms or kitchens, although the registered humidity contents do not show extreme values that support this hypothesis. The statistical analysis of the data (Table 4), in which beams VA-8 and VA-28 were excluded, show a dispersion for UPV of less than 10%, with a reliability of 95%, so that for the rest of the values the population of data obtained is accepted.

Table 4: Statistical calculations of the results obtained in the beams classified as SW.

Statistical parameters	w (%)	Tp,12 (mm)	p12 (g/cm ³)	UPV, 12 (m/s)	fk (MPa)	MOE (MN/m ²)
X _{AVG}	15.1	10.8	0.4	2059.5	25.4	1898.3
sd	2.1	1.0	0.0	197.3	4.2	400.3
CV(%)	14.0	9.2	5.8	9.6	16.5	21.1
Min.	11.8	9.0	0.4	1485.1	13.2	976.8
Max.	19.9	12.3	0.5	2565.0	36.1	3140.7

The minimum density of the beams was 0.4 g/cm³. This corresponds to a resistance class classification higher than C35, according to (Documento Básico SE-M, 2019). The UPV results of less than 1400 m/s obtained for VA-8 and VA-28 infer that the deterioration due to rot and cracks extends towards the interior of the element. However, their penetration depth results were not significant compared to the other beams.

This shows that the estimation of the state of conservation of wood based on the density calculated by penetrometer, can lead to false positives if it is not combined with other measurement techniques. The hardness of the wood at the point of impact of the needle can result in a high value that does not reflect the deterioration inside the material. Figure 13 shows the general analysis of results that correlate the moisture content/penetration/calculated density. In the cases of VA-9 and

VA-16, it is identified how they reach a penetration value ≥ 11.0 mm for humidity close to 20%, in which a softening of the wood would be expected that result in greater penetration, as happens with the VA-28. The moisture content comparison between these beams is very similar but with opposite results. In the case of VA-9 and VA-16 they do not present any lesions and they maintained a UPV higher than 2000 m/s, while in VA-28 the progression of the damages towards the interior of the beam was confirmed with UPV results less than 1400m/s.

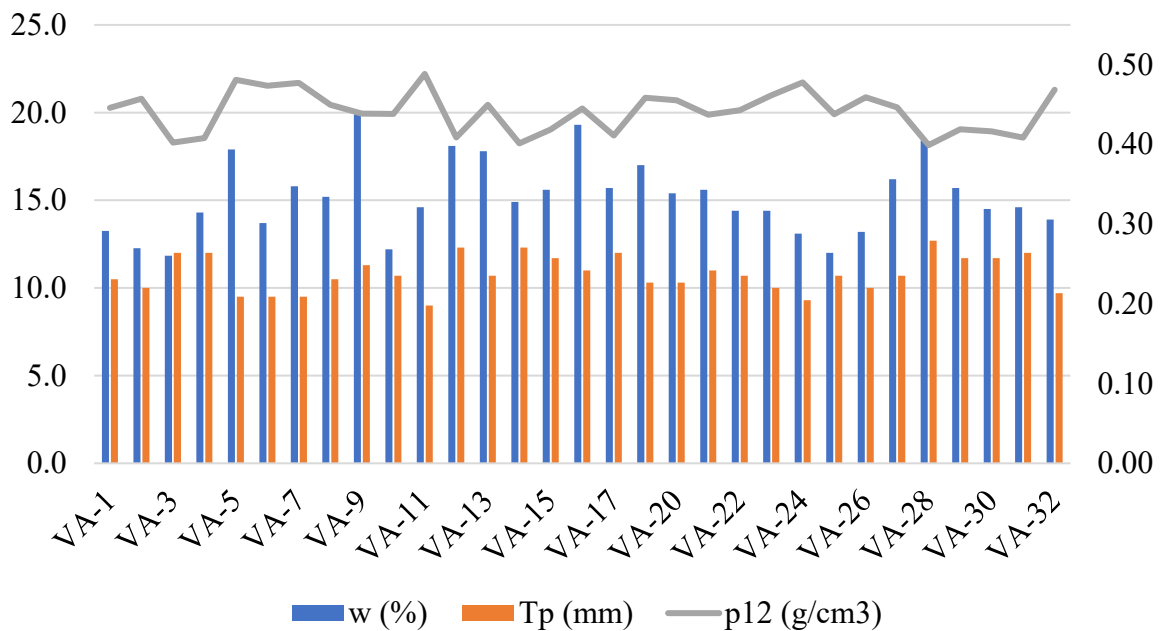


Figure 13. Relationship of results of moisture content, penetrometer and density calculated at 12% for all the wooden beams studied

Of the total UPV measurements made, 82% fluctuated in a penetration depth between 9.0 mm and 12.0 mm. In the graphical analysis (Figure 14) it can be seen how the majority set of results occupies the range between 1800 m/s and 2400 m/s for the aforementioned interval. The graph allowed to identify beam VA-22 as a variable distant from the population mean with a result of UPV= 1485.10 m/s. If the calculated standard deviation and the damages present in the beam are taken into account, it would be reasonable for structural safety reasons to replace it with a new one. The values obtained from the proposed equations for estimating the f_k and the MOE show a high correlation between them (Figure 15), characterizing the beams in structural class ME-2 (UNE 56544, 2011), on which they must apply all the restoration and consolidation actions necessary for its reuse.

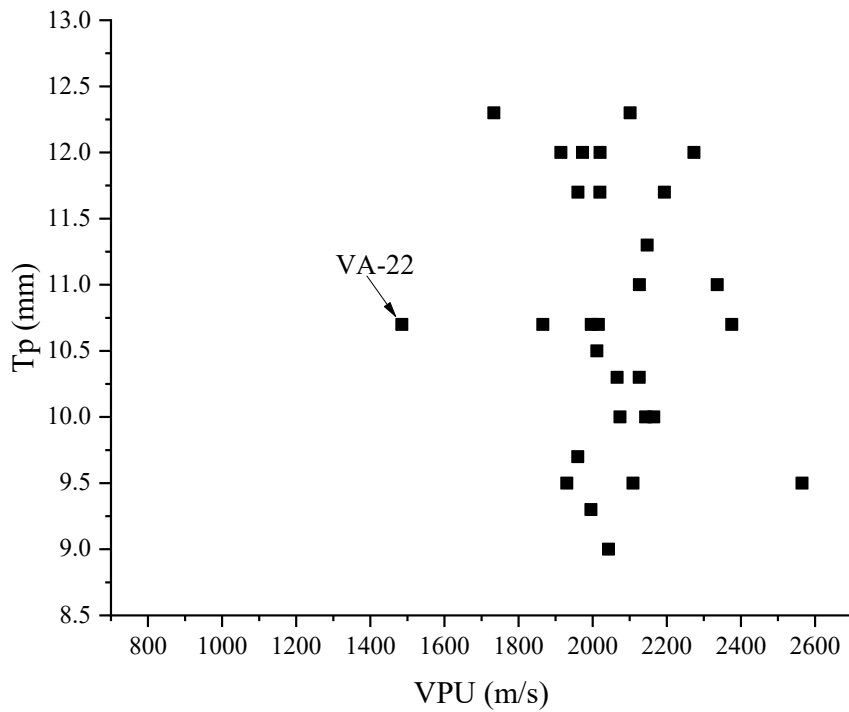


Figure 14. Relationship of results of UPV vs Tp for the beams evaluated as Sound Wood

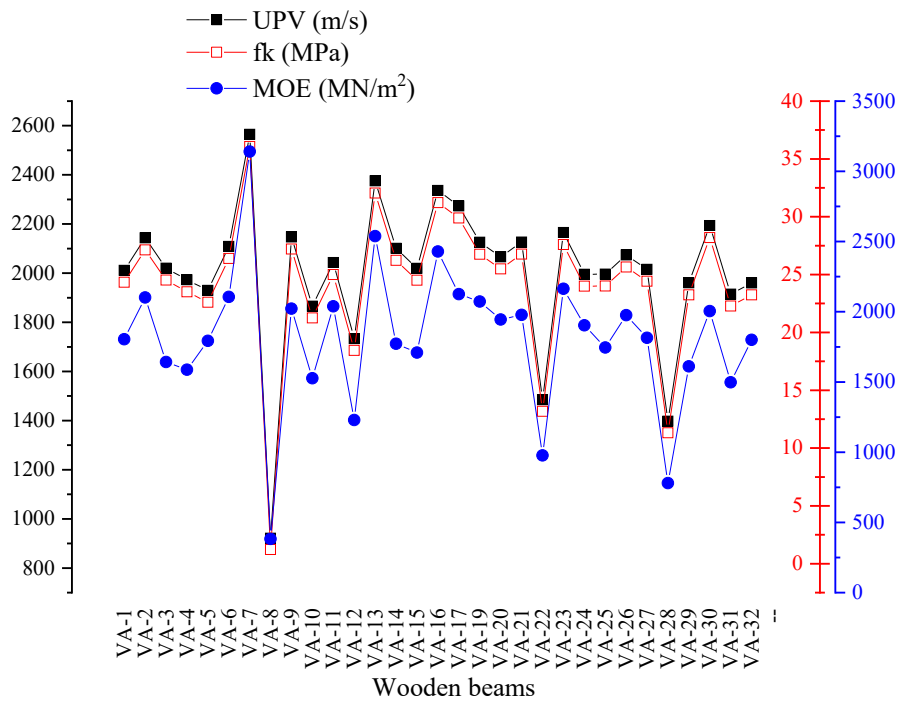


Figure 15. Correlation of results obtained from UPV, fk and MOE for wooden beams

4 CONCLUSIONS

Of the 32 beams diagnosed to evaluate their possible reuse as structural timber in the rehabilitation of the property, the following conclusions are reached:

The most recurrent injuries found during the visual inspection were the deterioration of the heads due to excess moisture in the joints, by the development of rotting fungi, as well as fissures and discontinuous cracks on the faces and edges. Among the most common restoration and reinforcement techniques for these types of deterioration are the use of metal caps and brackets to guarantee the fastening of the beams at the support points. Pickling or brushing of the faces and edges until reaching a surface with the fewest possible number of injuries. The fissures, on the other hand, can be sealed using resins, or from the preparation of a paste of carpenter's glue mixed with sawdust. Fumigation and treatment with biocide products, and finally the structural recalculation for the new dimensions of the beams.

The combined study of visual evaluation and non-destructive tests made it possible to identify that beams VA-8, VA-18, VA-22 and VA-28 must be replaced due to advanced lesions and poor density to be reused as a structural element.

The current regulations for visual classification of sawn wood for structural use is very conservative with regard to deterioration, which can result in the total replacement of old wooden elements. In rehabilitation and conservation projects of patrimonial assets, the evaluation of the state of conservation is more effective through the application of measurement tests on the pieces of wood. According to the results obtained in this study, the UPV technique showed more accurate results with respect to the density condition of the wood compared to the penetrometer technique, in which, through the equations used, no affectations were reflected in the densities for moisture content variations between 11.8% and 19.9%.

5 ACKNOWLEDGMENT

This study was financed by the Investment Group Avenida del Puerto, belonging to the Directorate of Investments of the OHCH under contract S-No. 4DG /2021 to Contract 6DG/2020. The authors wish to thank the support of the technicians Lázaro Y. Martínez García and Raúl de Jesús Expósito Mendez, as well as acknowledge the work and collaboration of the workers and carpenters on the site.

6 REFERENCES

- Alquicira, I. M., Castellanos, J. R. S. (2021), *Densidad, velocidad del ultrasonido y módulo dinámico de madera sólida y laminada de Pinus pseudostrabus*. Madera y Bosques, 27(3): e2732235-e2732235. <https://doi.org/10.21829/myb.2021.2732235>
- Arriaga, F., Íñiguez, G., Esteban, M., Fernández-Golfín, J. I. (2006), *Structural Tali timber (Erythrophleum ivorense A. Chev., Erythrophleum suaveolens Brenan.): Assessment of strength and stiffness properties using visual and ultrasonic methods*. Holz als Roh-und Werkstoff, 64(5): 357-362. <https://doi.org/10.1007/s00107-006-0100-5>
- Bratasz, L., Rachwal, B., Kozłowski, A., Kozłowski, R. (2010). *Sorption of Moisture and Dimensional Change of Wood Species Used in Historic Objects, Wood science for conservation of cultural heritage-Braga 2008 : proceedings of the international conference held by Cost action IE0601 in Braga (Portugal) 5-7 November 2008. - (Proceedings e report ; 67)*. Firenze University Press, Firenze.

- DIN EN 338:2016-07. (2016). *Structural timber - Strength classes*. Germany. <https://dx.doi.org/10.31030/2463437>.
- Documento Básico SE-M. (2019). *Seguridad Estructural. Madera*.
- Ettelaei, A., Layeghi, M., Hosseinabadi, H. Z., Ebrahimi, G., (2018), *Prediction of Modulus of Elasticity of Poplar Wood Using Ultrasonic Technique by Applying Empirical Correction Factors*. Measurement. <https://doi.org/10.1016/j.measurement.2018.11.076>
- ISO 9709:2018. (2018). *ISO 9709:2018(en) Structural timber — Visual strength grading — Basic principles*.
- Kuklík, P. (2007). *Determinación de las propiedades estructurales de la madera*, Praha.
- Liñán, C. R., Conde, J. M., Hita, P. R. D., Gálvez, F. P. (2011), *Inspección mediante técnicas no destructivas de un edificio histórico: oratorio San Felipe Neri (Cádiz)*. Informes de la Construcción, 63(521): 13-22. <http://dx.doi.org/10.3989/ic.10.032>
- Manavella, R. D., Guillaumet, A. A., Filippetti, M. C., Meyer, L. C. (2019), "*Determinación del módulo de elasticidad por ultrasonido y vibraciones en vigas de pino ponderosa*". 4to Congreso Latinoamericano de Estructuras de Madera. Montevideo, Uruguay.
- Nuere, E., (2007), *Madera, en restauración y rehabilitación*. Informes de la Construcción, 59(506): 123-130.
- Rello, L. A., Barra, R. D., Sanz, M. C., Fernández, A. L., Sánchez, M. T. L., Basterra, A. (2007). *Clasificación de madera estructural de P. pinaster Ait. Mediante ultrasonidos*, Congreso Iberoamericano de productos forestales - Iberomadera, Buenos Aires, Argentina.
- Salazar, D. V., Delgado, J. C., Yoza, L. Y., Mallque, M. A. (2018), *Propuesta metodológica para la evaluación de estructuras de madera en monumentos históricos – Caso Hotel El Comercio*. Revista Forestal del Perú, 33(2): 117-132. <http://dx.doi.org/10.21704/rfp.v33i2.1225>
- Sotomayor Castellanos, J. R. (2015), *Densidad, velocidad del ultrasonido y módulo de elasticidad de la madera de Pinus douglasiana, en relación a su contenido de humedad*. Revista de Ciencia y Tecnología(23): 25-30.
- Szostak, B., Trochonowicz, M., Kowalczyk, M. (2020), *Determination of the strength parameters of pinewood based on the non-destructive sclerometric test with a wood hammer*. Civil and Environmental Engineering Reports, 30(1): 43-52. <https://doi.org/10.2478/ceer-2020-0004>
- UNE 56544. (2011). *Norma Española UNE 56544:2011 Clasificación visual de la madera aserrada para uso estructural. Madera de coníferas*. Madrid. España.
- Zielińska, M., Rucka, M. (2021), "*Using the ultrasonic tomography method to study the condition of wooden beams from historical building*". 12th International Conference on Structural Analysis of Historical Constructions (SAHC). International Institute for Conservation of Historic And Artistic Works.

Concrete degradation by the formation of biogenic sulfuric acid in a Sewage Pumping Station

G. Coni^{1*} , A. Tafuri² , A. Costa¹ , G. Sakuma¹ 

*Contact author: conigabriella@gmail.com

DOI: <https://doi.org/10.21041/ra.v12i2.571>

Reception: 06/12/2021 | Acceptance: 04/03/2022 | Publication: 01/05/2022

ABSTRACT

This work presents the study carried out in a Sewage Pumping Station after severe degradation was observed. The attack by biogenic sulfuric acid in sanitary sewage systems is widely studied in the literature, however, data on real work situations are still quite limited. Analyzes of the concentration of H₂S in the air, carbonation depth, compressive strength, petrography, SEM/EDS, XRD and chemical determinations were carried out in concrete cores extracted above the effluent level. The products identified on the surface were Gypsum, Jarosite, Ferrous Hydroxide, Ferrous Chloride and possibly Hisingerite. The results demonstrate the presence of products on the surface, from the dissolution of cement paste as well as from the 16 mm steel bars located in the attacked region.

Keywords: biogenic sulfuric acid attack; degradation; reinforced concrete.

Cite as: Coni, G., Tafuri, A., Costa, A., Sakuma, G. (2022), "Concrete degradation by the formation of biogenic sulfuric acid in a Sewage Pumping Station", Revista ALCONPAT, 12 (2022), pp. 279 – 295, DOI: <https://doi.org/10.21041/ra.v12i2.571>

¹ Companhia de Saneamento Básico do Estado de São Paulo S.A (Sabesp), São Paulo, State of São Paulo, Brasil.

² Escola Politécnica da Universidade de São Paulo, São Paulo, Brasil.

Contribution of each author

In this work, the author Gabriella contributed with the activities: data collection 25%, work writing 35%, discussion of results 30%, author Amanda contributed data collection 25%, work writing 35%, discussion of results 30%, author Guilherme contributed data collection 25%, paper writing 15%, discussion of results 20% and author Adriana contributed data collection 25%, paper writing 15%, discussion of results 20%.

Creative Commons License

Copyright 2022 by the authors. This work is an Open-Access article published under the terms and conditions of an International Creative Commons Attribution 4.0 International License ([CC BY 4.0](https://creativecommons.org/licenses/by/4.0/)).

Discussions and subsequent corrections to the publication

Any dispute, including the replies of the authors, will be published in the first issue of 2023 provided that the information is received before the closing of the third issue of 2022.

Degradação do concreto através da formação de ácido sulfúrico biogênico em uma Estação Elevatória de Esgoto

RESUMO

Este trabalho apresenta o estudo realizado em uma Estação Elevatória de Esgoto após ser constatado severa degradação. O ataque por ácido sulfúrico biogênico em sistemas de esgoto sanitário é amplamente estudado na literatura, entretanto, dados em situações reais de obra ainda são bastante limitados. Foram realizadas análises da concentração de H_2S no ar, profundidade de carbonatação, ensaio de resistência à compressão, petrografia, MEV/EDS, DRX e determinações químicas em testemunhos de concreto extraídos acima do nível do efluente. Os produtos identificados na superfície foram Gipsita, Jarosita, Hidróxido Ferroso, Cloreto Ferroso e possivelmente Hisingerita. Os resultados demonstram a presença na superfície tanto de produtos oriundos da dissolução da pasta cimentícia quanto das barras de aço de 16 mm localizadas na região atacada.

Palavras-chave: ataque por ácido sulfúrico biogênico; degradação; concreto armado.

Degradación del hormigón mediante la formación de ácido sulfúrico biogénico en una Estación de Bombeo de Aguas Residuales

RESUMEN

Este trabajo presenta el estudio realizado en una Estación de Bombeo de Aguas Residuales luego de que se observara una severa degradación. El ataque por ácido sulfúrico biogénico en los sistemas de alcantarillado sanitario es ampliamente estudiado en la literatura, sin embargo, los datos sobre situaciones reales de trabajo aún son bastante limitados. Se realizaron análisis de concentración de H_2S en el aire, profundidad de carbonatación, prueba de resistencia a la compresión, petrografía, SEM/EDS, XRD y determinaciones químicas en núcleos de concreto extraídos por encima del nivel del efluente. Los productos identificados en la superficie fueron yeso, jarosita, hidróxido ferroso, cloruro ferroso y posiblemente hisingerita. Los resultados demuestran la presencia en la superficie de productos de la disolución de pasta de cemento y barras de acero de 16 mm ubicadas en la región atacada.

Palabras clave: ataque de ácido sulfúrico biogénico; degradación; hormigón armado.

Legal Information

Revista ALCONPAT is a quarterly publication by the Asociación Latinoamericana de Control de Calidad, Patología y Recuperación de la Construcción, Internacional, A.C., Km. 6 antigua carretera a Progreso, Mérida, Yucatán, 97310, Tel.5219997385893, alconpat.int@gmail.com, Website: www.alconpat.org

Reservation of rights for exclusive use No.04-2013-011717330300-203, and ISSN 2007-6835, both granted by the Instituto Nacional de Derecho de Autor. Responsible editor: Pedro Castro Borges, Ph.D. Responsible for the last update of this issue, Informatics Unit ALCONPAT, Elizabeth Sabido Maldonado.

The views of the authors do not necessarily reflect the position of the editor.

The total or partial reproduction of the contents and images of the publication is carried out in accordance with the COPE code and the CC BY 4.0 license of the Revista ALCONPAT.

1. INTRODUCTION

The sanitary sewer environment favors the formation of biogenic sulfuric acid (H_2SO_4) due to the presence of sulfur-oxidizing and sulfate-reducing bacteria (Estokova et.al., 2012). This acid produced by oxidizing bacteria is extremely aggressive to concrete as it attacks the cement paste, decalcifying the cement hydration products and leading to a progressive disintegration of the material (Wu et.al., 2018).

Another critical point is the reduction of the pH of the concrete to an extremely low value, reaching values around pH 1-2. Consequently, the depassivation of the reinforcement occurs and the oxidation process begins (Estokova et.al., 2012). So, the acid attacks the concrete as well as the steel bars in a short period, being able to reach deterioration rates of 12 mm/year in many sanitary sewage systems (Wu et.al., 2018). In a study conducted by Fernandes et.al., (2012), a 300 km-long sewage system showed superficial deterioration of concrete just 2 years after its construction. Strategies are currently being studied to mitigate the degradation of sewage infrastructure, for example, the use of bio-concretes that reduce the number of sulfur-oxidizing bacteria (Song et.al., 2021).

The degradation process of concrete by biogenic sulfuric acid, despite being widely discussed in the literature, data from research carried out in real situations are still quite limited (O'Connell et.al., 2010; Wu et.al., 2020). According to Wu et.al., (2020), the corrosion rates obtained in the site and laboratory tests generally show great variation and it is still difficult to establish a quantitative relationship between them based on existing knowledge. This paper presents a case of study in a Sewage Pumping Station from the Basic Sanitation Company of São Paulo State - SABESP severely deteriorated within only 20 years of construction and operation. It is expected that the results from this study will provide parameters able to validate experiments carried out on laboratory scale and further enable the development of strategies to increase the service life of sanitary infrastructures.

2. FUNDAMENTALS OF SEWER CORROSION

The attack of biogenic sulfuric acid begins with the formation of aqueous hydrogen sulfide (H_2S) by the activity of anaerobic sulfate-reducing bacteria, e.g. *Desulfovibrio desulfuricans*, present on the slime layer - below the waterline (Wu et. al., 2018). These bacteria, under anaerobic conditions and with a dissolved oxygen concentration (DO) lower than 0.1mg/L, convert the sulfur compounds present in the waste stream to aqueous hydrogen sulfide (H_2S)(aq) (House and Weiss, 2014; Wu et.al., 2018).

Part of the H_2S (aq) is released from sewage into the gas phase H_2S (g) above the waterline. The passage of H_2S (aq) to the gas phase is strongly influenced by the pH of the wastewater, as well as the equilibrium conditions between the gas and liquid phase, temperature, and turbulence of the flow (Wells et.al., 2009; Wu et.al., 2020). The released hydrogen sulfide condensate on the concrete surface where it is subjected to multiple stages of oxidation by sulfur-oxidizing microorganisms, such as species of the aerobic bacteria *Thiobacillus*, which act in different pH ranges, converting it to sulfuric acid (House e Weiss, 2014; Monteny et.al., 2000; Wu et.al., 2018).

The colonization of microorganisms in concrete depends on the availability of nutrients (organic matter), moisture, and the reduction of pH. The reduction of the pH of the concrete occurs by the carbonation and by the acidification of the surface caused by the H_2S (g) (Jiang et.al., 2014). When the surface pH is lowered to ~ 9 , the environment already presents sufficient conditions to initiate the colonization of *Thiobacillus thioparus* (Wu et.al., 2018).

Hereafter, bacterial activity is responsible for governing the gradual pH decrease of the concrete surface simultaneously altering the microbial communities. *Thiobacillus novellus*, *Thiobacillus intermedius* and *Thiobacillus neapolitanus* bacteria start to proliferate until reaching $\text{pH} \approx 3.0$, then there is a decline in the bacteria previously colonized, resulting in rapidly increasing proliferation of *Thiobacillus thiooxidans* bacteria, whose presence is associated with severe corrosion (Scrivener and Belie, 2013).

Portlandite $\text{Ca}(\text{OH})_2$, which is mainly responsible for the alkalinity ($\text{pH} \approx 13.0$) of the cement matrix, is the first compound to react with sulfuric acid, forming gypsum ($\text{CaSO}_4 \cdot 2\text{H}_2\text{O}$). Subsequently, gypsum can react with aluminate-containing phases to form ettringite ($(\text{CaO})_3 \cdot \text{Al}_2\text{O}_3 \cdot (\text{CaSO}_4)_3 \cdot 32\text{H}_2\text{O}$) (House and Weiss, 2014; Wells et.al., 2009). The formation of ettringite results in expansive pressure that can lead to internal cracking of the concrete, allowing the penetration of more acid and the degradation of the structure (Wu et.al., 2018). Furthermore, if pH falls below 10.6, ettringite turns out unstable and starts to dissolve (Duchesne and Bertron, 2013). For that reason, ettringite is an intermediate product, and gypsum is the final product of the sulfuric acid attack (Davis et.al., 1998). As the reserve of calcium ions provided *a priori* by Portlandite is consumed, the following reactions focus on the decalcification of hydrated calcium silicate (C-S-H), the major product of Portland Cement responsible for the concrete mechanical strength. The product of this reaction is silica gel, a material with no bearing capacity (Monteny et.al., 2000). In summary, the degradation of the concrete occurs above the waterline, starting from the surface and gradually advancing inside the structure.

3. METHODOLOGY

This paper presents a case study on a strongly deteriorated wet-well of a Sewage Pumping Station from the Basic Sanitation Company of São Paulo State (SABESP) put into operation in December of 1999. Internal inspections of the structure were carried out to obtain photographic records and extract concrete core from wet-well's wall for analysis.



Figure 1. (a) wet-well (b) Degradation of concrete and steel bars observed by site inspection

The structure has two concentric circular wells, dry and wet, with a diameter of 25.60 m and 13.70 m, respectively. The first was built in reinforced concrete, with a metallic cover, and the second one in prestressed concrete. The dry well is where six sets of pumps are located and the wet well, the object of this study, with 18.70 m in height, is the part of the structure that receives and sends the sewage to the treatment plant.

The inspection of the structure was carried out in the wet well (Figure 1a) and restricted to the gas area (above the waterline). In this region, the concrete surface presented an atypical condition with layers up to 15 cm thick with no cohesive properties, very easy to remove with a spatula (Figure 2a). The wall's thickness specified in the project is 35 cm. The passive reinforcement with 16 mm diameter was oxidized (Figure 2b), with loss of section and sectioned and/or completely dissolved parts.

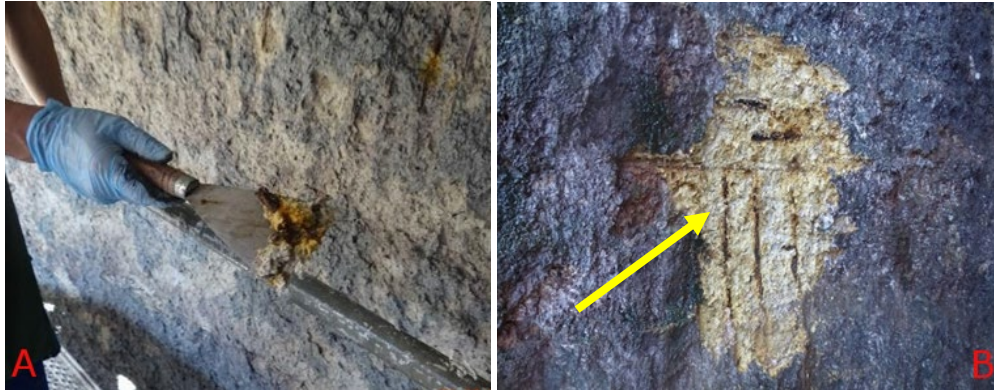


Figure 2. (a) removal of the degraded concrete layer using a spatula and (b) parts of completely reinforcement dissolution

The following tests were performed in the present study:

3.1 Gas concentration

Daily measurements of hydrogen sulfide (H_2S) concentrations were carried out in the headspace of the pumping station, during the period 02/07/2020 to 11/30/2020, by using myDataSens H_2S from Microtronics, with a measurement capability ranging from 0-1000 ppm. The equipment automatically collects and stores data every 5 minutes.

3.2 Carbonation front

The qualitative test to determine the carbonation front of the concrete was carried out using a solution composed of phenolphthalein, which is a colorless acid/base indicator that changes its color to purple at pH above 9 (alkaline), indicating the presence of $Ca(OH)_2$.

3.3 Compressive strength

Four (04) cylindrical concrete cores were extracted for a compressive strength test, according to ABNT NBR 7680-1/15, from the wall with a nominal diameter of 75 mm. The compression test of cylindrical specimens was performed in accordance with ABNT NBR 5739/18.

3.4 Petrographic analysis

The petrographic analysis was based on ASTM C 856/2017 - "Standard Practice for Petrographic Examination of Hardened Concrete". Two of the extracted concrete cores were used to make thin sheets with dimensions of 2.5 cm x 4.0 cm to characterize the interface between the sound and attacked concrete. A microscope model DM4500 P coupled to a digital camera DFC7000 T, both from Leica, and a stereoscopic binocular magnifier model M-8, from Wild, were used. Image editing was performed using the LAS X software. The photographic technique through photomicrography was used in the test to obtain enlarged images of the material's microstructure.

3.5 Scanning electron microscopy, X-ray diffraction and chemical determinations

In the same core, analyzes were carried out in three different layers: an outer layer, obtained by scraping the concrete with no cohesive properties; an intermediate layer; and an inner layer, apparently not attacked. For scanning electron microscopy, the scraped sample was dried in a sealed desiccator at room temperature for 4 days. The dry fragments were carefully mounted in the aluminum sample holder, with the aid of carbon tape and aluminum tape. The intermediate and innermost samples were broken with the aid of a hammer, at each end of the concrete core. The fragments were collected, carefully selected, and promptly mounted in an aluminum sample holder, with the aid of carbon tape and aluminum tape and covered with a thin layer of gold-palladium.

For the X-ray diffraction analysis, an aliquot of the scraped sample was dried at (45 ± 5) °C for 7 days, while the fragments of the intermediate and innermost samples were crushed in a mortar to obtain the mortar, then they were grounded in a porcelain mortar until completely passed through an ABNT No 200 sieve (75 μm). The EMPYREAN model Panalytical X-ray diffraction equipment was used, operating in copper $K\alpha$ radiation at 45 kV – 40 mA and scanning at $2^\circ 2\theta/\text{min}$. The identification of compounds was performed using Panalytical's X-pert HighScore Plus software (version 4.9) and diffraction patterns provided by the ICDD (International Center for Diffraction Data) with update until 2017.

Chemical determinations were performed only on the scraped material, as follows:

Determination of water-insoluble residue in acid, based on the general guidelines of ASTM C114-18 "Standard Test Methods for Chemical Analysis of Hydraulic Cement" and ABNT NBR 13810:1997 "Water - Determination of metals - Atomic absorption spectrometry method by flame". Determination of sodium (Na), potassium (K), iron (Fe), magnesium (Mg) and calcium (Ca), soluble in water and acid, based on general guidelines from ASTM C114-18 "Standard Test Methods for Chemical Analysis of Hydraulic Cement" and ABNT NBR 13810:1997 "Water - Determination of metals - Flame atomic absorption spectrometry method". Determination of soluble chloride ions and sulfate ions, according to the general guidelines of NBR 9917:2009 "Aggregates for concrete - Determination of soluble salts, chlorides and sulfates".

4. RESULTS AND DISCUSSION

4.1 Gas concentration

Hydrogen sulfide concentration in the air tends to increase with the temperature, as observed in figure 3. The increase in temperature reduces the solubility of H_2S (aq) in wastewater and encourages the release in the gaseous form H_2S (g) (Wu et.al., 2018). However, the temperature is not the only influencing factor, since the concentration of H_2S (g) inside the Sewage Pumping Station is also influenced by turbulence, which is directly related to the number of pumps in operation at the time of measurement.

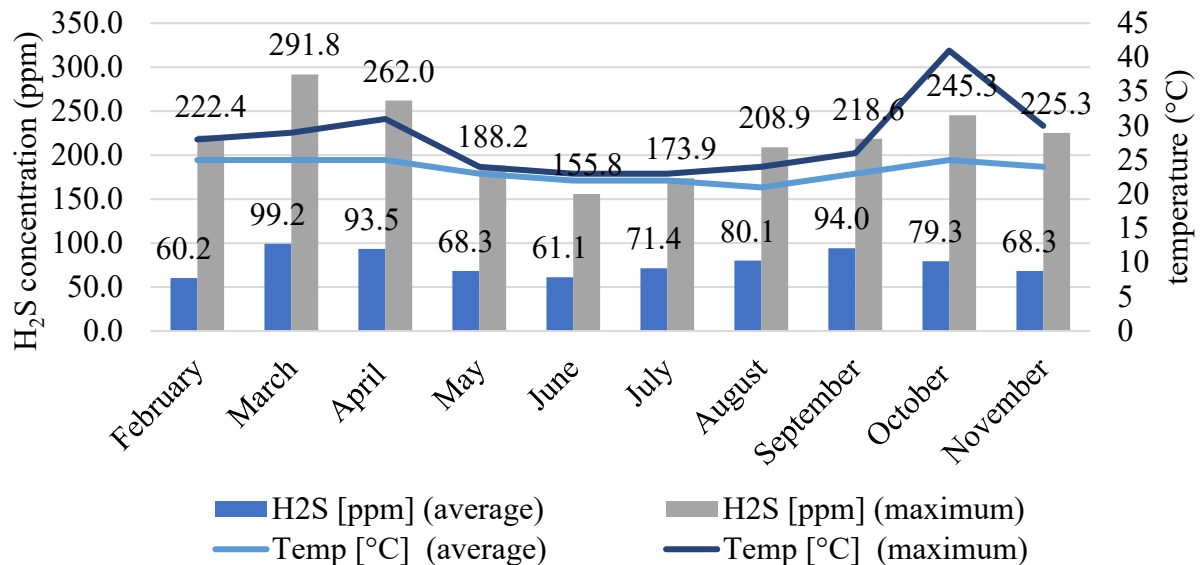


Figure 3. H₂S concentration and temperature over the months

4.2 Carbonation front

After removing the layer with no cohesive properties of approximately 8 cm from the wet-well’s wall, it was observed that the concrete was carbonated as it did not change color with the phenolphthalein’s solution application. Then, a 5 cm hole was made, observing that the innermost region of the concrete was still alkaline, as illustrated in Figure 4.



Figure 4: wet-well’s wall - alkaline concrete

4.3 Compressive strength of concrete

In the compressive strength tests results, illustrated in Table 1, it was observed that all the extracted cores presented higher strengths than those specified in the project (20 MPa). Despite the atypical condition observed on the surface of the concrete, this result was already expected, since the part used in the test was the inner part of the sample, which did not appear to have been contaminated by biogenic sulfuric acid yet.

Table 1. Direct compressive strength results

n° C. P	average dimensions (mm)		f _{ci,ext, inicial} (MPa)	k1	k2	k3	k4	f _{ci,ext (*)} (MPa)
	height (h)	Diameter (d)						
1	109,2	73,6	56,3	-0,04	0,09	0,05	-0,04	59,7
2	111,2	73,6	55	-0,04	0,09	0,05	-0,04	58,3
3	93,0	73,6	56	-0,07	0,09	0,05	-0,04	57,7
4	145,3	73,6	54,1	0,00	0,09	0,05	-0,04	59,5

NOTE - (*) Corrected results of the resistance obtained in the rupture of the cores extracted by the coefficients k1, k2, k3 and k4, according to item 5.2 of ABNT NBR76801:2015.

4.4 Concrete petrography

The identified thickness of the attacked region in the prepared slides corresponds to 1.6 mm to 4.1 mm for core 1 and 500 μm to 3.7 mm for core 2. Figure 5 shows the interface location between the attacked region (above) and the apparently unaffected region (bottom) for both cores. Note, in blue tones, the presence of microcracks and microporosity. The attacked region of both cores presents three zones of distinct alterations, namely:

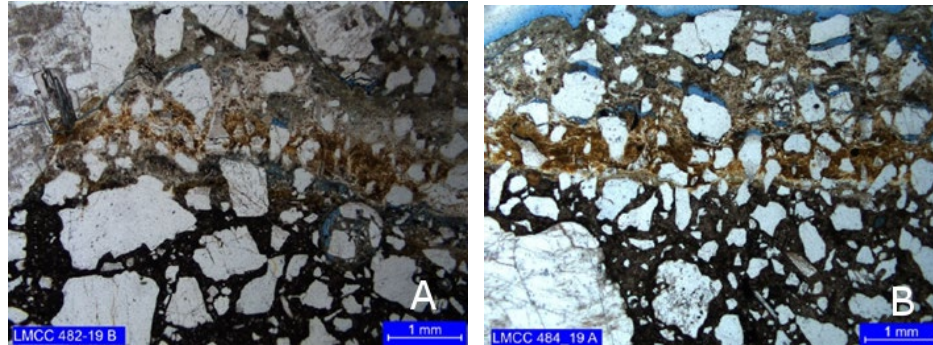


Figure 5. Interface location between the core regions (a) 1 and (b) 2. Simple polarization with capacitor.

Primary zone (outermost): characterized by intense substitution of the paste by low birefringence crypt to microcrystalline material, possibly gypsum, with a texture like “mortar” (Figure 6). Core 1 also exhibit punctual presence of carbonation.

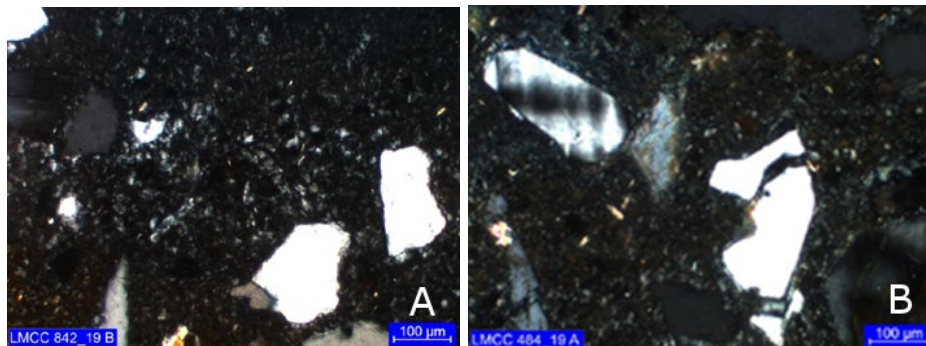


Figure 6. First alteration layer, possibly gypsum cores (a) 1 and (b) 2. Cross polarization, with capacitor.

Secondary (intermediate) zone: shows partial replacement of the paste, with impregnation of iron hydroxides and possible organic matter (Figure 7). In the work Sun (2015), Fe enrichment, due to rust precipitation, was attributed as one of the causes of the presence of microcracks in the concrete alteration zones.

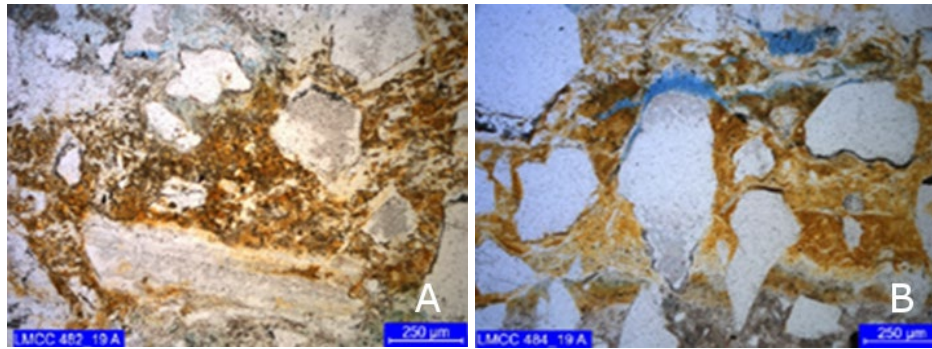


Figure 7. Impregnation of iron hydroxides (reddish tones) from cores (a) 1 and (b) 3. Simple polarization with capacitor.

Tertiary zone: this is a discontinuous carbonation zone at the interface with the apparently unattacked concrete (Figure 8).

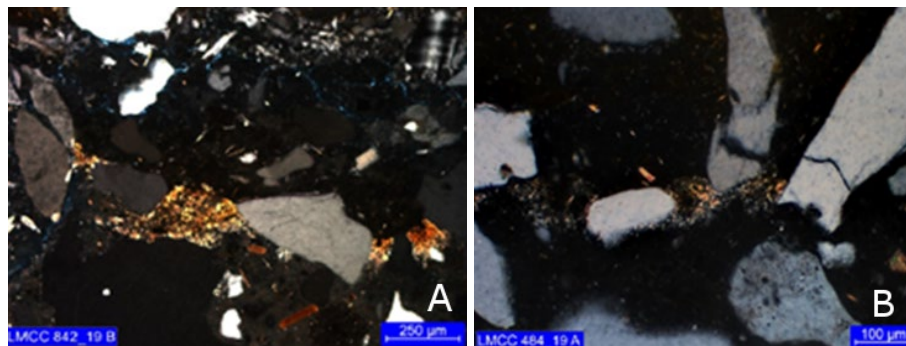


Figure 8. Presence of carbonation (yellowish tones) at the interface between the attacked regions (top) and apparently not attacked (bottom) cores (a) 1 and (b) 2. Cross polarization with capacitor.

In both cores (Figure 9), the three zones show abundant microcracks, unfilled or partially filled by low birefringence crypt to microcrystalline material, gypsum.

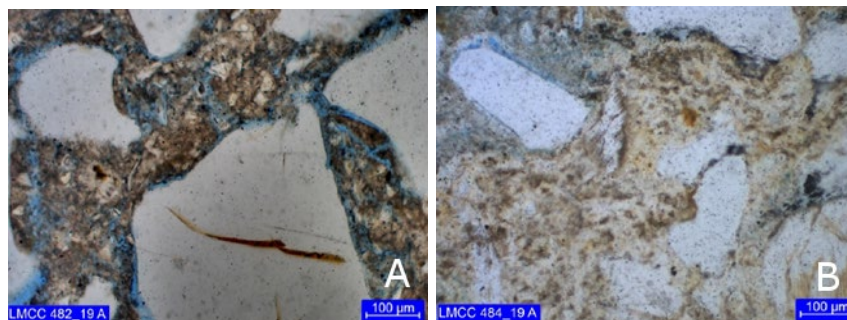


Figure 9. Microporosity zones in the paste associated with microcracks in blue tones (a) 1 and (b) 2. Simple polarization, with capacitor.

4.5 Scanning Electronic Microscopy - SEM

Microstructure analysis revealed considerable mineralogical changes on the attacked surface (Figure 10). Crystals of crystalline sulfoaluminosilicate phases were identified in the sample, containing Ca, Fe and K. In figure 10, the arrows point out to the locations of analysis by energy dispersive system (EDS – Figure 11).

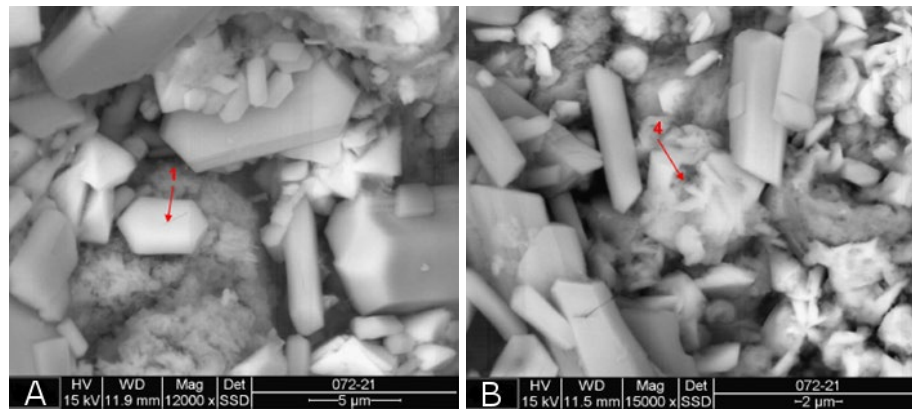


Figure 10. SEM scraped material - sulfoaluminosilicate crystalline phases, containing Ca, Fe and K.

In the micrograph of the scraped material, the presence of portlandite crystals was not identified, indicating that it has completely dissociated. Also, the acid has reduced the matrix to a more porous material, consisting of smaller particles.

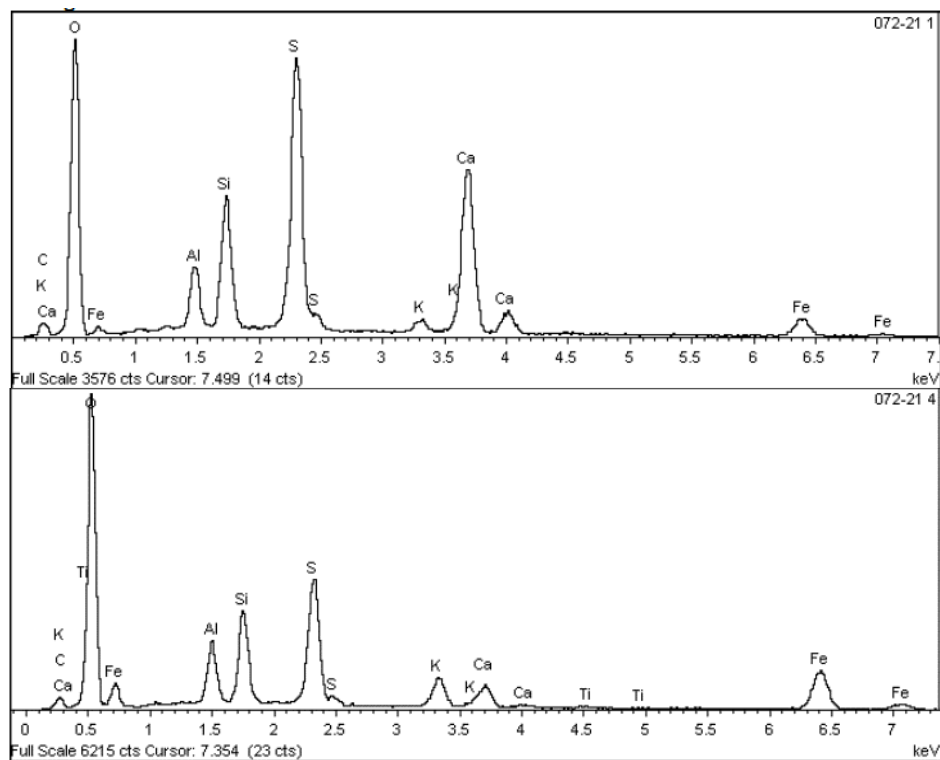


Figure 11. EDS spectra indicated in figure 10 (a) and (b)

In the intermediate sample, two fragments of the light and dark portions were analyzed. In the lighter portion, crystals of rectangular morphology of hydrated calcium sulfate were identified (Figura 12.a), according to the EDS spectrum (Figure 13) with strong S and Ca signals, suggesting gypsum as the main component and ettringite crystals (Figure 12.b).

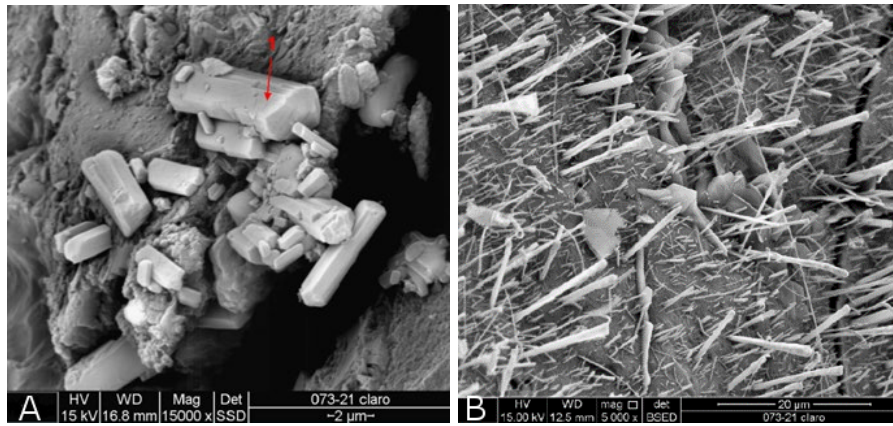


Figure 12. SEM intermediate sample - fragments of the clear portion (a) hydrated calcium sulfate and (b) ettringite crystals.

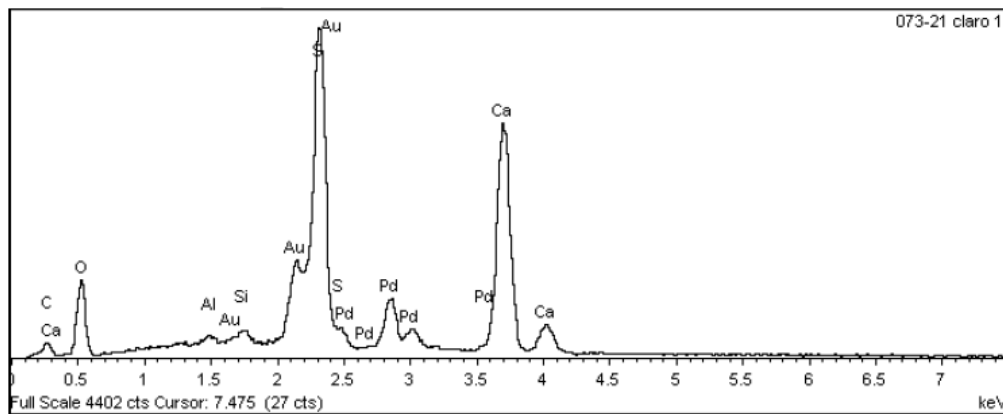


Figure 13. EDS spectra indicated in figure 12.a

In the analyzed fragments of the darker portion of the intermediate sample, crystals of calcium aluminosilicate with sulfur or calcium sulfoaluminosilicate were identified (Figure 14).

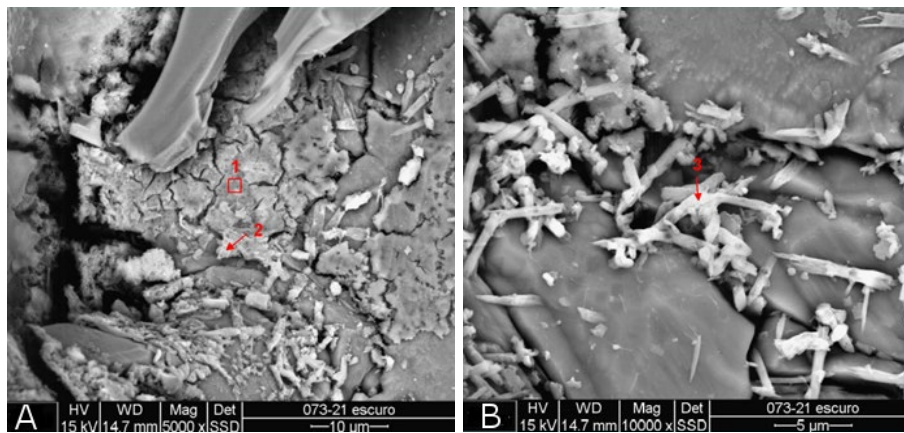


Figure 14. SEM intermediate sample - fragments of the dark portion calcium aluminosilicate crystals with sulfur or calcium sulfoaluminosilicate.

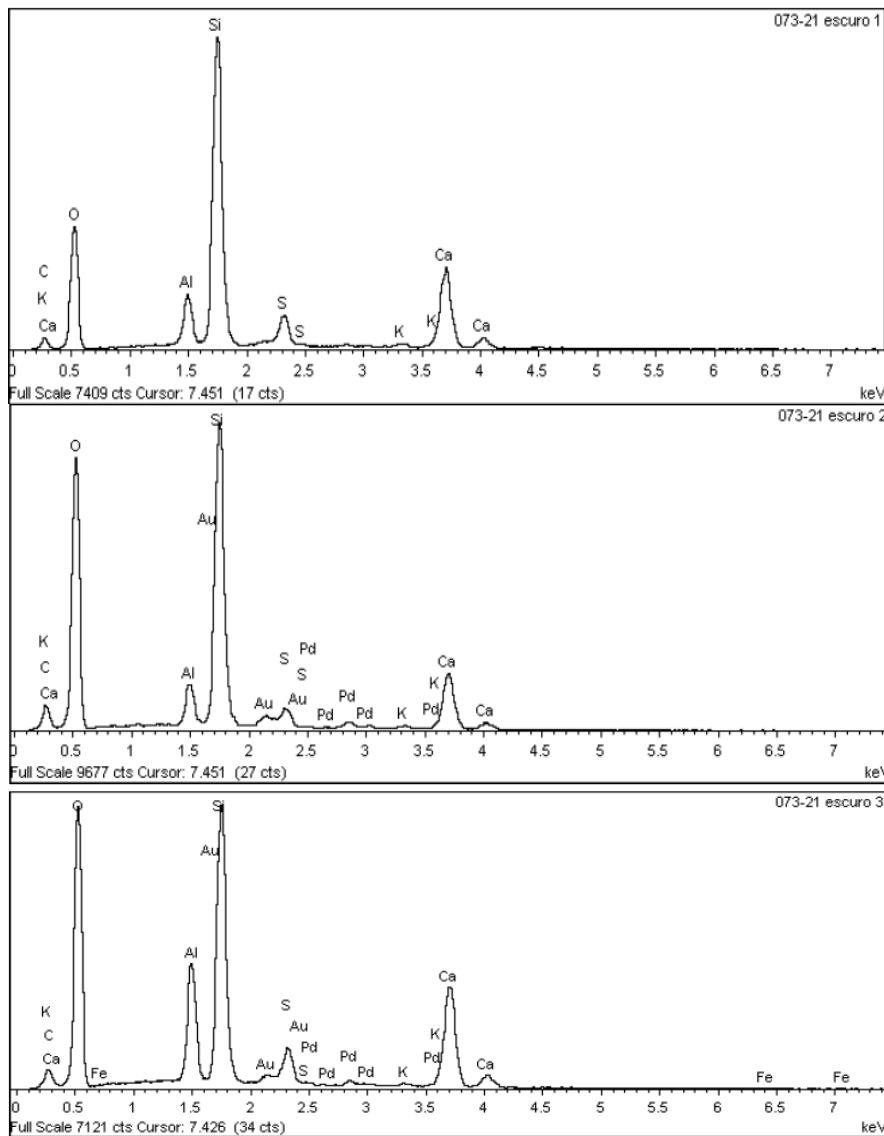


Figure 15. EDS spectra indicated in figure 14 and b.

In the innermost sample, apparently not attacked, portlandite plates larger than 10µm can be observed with non-pathological ettringite needles in a C-S-H weave (Figure 16).

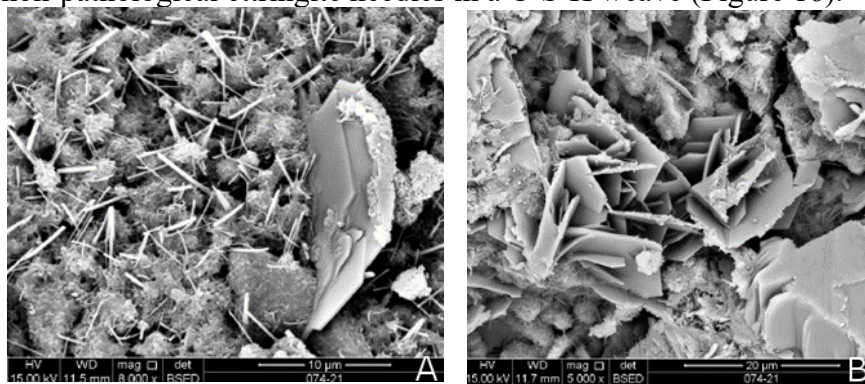


Figure 16. SEM innermost sample - magnification of (a) 10µm and (b) 20µm.

4.6 X-Ray Diffraction – XRD

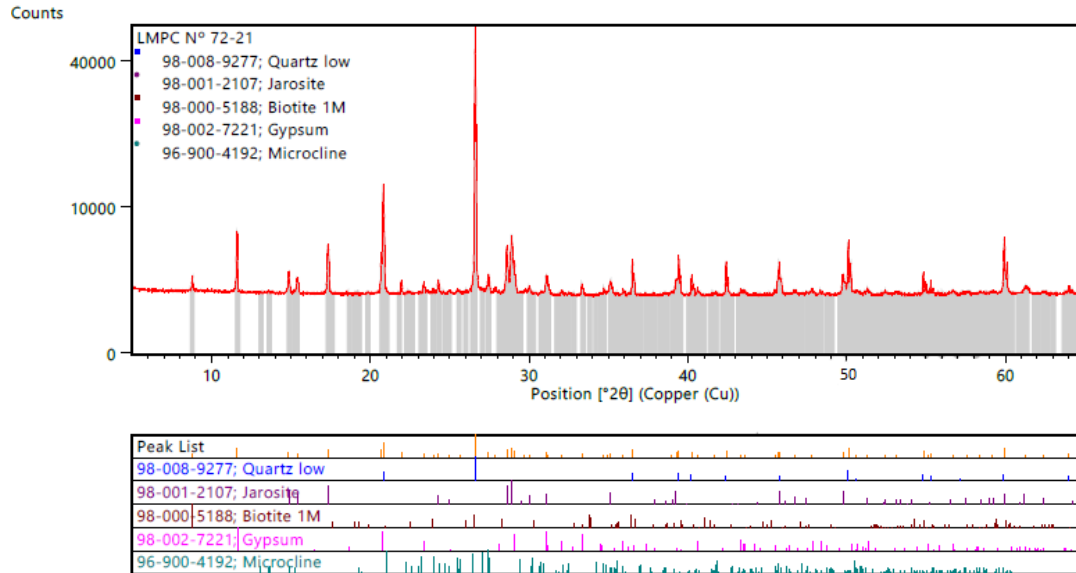


Figure 17. X-Ray diffractogram – scraped material.

In the scraped sample (Figure 17) the presence of Jarosite and Gypsum was identified in a higher concentration. Similar results were found by Tazaki et.al., (1992) in severely corroded concrete pipes. According to the authors, under extremely low pH conditions, bacterial activity can break down Pyrite (iron disulfide, FeS₂) to form Jarosite. Usually, the main microorganisms involved in these reactions are identified as *Thiobacillus ferrooxidans* and/or *Thiobacillus thiooxidans*. In the study by Song et.al., (2020), when the acid attack reaches the surface of the steel bars, the corrosion process of the bars is accelerated by H₂S forming iron sulfide, one of the compounds identified being FeS₂. Thus, it is possible that Jarosite formation comes from FeS₂, formed by the oxidation of the steel bars located in the attacked region. Gypsum was also identified as the most abundant compound on the concrete surface by authors such as Fernandes et.al., (2012), Davis et.al., (1998), Song, et. al., (2018) and Song et. al., (2020).

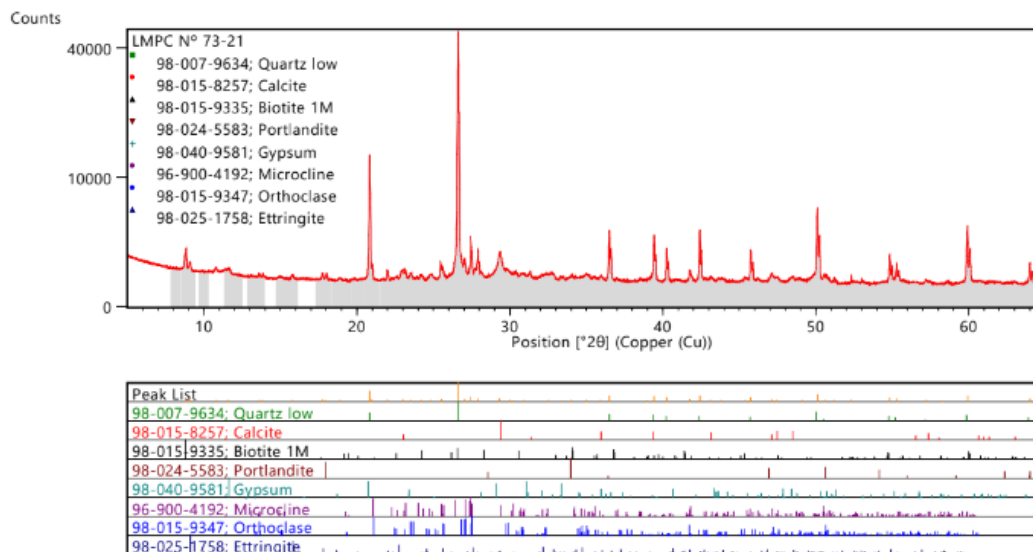


Figure 18. X-ray diffractogram – intermediate sample.

The results obtained by XRD confirm the presence of gypsum in the concrete in all analyzed layers. The presence of gypsum identified in the innermost layer (Figure 19), apparently not attacked, also indicates the beginning of degradation in this layer. From the intermediate sample, it is already possible to identify the presence of ettringite, probably due to a higher pH capable of guaranteeing the stability of that phase. The presence of calcite in the intermediate and innermost samples may come from the product of the carbonation reaction between calcium hydroxide and carbon dioxide.

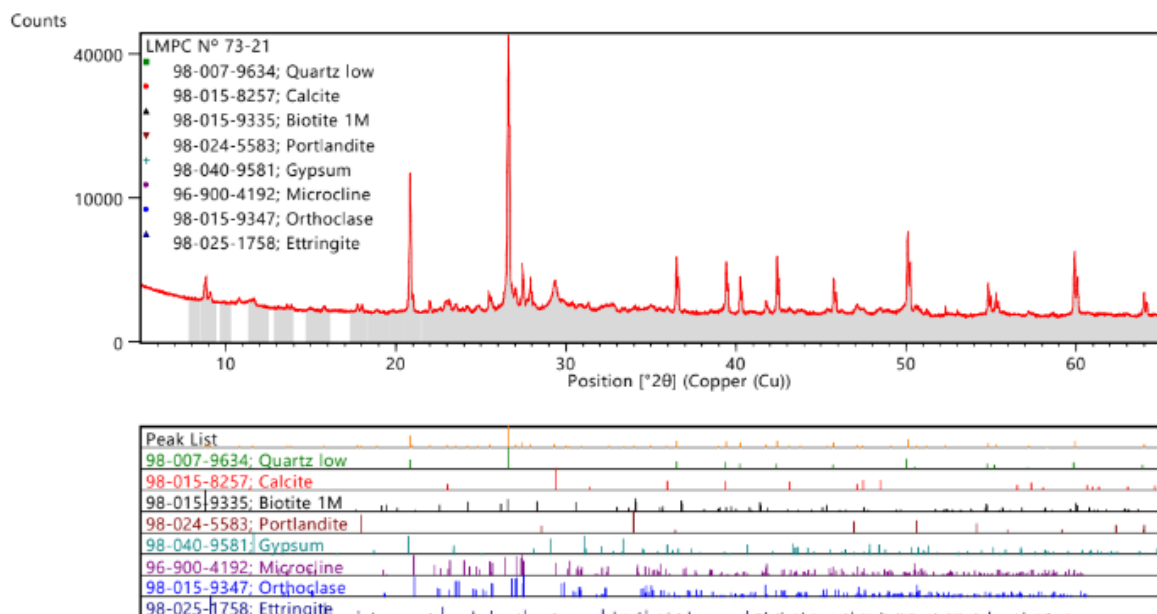


Figure 19. X-ray diffractogram – innermost sample.

4.7 Chemical determinations

The results obtained in the chemical determinations of the materials, expressed on the original basis and on the dry basis, are presented in Table 2.

Table 2. Results of surface chemical determination

Determinations	Results, in %		
	attack with nitric acid (HNO ₃)	water attack (water soluble fraction)	Difference (acid-soluble fraction)
Resíduo insolúvel	65,1	56,7	8,4
Ferro (Fe)	0,73	0,01	0,72
Sódio (Na)	0,04	0,02	0,02
Potássio (K)	0,11	0,01	0,10
Cálcio (Ca)	0,74	0,73	0,01
Magnésio (MgO)	0,01	0,01	0,00
Íons silicato (SiO ₃ ²⁻)	0,49	0,38	0,11
Íons sulfato (SO ₄ ²⁻)	0,41	0,40	0,01
Íons cloreto (Cl ⁻)	0,11	0,05	0,06

NOTE – (*) The missing amount for 100% in the results of table 2 refers to undetermined water. It is emphasized that both results of the determinations are in the same calculation basis and, therefore, it was possible to determine the difference between them.

The elements found in the water-soluble fraction are associated with the acidic gel formed from silicates, sulfates, sodium chlorides, potassium, magnesium, and calcium. The analyzed sample presented pH 2.8 at 19.8°C. This condition favors the colonization of acidophilic sulfur-oxidizing microorganisms (eg *Acidithiobacillus Thiooxidans* and *Acidithiobacillus Ferrooxidans*), which are associated with severe oxidation of steel (Wu et.al., 2020), justifying the steel bars corrosion/dissolution of 16 mm diameter. The pH result also justifies the absence of ettringite in the surface layer. Acidophilic microorganisms, in addition to oxidizing H₂S in sulfuric acid, can oxidize thiosulfate and elemental sulfur that may be deposited on the concrete surface (Wells et.al., 2009).

As for the significant levels of elements found in the soluble fraction in nitric acid attack (HNO₃) (insoluble in water, under the attack conditions proposed in the aforementioned test), they are associated with Jarosite [K₂Fe₆(OH)₁₂(SO₄)₄] and the possible presence of hisingerite [Fe₃Si₂O₅(OH)₄·2H₂O], ferrous hydroxide [Fe(OH)₂] and ferrous chloride [FeCl₂]. According to Alexander and Fourie (2011), aluminum hydroxide [Al(OH)₃] and iron hydroxide [Fe(OH)₃] can precipitate in the layer after the dissolution of the aluminate and/or iron-aluminate phases depending on the concentration of hydrogen ion in the solution - precipitates iron hydroxide at a pH greater than 1.0 and aluminum hydroxide precipitates at a pH greater than 3.0.

The biogenic sulfuric acid causes the loss of concrete alkalinity that initially protects the steel bars, leading to reinforcement corrosion. The traditional corrosion of rebar is an electrochemical process that causes the dissolution of iron, forming various corrosion products, usually iron oxides, and hydroxides. However, as pointed out by Song et.al., (2020), when the biogenic sulfuric acid reaches the steel surface, the reactions and corrosion products can be different. In the authors' work, the main corrosion products of steel bars included iron oxides, iron oxyhydroxides, iron sulfides, iron chlorides, and iron sulfate.

Although iron-containing compounds are mostly formed from the dissolution of steel bars located in the attacked region, these compounds may also come from the dissolution of cement paste, since Portland cement contains about 3% Fe₂O₃ (Jiang et.al., 2014). The formation of hisingerite, for example, may indicate the interaction of Fe, a product of corrosion of steel and/or cement paste, with Si from the dissolution of C-S-H.

5. CONCLUSIONS

From the inspection and results analysis of the Sewage Pumping Station the following conclusions can be drawn:

1. Factors such as the temperature and turbulence of the wastewater influence the speed degradation of concrete structures, due to the greater release of hydrogen sulfide in the air.
2. The compressive strength was preserved in the sounded part of the concrete, as well as its alkalinity, despite the severe deterioration and carbonation in the outermost region of the concrete.
3. The petrographic test shows that the attacked region presents zones of distinct alterations, all with the abundant presence of microcracks.
4. Acid attack includes dissolution of cement phases, transport of dissolved chemical species, and (re)precipitation as secondary minerals, as observed in XRD and SEM/EDS. Gypsum, responsible for the whitish appearance observed on the surface of the concrete, and Jarosite were the main compounds identified on the attacked surface. In addition to the aforementioned compounds, ferrous hydroxide [Fe(OH)₂] and ferrous chloride [FeCl₂] and possible presence of hisingerite were identified, indicating the interaction of silica from the dissolution of C-S-H with other products of steel corrosion and/or cement paste. The results show that when the acid reaches the reinforcement, the steel bars lose their passive

protection layer, allowing the existence of both corrosion products on the surface, from the dissolution of the cement paste and the steel bars, as well as a possible interaction between them. Ettringite was only detected from the intermediate layer of the concrete, confirming it to be an intermediate product of the reaction.

5. The analyzed structure showed a rapid deterioration in a short period of construction and the need for intervention before the end of the expected service life, indicating that the standard specifications in force without other protection measures do not guarantee the durability of the concrete in environments with high concentration of hydrogen sulfide.

6. ACKNOWLEDGMENTS

The authors would like to thank the Basic Sanitation Company of the State of São Paulo (SABESP) for allowing the availability of the structure analysis and for funding all the tests presented.

7. REFERENCES

- Associação Brasileira de Normas Técnicas. (2007). *NBR 5739: Concreto – Ensaio de compressão de corpos-de-prova cilíndricos*. Rio de Janeiro, Brasil.
- Associação Brasileira de Normas Técnicas. (2007). *NBR 7680: Concreto – Extração, preparo e ensaio de testemunhos de concreto*. Rio de Janeiro, Brasil.
- Associação Brasileira de Normas Técnicas. (2009). *NBR 9917:2009 Agregados para concreto - Determinação de sais, cloretos e sulfatos solúveis*. Rio de Janeiro, Brasil.
- Associação Brasileira de Normas Técnicas. (1997). *NBR 13810:1997 Água - Determinação de metais - Método de espectrometria de absorção atômica por chama*. Rio de Janeiro, Brasil.
- ASTM International. (2018). *ASTM C114/2018 Standard Test Methods for Chemical Analysis of Hydraulic Cement*
- ASTM International. (2017). *ASTM C 856/2017 Standard Practice for Petrographic Examination of Hardened Concrete*
- Alexander, M. G., Fourie, C. (2011), *Performance of sewer pipe concrete mixtures with portland and calcium aluminate cements subject to mineral and biogenic acid attack*. Materials and Structures, v. 44, pp. 313–330. DOI: [10.1617/s11527-010-9629-1](https://doi.org/10.1617/s11527-010-9629-1)
- Davis, J. L., Nica D., Shields K., Roberts D. J. (1998), *Analysis of concrete from corroded sewer pipe*. International Biodeterioration & Biodegradation, v. 42, pp. 75–84. DOI: [https://doi.org/10.1016/S0964-8305\(98\)00049-3](https://doi.org/10.1016/S0964-8305(98)00049-3)
- Duchesne, J., Bertron, A. (2013), *Leaching of cementitious materials by pure water and strong acids (HCl and HNO3)*. In: Performance of Cement-Based Materials in Aggressive Aqueous Environments: State-of-the-Art Report, RILEM TC 211 - PAE, 2013. DOI: https://doi.org/10.1007/978-94-007-5413-3_4
- Eřtoková, A., Harbul'áková, V. O., Luptáková, A., Števílová, N. (2012), *Study of deterioration of concrete influenced by biogenic sulphate attack*. Procedia Engineering, v. 42, pp. 1731-1738. DOI: <https://doi.org/10.1016/j.proeng.2012.07.566>.
- Fernandes, I. et al. (2012), *Identification of acid attack on concrete of a sewage system*. Materials and Structures, v. 45, n. 3, p. 337–350. DOI: <https://doi.org/10.1617/s11527-011-9769-y>.
- House, M. W., Weiss, W. J. (2014), *Review of Microbially Induced Corrosion and Comments on Needs Related to Testing Procedures*. Proceedings of the 4th International Conference on the Durability of Concrete Structures, pp. 94-103. DOI: <https://doi.org/10.5703/1288284315388>.
- Jiang, G., Wightman, E., Donose, B., Yuan, Z., Bond, P., Keller, J. (2014), *The role of iron in sulfide induced corrosion of sewer concrete*. Water research. V.49. pp. 166-174. DOI: <https://doi.org/10.1016/j.watres.2013.11.007>.

- Monteny, J., Vincke, E., Beeldens, A., De Belie, N., Taerwe, L., Van Gemert, D., Verstraete, W. (2000), *Chemical, microbiological, and in situ test methods for biogenic sulfuric acid corrosion of concrete*. Cement and Concrete Research, v. 30, pp. 623-634. DOI: [https://doi.org/10.1016/S0008-8846\(00\)00219-2](https://doi.org/10.1016/S0008-8846(00)00219-2).
- O'Connell, M., McNally, C., Richardson, M. (2010), *Biochemical attack on concrete in wastewater applications: A state of the art review*. Cement and Concrete Composites, v 32, p 479–485. DOI: <https://doi.org/10.1016/j.cemconcomp.2010.05.001>.
- Scrivener, K., Belie, N. (2013), *Bacteriogenic Sulfuric Acid Attack of Cementitious Materials in Sewage Systems*. In: Performance of Cement-Based Materials in Aggressive Aqueous Environments, pp.305-318. DOI: https://doi.org/10.1007/978-94-007-5413-3_12.
- Song, Y., Tian, Y., Li, X. Wei, J., Zhang, H., Bond, P., Yuan, Z., Jiang, G. (2018), Distinct microbially induced concrete corrosion at the tidal region of reinforced concrete sewers. Water Research. 150. <https://doi.org/10.1016/j.watres.2018.11.083>.
- Song, Y., Wightman, E., Kulandaivelu, J., Bu, H., Wang, Z., Yuan, Z., Jiang, G. (2020), *Rebar corrosion and its interaction with concrete degradation in reinforced concrete sewers*, Water Research. DOI: <https://doi.org/10.1016/j.watres.2020.115961>.
- Song, Y., Chetty, K., Garbe, U., Wei, J., Bu, H., O'moore, L., Jiang, G. (2021), *A novel granular sludge-based and highly corrosion-resistant bio-concrete in sewers*. Science of The Total Environment, 791, 148270. doi: <https://doi.org/10.1016/j.scitotenv.2021.148270>.
- Tazaki, K., Mori, T., Nonaka, T. (1992), *Microbial jarosite and gypsum from corrosion of Portland Cement concrete*. Canadian Mineralogist. v. 30, pp. 431-444.
- Wells, T., Melchers, R. E., Bond, P. (2009), Factors involved in the long term corrosion of concrete sewers. In: Annual Conference of the Australasian Corrosion Association, 49th.
- Wu, L., Hu, C., Liu, W.V. (2018), *The Sustainability of Concrete in Sewer Tunnel—A Narrative Review of Acid Corrosion in the City of Edmonton, Canada*. Sustainability. v. 10, 517. DOI: <https://doi.org/10.3390/su10020517>.
- Wu, M., et al. (2020), *Microbiologically induced corrosion of concrete in sewer structures: A review of the mechanisms and phenomena*. Construction and Building Materials, v. 239. DOI: <https://doi.org/10.1016/j.conbuildmat.2019.117813>.
- Yuan, H. (2013), *Degradation modeling of concrete submitted to biogenic acid attack*. Tese de Doutorado, Université Paris-Est. DOI: <https://doi.org/10.1016/j.cemconres.2015.01.002>.

Diagnosis and solutions proposal to the damages present in the ceiling of the Convent of Santa Clara de Asís

A. Hernández Oroza^{1*} , A. Diomedes Almeida¹, A. Romeo Sáez¹, P. R. Cuétara Pérez¹ 

*Contact author: ahernandez@proyectos.ohc.cu

DOI: <https://doi.org/10.21041/ra.v12i2.584>

Reception: 11/01/2022 | Acceptance: 20/04/2022 | Publication: 01/05/2022

ABSTRACT

For the restoration of the wooden ceilings of the Convent of Santa Clara, resistography and penetrometer tests, biological studies of the wood, and geomatic techniques for analysis of deformation and dimensioning of the beams were applied. In the present work, the results of the diagnosis showed that 65% of 98 beams is affected by rot and the presence of xylophagous organisms. Density studies by comparison with reference values, showed a loss in the hardness of the wood. The results conclude in the need to replace 17 beams, and the reinforcement of the wood pillars and sections of sliding beams.

Keywords: non-destructive testing, diagnosis, buildings, heritage, geomatics.

Cite as: Hernández Oroza, A., Diomedes Almeida, A., Romeo Sáez, A., Cuétara Pérez, P. R. (2022), “*Diagnosis and solutions proposal to the damages present in the ceiling of the Convent of Santa Clara de Asís*”, Revista ALCONPAT, 12 (2), pp. 296 – 310, DOI: <https://doi.org/10.21041/ra.v12i2.584>

¹Departamento de Diagnóstico y Levantamiento. Empresa Filial RESTAURA, Oficina del Historiador de La Habana, La Habana Vieja, Cuba.

Contribution of each author

In this work, the author A. H. Oroza contributed with the design of the research and the carrying out of tests on site (100%), the writing of the text (50%), the discussion of results (100%) and review (50%). The author A. Diomedes Almeida contributed with the design of the research and the carrying out of essays on site (100%), writing of the text (20%) and revision (25%). The author A. Romeo Sáez contributed to the biological research (100%), writing the text (20%) and revision (25%). The author P. R. Cuétara Pérez contributed with the survey with laser scanner and 3D/orthoimage digital processing (100%) and writing of the text (10%).

Creative Commons License

Copyright 2022 by the authors. This work is an Open-Access article published under the terms and conditions of an International Creative Commons Attribution 4.0 International License ([CC BY 4.0](https://creativecommons.org/licenses/by/4.0/)).

Discussions and subsequent corrections to the publication

Any dispute, including the replies of the authors, will be published in the first issue of 2023 provided that the information is received before the closing of the third issue of 2022.

Diagnóstico y propuesta de solución a las lesiones presentes en el forjado del Convento de Santa Clara de Asís

RESUMEN

El objetivo de este trabajo es diagnosticar y proponer solución a las lesiones presentes en los forjados de madera del Convento de Santa Clara. Para ello, se aplicaron ensayos no destructivos de resistografía y penetrómetro, estudios biológicos a la madera, y técnicas geomáticas para análisis de deformación y dimensionamiento de las vigas. Los resultados del diagnóstico demostraron que el 65% del forjado compuesto de 98 vigas, está afectado por pudrición y organismos xilófagos. Los estudios de densidad mediante comparación con valores de referencia mostraron pérdida en la dureza de la madera. Los resultados concluyen que la restauración implica la necesidad de sustituir 17 vigas, y el refuerzo de los pies derechos y secciones de vigas de corredera.

Palabras clave: ensayos no destructivos, diagnóstico, edificaciones, patrimonio, geomática.

Diagnóstico e proposta de solução para as lesões presentes na laje do Convento de Santa Clara de Asís

RESUMO

Para a restauração dos pisos de madeira do Convento de Santa Clara, foram aplicados ensaios de resistografia não destrutiva e penetrometria, estudos biológicos da madeira e técnicas geomáticas para análise de deformação e dimensionamento das vigas. No presente trabalho, os resultados do diagnóstico mostraram que 65% da laje de 98 vigas é afetada por podridão e organismos xilófagos. Estudos de densidade por comparação com valores de referência, mostraram uma perda na dureza da madeira. Os resultados concluem na necessidade de substituição de 17 vigas, e do reforço dos pés direitos e seções de vigas deslizantes.

Palavras-chave: ensaios não destrutivos, diagnóstico, edificações, patrimônio, geomática.

Legal Information

Revista ALCONPAT is a quarterly publication by the Asociación Latinoamericana de Control de Calidad, Patología y Recuperación de la Construcción, Internacional, A.C., Km. 6 antigua carretera a Progreso, Mérida, Yucatán, 97310, Tel.5219997385893, alconpat.int@gmail.com, Website: www.alconpat.org

Reservation of rights for exclusive use No.04-2013-011717330300-203, and ISSN 2007-6835, both granted by the Instituto Nacional de Derecho de Autor. Responsible editor: Pedro Castro Borges, Ph.D. Responsible for the last update of this issue, Informatics Unit ALCONPAT, Elizabeth Sabido Maldonado.

The views of the authors do not necessarily reflect the position of the editor.

The total or partial reproduction of the contents and images of the publication is carried out in accordance with the COPE code and the CC BY 4.0 license of the Revista ALCONPAT.

1. INTRODUCTION

The conservation of heritage buildings continues to be one of the most complex problems in the field of construction today. As a consequence of the centuries of exposure, these structures have been subjected to the influence of the effects of climate change and the increase in the atmosphere of corrosive gases (SO₂, NO_x, O₃), leading to an accelerated deterioration of its constituent materials (stone, metal, wood) due to chemical reactions, biological colonization and formation of black crusts (Kherais et al., 2021; Kumar and Imam, 2013; Sesana et al., 2021). This can mean a significant risk to the durability of cultural heritage, which must be duly evaluated by a multidisciplinary work group, supported by different testing techniques, many of which are based on destructive techniques such as extracting of test cores and carrying out coves. However, when dealing with the conservation of the built heritage, this type of invasive studies should be avoided in order to maintain the integrity of the work, its structural elements and, consequently, its heritage value.

Currently there are new non-destructive testing (NDT) techniques that provide information with a high level of precision, accuracy, repeatability and reliability. The applications developed are based on different principles, such as electromagnetic (ultrasound, potential, resistivity), impact (Schmidt hammer, penetrometer), geomatics (laser scanner, photogrammetry), emissive (thermography), among others.

The quantitative analysis obtained from these results during the diagnosis allows identifying the causes of deterioration, evaluating the degree of decay or rotting (Liñán et al., 2011) and then the taking of necessary corrective and conservation actions.

The Convent of Santa Clara de Asís was inaugurated in Havana in 1644, becoming the first religious convent founded in Cuba. In 2018, the Office of the Historian of Havana (OHCH) began a restoration and recovery project that has involved professionals and students from different branches of technical careers, and professionals linked to the field of construction and conservation of built heritage. The results that have been obtained from these investigations allowed the establishment of priorities and methodologies for its gradual intervention and recovery (Guevara et al., 2019).

The objective of this work is to evaluate the state of conservation in the structure of the wooden ceiling of the circulation gallery located on the upper floor of the first cloister, for which a series of NDTs were combined that allowed identifying the pathologies present and determining the magnitude of the injuries in the beams and wood stud that make it up. This implies a proposed solution that is discussed at the end of the work.

2. CASE STUDY AND METHODOLOGY

2.1 Identification of the object of study

The structure is located on the upper floor of the first cloister, towards block A (Figure 1). It is based on a wood and plank slab made up of 98 beams of 9 cm x 13 cm (base x height), spaced between 43 cm and 45 cm with an inclination of 17 degrees from the wall towards the wood studs, supported on the 3rd axis on the rammed earth wall that forms the church, and along the axis 4 on a sliding beam that rests on 13 wood studs. The slide beam is made up of 12 beams joined by scarf joint, which rest on the right feet (Table 1). The roof is made up of red ceramic tiles.

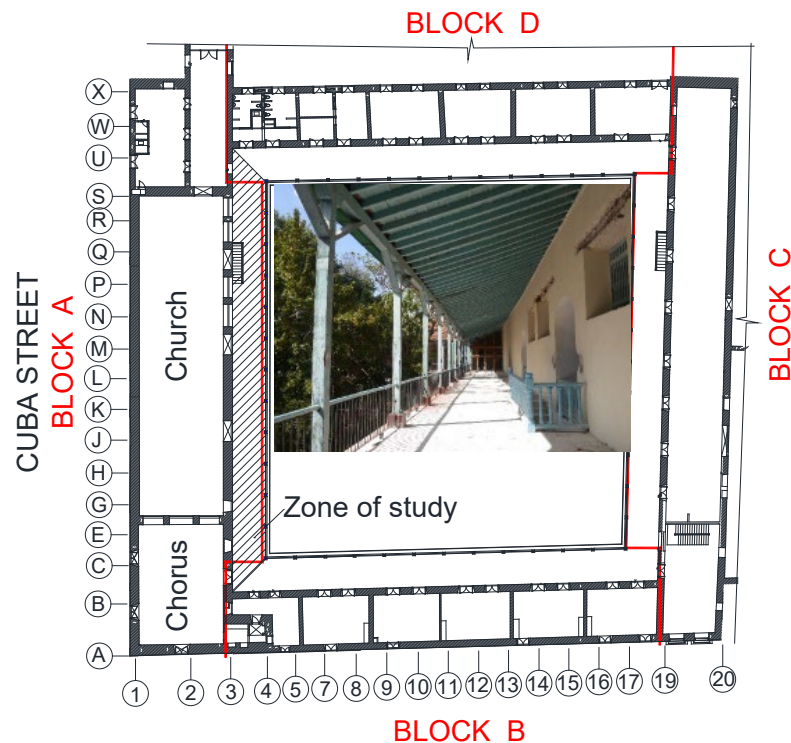


Figure 1. Floor plan sketch of the first cloister, signs and photograph of the gallery studied

2.2 Analysis and selection of non-destructive tests

The purpose of the NDT is to determine the quality and completeness of the material and its component parts without affecting their properties, functions and usefulness through inspection, measurement or evaluation (Helal et al., 2015; Workman and Moore, 2012). The application of this type of techniques to study the state of conservation of historic buildings has gained validity, mainly due to the advantage of not requiring additional deterioration in the structural elements of the building, to know its state of conservation (Binda and Saisi, 2009; Liñán et al., 2011; Ortega and Ripani, 2007). Due to the fact that wood is an organic material, it is susceptible to degradation processes caused by xylophagous insects, mechanical actions, exposure to weathering, rotting by fungi or the action of fire.

In heritage buildings, the use of NDT adds a high value to the diagnostic study, because the structural elements of wood are not affected or receive a negligible impact. As a result, it is possible to obtain technical information with sufficient precision to estimate the state of conservation, quality and durability of the work or work object studied (Hasníková and Kuklík, 2014; Morales-Conde et al., 2013; Palaia et al., 2008).

The techniques applied were:

- Visual inspection of the damages presents on the structural elements
- Measurement of environmental parameters and superficial moisture content of wood elements
- Identification of wood species
- Sizing of the wooden elements that form the wooden roof
- Application of infrared thermography
- Detection of inner damages present inside the timbers by the use of resistography
- Estimation of wood hardness by the use of penetrometer
- Structural evaluation from 3D models obtained by terrestrial laser scanner (TLS)
- Preparation of floor plans and sections in CAD platform

2.2.1 *Infrared thermography*

Infrared thermography is a non-destructive technique that allows pathological analysis through the emission of heat energy by materials. The reading of the radiation emitted in the infrared band makes it possible to interpret the temperature of the material based on the thermal conductivity or the specific heat. Depending on the characteristics and exposure conditions, this material can retain or emit heat. Emissivity is defined by the Stefan-Boltzman Law, which states that radiation is proportional to the temperature of the body and the thermal properties of the material (Morales-Conde et al., 2013). Images were taken with a FLIR E75 camera and post-processed using the software FLIR Tools.

2.2.2 *Resistography*

The resistograph is a piece of equipment specially designed to easily identify areas with cavities, deformations, softening, among other wood damages (Ortiz et al., 2017). An IML Resi PD400 equipment was used and the results were processed with the PD-Tools software. Resistography was performed on the selected elements based on the damage found during puncturing and visual inspection. In the beams, the measurements were made mainly at the ends of the beams that are embedded within the wall, in three directions: diagonal, horizontal and vertical depending on the pathologies of each element tested. In the wood stud, the measurements were made diagonally at the bases to determine the state of conservation in the support, and horizontally at different heights, from the base with a separation of 150 mm between each resistographic measurement point.

2.2.3 *Hardness by Pilodyn penetrometer*

It is a tool that allows estimating the hardness of wood through the penetration of a 1.5 mm diameter steel rod, from a shot towards the wooden element (Palaia et al., 2008). The depth of penetration of the rod varies depending on the density of the material. Due to the fact that the result obtained is dimensionless, it is necessary for its correct interpretation to carry out several measurements on the same element and reference it against a wooden specimen of the same species, at a known moisture content (Kloiber, 2007; Kuklík, 2007).

2.2.4 *Identification of timber species*

The test was carried out to know the timber species present in the elements that make up the forging of the gallery and the uprights that support it. Samples of 1 cm³ volume were taken from the wood elements present in the analysis area. Histological sections were made in the three directions (transversal, tangential and radial), to observe the disposition of the constituent elements by species and they were compared with the reference anatomical descriptions and the identification keys reported and classified within a xylotheque. The macroscopic anatomical characters evaluated were color, texture, smell (in those that possessed it), luster and the presence of growth rings. Microphotographs were taken with a Nikon digital camera model SMZ745 attached to a microscope. The images were processed using the program IC Capture version 2.4. The wood species were graphically identified using the following symbols (Table 1).

Table 1. Graphical representation of the wood species identified in the slab studied

Icon/Name		
 Ácana	 Pine	 Caguairán
 Cedar	 Baría	 Najesí

2.2.5 3D Survey and digital processing

The laser scanner Z+F Imager® 5010c was used. Eleven positionings were made, with an average distance between each one of 5 m. In the equipment, the resolution and quality during the sweep were configured in “High” (High), in addition to the acquisition of photos. This configuration in the TLS implies that at 10 meters from the emitter location, the maximum error distance between the points marked by the laser is 6 mm. With this work scheme, the approximate delay time is 8 minutes for each positioning, in which a final model of points with known x and z coordinates is obtained, with their RGB values.

2.2.6 Generation of 3D models and extraction of orthoimages

For the different types of analysis (geometric, structural, etc.), which can be done on a finite element, it is necessary to obtain a 3D model that can be easily manipulated and measurable by existing conventional programs. The information obtained from a 3D survey provides an almost continuous description of the scanned surface, which makes it possible to identify and quantify anomalies in the elements such as asymmetries, deformations, discontinuities, among other injuries that may be difficult or impossible to identify with the naked eye (Tucci and Bonora, 2017). Orthoimages can be extracted from the 3D models, which makes it possible to obtain an orthogonal projection of the point model, which has the same metric validity as a traditional scale drawing (Figure 2). Commercial software based on CAD allows the import of the orthoimage, making it possible to make precise drawings that can later be viewed and analyzed in other digital environments.



Figure 2. Orthoimage obtained from the gallery of block A

3. RESULTS AND DISCUSSION

3.1 Results of visual inspection

From beam 1 to 17, the floor is supported by a shoring system due to the risk of collapse caused by advance deterioration as a result of decay, as well as the absence of several boards and flashings. This situation has caused a drop in the rest of the slab and the failure of some elements.

The roof is affected by the proliferation of invasive plants throughout the gallery, which leads to an increase in the moisture content in the wood, mainly in rainy seasons, as well as the additional weight that compromises the durability of the roof. The result of the diagnosis identified rotting as the most recurrent lesions, mainly in the head of the timber due to colonization by fungi, dismemberment as a result of the attack of subterranean termites of the genus *Coptotermes*, and bending failures in beams associated with the loss of the bearing capacity of the element. The wood studs that support the slab have a concrete base as support, which responds to an intervention carried out in the 1980s. In most of these, the base is cracked as a result of the increase in volume suffered by the section of embedded wood, as a consequence of the accumulation of moisture inside of it. The concrete is not capable of absorbing the stresses generated within the material due to the volume changes suffered by the wood, which causes them to fracture. Some wood studs are more deteriorated than others due to the fact that woods of a different nature were used, which is why

their absorption capacities and the stresses exerted vary in each case.

3.2 Sizing and deformation obtained from TLS data

The high precision of the data obtained by the laser scanner from the union of the point clouds and the obtaining of the 3D model, allows the measurements of the slab elements to be carried out without the need to intervene on them. To work with representative sections and the wood studs, regions were established and the views were adjusted to obtain measurable images. In the case of the wooden ceiling, a section between beams 35 to 49 was extracted, while for the support elements, a section from studs 5 and 6 was selected. The results are shown in figure 3. Summary of the sizing is indicated in table 2.

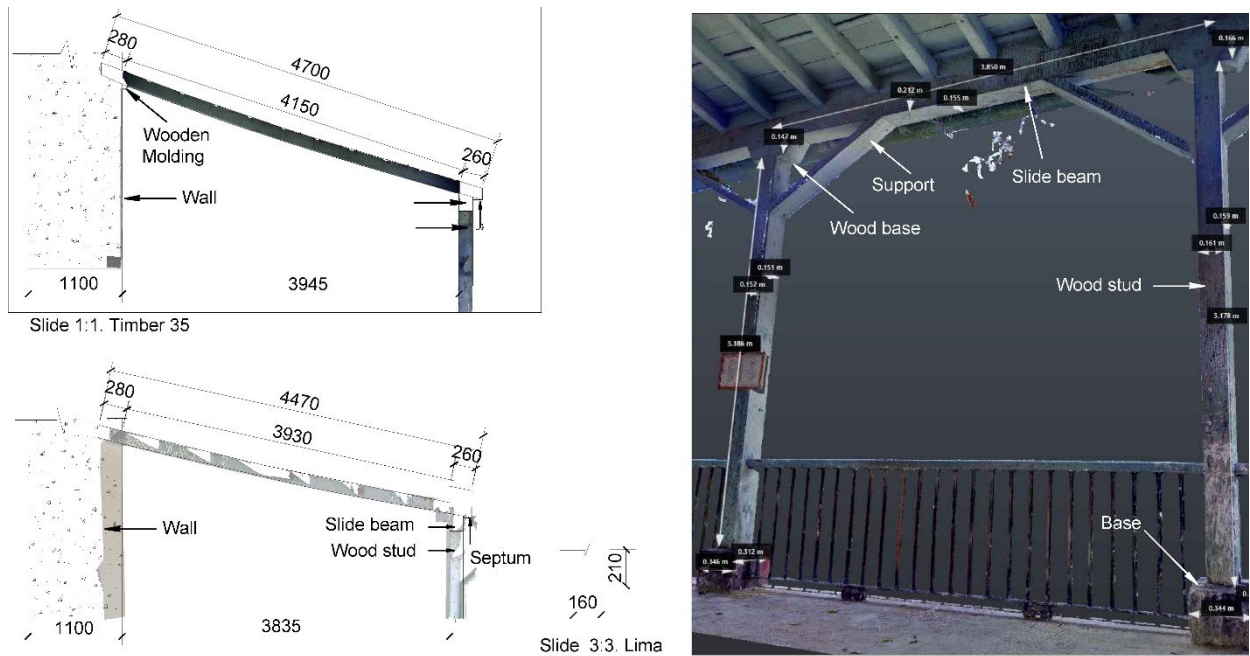


Figure 3. Dimensioning and deformation (in mm) of the wooden elements from the 3D models

Table 2. General dimensions of the floor elements

Element	Base (cm)	Height (cm)	Spacing (cm)
Wood beam	9-10	13	43-45
Table	45-48	18-24	-
flashing	45-48	5-6	31-38
Lima	16	21	-
Slide beam	15-16	21	-
Wood base	15-16	16-17	-
Wood rest-food	5	16	-
Wood stud	15-16	334-372	360-370
Wood stud's base	30-40	27-30	-

For the structural analysis of the slab beams, orthoimages were extracted using the Reconstructor software, and cuts were made using the Autodesk Recap software from beam number 17 to 98. All the beams that make up the slab present deformations to a greater or lesser extent, and some show flexural failures due to a decrease in their bearing capacity. The Cuban standard (NC 53-179:88, 1988), establishes that the maximum admissible deflection is $\frac{1}{240}$ of length for full load. This indicates that the admissible deflection for the wood beams is approximately 1.5 cm, but the values obtained on site are 2 cm to 4 cm higher than those acceptable by calculation. The standard establishes that the deflection of the beams will increase for load periods of more than 10 years by 50% for dry wood, and 100% for wet wood. Considering this, the allowable deflection would increase by 2.25 cm and 3.0 cm, respectively, for which there are still differences between allowable and actual values (Figure 4). It is important to note that not all the maximum deformations found are located in the center of the span, for the reason that there are areas where the element is more deteriorated than others; that is why the beams deform and fail in the most vulnerable area. It was identified that not all the beams are of the same wood species, which is why their hardness and resistance to bending also vary. In the right feet 1 and 7, the deterioration in the joints has caused the displacement of the same and of all the elements that adjoin it. These vertical movements that the right feet have suffered vary between 3.5 cm - 20 cm approximately, and the separation in the scarf joint between the beams that make up the sliding beam ranges between 1 cm to 2 cm, which represents considerable displacements.

To evaluate the deformation of the beams and the density they present, the identification of the timber species was carried out, from the taking of samples directly from the beams and uprights. The wood species were identified in a biological laboratory and the densities obtained with a penetrometer were compared with the reference values reported by the National Institute of Agro-Forest Research (INAF).

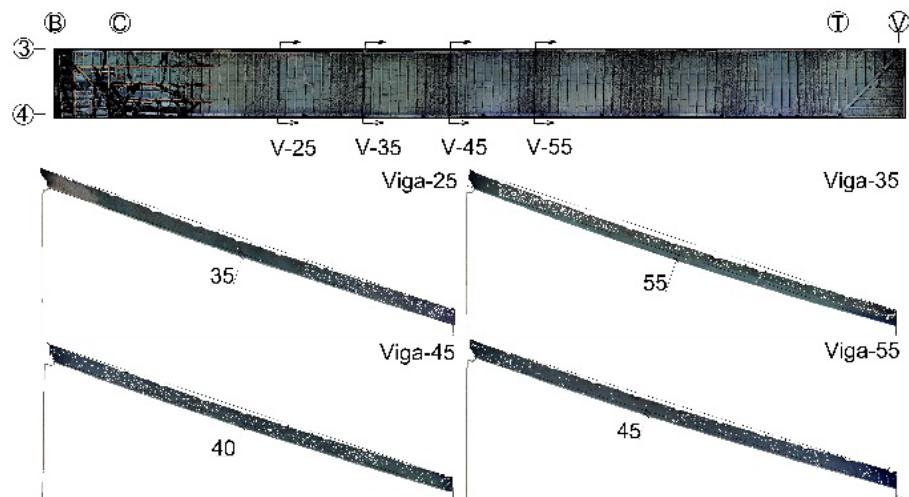


Figure 4. Deformations (in mm) of some wood beams

3.3 Identified timber species

Through the application of the comparative anatomy method from the histological sections made in transverse, tangential and radial directions, it was obtained as a result that the species of wood that form the structure of the roofing and the support system of the wood stud are: cedar (*Cedrela odorata*), pine (*Pinus sp.*), baría (*Cordia gerascantus*), caguairán (*Guibourtia hymenifolia*) and ácana (*Manilkara grisebachii*). Figure 5 shows the histological sections made to identify the existing wood species.

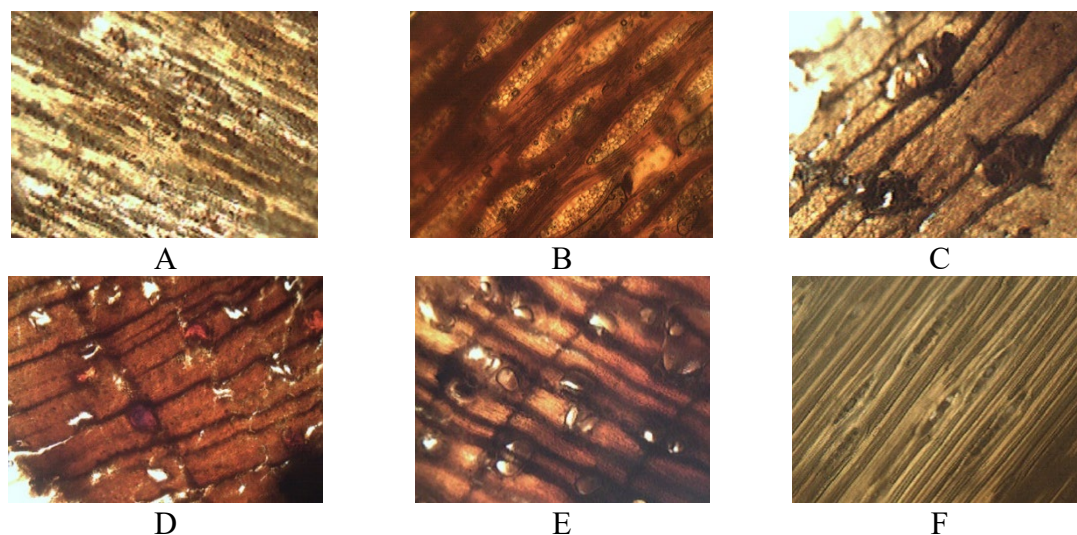


Figure 5. Histological sections at 40x of the identified wood species: A- ácana (longitudinal cut), B- baría (longitudinal cut), C- caguairán (cross-section), D- cedar (longitudinal cut), E- najesí (cross cut), F- pine (lengthwise cut)

3.4 Analysis of diagnostic results

The moisture content measured in the floor beams is between 9%-19%, in the wood studs between 11%-17% and the sliding beam between 11%-12%. The thermographic images obtained reflected how the support wall presents areas of high humidity, which favors the absorption of water in the wood as it is a hygroscopic material.

In the case of the uprights and the sliding beam, the elements were partially wet because they are exposed to sunlight and their drying and ventilation conditions are more favorable than those of the wood beams. However, in times of rain and extreme weather events, this same exposure causes deterioration to be more accelerated and favors the proliferation and attack of wood-degrading organisms.

In the analysis with the thermographic camera, temperature changes of $\pm 2^{\circ}\text{C}$ were identified at different points of the same element, which leads to thermal deformations of the roof. In the case of the beams, the coldest values are found near the boards and in the wall of axis 3, where the most considerable differences appear in the propped area and close to the floor. When it rains, the water infiltrates mainly through the areas where the waterproofing system is least preserved and where there is a greater presence of invasive plants, which causes the accumulation of water, both in the roof and in the wall. The degree of saturation of the wood elements varies depending on the species, the level of exposure and the environmental conditions, which leads to the triggering of pathological processes that weaken their mechanical properties. Other injuries identified with the thermography were temperature variations on the floor, associated with unevenness or damage that favor the accumulation of rainwater, and favor absorption by capillarity in the right feet of the gallery. Being embedded in a concrete base that works as a waterproof layer, drying inside the base is very inefficient and accelerates the decaying of the wood.

The analysis carried out with the resistograph allowed us to identify that of the 98 beams that make up the roof, 64 of them present different pathological manifestations associated with decay due to exposure to wetting and drying cycles. The resistography began in the area of the junction because it is the most vulnerable area, and depending on the damage detected, measurements were also made in the center of the span or near the supports (Figures 6 and 7).

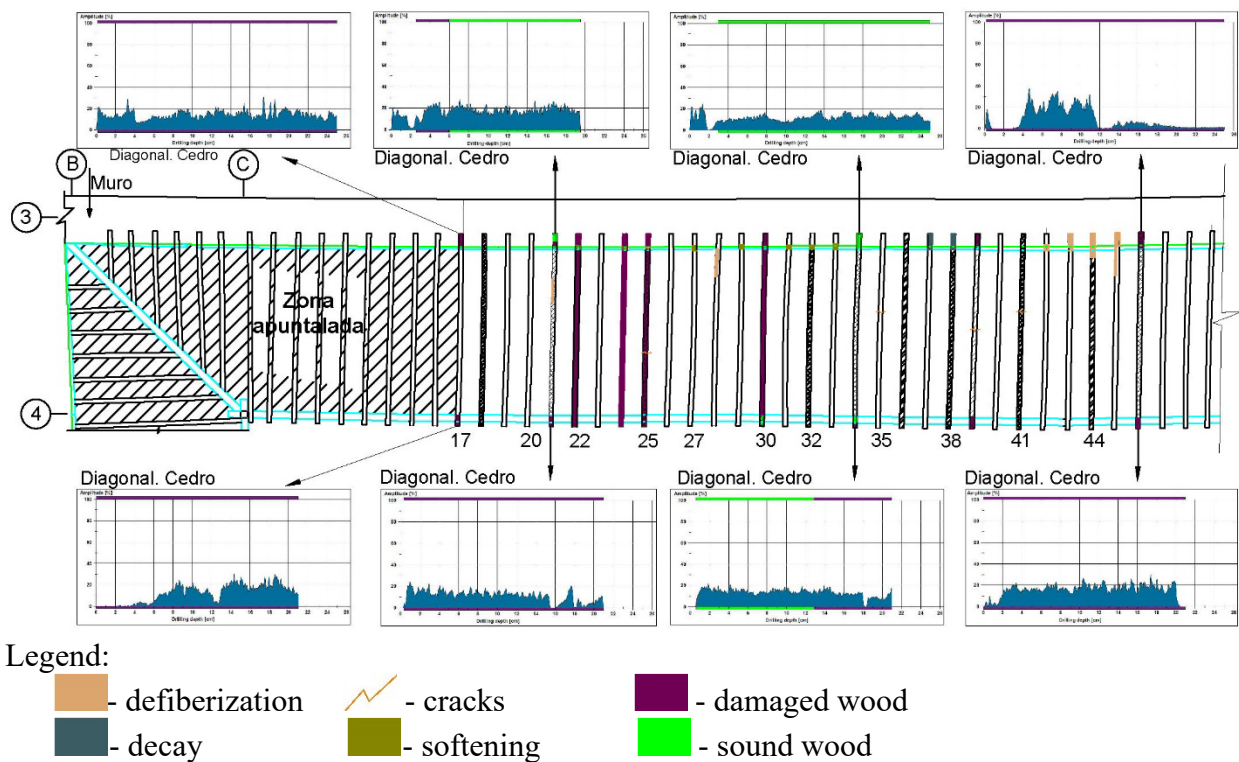


Figure 6. Results of resistography tests and damages in wooden elements between beams 1-49

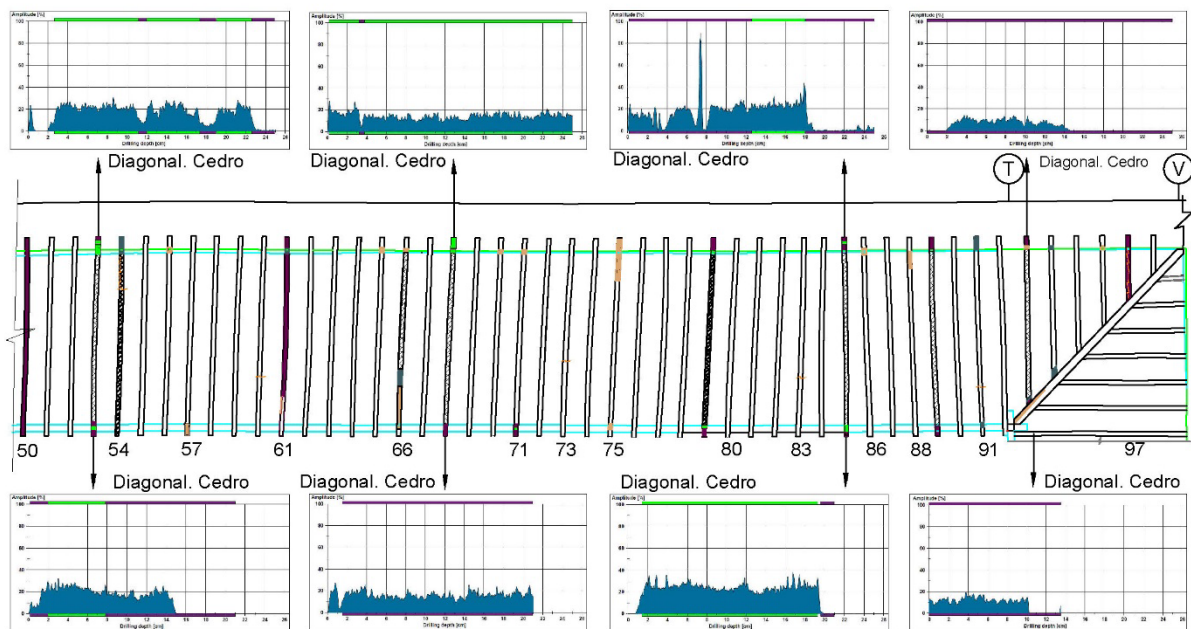


Figure 7. Results of resistography tests and damages in wooden elements between beams 50-98

In the case of the wood studs, the resistography showed low penetration resistance values for all of them, and anomalies similar to those detected in the wooden beams. The extension of the lesions is between 150 mm and 750 mm from the concrete base upwards, and in more than 50% of the wood studs, it is located in the first 150 mm of height.

The sliding beam, with an extension of 45.5 m, is made up of sections, and each section of beams of different wood species. Due to the fact that the most vulnerable area is the exterior side, the

resistography was carried out from the interior side (gallery) to the exterior (patio), with the purpose of identifying the progress in the deterioration based on the width of the beam. In the section between the wood studs 8 and 9, the resistography shows areas with defibration due to the attack of termites. These xylophagous organisms feed on the wood and leave tunnels inside it, consequently, the resistographic curve suddenly changes as a result of the lack of resistance during their advance (Figures 8 and 9). When carrying out the penetrometer tests and the corresponding adjustment calculations, it was evaluated that the wooden elements have a hardness lower than the tabulated values for Cuban woods. These results are in correspondence with the low resistances obtained in the resistography tests. Table 3 presents a sample of some of the elements studied.

Table 3. Hardness calculation results from the penetrometer

Element	Location	Wood species	Moisture content (%)	Penetration 12% humidity (mm)	Calculated density 12% humidity (g/cm ³)	Tabulated density 12% humidity* (g/cm ³)
Lima	axis 3	Pine	14	14	0.35	0.74
Beam 30	axis 4	Cedar	13	17	0.27	0.37
Beam 50	axis 3	Cedar	13	21	0.16	0.37
wood stud 8	at 30 cm from base	Pine	14	9.5	0.47	0.74
wood stud 9	at 30 cm from base	Baría	13	11	0.43	0.84

*- reference values provided by INAF

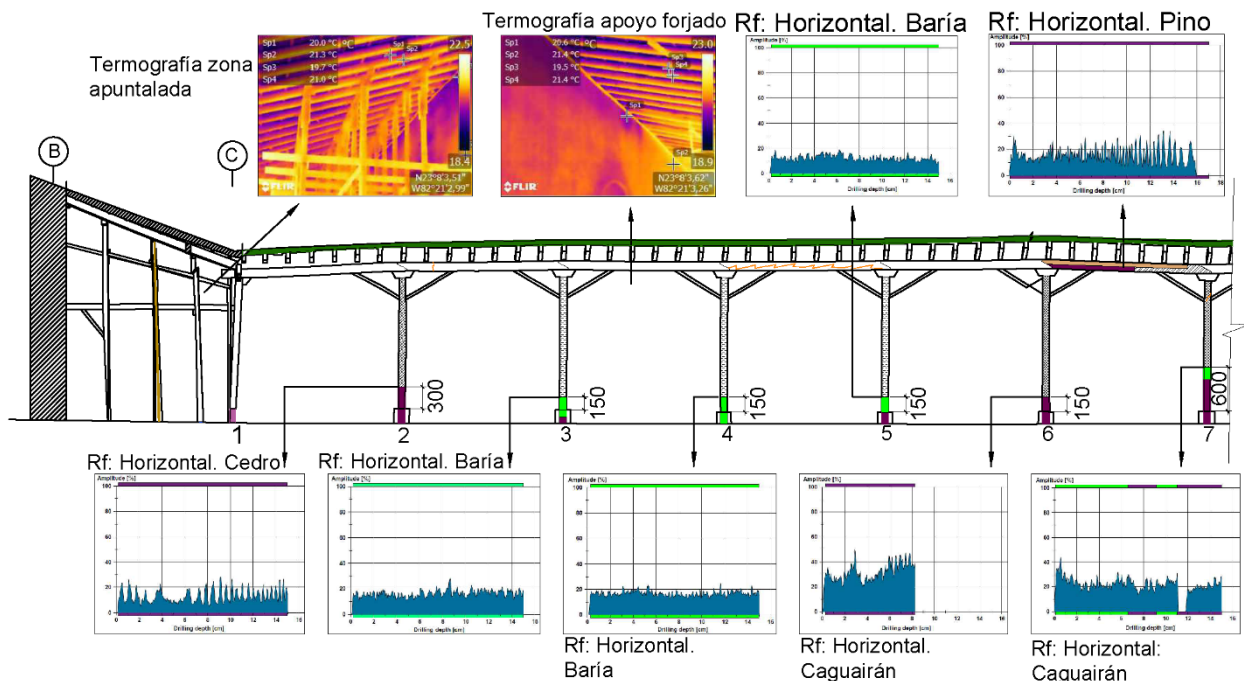


Figure 8. Results of tests on elements of the slab between wood studs 1-7, where the thermography reflects the humidity present in the wall of axis 3 in the support area of the beams, and the resistography in the wood stud and sliding beam of the axis 4

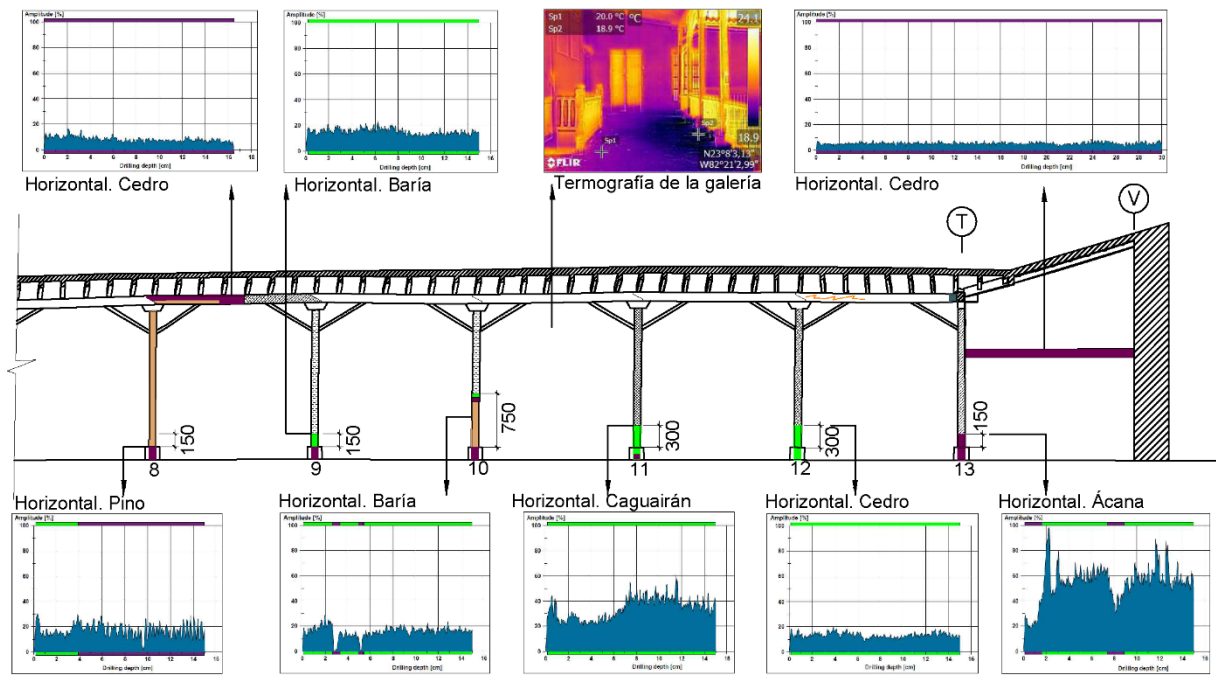


Figure 9. Results of tests on elements of the slab between wood stud 8-13, showing the thermography of the gallery with a high level of humidity in the supports of the wood stud, and the resistography in the wood stud and slide beam at axis 4.

3.5 Solution proposals

In the floor beams, it was determined that 17 of them need to be replaced as a result of their advanced deterioration. Additionally, another 45 beams must be structurally reinforced in different areas, depending on the pathologies developed in each one. Of the remaining 34 beams for which no significant injuries were identified, it will be necessary to disassemble and strip 2 of them due to superficial damages, in order to subsequently recalculate the load for the new beam section (Figures 10 and 11). All the wood studs showed deterioration that required structural reinforcement actions, as well as in the sliding beams, where it will be necessary to replace two sections and reinforce another 3 sections (Figures 12 and 13). The significant decrease in the density of the wood is the result of exposure to wetting and drying cycles, mainly in the rainy months, with the consequent proliferation of fungi and termite infestation. The deformations present in the beams are not only the result of the increase in weight due to excess water and the growth of higher plants, but also due to the loss of their timber properties, which increases the risk of structural failure.

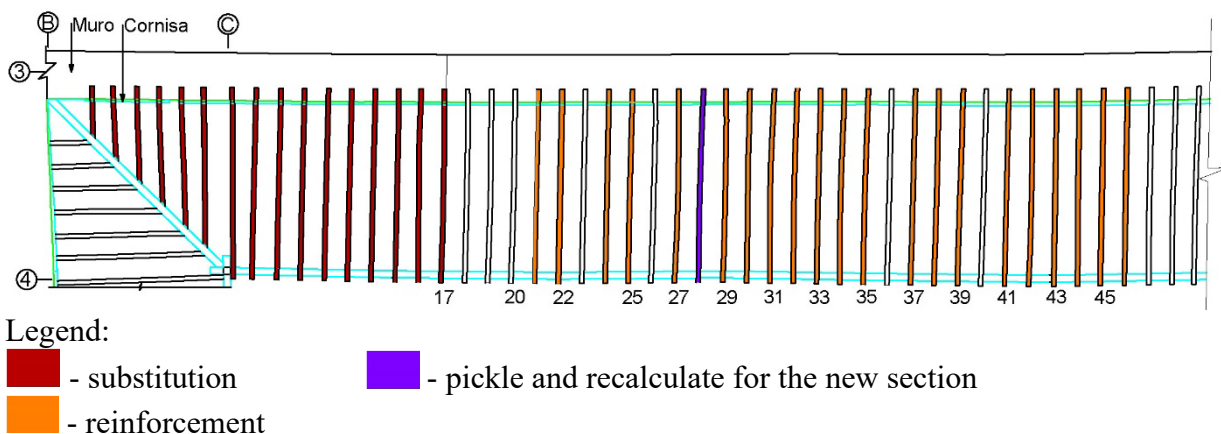


Figure 10. Proposal for a solution to the ceiling between beams 1-49

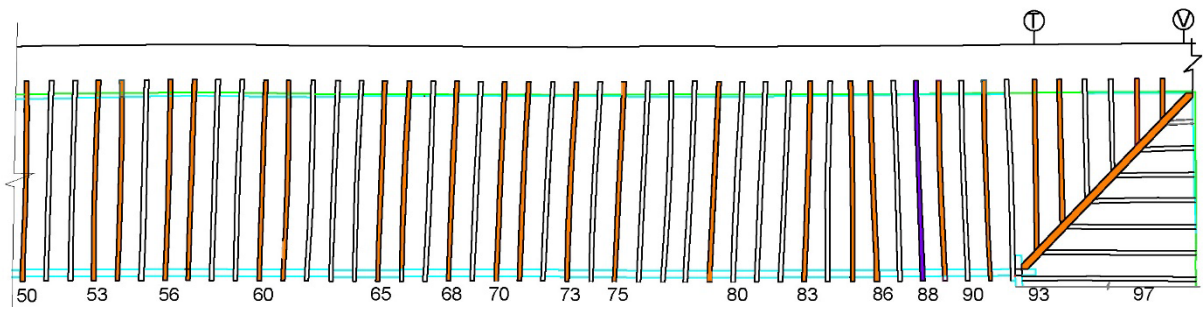


Figure 11. Proposal for a solution to the ceiling between beams 50-98

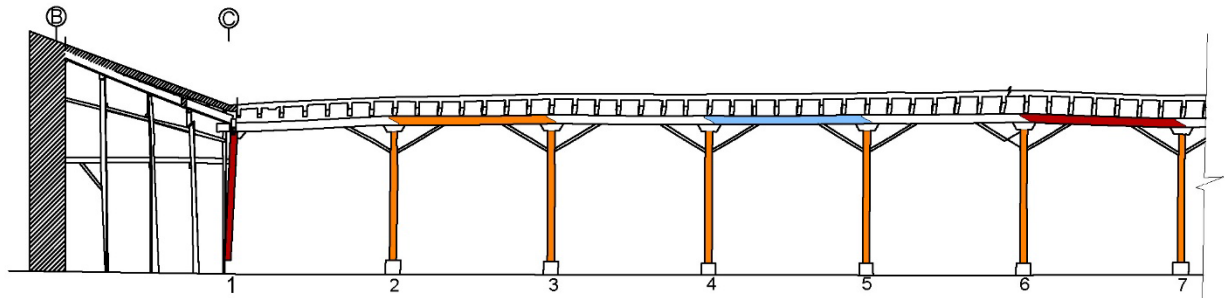


Figure 12. Proposal for a solution to the wood stud 1-7 and section of the sliding beam

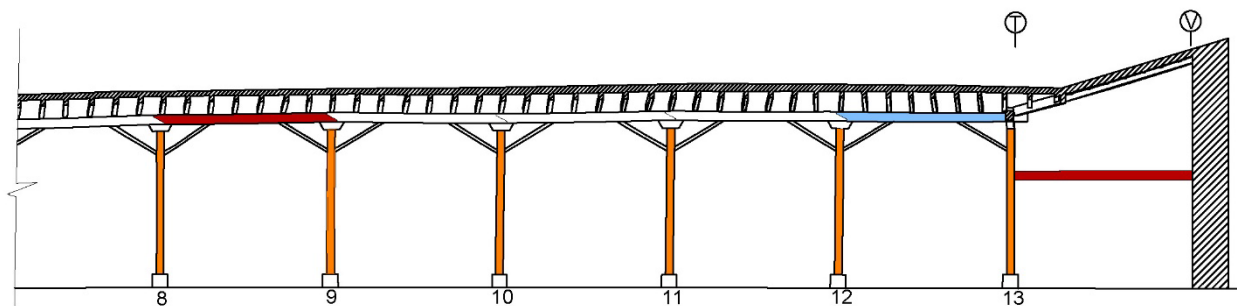


Figure 13. Proposal for a solution to the wood stud 8-13 and section of the sliding beam

4. CONCLUSION

The structure of the wooden ceiling of the gallery studied shows advanced deterioration, caused by reasons such as excess of moisture and the growth of invasive plants on the roof. This situation led to colonization by fungi and the attack of xylophagous organisms, which provoke losses in the properties of the wood used,

Applied density studies showed affectations in hardness as a result of exposure to wetting and drying cycles, and biological colonization. This had caused deformations in the beams and a decrease in the bearing capacity of the structural elements.

As a result of the diagnosis carried out, the need to replace 17 roof support beams and the structural reinforcement of another 45 was demonstrated. The wood stud must also be reinforced, while one of them will have to be replaced due to advanced deterioration, as well as some slide beam sections.

5. AKNOWLEDGMENT

The authors wish to thank the OHCH Patrimonial Rehabilitation Investor Group for financing this research under contract No. S-5AI/2020 Ccto. 22DG/2019. It was carried out with the support of the Materials Division of the Tecnalia Research & Innovation Foundation under the FOCAD 2018

collaboration project.

Likewise, we would like to thank the specialists and technicians of the Diagnostic and Survey Department for their participation, in particular the Engineers Rafael González Hernández and Dainelys Guerra Bouza for their considerable contribution, all the technicians from the Department of Diagnostic and Surveying, as well as to the Biologist Maider Arana of the Tecnalia Foundation in the elaboration of the termite control and eradication plan, and of the International Cooperation to Ing. Ingrid Alonso Esquivel.

6. REFERENCES

- Binda, L. and Saisi, A. (2009), *Application of NDTs to the diagnosis of Historic Structures*, Non-Destructive Testing in Civil Engineering, Nantes, France.
- Guevara, J. L., Toirac, Y. A., Marisy, C. M. C. (2019), *Un acercamiento al convento de Santa Clara de Asís de La Habana. Estudio de su estado de conservación y propuestas de intervención*. Revista ALCONPAT, 9(2): 228-246. <http://dx.doi.org/10.21041/ra.v9i2.354>
- Hasníková, H., Kuklík, P. (2014), *Various non-destructive methods for investigation of timber members from a historical structure*. Wood research, 59(3): 411-420.
- Helal, J., Sofi, M., Mendis, P. (2015), *Non-destructive testing of concrete: A review of methods*. Electronic Journal of Structural Engineering, 14(1): 97-105.
- Kherais, M., Csébfalvi, A., Len, A. (2021), *The climate impact on timber structures*. International journal of optimization in civil engineering, 11(1): 143-154.
- Kloiber, M. (2007), *"Ensayos no destructivos de las propiedades de la madera"*, Mendel University, Czech Republic, 208 pp.
- Kuklík, P. (2007), *Determinación de las propiedades estructurales de la madera*, Praha.
- Kumar, P., Imam, B., (2013), *Footprints of air pollution and changing environment on the sustainability of built infrastructure*. Science of The Total Environment, 444: 85-101. <http://dx.doi.org/10.1016/j.scitotenv.2012.11.056>
- Liñán, C. R., Conde, J. M., Hita, P. R. D., Gálvez, F. P. (2011), *Inspección mediante técnicas no destructivas de un edificio histórico: oratorio San Felipe Neri (Cádiz)*. Informes de la Construcción, 63(521): 13-22. <http://dx.doi.org/10.3989/ic.10.032>
- Morales-Conde, M. J., Rodríguez-Liñán, C., Rubio de Hita, P. (2013), *Application of non-destructive techniques in the inspection of the wooden roof of historic buildings: A case study*. Advanced Materials Research, 778: 233-242. 10.4028/www.scientific.net/AMR.778.233
- Norma Cubana (1988), *NC 53-179:88 - Estructuras de madera. Método de cálculo*. La Habana, Cuba.
- Ortega, N. F., Ripani, M. (2007), *Experiencias en el empleo de ensayos no destructivos, en el análisis de estructuras de hormigón afectadas por diferentes situaciones patológicas*, IV Conferencia Panamericana de END Buenos Aires – Octubre 2007. Asociación Argentina de Ensayos no Destructivos y Estructurales (AAENDE), Argentina, pp. 1-12.
- Ortiz, R., Fuentes, N., Jamet, A., Moya, A., González, M., Varela, M. P., Ramírez, A., Adofacci, G., Martínez, P. (2017), *Evaluación resistográfica en elementos de maderas desfibradas de la torre de lixiviación de la oficina salitrera Santa Laura en Chile. Patrimonio de la Humanidad*. Informes de la Construcción, 69(547): 1-6. <http://dx.doi.org/10.3989/id54678>
- Palaia, L., Monfort, J., Sánchez, R., Gil, L., Álvarez, A., López, V., Tormo, S., Pérez, C., Navarro, P. (2008), *"Assessment of timber structures in service, by using combined methods of non-destructive testing together with traditional ones"*. 9th International Conference on NDT of Art. Jerusalem, Israel.

- Sesana, E., Gagnon, A. S., Ciantelli, C., Cassar, J., Hughes, J. J. (2021), *Climate change impacts on cultural heritage: A literature review*. Wiley Interdisciplinary Reviews: Climate Change: e710. <https://doi.org/10.1002/wcc.710>
- Tucci, G., Bonora, V. (2017), *Towers in San Gimignano: metric survey approach*. Journal of performance of constructed facilities, 31(6). [http://doi.org/10.1061/\(ASCE\)CF.1943-5509.0001085](http://doi.org/10.1061/(ASCE)CF.1943-5509.0001085)
- Workman, G. L., Moore, P. O. (2012), "*Nondestructive Testing Handbook 10: Overview*". American Society for Nondestructive Testing.